SYNTHESIS OF MODIFIED HYDROCALUMITE: A NOVEL KATOITE/PORTLANDITE PRECURSOR METHOD

UNIVERSITEIT VAN PRETORIA
UNIVERSITY OF PRETORIA
YUNIBESITHI YA PRETORIA
Denkleiers • Leading Minds • Dikgopolo tša Dihlalefi

Monique J. Schmidt

SYNTHESIS OF MODIFIED HYDROCALUMITE: A NOVEL KATOITE/PORTLANDITE PRECURSOR METHOD

Monique J. Schmidt

UNIVERSITEIT VAN PRETORIA
UNIVERSITY OF PRETORIA
YUNIBESITHI YA PRETORIA
Denkleiers • Leading Minds • Dikgopolo tša Dihlalefi

Submitted to partial fulfilment of part of the requirements for the degree of Masters of Engineering in the Faculty of Engineering, the Built Environment and Information Technology, University of Pretoria, Pretoria

2015

SYNTHESIS OF MODIFIED HYDROCALUMITE: A NOVEL KATOITE/PORTLANDITE PRECURSOR METHOD

Monique J. Schmidt

Supervisor: FJWJ Labuschagne

Department: Chemical Engineering

Degree: MEng (Chemical Engineering)

SYNOPSIS

A novel method of synthesising calcium/aluminium layered double hydroxides (LDHs) was developed, which makes use of a katoite/portlandite mixture as a precursor. The precursor mixture is synthesised by reacting CaO and $Al(OH)_3$ in water. The synthesis has no expensive heating steps and does not produce any effluent, making the synthesis a "green" method. (Van der Westhuizen, 2011) The purpose of this investigation was to launch an exploratory study on the effectiveness and limitations of the novel synthesis method when synthesising intercalated calcium/aluminium LDHs.

The novel synthesis method was compared to two traditional synthesis methods: co-precipitation and reconstruction. The novel synthesis method is equally as effective as the reconstruction method for the synthesis of organically modified Ca/Al LDHs. In most intercalations, the precursor method yielded more crystalline products than the reconstruction method. The co-precipitation method with nitrate salts was the least effective, since nitrate was more stable in the interlayer than the majority of the organic anions. For this reason, a Ca/Al-nitrate phase was the dominant crystalline species in these samples. Since the novel synthesis method produces organically modified LDHs of equal or higher quality than the traditional synthesis methods, it is a feasible method for producing LDHs. Since the method

is also cheaper and more environmentally friendly than traditional synthesis methods, it is the preferential method for producing organically modified Ca/Al LDHs on a large scale.

When the precursor mixture was hydrated in a reaction vessel that was left open to air from 2 h to 24 h, at temperatures ranging from room temperature to 80 °C, the maximum conversion to hydrocalumite was 15 wt.%. This means that if the reactor is left open to air, there will only be 15 wt.% carbonate contamination from air in the form of hydrocalumite. If a sealed vessel is used, the conversion will be drastically less, since there is a negligible amount of carbon dioxide in the small volume of air trapped in the vessel. For this reason, it is not necessary to synthesise intercalated hydrocalumites in an inert atmosphere, unless 100 % purity is needed.

Chloride-intercalated Ca/Al LDHs form readily at temperatures from room temperature to 60 °C when aged for 2 h to 24 h. A maximum conversion of 64 wt.% occurs when the sample is aged for 12 h at 40 °C. In general, if the sample is aged for extended periods or at elevated temperatures, conversion decreases. A decrease in conversion is always accompanied by an increase in amorphous material, indicating that a more stable, amorphous phase forms if the LDH is aged for too long or at temperatures that are too high. Since no general trends could be found when intercalating chloride, further tests should be performed to determine what other factors influence the ability of the precursor to form an intercalated hydrocalumite.

In general, the conversion of the precursor to a benzoate-intercalated LDH increases with increasing reaction time and decreases with increasing temperature. Benzoate-intercalated LDH did not form at a temperature of 60 °C at any of the aging times tested, indicating that Ca/Al-benzoate is not stable at elevated temperatures. When the samples were aged for 24 h, there are two new primary peaks present on the XRD patterns. For this reason, there is either a new configuration of benzoate in the interlayer or a new crystalline symmetry present in the samples. As the temperature increased, a smaller d-spacing spacing was favoured.

Instead of using a katoite/portlandite mixture, a calcium source in the form of calcium oxide [CaO] or calcium hydroxide [$Ca(OH)_2$] can be added to pure katoite prior to intercalating with an anion. Using an extra calcium source in combination with katoite, instead of the precursor mixture, renders similar results. The CaO converts rapidly to $Ca(OH)_2$; therefore, both calcium sources are equally effective.

Contrary to popular belief, an intercalated LDH material does not necessarily have to be synthesised at a high pH. All the weak acids with low solubility tested were able to intercalate at a pH as low as 5. This is not the case for soluble acids. Both strong and weak soluble acids tend to break down the layered material as soon as the pH drops below 10, as reported in literature. However, even for organic acids, it is recommended to keep the pH above 10, in order to maximise retention of layered material. The only benefit to intercalating organic acids at a lower pH is that the precursor and carbonate-intercalated LDH are broken down to a larger extent, making the final product purer.

When a katoite/portlandite precursor material is titrated with different acids, the top-down titration curves display two distinct plateaus for most acids. However, titrations with anthranilic acid shows only one distinct plateau, and titration with OH-substituted benzoic acid rings tend to exhibit an extra plateau. This is because the OH group dissociates at a high pH.

There are several factors affecting intercalation that have not been studied, which may have a large impact on the degree of intercalation. It is, therefore, recommended that the following factors also be investigated:

- Mixing efficiency
- Boiled vs. non-boiled water
- Size of the anion

In order to determine the success of the intercalation experiments, the most important factor to test would be the properties of the intercalated LDH materials in their final applications.

KEYWORDS: layered double hydroxide, precursor, katoite, intercalation

Acknowledgements

I would like to thank:

- My enthusiastic and dedicated supervisor, Dr. Johan Labuschagne, for his help and guidance throughout my thesis. I could not have had such an amazing experience during these past 2 years if it was not for him.
- Mr. Jan Mentz for aiding in the development of this research project.
- Dr. Andreas Leuteritz for his knowledge and input during the time spent at the Leibniz Institute for Polymer Research, Dresden.
- Mrs. Wiebke Grote for her extensive help with X-ray diffraction analysis, as well as her stimulating conversation during analysis sessions.
- Mrs. Liane Häußler and Mr. Gerard Puts for their help with thermogravimetric analysis.
- The National Research Foundation (NRF) for contributing to the funding of this project.
- My family: Christine Schmidt, Dieter Schmidt and Claudia Schmidt for their moral support and constant reminders not to take life too seriously.
- Gerard Potgieter, even though I can’t find the words.

Contents

List of Figures

List of Tables

1. Introduction

Layered double hydroxide (LDH) materials are becoming increasingly more important in the field of nanotechnology. The positive charge on the LDH layers allows LDH materials to theoretically incorporate any negatively charged anion between the layers. Since the intercalated anions change the properties of the LDH, the applications of LDHs are vast. The main applications of LDHs include: catalysts; pharmaceuticals; flame retardants; adsorbents and anion stabilisers. (Cavani, Trifiro & Vaccari, 1991) LDHs are synthesised using various methods. Most of these synthesis methods are extremely energy intensive and/or produce a large amount of effluent (Duan *et al*, 2008). If LDHs are to be synthesised on an industrial scale, a cheaper, more environmentally friendly synthesis method must be developed.

A novel synthesis method of Ca/Al LDHs, which makes use of a precursor material, has been discovered by Van der Westhuizen (2011) and investigated by Venter (2013) and Van Graan (2012). The precursor method uses calcium oxide and aluminium hydroxide as raw materials, making the novel synthesis method very affordable. The largest cost will, therefore, most likely be attributed to the anion used in the intercalation. Since the synthesis method is novel, an exploratory study was launched into the factors affecting the method.

The purpose of this investigation was to launch an initial study on:

- the optimum reaction time for intercalation,
- the optimum intercalation temperature,
- the pH stability range for intercalated LDHs,
- the effect of anion steric hindrances and functional groups on the ability of the anion to intercalate and
- the effect of anion acid strength and solubility on the stability of the LDH.

The limitations and effectiveness of the novel synthesis method versus traditional synthesis methods can determine whether it is a viable method for the synthesis of organically and inorganically modified LDHs on an industrial scale.

All the experiments were performed on a lab-scale, with a maximum of 100 g of sample being produced at a time. X-ray diffraction analysis was the main analytical method used to characterise the LDH samples.

2. Literature

2.1 Basic structure of layered double hydroxides (LDHs)

Layered double hydroxides (LDHs) are clay materials that have the general formula: $M^{II}_xM^{III}_y(OH)_{2(x+y)}A^{n-}_{y/n}\cdot mH_2O$ (Cavani *et al*, 1991), more commonly written in the short-hand notation: M^{II}/M^{III}-A (Forano *et al*, 2013: 746). LDH materials can be divided into two distinct sections: the layers and the interlayer region (Brown & Gastuche, 1967). The general structure of an LDH is shown in Figure 2-1. The layers of the LDH, represented by $[M^{II}_xM^{III}_y(OH)_{2(x+y)}]^{y+}$, are made up of divalent (M^{II}) and trivalent (M^{III}) metal cations. Due to the trivalent cation substitution in the layers of the clay, the layers tend to have a net positive charge. For this reason, LDHs can incorporate negatively charged anions (A^{n-}) between their layers, through a process called intercalation (Cavani *et al*, 1991). The ability of LDHs materials to take up anions has led to the name 'anionic clays'.

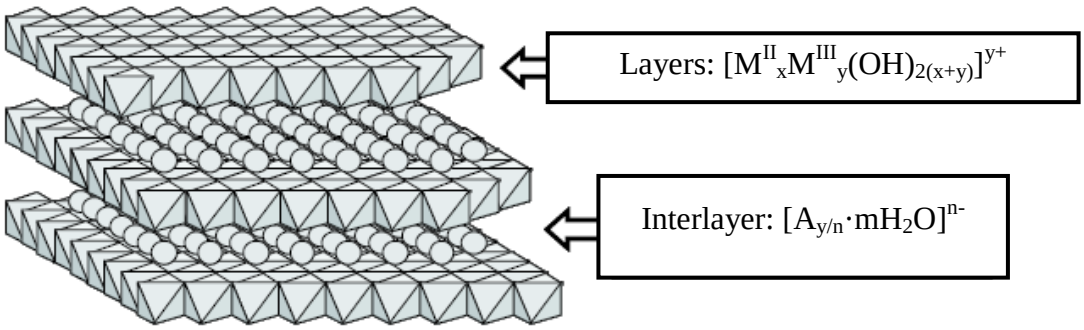

Figure 2-1: General structure of a LDH (Forano *et al*, 2006: 1022)

The first accurate structure of layered double hydroxides was reported by Allmann (1968) and Taylor (1969), while studying Mg/Fe LDHs. They discredited the model put forth by Feitknecht and Gerber (1942), and proved that the Mg and Fe ions surrounded by hydroxide ions make up the layers of the LDH, while water and carbonate make up the interlayer region.

2.1.1 Cationic layers

The most common combinations of divalent and trivalent metal cation in the layer of an LDH are magnesium and aluminium, respectively. Mg/Al LDHs with carbonate in the interlayer

are more commonly referred to as hydrotalcite (Forano *et al*, 2006: 1021). The general formula for hydrotalcite is: $Mg_6Al_2(OH)_{16}CO_3 \cdot 6H_2O$ (Brindley & Kikkawa, 1980). The structure of hydrotalcite is fundamentally derived from brucite, in which magnesium ions are surrounded by hydroxide ions in an octahedral configuration (Reichle, 1986). In hydrotalcite, however, the magnesium in the brucite layers is partially substituted by aluminium ions (Allmann, 1968), giving the layers a net positive charge. Hydrotalcite specifically refers to a Mg/Al-CO_3 LDH. Any LDH with other cation configurations or interlayer anions are, therefore, referred to as hydrotalcite-like materials (Miyata & Kumura, 1973).

The system for the formation of hydrotalcite from a mixture of magnesium and aluminium oxides in the presence of a carbonate source has been described in detail by Roy, Roy and Osborn (1953). The products of this system at various temperatures can be seen in Figure 2-2. Hydrotalcite can only form at temperatures lower than 325 °C and is also a metastable phase.

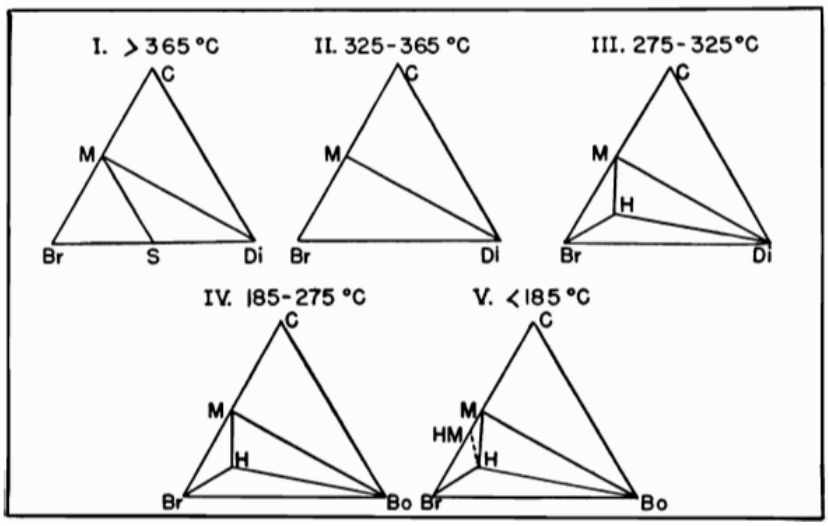

Figure 2-2: Temperature and concentration effects in the MgO-Al_2O_3-CO_3^{2-}-H_2O system. C = CO_2, Di = diaspore, S = spinel, Br = brucite, M = magnesite, H = hydrotalcite, HM = hydromagnesite and Bo = boehmite (Roy *et al*, 1953)

The effect of increasing the aluminium content on the thickness of the LDH layer is shown in Figure 2-3. When there is a small amount of aluminium in the sample, the width of the LDH layer corresponds to that of pure brucite. At a Al/(Mg + Al) ratio of 0.2, which corresponds to a Mg:Al ratio of 4:1, the LDH starts to form. The width of the layer decreases, until a Al/(Mg + Al) ratio of 0.33. This corresponds to a Mg:Al ratio of 2:1. At this ratio, the layers take on the width of a pure $Al(OH)_3$ unit cell. For this reason, the optimum Al/(Mg + Al)

ratio for the formation of an LDH is in the range of: 0.20 – 0.33. Different LDHs have different optimum M^{II}:M^{III} ratios (Sato *et al*, 1988).

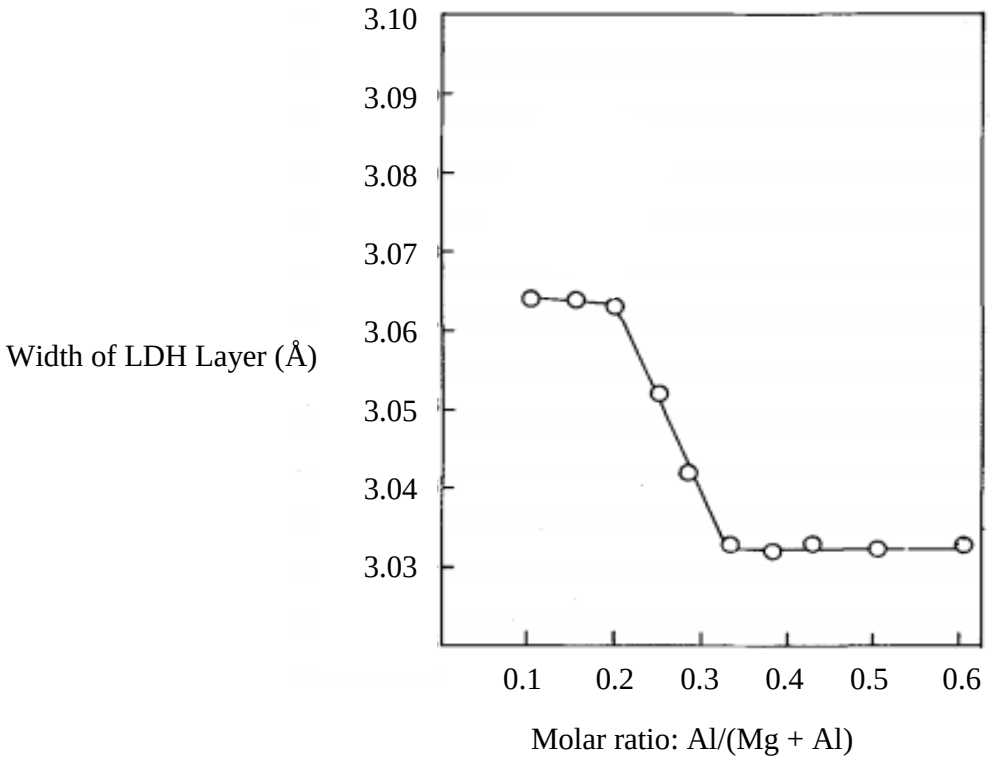

Figure 2-3: Ideal cation ratios for Mg/Al-CO_3 LDH (modified from: Miyata, 1980)

The most common configuration of LDHs is layers consisting of one divalent metal cation and one trivalent metal cation. However, several combinations of multiple divalent and trivalent metal cations have been produced (Auerbach, Carrado & Dutta, 2004: 391). Taylor (1984) also proved that it was possible to combine trivalent with trivalent metal cations, or even trivalent or divalent with tetravalent metal cations. Only one monovalent metal cation has been reported to have formed an LDH successfully, in the form of a Li/Al LDH (Fogg & O'Hare, 1999).

One subgroup of hydrotalcite-like materials is called the hydrocalumite group. The hydrocalumite group contains calcium as the divalent metal cation. The name hydrocalumite was proposed by Tilley, Megaw and Hey (1934), who analysed the hydrated form of calcium aluminate in detail. More specifically, hydrocalumite refers to a clay with the following formulas: $Ca_4Al_2(OH)_{12}Cl_2{\cdot}4H_2O$ (Rousselot *et al*, 2002) or $Ca_4Al_2(OH)_{12}CO_3{\cdot}6H_2O$ (Buttler, Dent Glasser & Taylor, 1959). Roberts (1957) noted that Ca/Al LDHs form more

readily in the presence of a carbonate source; therefore, hydrocalumite will be used to refer to a carbonate-containing Ca/Al LDH. An LDH with any other trivalent metal cation or interlayer anion is referred to as a hydrocalumite-like material (Lopez-Salinas *et al*, 1996). The thickness of a Ca/Al LDH layer can be taken as 2.02 Å (Rousselot *et al*, 2002).

In most LDH materials, the metal cations in the layers are surrounded by six hydroxide ions, in an octahedral configuration. This is not the case, however, for calcium aluminium LDHs, in which the calcium is surrounded by 7 hydroxide ions and the aluminium is still surrounded by 6 hydroxides (Rapin *et al*, 1999).

2.1.2 Anionic interlayer

The geometry of the layers can easily be calculated using X-ray diffraction (XRD) analysis. However, this is not true of the interlayer anion geometry. The anions in the interlayer are less static than the cationic layers, since the anions are constantly changing their hydrogen bonds with the surrounding water molecules (Allmann, 1968).

Many studies have been performed on the relative stabilities of anions in the layers of LDHs (Miyata, 1983). In most cases, carbonate is the most stable anion, which is why it is also the most common anion found between the layers of naturally occurring LDH materials (Auerbach *et al*, 2004: 380). Theoretically, any anion can be incorporated between the layers of an LDH; however, the ease of intercalation varies between anions. Anions with carboxylate functional groups are generally easier to intercalate because of their low dissociation constants (Carlino, 1997).

A large variety of anions have been intercalated using various different methods. For a comprehensive overview of intercalated anions, refer to Auerbach *et al* (2004: 392). More complex anions have been intercalated into a Ca/Al LDH by Meyn, Beneke and Lagaly (1990).

Anions can either be in monolayer, bilayer (Carlino, 1997) or overlapping (Clearfield *et al*, 1991) arrangements, as shown in Figure 2-4. Miyata and Kumura (1973) proved that there is a linear relationship between the interlayer distance and the length of the chain intercalated between the layers. When dicarboxylic acids of different lengths are

intercalated between the layers of a Zn/Al LDH, they have a straight-line relationship, as shown in Figure 2-5.

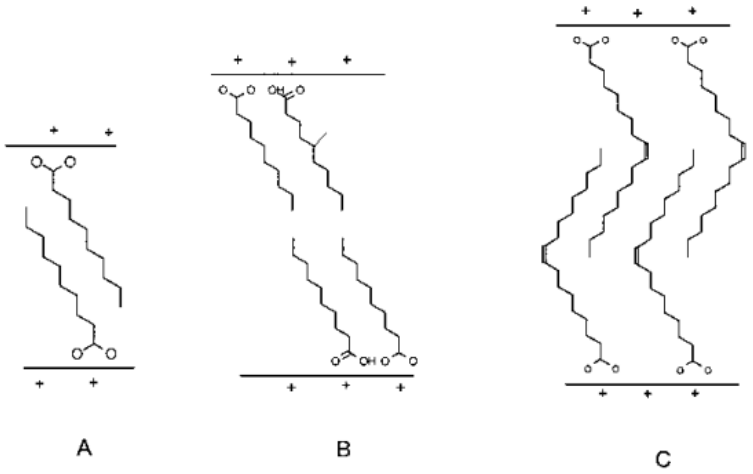

Figure 2-4: Arrangement of interlayer: A. monolayer; B. bilayer and C. overlapping (Auerbach *et al*, 2004: 395)

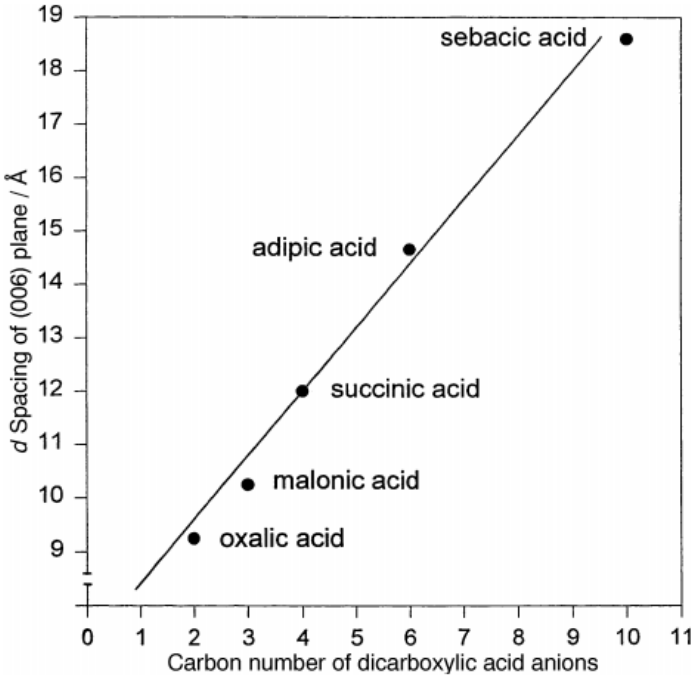

Figure 2-5: Distance between layers vs. length of dicarboxylate group in interlayer of Zn/Al LDH (modified from: Newman & Jones, 1998)

The same anion can also be found at different orientations within the LDH. According to Vucelic, Moggridge and Jones (1995), the angle at which benzoate intercalates decreases

with increasing temperature. This means that at a higher temperature, benzoate will have a flatter orientation in the interlayer, and the interlayer distance will decrease. The different orientations of nitrate in the interlayer are shown in Figure 2-6.

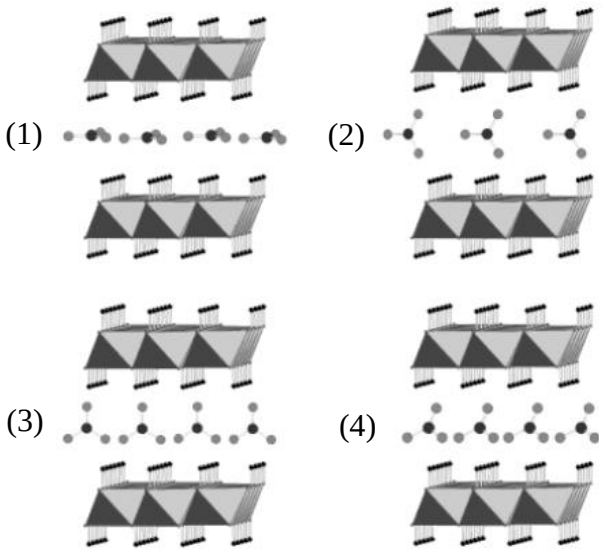

Figure 2-6: Orientation of nitrate ions in the interlayer (modified from: Bontchev *et al*, 2003)

2.1.3 Interlayer water

Weakly held interlayer water is trapped between the layers, along with the interlayer anion. The amount of water varies between LDH materials (Frunza *et al*, 2007); however, the interlayer waters can be eliminated without jeopardising the structure of the LDH (Buttler *et al*, 1959). Layer thickness increases with increasing water content, as seen in Table 2-1.

Table 2-1: Layer thickness of Ca/Al LDH varying with number of crystalline waters in the interlayer (Taylor, 1973)

Composition	Layer thickness (Å)
$Ca_4Al_2(OH)_{12}(OH)_2 \cdot 12H_2O$	10.9
$Ca_4Al_2(OH)_{12}(OH)_2 \cdot 6H_2O$	7.9
$Ca_4Al_2(OH)_{12}(OH)_2 \cdot 4H_2O$	7.4
$Ca_4Al_2(OH)_{12}(OH)_2$	5.8

As seen from Figure 2-7, water is hydrogen bonded to the layers of the LDH. For this reason, water is capable of rotating about an axis perpendicular to the clay layers (Van der Pol *et al*, 1994). Water also has the ability to hydrogen bond with the anion in the interlayer (Kumar, Kalinichev & Kirkpatrick, 2006).

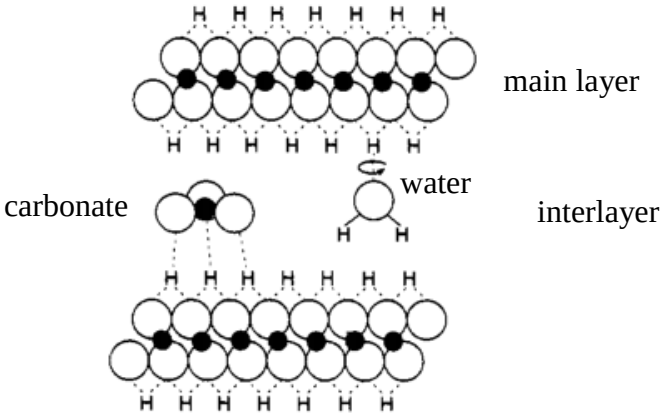

Figure 2-7: Interaction of water molecules and interlayer anion with the layers in an LDH (modified from: Van der Pol *et al*, 1994)

2.2 Crystal Symmetry

2.2.1 Unit Cell Parameters

The unit cells of LDHs describe both the interlayer region and the layers themselves. LDHs tend to have unit cells with two sides of equal length ($a = b$), and a third side, c, of a different length. For this reason, the unit cell of an LDH is described by either hexagonal (2H) or rhombohedral (3R) symmetry (Cavani *et al*, 1991). The general structure of an LDH with 3R symmetry is shown in Figure 2-8. The interlayer space of the LDH is the space occupied by the anion. The layer, on the other hand, is composed of cations surrounded by hydroxide ions. The total height of the layer and the interlayer space corresponds to the d-spacing of the LDH, c'.

The same type of LDH can also be present with different symmetries. For example, $Mg_6Al_2(OH)_{16}CO_3{\cdot}4H_2O$ that has 3R symmetry is referred to as hydrotalcite, while the same LDH with 2H symmetry is known as manasseite (Frondel, 1941).

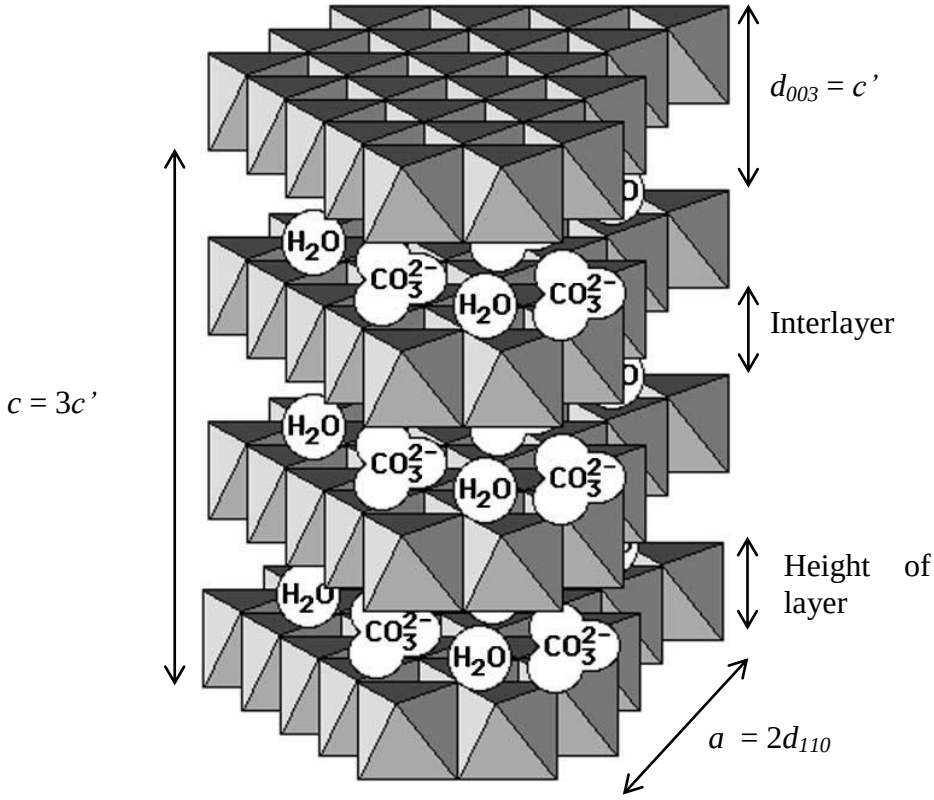

Figure 2-8: LDH structure (adapted from: Rives, 2002)

The earlier research into hydrocalumite produced three different proposed crystalline geometries: hexagonal, rhombohedral and monoclinic. Hydrocalumite can also be present in a mixture of these symmetries (Buttler *et al*, 1959). The first hydrocalumites were identified and characterised with hydroxide in the interlayer and general formula: $4CaO{\cdot}Al_2O_3{\cdot}xH_2O$ (Mylius, 1933; Assarsson, 1931). Tilley *et al* (1934) were the first to characterise a carbonate-intercalated LDH that occurred naturally in cement. Hydrocalumite was found to have monoclinic (pseudo-hexagonal) geometry, with a = 9.9 Å, b = 11.4 Å, c = 16.84 Å and β = 111° (angle between the a and c axes). However, a hexagonal symmetry can also be fit to the structure, with a = 5.74 Å and a layer thickness of 7.92 Å (Buttler *et al*, 1959).

Several different simple anions have been incorporated between the layers of a Ca/Al LDH. Common unit cell parameters for Ca/Al LDHs intercalated with simple anions can be found in Table 2-2.

Table 2-2: Common unit cell parameters for Ca/Al LDHs with different interlayer anions (Feitknecht & Buser, 1951)

Anion	*a* (Å)	*c* (Å)
CO_3^{2-}	5.74*	7.9*
Cl^-	5.74	7.8
Br^-	5.75	8.1
I^-	5.75	8.8
NO_3^-	5.74	8.6
ClO_3^-	5.74	9.2
IO_3^-	5.75	10.3
ClO_4^-	5.75	9.5
MnO_4^-	5.75	9.6
Picrate	5.74	12.7
SO_4^{2-}	5.75	8.9
CrO_4^{2-}	5.75	10.0
WO_4^{2-}	5.75	10.3
$S_2O_3^{2-}$	5.75	10.4
$Fe(CN_6)^{3-}$	5.75	10.8

* Buttler *et al*, 1959

2.2.2 Planes of Symmetry

LDH unit cells contain either a (003) or a (002) plane of symmetry. This implies that the unit cell either incorporates 3 layers or 2 layers of the LDH (Cavani *et al*, 1991). The amount of layers needed to describe the unit cells is determined by the shifting of the layers with respect to one another. Figure 2-9 shows the two structures typically found in LDHs. If the layers are sequenced BC-CA-AB-BC then the LDH must be described by 3 layers. On the other hand, if the layers are sequenced BC-CB-BC then two layers will be sufficient in describing the unit cell (Allmann, 1970). The typical planes present for both rhombohedral and hexagonal crystalline symmetry is shown in Table 2-3 (Cavani *et al*, 1991).

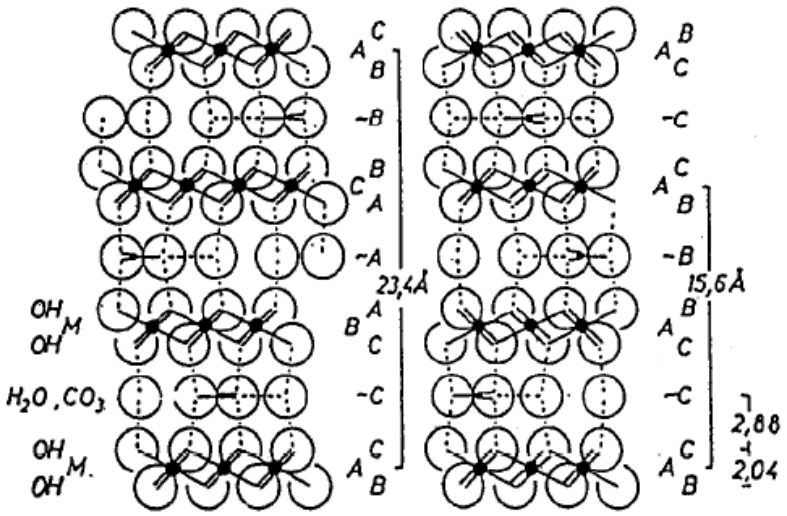

Figure 2-9: Stacking of LDH layers (Cavani *et al*, 1991)

Table 2-3: Planes of symmetry (Cavani *et al.*, 1991)

Symmetry	Planes
Hexagonal (2H)	(002)
	(004)
	(006)
	(102)
	(103)
	(104)
	(105)
	(106)
	(108)
	(110)
	(112)
Rhombohedral (3R)	(003)
	(006)
	(009)
	(012)
	(015)
	(018)
	(110)
	(113)

There are situations in which neither 3R nor 2H symmetry fits perfectly to the LDH XRD pattern. In such situations, the (110) plane separates into two planes, defined by (200) and (110). In this case, orthorhombic coordinates can be used to describe the symmetry of the unit cell. In the case of LDHs, $b \approx a\sqrt{3}$ (Rives, 2002). For imperfect LDHs with orthogonal symmetry, only one layer is described by the unit cell, meaning that a (001) plane represents the primary peak. It is also important to note that the larger the difference in atomic radii between the two cations present in the layers, the less crystalline the sample will be (Taylor, 1984). Therefore, the larger the difference in atomic radii, the higher the chance that neither 3R nor 2H symmetry will be sufficient to describe the unit cell of the LDH, as in the case of Ca/Al LDHs.

2.2.3 Bragg's Law

The exact distance between the layers of the LDH (the interlayer space) can be calculated using Bragg's Law (Equation 1).

$$n\lambda = 2\,d_{hkl}\sin\theta_{hkl} \qquad (1)$$

The order of reflection, n, is an integer and the wavelength of the electrons fired at the lattice is defined by λ. The distance between two planes of symmetry is denoted by d_{hkl}, and the angle of deflection is θ_{hkl}, both of which are shown in Figure 2-10.

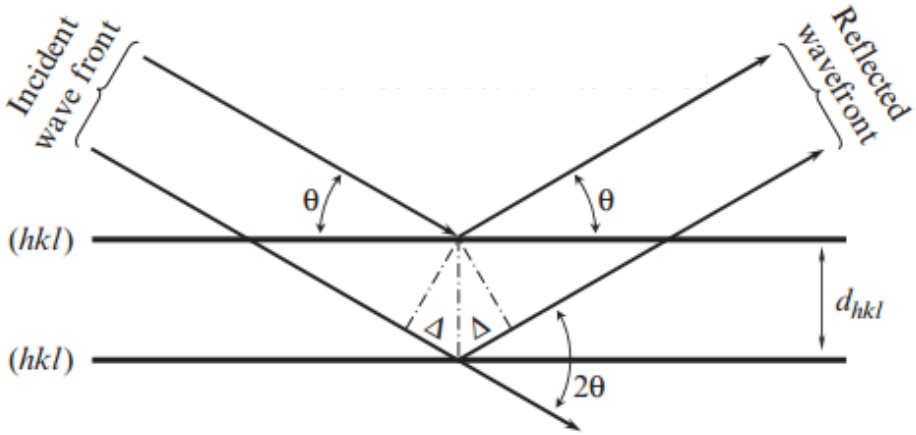

Figure 2-10: X-Ray diffraction and Bragg's law (Pecharsky & Zavalij, 2009: 143)

The parameters *h*, *k* and *l* are integers that describe the plane of symmetry. For the purpose of the experiments, $n = 1$ and the wavelength $\lambda = 1.789$ Å for a cobalt (Co) source (Dinnebier & Billinge, 2008: 4).

2.2.4 Parameter Calculations

The *c* parameter for a rhombohedral LDH unit cell can be calculated using Equation 2 (Forano *et al*, 2013: 763). If the unit cell only incorporates 2 layers, then the d-spacing of the primary peak, d_{002}, is multiplied by 2 to get the *c* parameter. Since a d_{003} primary peak is the more common configuration, it will be used throughout the rest of this section for calculation purposes.

$$c = 3c' = 3d_{003} \tag{2}$$

The crystal planes of symmetry represented by each of the 3 main peaks are shown in Figure 2-11.

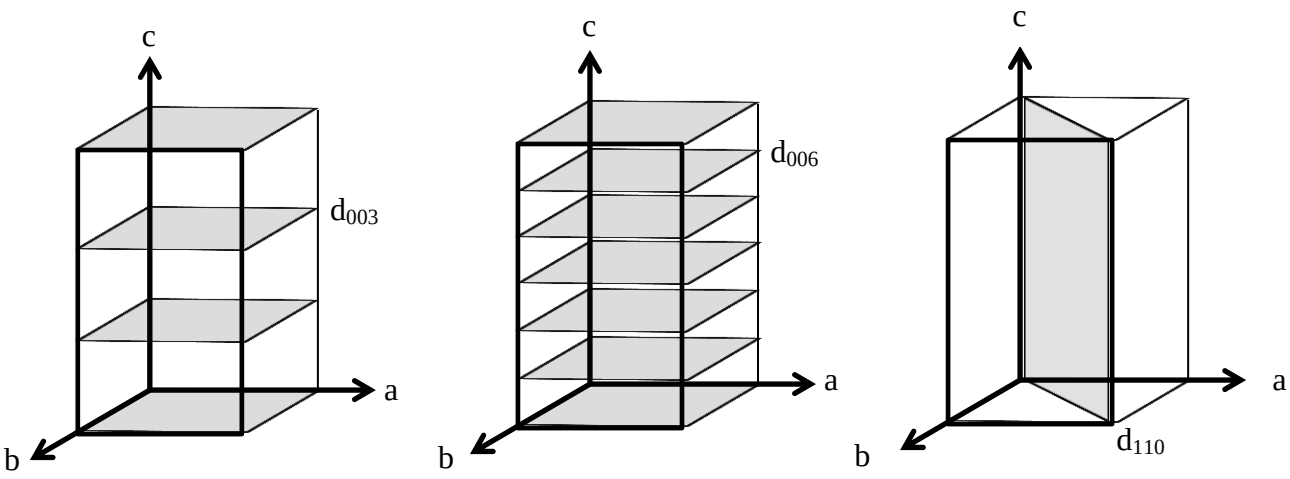

Figure 2-11: Planes of symmetry of rhombohedral LDHs

Similarly, as portrayed in Figure 2-11, the *c* parameter for rhombohedral LDH unit cells can be calculated using:

$$c = 6\, d_{006} \quad (3)$$

Combing Equations 2 and 3 gives:

$$d_{003} = 2\, d_{006} \quad (4)$$

In order to calculate the d-spacing of the LDH, in other words, the total height of the layer and the interlayer space, Equation 5 can be used, which is taken from Bragg's law (Equation 1). The d-spacing of an LDH corresponds to the spacing of the *003* plane.

$$d_{003} = n\lambda / (2 \sin\theta_{003}) \quad (5)$$

Parameter *a* can be calculated using the (110) peak according to Equation 6 (Goh, Lim & Dong, 2008). This equation can be applied to both 3R and 2H symmetries.

$$a = 2\, d_{110} \quad (6)$$

A (009) peak can also be present in the XRD pattern for 3R symmetries. The (009) peak can be used to calculate the *c* parameter and the d-spacing of the LDH. The peaks are related in that $d_{003} = 2d_{006} = 3d_{009}$. A more accurate *c* parameter can also be calculated using the average d-spacing represented by these 3 peaks, according to Equation 7 (Li, Hou & Zhu, 2007).

$$c = 1/3\,(d_{003} + 2d_{006} + 3d_{009}) \quad (7)$$

2.2.5 Crystalline Symmetry

Frondel (1941) was the first to distinguish between two types of Mg/Al-CO_3 LDHs: hydrotalcite and mannesite. These two LDHs have identical chemical formulas; however, they differ in structure. The common parameters of both symmetries of hydrotalcite are laid out in Table 2-4. A rhombohedral crystalline symmetry usually corresponds to a space group of $R\bar{3}m$, while a space group of P6/mmc is normally associated with hexagonal symmetry.

Table 2-4: Properties of manasseite and hydrotalcite (Frondel, 1941)

	Manasseite	Hydrotalcite
Space Group	P6/mmc	$R\bar{3}m$
a (Å)	3.060	3.065
c (Å)	15.34	23.08

2.3 Structural analysis techniques

2.3.1 X-ray diffraction (XRD) analysis

The general XRD peak pattern for an LDH is shown in Figure 2-12. The primary peak (the most intense peak) for LDHs is usually the first peak on the XRD pattern. From the primary peak and the (110) peak, which usually occurs between 71° and 77° for a cobalt source, the main parameters of the LDH can be calculated (Rives, 2002).

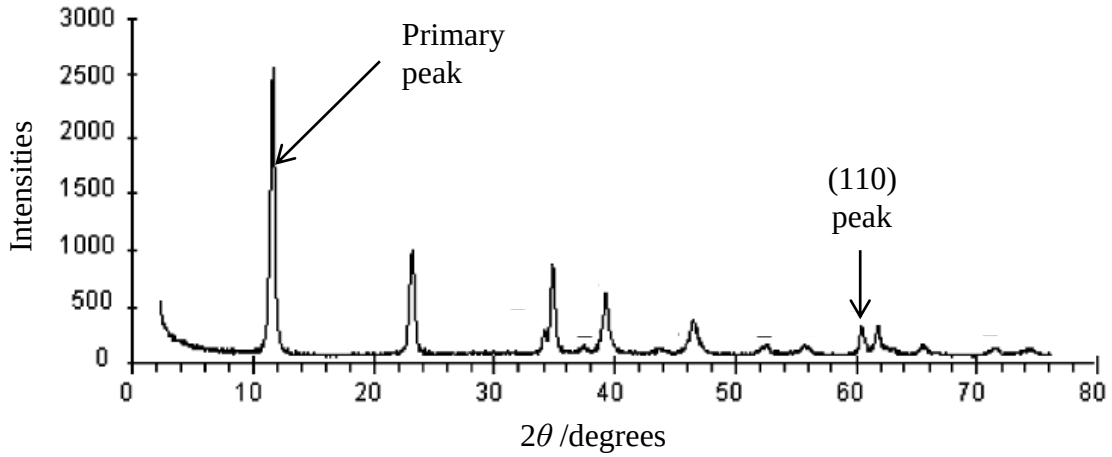

Figure 2-12: XRD pattern for a Mg/Al-CO_3 LDH using a Cu-Kα source (modified from: Forano *et al.*, 2006: 1039)

The XRD pattern with relevant peaks for a rhombohedral (3R) LDH is shown in Figure 2-13. The primary peak of the LDH is the first peak, which is representative of the (003) plane for rhombohedral LDHs. If the LDH has hexagonal symmetry, the primary peak represents the (002) plane. Not all peaks in Figure 2-13 are present for all the LDHs; however, the relative peak intensities must be approximately the same. Furthermore, extra planes can be present in

the XRD pattern if crystalline imperfections are present in the sample (Giacovazzo *et al*, 2002: 229).

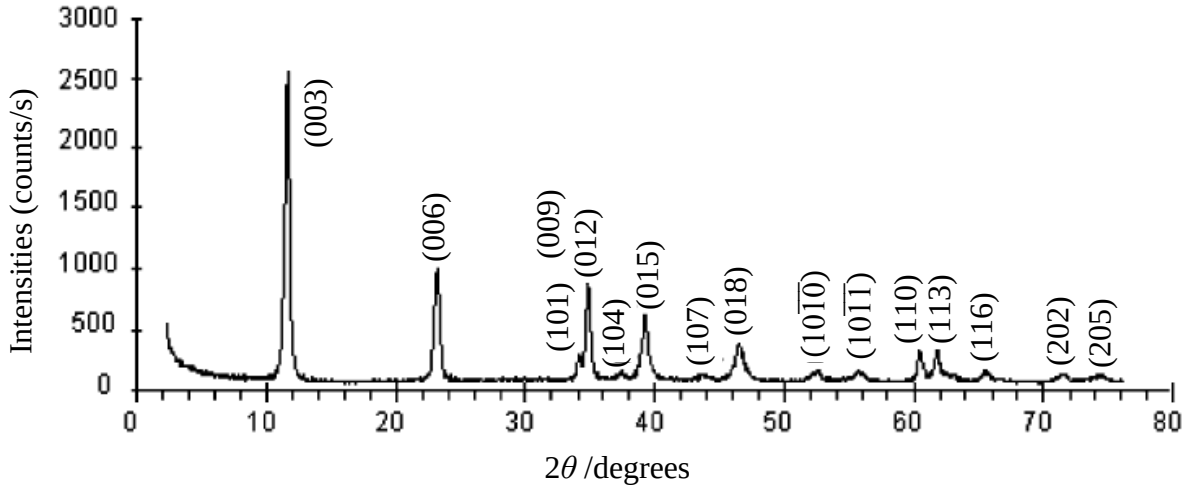

Figure 2-13: XRD for rhombohedral LDH symmetry (Forano *et al*, 2006: 1039)

There are two situations in which the primary peak of the LDH shifts: through intercalation of another anion in the interlayer space or through substitution of the cations in the layers. If the layer composition remains the same, any change in d-spacing will be related to a change in interlayer spacing. If the d-spacing increases, the primary LDH peak will shift to the left. Similarly, a decrease in d-spacing is represented by a shift to the right of the primary peak on the XRD pattern. The *a* parameter of the LDH, however, will remain the same, provided that the same cations in the same ratio are present in the layer (Cavani *et al*, 1991). Bigger anions in the layer will cause the height of the layer to increase, which is accompanied by a shift to the left of the primary peak. Even a change in the ratio of layer anions can change the height of the layer (Cantrell *et al*, 2005).

When anions intercalate between the layers of an LDH, water is pulled into the interlayer space, mainly due to hydrogen bonding between the water and the anion. The amount of water and orientation of the water molecules will also have an effect on the d-spacing of the LDH (Frunza *et al*, 2007).

2.3.2 Thermal gravimetric analysis (TGA)

Miyata (1980) found that upon calcining hydrotalcite at 300 °C for 2 h, there was still hydrotalcite present. However, at temperatures between 400 °C and 800 °C, MgO was detected, with slight aluminium substitution. At 900 °C MgO, $MgAl_2O_4$ and traces of γ-Al_2O_3 were present. Pure MgO is the only phase present at 1 000 °C.

A typical TGA curve for hydrotalcite is shown in Figure 2-14. Normally, there are two distinct weight loss regions in a TGA curve for LDHs. The first represents the loss of water, which occurs up to a temperature of 225 °C (Vaysse *et al*, 2002). The second can be attributed to loss of CO_2 and dehydroxylation (Sato *et al*, 1988). The same is true for a Ca/Al LDH with simple intercalated anions (Xu *et al*, 2009). There are two different types of water present in LDHs: intrinsic and extrinsic water. Extrinsic water (lose and surface-bound water) is released at temperatures up to 110 °C. Intrinsic water (interlayer water) is released from 110 °C up to 250 °C (Yun & Pinnavaia, 1995).

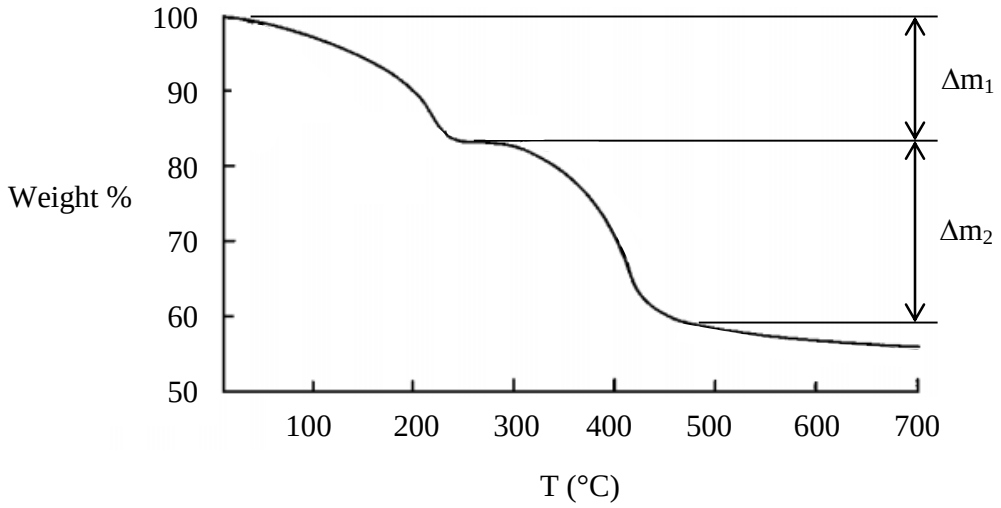

Figure 2-14: TGA curve for Mg/Al-CO_3 LDH (modified from: Stanimirova *et al*, 1999)

From the TGA curve, the amount of interlayer water and interlayer anion can be calculated. The first bulk of mass loss (Δm_1) can directly be associated with the amount of interlayer waters present in the LDH. The second mass loss (Δm_2) is attributed to the following reaction:

$$Ca_4Al_2(OH)_{12}A_{2/n} \rightarrow Ca_4Al_2O_6 + 2/nA^{n-} + 6H_2O \quad (8)$$

The reaction can then be used to calculate the amount of anion in the interlayer of the original LDH. In some cases, like with Co/Al-CO_3 LDH, there is only one bulk mass loss, meaning that interlayer water loss, anion loss and dehydroxylation occur simultaneously (Sato *et al*, 1988). The range at which the mass losses occur varies drastically, depending on the cations present in the layer and the anions present in the interlayer (Vaccari, 1998).

The typical dehydration curve for $4CaO{\cdot}Al_2O_3{\cdot}13H_2O$ LDH is shown in Figure 2-15. As can be seen from the figure, Ca/Al-OH LDH starts losing the interlayer water at a temperature of 50 °C. Another dramatic drop in the amount of interlayer waters occurs at a temperature of roughly 100 °C. At a temperature of 300 °C, most or all of the interlayer water has been evaporated from the LDH (Buttler *et al*, 1959).

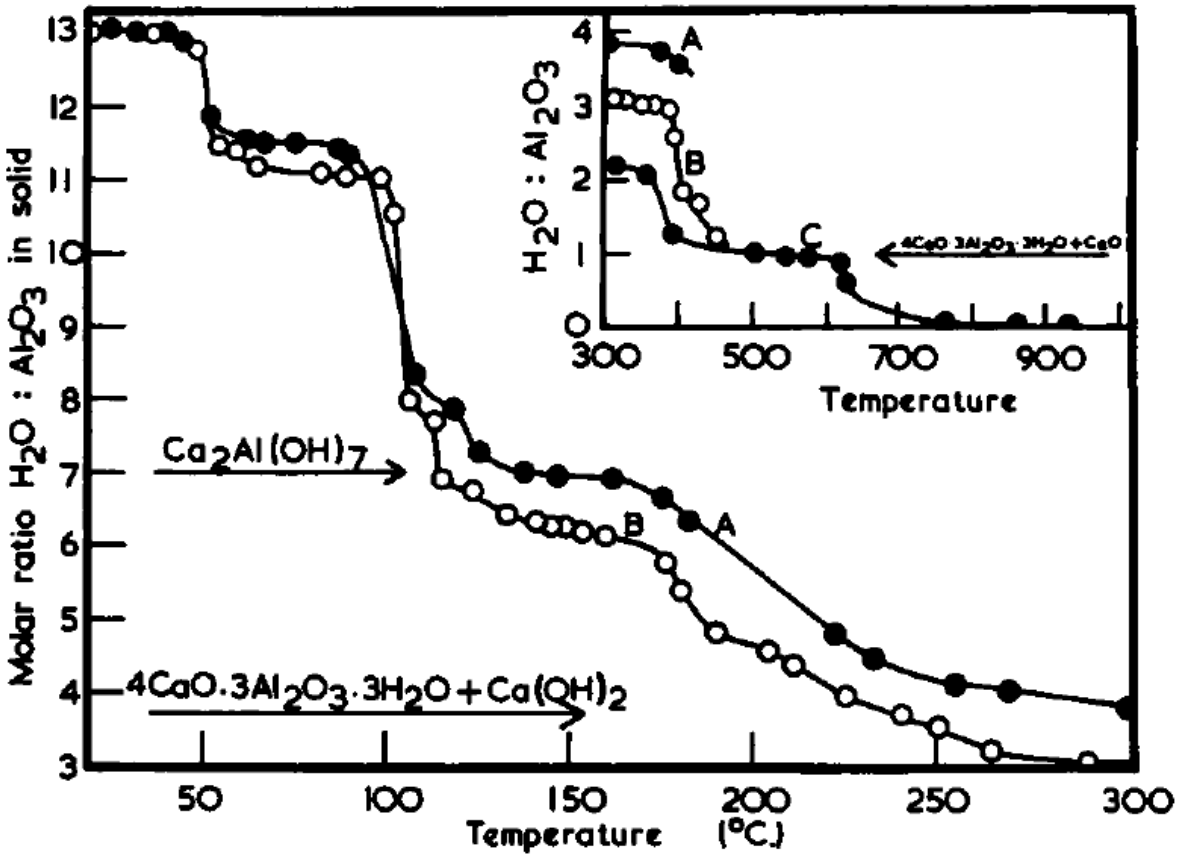

Figure 2-15: Dehydration curve of $4CaO{\cdot}Al_2O_3{\cdot}13H_2O$, where A, B and C are different calcination methods (Buttler *et al*, 1959)

2.3.3 Scanning electron microscopy (SEM)

The same crystalline symmetry can render different 3-dimentional macro structures for different LDH materials. Figure 2-16 shows 4 different macro structures for LDH materials that have hexagonal symmetry (Okamoto, Iyi & Sasaki, 2007). Fibrous hydrotalcites have also been produced. These are hydrotalcite materials with hexagonal symmetry and long, needle-like macro structure (Miyata & Okada, 1982).

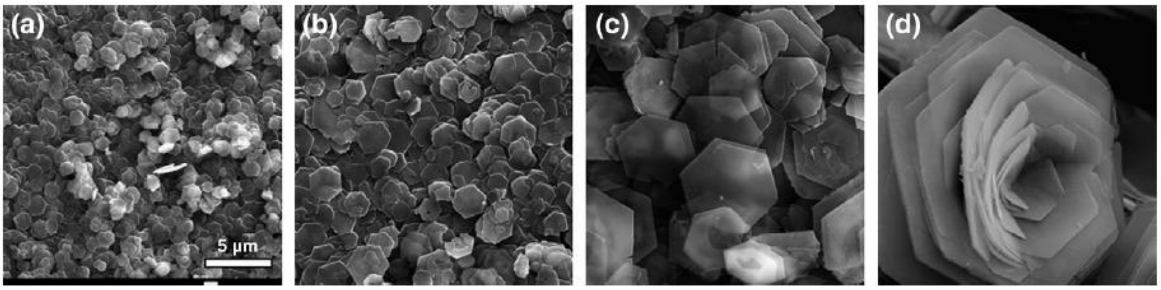

Figure 2-16: Macro 3D structures of hexagonal LDHs (Okamoto *et al*, 2007)

2.3.4 Fourier transform infrared spectroscopy (FTIR)

Infrared spectroscopy (IR) is a useful analytical technique that can indicate the type of bonds present in a sample. For this reason, it can give an indication to the general chemical structure of a given sample and has frequently been used when analysing clay materials (Madejova, 2003). The typical bands found in the FTIR pattern of the precursor material are listed in Table 2-5 and other bands found in a Ca/Al-CO_3 LDH are listed in Table 2-6.

Table 2-5: Precursor FTIR bands

Wavenumber (cm^{-1})	Component	Reference
700 - 950 1 100 3 650 3 200 – 3 750	Synthetic katoite	Passaglia & Rinaldi, 1984
3 646 3 487	Superficial OH bond associated with $Ca(OH)_2$	Campos-Molina *et al*, 2010

Table 2-6: Potential bands present in LDH FTIR patterns

Wavenumber (cm^{-1})	Type of bond	Reference
430	O – M – O	Aisawa *et al*, 2002
550 590 840	M – O bonds	Aisawa *et al*, 2002
670 – 690 715 – 760	Mono-substituted benzene	Nicolet, *sa*
700 – 715 770 – 795	1:3-substituted benzene	Nicolet, *sa*
740 – 760	1:2-substituted benzene	Nicolet, *sa*
790 – 820 1 340 – 1 380	Nitrate	Nicolet, *sa*
3 000 1 620	Interlayer waters	Campos-Molina *et al*, 2010
1 400 2 850 2 925	C – H stretching and vibrations	Aisawa *et al*, 2002
1 360 3 000	Carbonate in interlayer	Dudek *et al*, 2012
800 – 835	1:4-substituted benzene	Nicolet, *sa*
920 – 970 1 400 – 1 440 1 650 – 1 700	COOH	Nicolet, *sa*
1 030 – 1 100	C – O bond (alcohols)	Nicolet, *sa*
1 480 – 1 525 1 610 – 1 620	Benzene ring	Nicolet, *sa*
1 560 – 1610	COO^-	Nicolet, *sa*
2550 – 3 200	Bonded O – H from carboxylic acid	Nicolet, *sa*
3 000 – 3 200	Aromatic C – H	Nicolet, *sa*
3 250 – 3 600	Bonded O – H	Nicolet, *sa*
3 500 – 3 700	Free O – H	Nicolet, *sa*

2.4 LDH synthesis and modification methods

There are various different methods of synthesising LDH materials, most of which are summarised by Forano *et al* (2013: 752 - 759). These methods have been proved efficient, yet costly. Since the focus of this investigation was calcium aluminium LDH with a 2:1 ratio, the example reactions for each synthesis method were chosen as the formation of a 2:1 Ca:Al LDH with an anion (A^{n-}) intercalated between the layers. Carlino (1997) gives a detailed comparison of the different synthesis methods.

2.4.1 Co-precipitation method

In the co-precipitation method, salts of the divalent and trivalent metal cations are mixed with a solution of the interlayer anion (Miyata & Kumura, 1973). Sodium hydroxide must be added to the solution, in order to encourage the formation of the clay layers (Feitknecht & Gerber, 1942). Co-precipitation is usually carried out at a pH between 7 and 10 (Vaccari, 1998). The most effective co-precipitation method was one in which the pH was held constant (Rousselot *et al*, 2002).

The salts of the divalent and trivalent metal cations are usually nitrate or chloride salts (Miyata, 1975). The chloride or nitrate anion associates with the sodium from the sodium hydroxide, while the hydroxide ions are free to form the clay layers. This mixture is then left to react at temperatures ranging from room temperature (Hwang, Han & Choy, 2001) to well above the boiling point of water (Zhang *et al*, 2008). However, Williams and O'Hare (2006) recommend temperatures above room temperature for LDH syntheses. The temperature range is usually between 60 °C and 80 °C (Vaccari, 1998). A co-precipitation reaction using nitrate salts for the formation of a calcium aluminium LDH is as follows:

$$4Ca(NO_3)_2 + 2Al(NO_3)_3 + 2/n\ A^{n-} + 12NaOH + xH_2O \rightarrow Ca_4Al_2(OH)_{12}A_{2/n}\cdot xH_2O + 14NaNO_3 \quad (9)$$

Even though the co-precipitation method is one of the oldest and most effective LDH synthesis methods, it has the main disadvantage of producing excess salt effluents (Othman *et al*, 2009).

2.4.2 Reconstruction/rehydration method

Carbonate is one of the most readily intercalated anions in LDHs, due to its stability in the interlayer. Carbonate-intercalated LDHs release carbon dioxide and water when heated, which leaves a mixture of divalent and trivalent metal oxides. The process of heating the LDH and reducing it to its mixed metal oxides is referred to as calcination. (Miyata, 1980) Increase in calcination temperature has been linked to an increase in crystal size (Clause *et al*, 1991; Miyata, 1980), as seen in Figure 2-17.

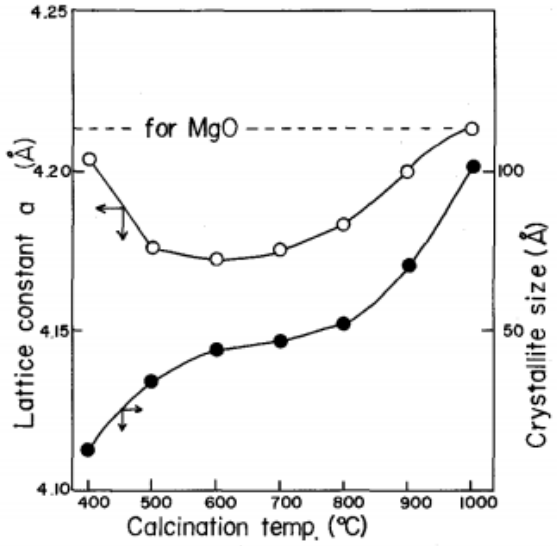

Figure 2-17: Crystallite size (●) and lattice constant *a* (○) vs. temperature for hydrotalcite calcined for 1 h (Miyata, 1980)

The reconstruction method relies on the "memory effect" of LDH materials. More specifically, it relies on the ability of the mixed metal oxides to reform LDH layers once rehydrated in water (Miyata, 1980). Once rehydrated, the LDH layers can incorporate anions between the layers that were not necessarily present before the calcination process (Vieille *et al*, 2003). In general:

$$Ca_4Al_2(OH)_{12}CO_3 \cdot xH_2O \rightarrow Ca_4Al_2O_6 + CO_2 + (6+x)H_2O \quad (10)$$

$$Ca_4Al_2O_6 + 2/nA^{n-} + (6+x)H_2O \rightarrow Ca_4Al_2(OH)_{12}A_{2/n} \cdot xH_2O \quad (11)$$

Heating above 800 °C jeopardises the integrity of the LDH (Miyata, 1980). According to Shumaker *et al* (2008), the optimum temperature of calcination is between 450 °C and 500 °C. The structure of the LDH at various temperatures is shown in Figure 2-18.

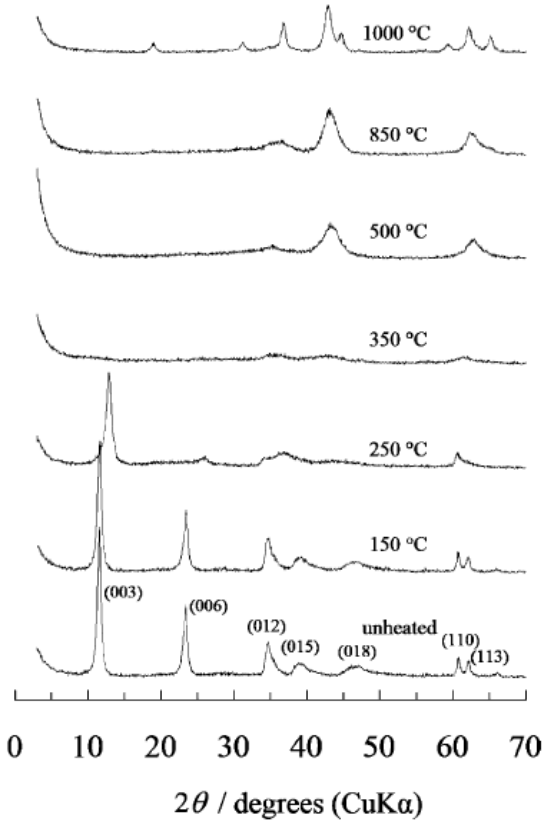

Figure 2-18: Structure of hydrotalcite at various temperatures (Forano *et al*, 2006: 1051)

The major economic issue to address when using the reconstruction method is the energy expended to calcine the LDH material. The added energy cost makes the reconstruction method one of the least economically viable synthesis methods.

2.4.3 Anion exchange method

As with the reconstruction method, the anion exchange method requires a pre-synthesised LDH as a starting material. Unlike the reconstruction method, however, the anion exchange method requires a lightly held anion in the interlayer of the precursor LDH, instead of the usual carbonate (Forano *et al*, 2013: 758). The concept of the anion exchange method is to mix an existing LDH with a solution/mixture of an anion that is more stable in the LDH

interlayer. The more stable anion (A^{IIm-}) will then replace the weakly held anion (A^{In-}) in the interlayer (Sato, Wakabayashi & Shimada, 1986; Guo & Tian, 2013), through the following reaction:

$$Ca_4Al_2(OH)_{12}A^{I}_{2/n}\cdot xH_2O + 2/m\ A^{IIm-} \rightarrow Ca_4Al_2(OH)_{12}A^{II}_{2/m}\cdot xH_2O + 2/n\ A^{In-} \quad (12)$$

Miyata (1983) found that the strength of simple anions in the interlayer of a Mg/Al LDH increased in the following order:

Monovalent anions: $I^- < NO_3^- < Br^- < Cl^- < F^- < OH^-$
Divalent anions: $SO_4^{2-} < NYS^{2-} < CO_3^{2-}$

It was also concluded that divalent anions are more stable in the interlayer than monovalent anions (Miyata, 1983).

There are several problems that arise from the anion exchange method. As seen with the co-precipitation method, the reaction produces an effluent in the form of a salt of the weakly held anion that was replaced.

2.4.4 Green synthesis methods

Several green synthesis methods of hydrocalumite have been proposed (Sánchez-Cantú *et al*, 2013; Zhang *et al*, 2015). One of the more common green synthesis methods is the hydrothermal method. The hydrothermal method involves the mixture of reagents at elevated temperatures and pressures, without the production of effluent (Reichle, 1986). Roy *et al* (1953) investigated the ideal pressure and temperature to form hydrotalcite using the hydrothermal method. Sauerwein *et al* (2011) and (Wen *et al*, 2015) proposed the following reaction to form a Ca/Al-CO_3 LDH:

$$4Ca(OH)_2 + 2Al(OH)_3 + CO_3^{2--} + xH_2O \rightarrow Ca_4Al_2(OH)_{12}CO_3\cdot xH_2O \quad (13)$$

The calcium hydroxide can be replaced with calcium oxide, and the carbonate is derived from multiple carbonate sources. The carbonate can also be partially substituted with perchlorate and triflate (Sauerwein *et al*, 2011).

2.5 Titration

Titration is the act of adding an acid to a base (or vice versa), while studying the pH of the solution. Usually, titrations are performed on a volume basis, with a known concentration of acid/base being added to a solution. Since an acid-base reaction is occurring, there will usually be a point where the pH buffers. This buffering effect is when the acid is being neutralised by the base to form water and a salt.

A top down titration is when a basic medium is titrated with an acid, while a bottom up titration is when an acidic medium is titrated with a base. Titrations of clays have already been performed to some extent. For example, the bottom-up titration of an LDH is shown in Figure 2-19. Sodium hydroxide was added to a solution of magnesium chloride and aluminium chloride in the titration.

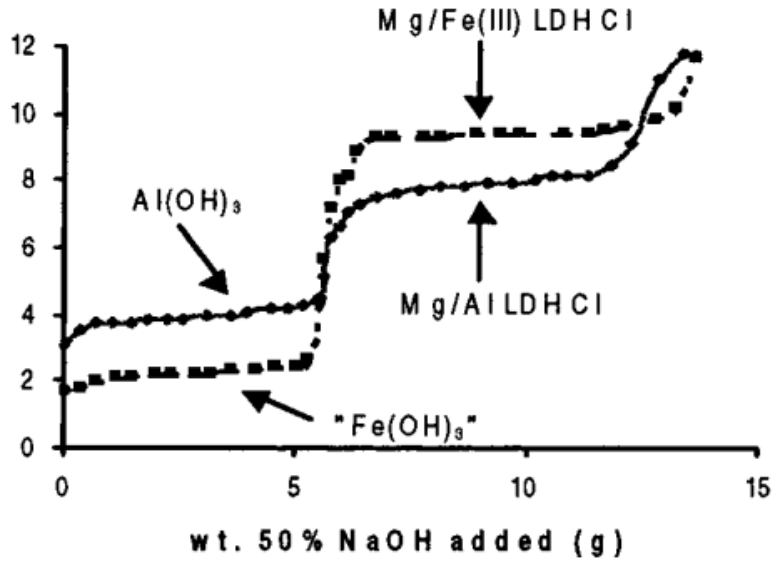

Figure 2-19: Bottom-up titration of Mg-Fe and Mg-Al LDH (Boclair & Braterman, 1999)

For clays, the plateaus generally indicate either the intercalation of the acid anion into the clay, or the disintegration of the clay itself (with the acid being neutralised by the hydroxide ions in the layers of the clay). Generally, titrations with LDHs exhibit one or two plateaus. LDHs usually exhibit 2 plateaus, as displayed in Figure 2-19 (Auerbach *et al*, 2004: 379).

2.6 Factors affecting intercalation

There are several factors that affect the formation of LDHs and their morphology. These factors include (Othman *et al*, 2009):

- Reaction time
- Temperature
- pH
- Nature of solution and anion

LDH materials can form at room temperature. There is, however, a limit to the temperature at which an LDH will form. According to Roy *et al* (1953), hydrotalcite will not form at temperatures above 325 °C. However, in order to ensure that the brucite sheets are not compromised at all, the temperature must be kept below 200 °C (Lombardo *et al*, 2008). Calcination temperature also affects the ability of the calcined material to absorb anions from solution: the optimum temperature being between 400 °C and 500 °C (Mandal & Mayadevi, 2008).

The stacking of the layers depends on temperature. For the formation of Mg/Fe LDHs, Allmann (1968) proved that lower temperatures favour rhombohedral symmetry, while higher temperatures favour hexagonal symmetry. However, decreasing the temperature will not change a hexagonal symmetry LDH into a rhombohedral symmetry.

According to Mandal and Mayadevi (2008), most fluoride ions are absorbed by a Zn/Al LDH in the first 5 min of contact. This implies that calcined LDH reactions with simple anions are quite rapid.

The exact effect of pH on the intercalation of LDHs is not known. The pH must, however, be above the point where the hydroxide layers of the LDH disintegrate. In many cases, experiments have adjusted the pH of the clays to above a pH of 10, in order to ensure that the clay layers do not disintegrate (Aisawa *et al*, 2007). However, there has been evidence in the past that LDH material can form at a pH of as low as 6.9 (Taylor, 1984). Mandal and Mayadevi (2008) proved an optimum pH for the intercalation of fluoride into a Zn/Al LDH using the reconstruction method (Figure 2-20).

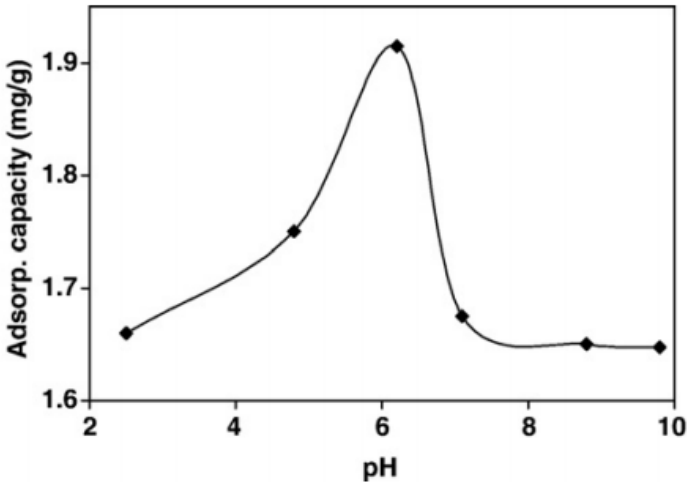

Figure 2-20: Intercalation of fluoride into a Zn/Al LDH (Mandal & Mayadevi, 2008)

Another reason why pH plays a major role in the intercalation of anions is due to the fact that acids dissociate from the H^+ ion at a higher pH. Figure 2-21 shows that at very high pH values, salicylic acid can be assumed to be divalent, since both the H^+ ions from the carboxyl and hydroxyl group have dissociated into the solution.

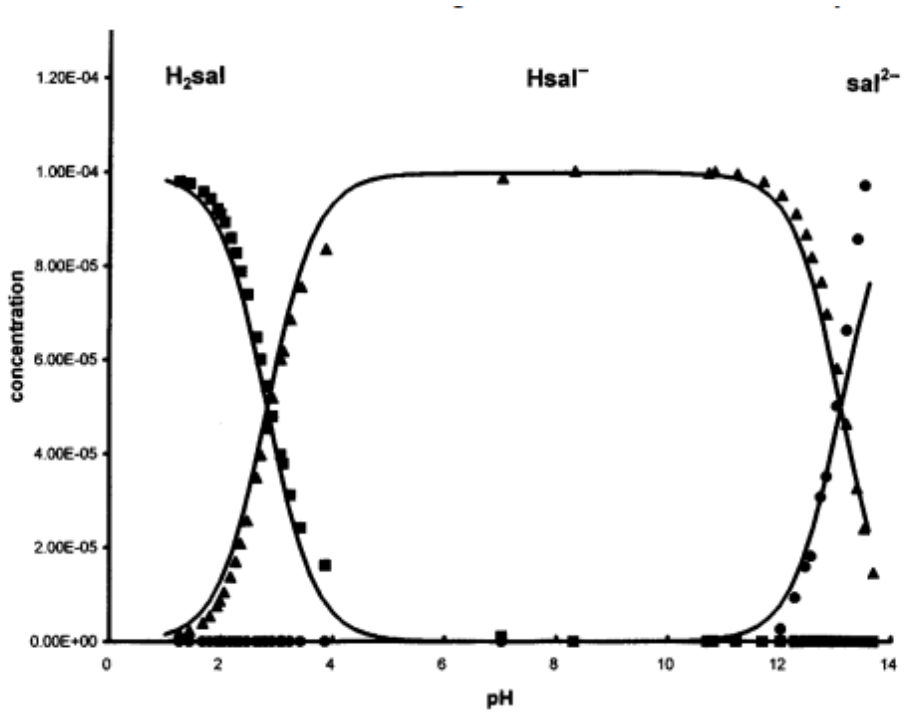

Figure 2-21: Salicylic acid dissociation in water, where ■ = [H_2sal], ▲ = [Hsal$^-$] and ● = [sal^{2-}] (Tauler, Marques & Casassas, 1998)

However, at pH values of below 13, salicylic acid is monovalent, with only the H^+ ion from the carboxyl group having dissociated. Below a pH value of 3, salicylic acid has no charge. For this reason, below a pH value of 3, there will be little to no driving force for salicylic acid to intercalate into the anionic clay.

Finally, the solubility of the anion in water plays a vital role in whether the anion will intercalate. The solubility of the metals also determines whether the layers form (Scheckel *et al*, 2000).

3. Experimental

3.1 Planning

3.1.1 Precursor method

Expensive heating steps and the production of effluent in the traditional synthesis methods add to the cost of production of LDHs. Sauerwein *et al* (2011) have addressed these issues by patenting the reaction of calcium oxide/hydroxide with aluminium hydroxide in water with a carbonate source. The temperatures tested in the patent are between 25 °C and 180 °C. The patent specifies that carbonate can be intercalated between the layers of a Ca/Al LDH with partial substitution of perchlorate and/or triflate. However, in theory, this synthesis method should be applicable to any type of anion, as shown in Equation 14.

$$4CaO + 2Al(OH)_3 + 2/nA^{n-} + yH_2O \rightarrow Ca_4Al_2(OH)_{12}A_{2/n}\cdot xH_2O \quad (14)$$

Van der Westhuizen (2011) noted that the formation of intercalated hydrocalumite from a mixture of CaO and $Al(OH)_3$ can also be separated into two distinct steps and/or reactions, as seen in Figure 3-1. The two steps of the reaction synthesis are:

$$4CaO + 2Al(OH)_3 + 8H_2O \rightarrow Ca_3Al_2(OH)_{12} + Ca(OH)_2 \quad (15)$$

$$Ca_3Al_2(OH)_{12} + Ca(OH)_2 + 2/nA^{n-} + xH_2O \rightarrow Ca_4Al_2(OH)_{12}A_{2/n}\cdot xH_2O \quad (16)$$

The first step (Equation 15) is the synthesis of the precursor material. The precursor is a mixture of katoite [$Ca_3Al_2(OH)_{12}$] and portlandite [$Ca(OH)_2$] in the correct stoichiometric ratio to form an intercalated Ca/Al LDH with a Ca:Al ratio of 2:1. In the second step of the novel synthesis method (Equation 16), the katoite/portlandite precursor is mixed with an anion in the correct stoichiometric ratio to form hydrocalumite or an intercalated hydrocalumite. In both steps of the reaction, water is in excess. The amount of water added must be just enough to wet the final product. The water concentration is generally taken as 0.1 g_{solids}/g_{water}. (Van der Westhuizen, 2011)

In all the prior investigations, an extra mole of calcium was added in the first reaction to form a precursor material that contained both katoite and portlandite. It is, however, possible to add the extra mole of calcium to pure katoite in the second step of the reaction. In this case, the first reaction is only performed with 3 mol of CaO, instead of 4 mol of CaO, according to:

$$3CaO + 2Al(OH)_3 + 3H_2O \rightarrow Ca_3Al_2(OH)_{12} \quad (17)$$

$$Ca_3Al_2(OH)_{12} + CaO + 2/nA^{n-} + (2+x)H_2O \rightarrow Ca_4Al_2(OH)_{12}A_{2/n}\cdot xH_2O \quad (18)$$

All three reaction pathways from CaO and $Al(OH)_3$ to hydrocalumite and modified hydrocalumite are shown in Figure 3-1. Only the two-step reaction mechanisms were addressed in the investigation; however, a direct synthesis is also possible.

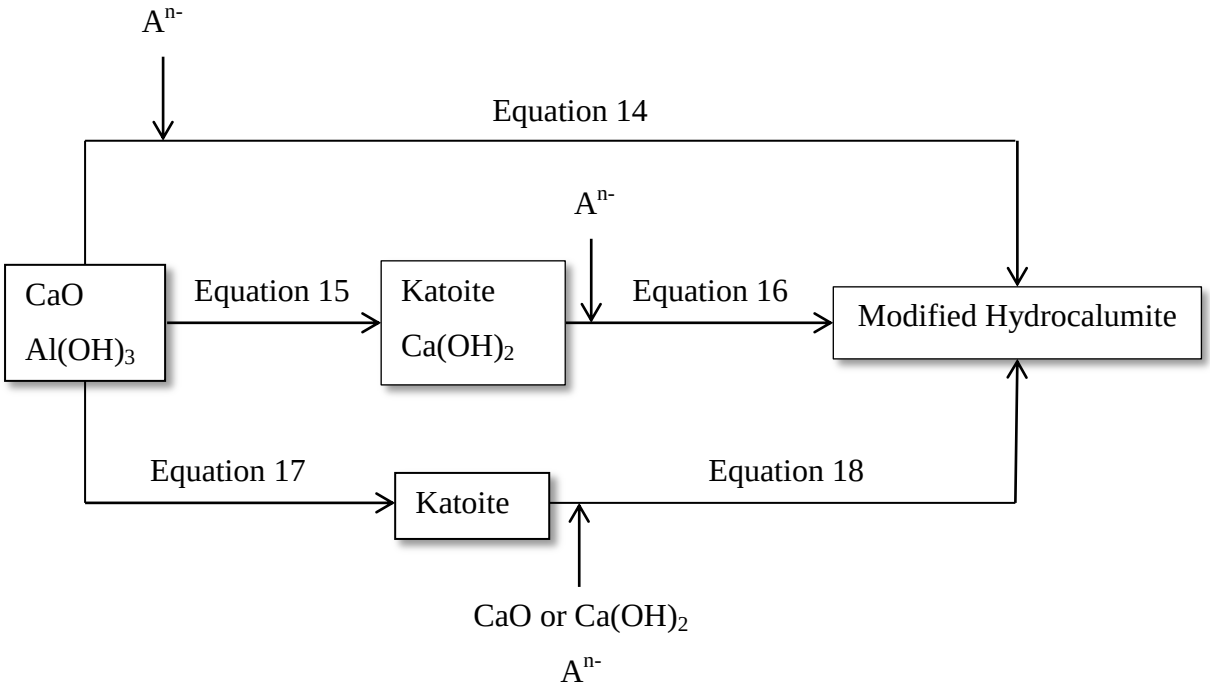

Figure 3-1: Reaction pathways from CaO and $Al(OH)_3$ to hydrocalumite and modified hydrocalumite

3.1.2 Experimental Scope

The emphasis of the investigation was placed on gathering a broad range of information on the optimum synthesis conditions, rather than on a detailed exploration of specific conditions. For this reason, more time was spent on exploring different reaction conditions, rather than

on repeats of experimental runs. This allows a general understanding of the optimum reaction conditions for future detailed experiments. All raw materials used for the experiments were reagent grade (≥95 wt.%).

In order to test the effects that the initial aging has on the reactivity of $Ca(OH)_2$ in the second step of the precursor reaction, pure katoite was synthesised. The katoite was then mixed with either CaO or pure $Ca(OH)_2$ (supplied by ACE Chemicals) and an anion. An intercalated Ca/Al LDH was synthesised using benzoic acid (Merck) and hydrochloric acid (Merck) as anions. These anions were selected because of their simple structure.

For the same reason, benzoic acid and hydrochloric acid were selected as the two anions used in the time and temperature experiments. For these experiments, a mixture of the precursor in the presence of one of the two anions was left to react for 2 h, 6 h, 12 h and 24 h, at ambient temperatures and temperatures of 40 °C, 50 °C, 60 °C and 80 °C.

Non-carbonate anions have traditionally been synthesised in an inert environment that is sealed from air (Clearfield *et al*, 1991; Cavani *et al*, 1991; Cota *et al*, 2010). This is due to the fact that carbon dioxide from the air intercalates between the layers of an LDH in the form of carbonate and is almost impossible to remove from the interlayer without the use of expensive heating steps. Running experiments in an inert atmosphere will increase the cost of production of the LDH; however, this precaution may not be necessary. To test whether an inert atmosphere is needed, the precursor was hydrated in a reaction vessel that was left open to air for the same time and temperatures used in the benzoic acid and hydrochloric acid experiments. The experiments tested how sensitive the precursor is to the uptake of CO_2 in the form of carbonate from air.

The effects of steric hindrances, functional groups and acid strength on the ability of anions to intercalate were tested. Experiments were performed using a variety of different anions at different pH values. These experiments were carried out primarily to gauge the limitations of the precursor method. Each anion was intercalated at 2 or 3 different pH values.

Many different benzene-ring containing anions have been intercalated between the layers of LDHs (Meyn *et al*, 1990). The success of the intercalation may be linked to the steric hindrances or nature of the functional groups present on the benzene ring. In order to test

which one of these two factors have a larger impact on intercalation, simple benzene-containing anions were intercalated. Benzoic acid was taken as the base anion, with no added functional groups and no steric hindrances. Benzoic acid rings with substitutions in the ortho-, meta- and para- positions were also selected (Table 3-1).

All the acids listed in Table 3-1 are weak acids with low solubility (except benzoic acid, which is slightly soluble in water). For this reason, strong, soluble acids were also selected to compare the intercalation behaviour at different pH values. Hydrochloric acid (Merck), nitric acid (ACE Chemicals) and sulphuric acid (ACE Chemicals) were used for this purpose.

Table 3-1: Benzoic acid substituted compounds (supplied by Merck)

Name	Functional group	Substitution	pK_a^{I}	pK_a^{II}
Benzoic acid	None	-	4.20[1]	-
Salicylic acid	OH	Ortho	2.97[1]	13.70[1]
Anthranilic acid	NH_2	Ortho	2.08[1]	4.96[1]
Thiosalicylic acid	SH	Ortho	4.65[3]	9.40[3]
3-Hydroxybenzoic acid	OH	Meta	4.06[2]	9.92[2]
3-Aminobenzoic acid	NH_2	Meta	3.11[4]	4.78[4]
4-Hydroxybenzoic acid	OH	Para	4.48[2]	9.32[2]
4-Aminobenzoic acid	NH_2	Para	2.50[2]	4.87[2]

[1]Harris, 2007
[2]Anon, *sa*
[3]Abu-Bakr, 1997
[4]Niazi & Mollin, 1987

Finally, for a complete understanding of the precursor method limitations, weak, soluble acids were also tested. These acids were: citric acid (ACE Chemicals), acetic acid (Merck), thioglycolic acid (Sigma Aldrich) and carbonic acid (Merck). These acids tested whether acid strength or acid solubility has a greater impact on intercalation behaviour. The pKa values of the strong and weak soluble acids can be found in Table 3-2.

Table 3-2: Dissociation constants of soluble acids

Acid	pK_a^I	pK_a^{II}	pK_a^{II}
Hydrochloric acid	-8.0[2]	-	-
Nitric acid	-1.3[2]	-	-
Sulphuric acid	-3.0[2]	1.99[2]	-
Citric acid	3.13[1]	4.76[1]	6.40[1]
Acetic acid	4.76[1]	-	-
Thioglycolic acid	3.64[1]	10.61[1]	-
Carbonic acid	6.35[1]	10.33[1]	-

[1]Anon, *sa*
[2]Reich, 2012

3.2 Methods

For all experiments, distilled water was used. The distilled water was boiled before each experiment and allowed to cool to room temperature in a sealed vessel. This eliminated all dissolved carbonate from the system. All powders with low solubility were added slowly to the water, while stirring, in order to ensure that the powder was fully whetted.

Samples that were sent for analysis were dried using a vacuum pump attached to a Buchner funnel. These samples were then placed in an oven overnight and ground using a mortar and pestle. The drying temperature varied between experiments.

3.2.1 Precursor synthesis

The precursor mixture was synthesised in bulk using a 5 000 mL round-bottom flask, in a heating mantle. The pre-boiled distilled water (4 000 mL) was added to a round-bottom flask. A mixture of 580 g CaO (supplied by ACE Chemicals) and 400 g $Al(OH)_3$ (supplied by ACE Chemicals) was added to the distilled water in the flask. The reagents were stirred using an overhead stirrer for 24 h at a speed of 1 500 rpm and at a temperature of 60 °C. While the mixture was aging, the flask was sealed off completely from air with rubber stoppers. After filtering, the filter cake was placed in the oven at 120 °C overnight and ground into a fine powder.

3.2.2 Titration

Pre-boiled distilled water (150 mL) was poured into a 250 mL Erlenmeyer flask. The flask was placed on a hotplate stirrer, with a Teflon-coated stirrer bar at a speed of 400 rpm. The precursor mixture (15 g) was then added to the flask.

Two different methods of titration were needed for the anions with high and low solubility. For the soluble anions, volume titrations were sufficient. The acid was placed in a 50 mL burette and slowly added to the precursor slurry in 1 mL increments. After each acid addition, the pH was measured using a CRISON BASIC 20 pH meter.

The acids with low solubility had to be titrated using mass additions. For the mass titration, the correct stoichiometric amount of anion needed to form an LDH was added in 10 equal increments. For monovalent anion, the first 2 mol of anion added will react according to Equation 16, in which n = 1:

$$Ca_3Al_2(OH)_{12} + Ca(OH)_2 + 2HA + xH_2O \rightarrow Ca_4Al_2(OH)_{12}A_2{\cdot}xH_2O + 2H^+ \qquad (19)$$

After the first 2 mole equivalents of acid have been added to the mixture, the mass increments are increased by a factor of six. This is due to the fact that seven times more anion is needed to completely react and neutralise the clay layers than is needed to intercalate. The neutralisation reaction for a monovalent anion is:

$$Ca_3Al_2(OH)_{12} + Ca(OH)_2 + 14HA + xH_2O \rightarrow 4CaA_2 + 2AlA_3\,A_2{\cdot} + (x+14)H_2O \qquad (20)$$

Theoretically, there will be two plateaus present in the titration curve. The first will continue until a mole equivalent of 2, and the second will continue until a mole equivalent of 14 for monovalent anions. The first plateau indicates the intercalation of the anion between the layers of the LDH, while the second indicates the neutralisation of the clay layers with excess acid.

3.2.3 Intercalation

3.2.3.1 Precursor method

Unless otherwise specified, all intercalation experiments using the precursor method were performed with 15 g of katoite/portlandite precursor, in 100 mL of water at ambient conditions for 48 h. The correct stoichiometric amount of anion to intercalate was used, except in the pH experiments.

All intercalation experiments were performed in 250 mL Erlenmeyer flasks on hotplate stirrers, as shown in Figure 3-2. The Erlenmeyer flask was modified with two holes on the sides that have different screw-on attachments. When no temperature or pH measurements were needed, two side attachments with no modification holes were screwed onto both sides, which sealed the flask off from air completely. If temperature or pH measurements were needed, different modified side attachments were screwed on. These attachments were modified with holes that allowed only the probes to fit through with no room for air to enter the flask. Finally, the top of the flask was sealed with a glass bung. The only exception was the experiments involving carbonate uptake from air.

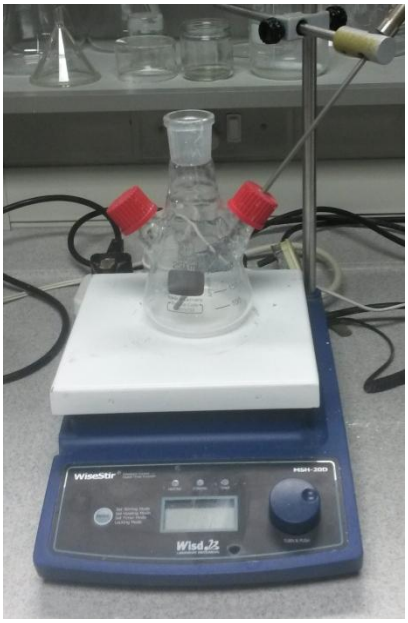

Figure 3-2: Experimental setup for intercalation experiments

For all experiments, approximately 100 mL pre-boiled water was added to the Erlenmeyer flask at the reaction temperature. If the reaction was run at room temperature, the water was allowed to cool to room temperature in the sealed vessel before being added to the Erlenmeyer flask. However, if the reaction was run at elevated temperatures, the water that was sealed from air was allowed to cool to approximately the reaction temperature before being added to the Erlenmeyer flask. A thermocouple was then placed through one of the modified side stoppers, as shown in Figure 3-2, and the temperature of the water was adjusted to the reaction temperature using the temperature controller on the stirrer plate. Once the temperature was adjusted to the reaction temperature, the stir speed was set at 300 rpm. The precursor (15 g) was added to the water slowly.

For the alternative calcium source experiments, the amount of katoite in the katoite/portlandite precursor was calculated and added to the water as pure katoite. The correct stoichiometric amount of CaO (ACE Chemicals) or $Ca(OH)_2$ (ACE Chemicals) was added to the mixture, while stirring.

Finally, the acid was slowly added to the slurry, while stirring at 300 rpm. For most of the experiments, the correct stoichiometric amount of acid was calculated and added to the slurry. However, different amounts of acids were used for the different pH experiments. For the intercalation experiments at different pH values, the acids that needed to be intercalated were used to adjust the pH. For low pH values, excess acid was used. The acid was added, while monitoring the pH. When the correct pH was reached, the bung was used to close off the top of the flask and seal the reaction off from air.

Unless a different time was specified, the intercalation reactions were run for 48 h, then filtered using a Buchner funnel. The filter cake was rinsed with water, before being placed on a petri dish. The petri dish was then placed in an oven overnight at 60 °C, after which the dry sample was ground into a fine powder using a mortar and pestle.

3.2.3.2 Co-precipitation Method

The co-precipitation experiments were also performed on the experimental setup in Figure 3-2. Pre-boiled distilled water (50 mL) was added to the Erlenmeyer flask. The anion, to the amounts specified in Table 3-3, was then added to the water, while the water was being

stirred at 300 rpm with a Teflon-coated stirrer bar. Two solutions were mixed for the experiments and placed in two separate burettes. The first solution was a mixture of 5.00 g $Ca(NO_3)_2 \cdot 4H_2O$ and 3.97 g $Al(NO_3)_3 \cdot 9H_2O$. The second solution was a 1M solution of sodium hydroxide. The first solution was slowly added, drop-wise, to the water-anion slurry in the flask. The second solution was used to keep the pH at approximately 10 throughout the addition of the first solution.

Table 3-3: Mass of anions needed in co-precipitation experiments

Anion	Mass (g)
Benzoic acid	1.29
Salicylic acid	1.46
Anthranilic acid	1.45
3-Aminobenzoic acid	1.45
4-Aminobenzoic acid	1.45

After the entire calcium nitrate and aluminium nitrate solution had been added to the flask and the pH had been adjusted to roughly 10, the flask was sealed with a glass bung and allowed to age for 48 h at 60 °C. Once the sample was aged, it was filtered, rinsed with distilled water and dried overnight at 60 °C. The dry sample was ground into a fine powder using a mortar and pestle.

3.2.3.3 Reconstruction Method

For the reconstruction method, CaAl-CO_3 LDH was synthesised using the novel synthesis method (as described in Section 3.2.3.1). Pre-boiled distilled water (1 500 mL) was added to a 2 000 mL Erlenmeyer flask that was stirred using a Teflon-coated stirrer bar, at a constant speed of 300 rpm. While stirring, 125.00 g of precursor and 21.84 g of $NaHCO_3$ was slowly added to the water in the flask. The flask was then sealed with a rubber bung and left to stir for 48 h at ambient temperatures. The sample was then filtered and rinsed with distilled water, before being placed in an oven overnight at 60 °C. Once completely dry, the sample was ground using a mortar and pestle.

The dry CaAl-CO_3 sample was placed in a crucible, which was placed in a furnace. The sample was calcined at 450 °C for 4 h, after which the crucible was placed in a desiccator to cool to room temperature. Once cool, the powder was sealed from air until it was used in the reconstruction experiments.

An Erlenmeyer flask setup, as specified in Figure 3-2, was also used for the reconstruction experiments. Pre-boiled distilled water (100 mL) was added to the Erlenmeyer flask and stirred at 300 rpm. The calcined powder was added to the Erlenmeyer flask, after which the anion in the correct stoichiometric amount was added to the slurry. The flask was sealed from air with a glass bung and left to stir at room temperature for 48 h. The sample was then filtered, dried and ground in the same way as the pre-synthesised LDH.

3.3 Characterisation

Four different characterisation techniques were carried out, in order to characterise the LDH samples: X-ray diffraction analysis (XRD); thermogravimetic analysis (TGA), Fourier transform infrared analysis (FTIR) and scanning electron microscopy (SEM).

Wide-angle X-ray scattering (WAXS) was performed on the samples using a PANalytical X'Pert-Pro Diffractometer. The scans were taken from an angle of 5.0° to an angle of 90.0°, using a cobalt (Co) source. HighScore Plus 4.1 software was used to identify crystalline species in the sample. Quantitative analysis could only be performed on samples in which all the crystalline species present in the sample were in the database. In these cases, Rietveld refinement using the Highscore Plus 4.1 software was used for the quantification.

All the samples that successfully intercalated were sent for TGA analysis, in order to quantify the intercalation and assess how much crystalline water was present between the layers. A TA Instruments Q 5 000 TGA machine was used, and the sample was run in an N_2 atmosphere. The sample was held at room temperature for 5 min, and then taken to a temperature of 800 °C at a rate of 10 °C/min.

FTIR was used primarily to identify whether organic anions had intercalated between the layers of the LDH. A Bruker Tensor 27 IR-spectrometer equipped with a Pike ATR-unit was

used to obtain the FTIR spectra. Each spectrum was collected at a resolution of 4 cm^{-1}. The scans were taken from 500 cm^{-1} to 4 000 cm^{-1}, with 128 scans performed per run.

Finally, SEM was performed on the chloride and benzoate uptake experiments, in order determine how time and temperature influence the crystalline nature of the sample. The samples were coated 8 times with graphite in a Polaron h/v coater. The samples were then analysed in an Ultrahigh Resolution Field Emission SEM (JEOL 6000F). The resolution was 0.6 nm, and the system had a Gatan Digital Micrograph imaging system.

3.4 Simulations

All molecular simulations were generated on Avogadro open-source molecular simulation software, version 1.1.1. For geometry optimisation, the UFF force field function was used, with 4 steps per update. The steepest descent algorithm was used for each run. The sizes of each molecule were calculated with a built-in measurement tool.

4. Results and Discussions

4.1 Temperature and time effects

All quantitative data was obtained using the Rietveld refinement method of the XRD patterns. The XRD patterns from which the quantitative values were derived are attached in Appendix A. Quantitative analysis could only be obtained if all the peaks on the XRD pattern were identifiable.

4.1.1 Carbonate uptake from air

The ability of the precursor to take up carbonate from air at different temperatures and times is shown in Table 4-1. At a temperature of 80 °C, the water evaporated. For this reason, the results at 80 °C cannot be taken as accurate. The influence of temperature on the uptake of carbonate from air is a balance between two competing mechanisms. An increase in temperature increases the reaction rate; however, an increase in temperature also decreases the amount of dissolved carbonate in the water. In general, however, an increase in temperature corresponds to an increase in conversion to a Ca/Al-CO_3 LDH (hydrocalumite).

Table 4-1: Carbonate uptake by precursor from air. Conversion to hydrocalumite (wt.%)

Time (h)	Temperature (°C)			
	Ambient	40	60	80
2	6.21	6.56	4.27	13.71
6	5.19	8.07	14.26	2.17
12	14.34	7.45	9.83	-
24	6.19	7.89	10.11	-

The aging time required to reach the maximum conversion to hydrocalumite differs depending on the temperature. When run for 2 h, the maximum amount of carbonate was taken up at 80 °C. For 6 h and 24 h, the maximum carbonate uptake occurs at 60 °C, and for 12 h, the maximum uptake occurred at room temperature. An increase in conversion to hydrocalumite corresponds to a decrease in the amount of leftover katoite in the sample (Table 4-2).

Table 4-2: Carbonate uptake by precursor from air. Residual katoite (wt.%)

Time (h)	Temperature (°C)			
	Ambient	40	60	80
2	75.07	75.43	78.18	69.82
6	76.82	75.27	68.51	77.58
12	66.88	76.38	69.43	-
24	74.01	75.41	73.20	-

Ca/Al-OH LDH formed as a new stable phase when the precursor was left open to air. At low temperatures and short reaction times, Ca/Al-OH LDH does not form (Table 4-3). Ca/Al-OH also does not form at a temperature of 40 °C. The maximum conversion to the new species is observed at 80 °C and 6 h; however, since the 80 °C results cannot be taken as accurate, the maximum conversion is observed at 60 °C and 12 h. At a temperature of 60 °C and a time of 12 h, there is a sharp drop in conversion to hydrocalumite (Table 4-1), which is accompanied by a sharp increase in conversion to Ca/Al-OH. This means that the mechanisms for the formation of these two species are competing.

Table 4-3: Carbonate uptake by precursor from air. Conversion to Ca/Al-OH (wt.%)

Time (h)	Temperature (°C)			
	Ambient	40	60	80
2	0.00	0.00	0.00	1.80
6	0.00	0.00	1.47	7.22
12	1.42	0.00	4.28	-
24	3.62	0.00	3.20	-

A new crystalline calcium carbonate phase was formed at certain conditions. These conditions include:

- room temperature for 24 h;
- 60 °C for 2 h, 12 h and 24 h and 80 °C for 6 h

In all cases, the conversion was less than 1 wt.%. However, this does not take into consideration the calcium carbonate in the amorphous phase (Cartwright *et al*, 2012).

If the reaction vessel is not sealed from air, carbonate from the air will intercalate between the layers of the LDH to form hydrocalumite. In order to ensure that the final product has 0 % carbonate contamination, the vessel must be sealed off from air and performed in an inert environment. However, even when the intercalation is performed in a vessel open to air under different conditions, the maximum hydrocalumite yield was 15 wt.%. If the reaction vessel is sealed off from air, and no new carbon dioxide can enter the vessel, carbonate contamination will decrease. This indicates that, unless 100 % pure products are needed, intercalation reactions can be run without the use of nitrogen. Running the experiments without the use of nitrogen will decrease the cost of production of intercalated LDH materials. For this reason, all intercalation experiments in this investigation were performed without the use of nitrogen.

4.1.2 Chloride uptake from hydrochloric acid

According to Table 4-4, temperature has a greater impact on conversion than time when attempting to synthesise a Ca/Al-Cl LDH using the precursor method. At 40 °C and 50 °C, the maximum conversions occur when the samples were aged for 12 h. At ambient temperatures, the maximum conversion occurs when the sample was aged for 24 h, while the maximum conversion at 60 °C occurs when the sample was aged for 6 h. When the sample is aged at elevated temperatures, a higher conversion to CaAl-Cl LDH is favoured at shorter times.

Table 4-4: Chloride uptake by katoite/portlandite mixture. Conversion to Ca/Al-Cl (wt.%)

Time (h)	Temperature (°C)			
	Ambient	40	50	60
2	11.82	19.53	20.63	18.84
6	15.23	18.05	36.83	51.31
12	16.26	64.23	46.09	30.39
24	32.12	24.05	23.38	44.15

There are two possible explanations for the lower conversion at longer aging times. The first explanation is that when the sample is aged for longer, a more stable phase is reached. The more stable phase would either be present in the sample as a new primary peak, or it would

be present in the amorphous phase. The second explanation is that the particles become smaller when aged; therefore, they are washed through the filter paper.

The amount of residual katoite increases with decreasing conversion to Ca/Al-Cl LDH (Table 4-5), which eliminates the latter theory that the particles are filtering through the filter paper. The maximum conversion to CaAl-Cl LDH at a time of 12 h and a temperature of 40 °C also corresponds to the conditions with the least amount of katoite. The same is true for the most amount of katoite at ambient temperatures and 2 h aging time, which yielded the least amount of CaAl-Cl LDH. This supports the theory that there is a new stable phase formed when the sample is aged at certain reaction conditions. Due to the fact that no unidentified peaks are present in the XRD patterns, it can be concluded that the new stable phase is not present as a crystalline species.

Table 4-5: Residual katoite in chloride uptake experiments (wt.%)

Time (h)	Temperature (°C)			
	Ambient	40	50	60
2	83.83	76.87	75.66	77.50
6	80.87	78.26	58.13	45.15
12	79.85	31.66	49.20	67.08
24	66.04	73.32	73.39	51.97

The only other difference between the samples is the amount of amorphous material present in the sample (Appendix A-15 – Appendix A-30). Upon visual inspection, the least amount of amorphous material appears to be present at 6 h when the sample is aged at 60 °C and at 12 h when the sample is aged at 40 °C and 50 °C. These three conditions correspond to the maximum conversions (Table 4-4). These results support the theory that a new stable phase is formed when the sample is aged for too long, or at a very high temperature. The new stable phase is, however, amorphous. For this reason, it is not identifiable on the XRD pattern.

There is no real trend for the conversion of precursor material to a Ca/Al-Cl LDH in the presence of hydrochloric acid. According to the results, the optimum condition for the formation of a Ca/Al-Cl LDH is 12 h at 40 °C.

Figure 4-1 shows SEM images for Ca/Al-Cl samples aged at different reaction conditions. There is still a lot of unreacted katoite in each of the samples, and there are no large observable differences between the samples.

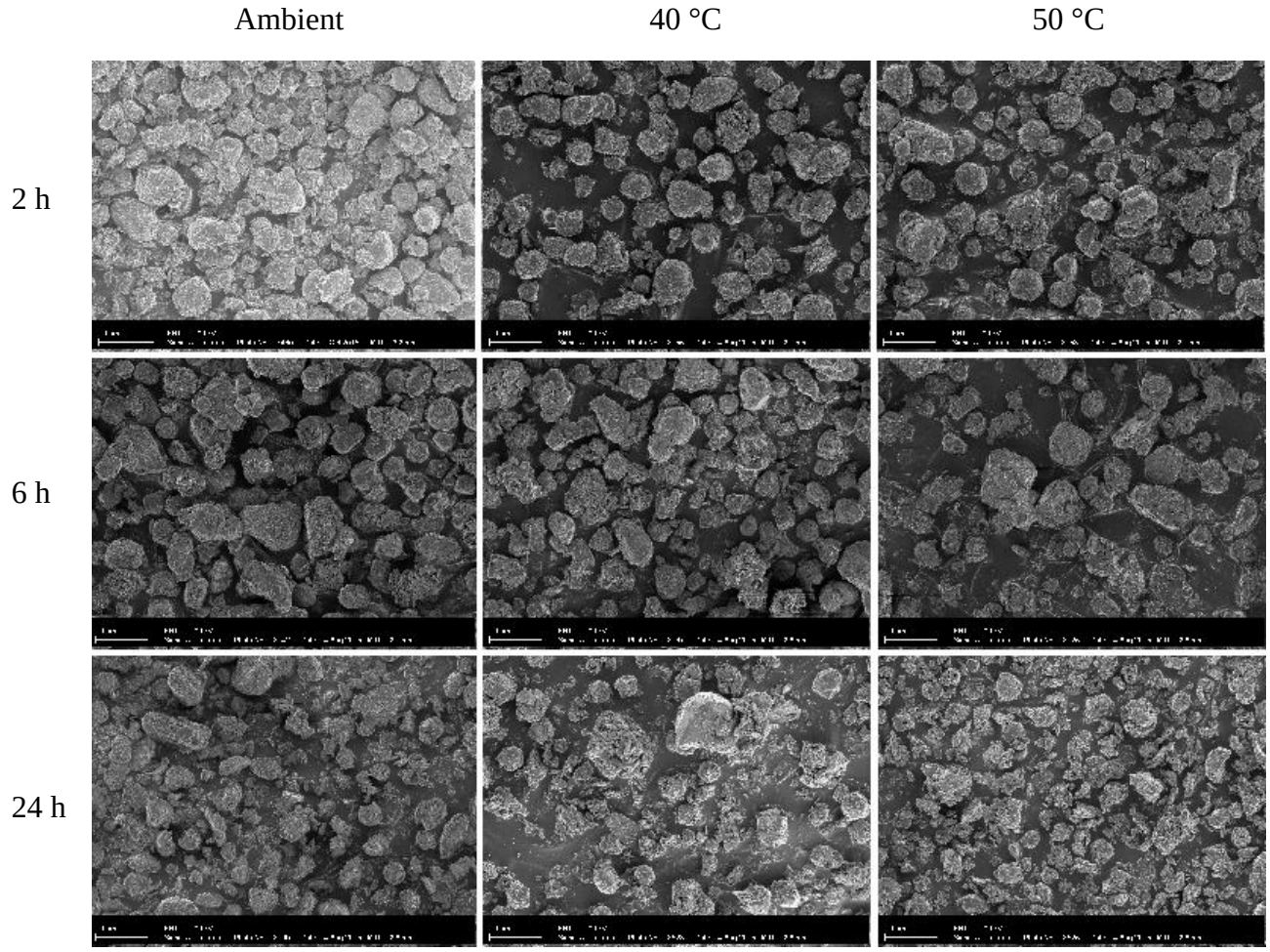

Figure 4-1: Scanning electron micrographs for chloride uptake samples aged at different reaction conditions (resolution = 4 000)

At 2 h and ambient temperatures, hexagonal plates start to form from the isomeric katoite structures (Figure 4-2). The number of hexagonal platelets increase as the temperature is increased to 60 °C (Figure 4-3). However, when the aging time is increased to 24 h, there is no significant increase in the number of plates (Figure 4-5). Finally, when the sample is aged for 24 h at 60 °C (Figure 4-6), the size of the platelets appears to increase. The platelet crystallinity, however, seems to be less than at a lower time and temperature. SEM images for the sample aged at 40 °C and 12 h have been included in Figure 4-4, since there is a drastic increase in conversion at these conditions. Upon inspection of the SEM images, the increase

in conversion appears to be accompanied by an increase in the amount of large hexagonal platelets present in the sample.

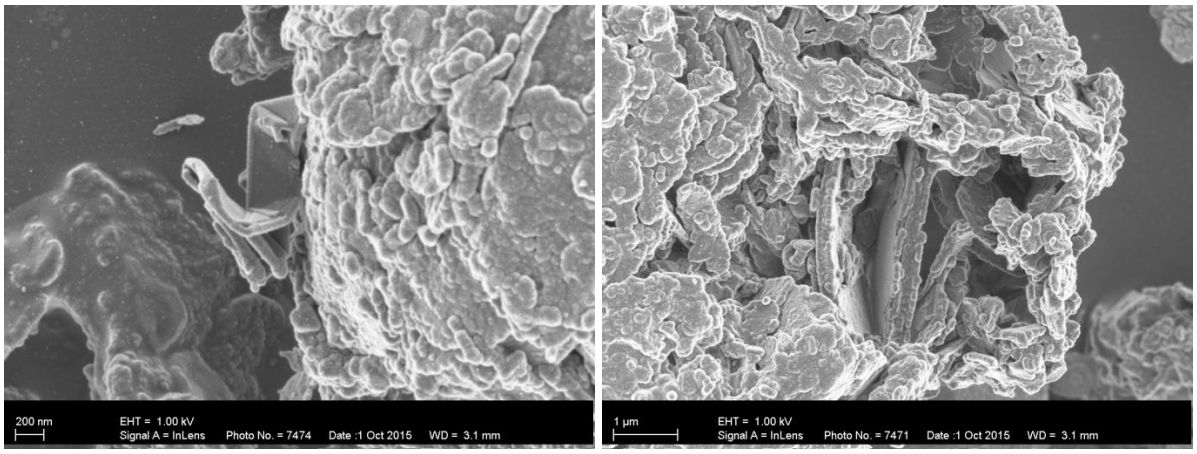

Figure 4-2: Scanning electron micrographs for chloride uptake samples aged at 2 h, ambient temperatures

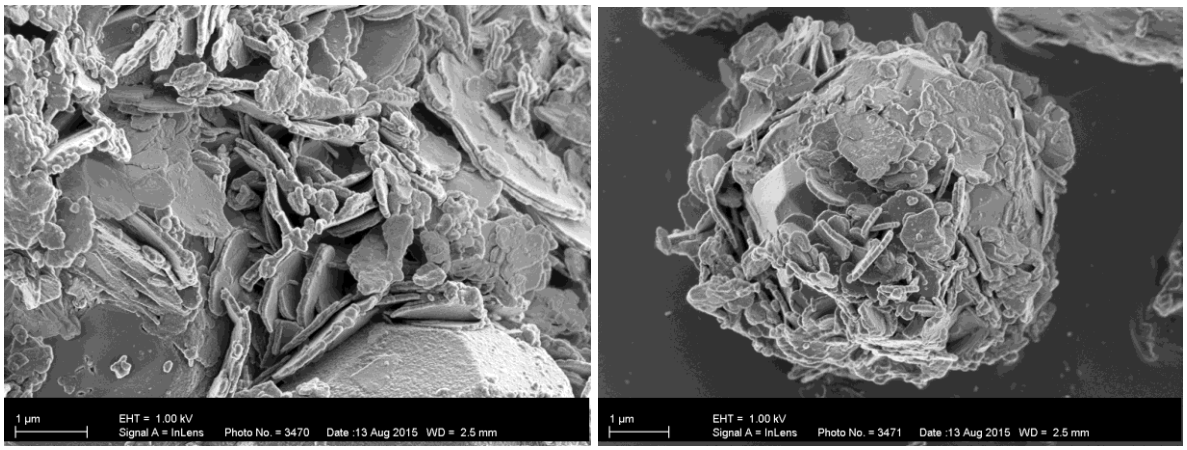

Figure 4-3: Scanning electron micrographs for chloride uptake samples aged at 2 h, 60 °C

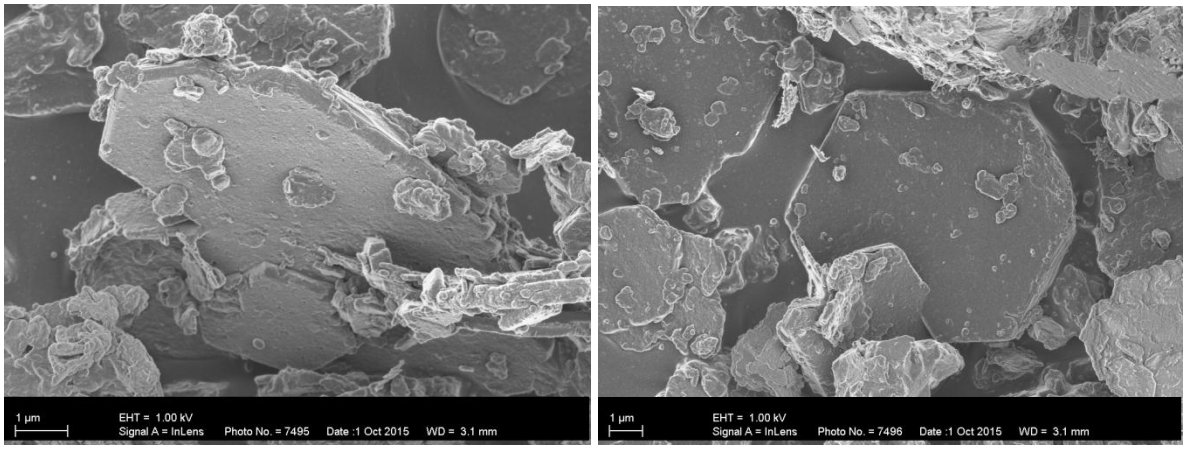

Figure 4-4: Scanning electron micrographs for chloride uptake samples aged at 12 h, 40 °C

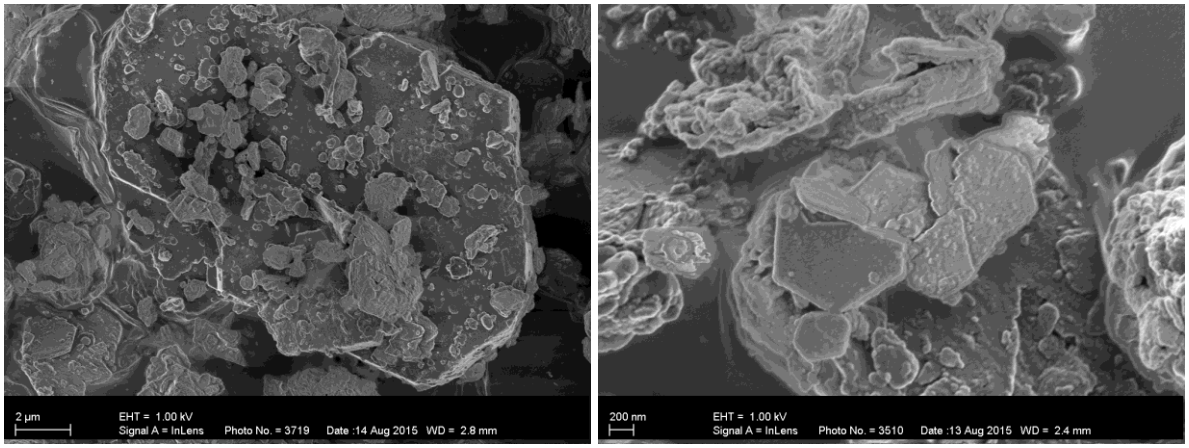

Figure 4-5: Scanning electron micrographs for chloride uptake samples aged at 24 h, ambient temperatures

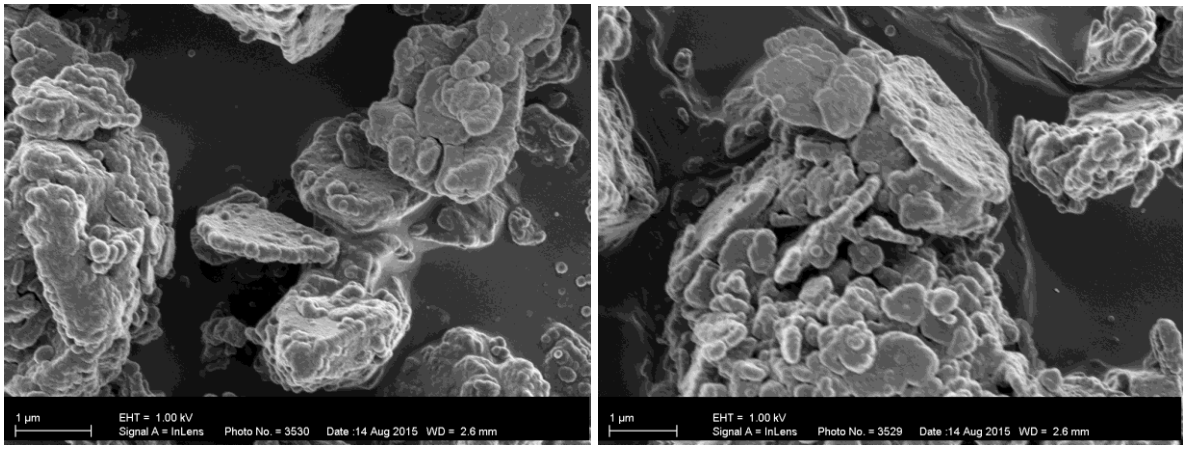

Figure 4-6: Scanning electron micrographs for chloride uptake samples aged at 24 h, 60 °C

4.1.3 Benzoate uptake from benzoic acid

When benzoic acid is reacted with a mixture of katoite and portlandite in water, a new primary peak appears on the XRD pattern at a 2θ value of 6.45° (Figure 4-7, Figure 4-8, Figure 4-9 and Figure 4-10). This new peak corresponds to a d-spacing of 15.91 Å (Equation 5). Regardless of the conditions used, there is still a large amount of unreacted katoite in the sample, which is shown by clear peak at a 2θ value of 20°. The relative intensity of the katoite primary peak versus the intensity of the Ca/Al-benzoate primary peak is large, indicating a low conversion to benzoate-intercalated LDH. However, as the reaction time increases, there is a general increase in the new primary peak intensity versus katoite primary peak intensity. This indicates that there is a general increase in the conversion to

intercalated LDH with increasing reaction time. Furthermore, there is no unreacted, crystalline benzoic acid left in any of the samples.

This general trend is not, however, true when the sample is aged at 50 °C, where the primary peak intensity of the intercalated LDH is highest when left to age for 6 h. The other two exceptions are when the sample is aged for 6 h at 40 °C and 12 h at ambient temperatures. In these two cases, the new primary peak of the intercalated material disappears entirely. This phenomenon could be attributed to experimental error. The new primary Ca/Al-benzoate peak is not present in the XRD pattern when the sample is aged at 60 °C for all times between 2 h and 24 h. This indicates that Ca/Al-benzoate is not stable at elevated temperatures. This theory is supported by the tendency of the LDH primary peak to decrease with respect to the katoite primary peak as the temperature increases. For this reason, the optimum synthesis conditions for a benzoate-intercalate Ca/Al LDH using the precursor method is at ambient temperatures.

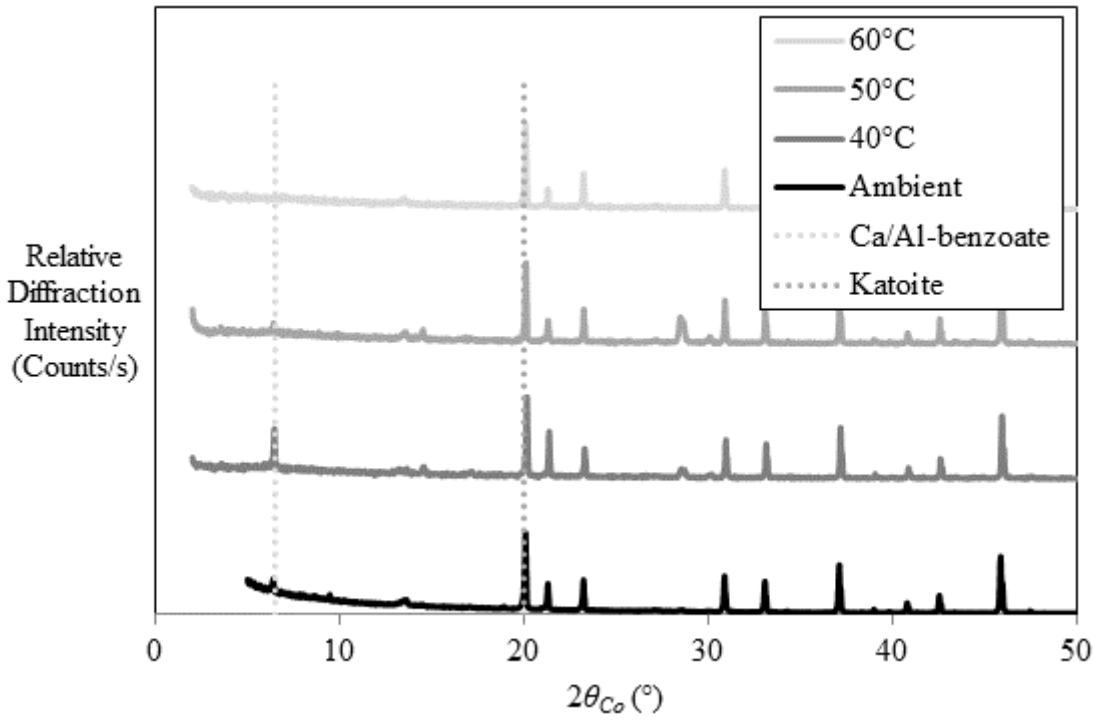

Figure 4-7: Benzoic acid uptake by precursor in water at different temperatures for 2 h

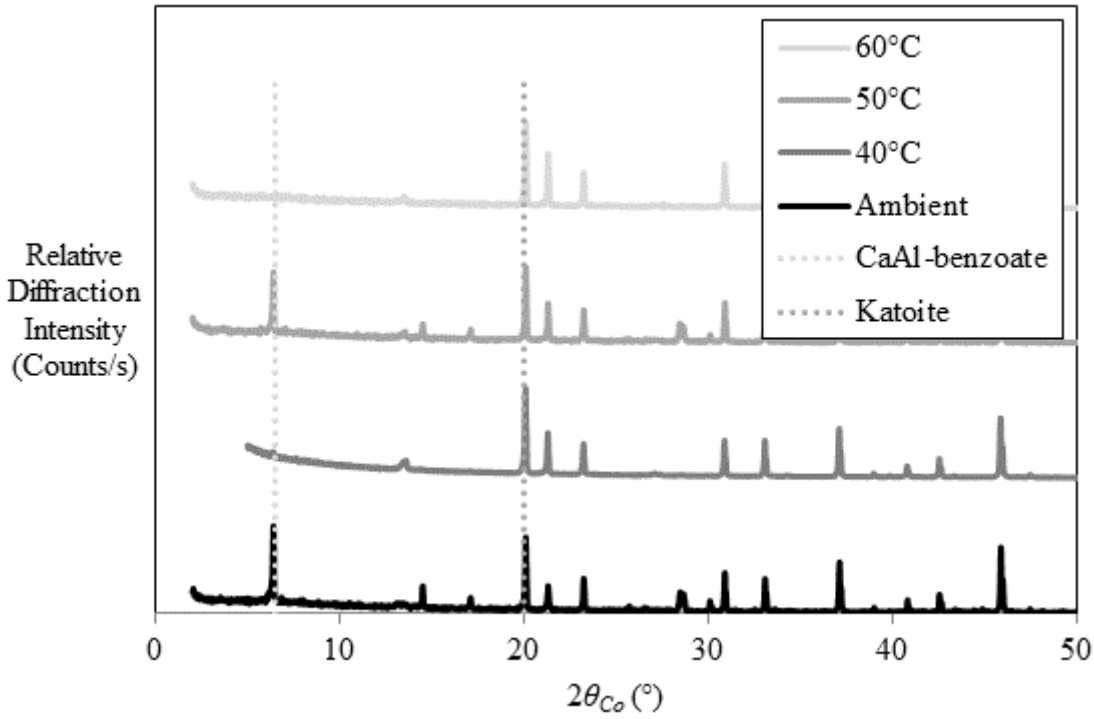

Figure 4-8: Benzoic acid uptake by precursor in water at different temperatures for 6 h

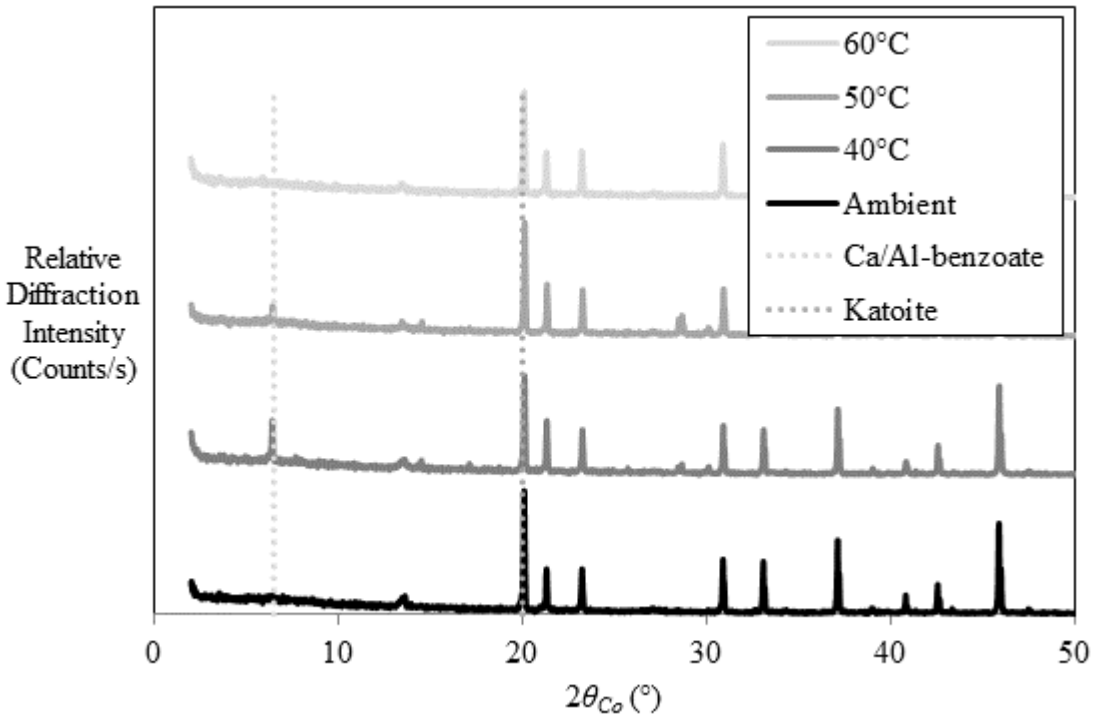

Figure 4-9: Benzoic acid uptake by the precursor in water at different temperatures for 12 h

When intercalated for 24 h, there are two new primary peaks present on the XRD pattern (Figure 4-10). The primary peak that occurs at a 2θ value of 6.45° is present for all reaction times tested. However, when aged for 24 h, there is a new primary peak at 7.09° at each temperature, except at 60 °C. This additional peak could indicate that benzoate intercalates at two different orientations when left to age for 24 h. The second primary peak becomes more intense with increasing temperature, indicating that the new orientation is favoured at higher temperatures. The additional primary peak corresponds to a d-spacing of 14.47 Å, which means that as the temperature increases, the orientation of benzoate between the layers becomes flatter. This supports the results found in literature (Vucelic *et al*, 1995).

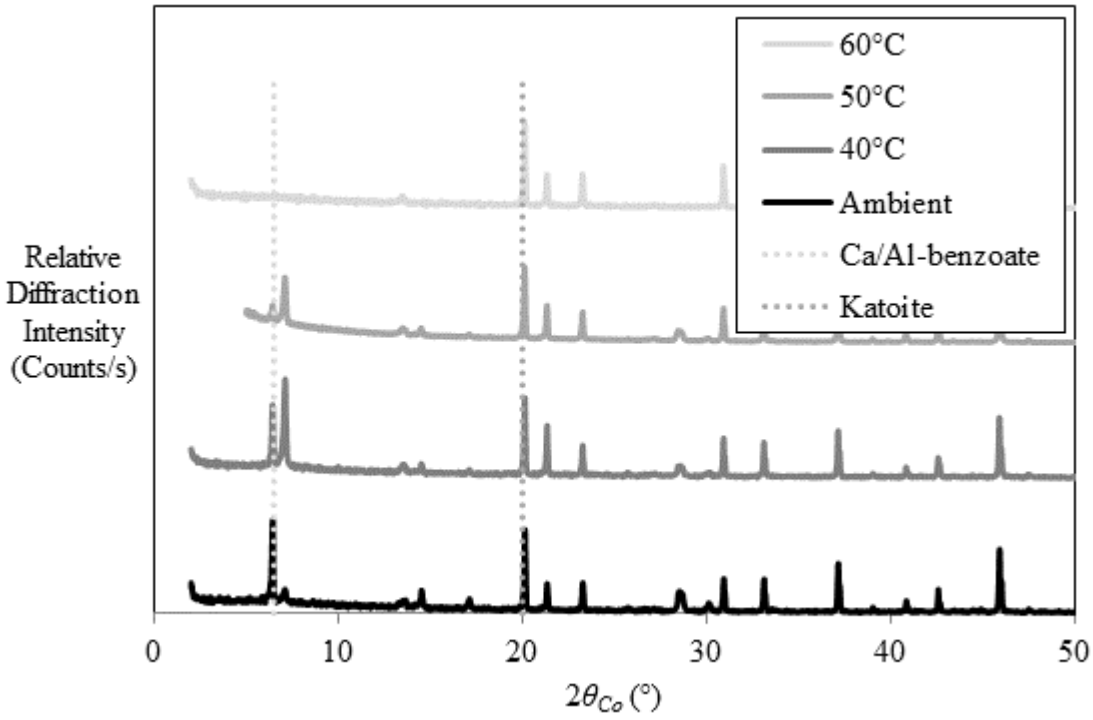

Figure 4-10: Benzoic acid uptake by the precursor in water at different temperatures for 24 h

Like chloride, benzoate struggled to intercalate at certain reaction conditions. However, there are several general trends that arise when intercalating benzoate. In general, as the aging time increases, the conversion increases. Intercalation at 60 °C is not possible between 2 h and 24 h. The combination of longer aging times and lower temperatures has the best yield when synthesising a Ca/Al-benzoate LDH.

The SEM images for the benzoate uptake experiments at different conditions are similar to that of the chloride uptake experiments (Figure 4-11). There are still a lot of large isometric shapes that can be attributed to unreacted katoite.

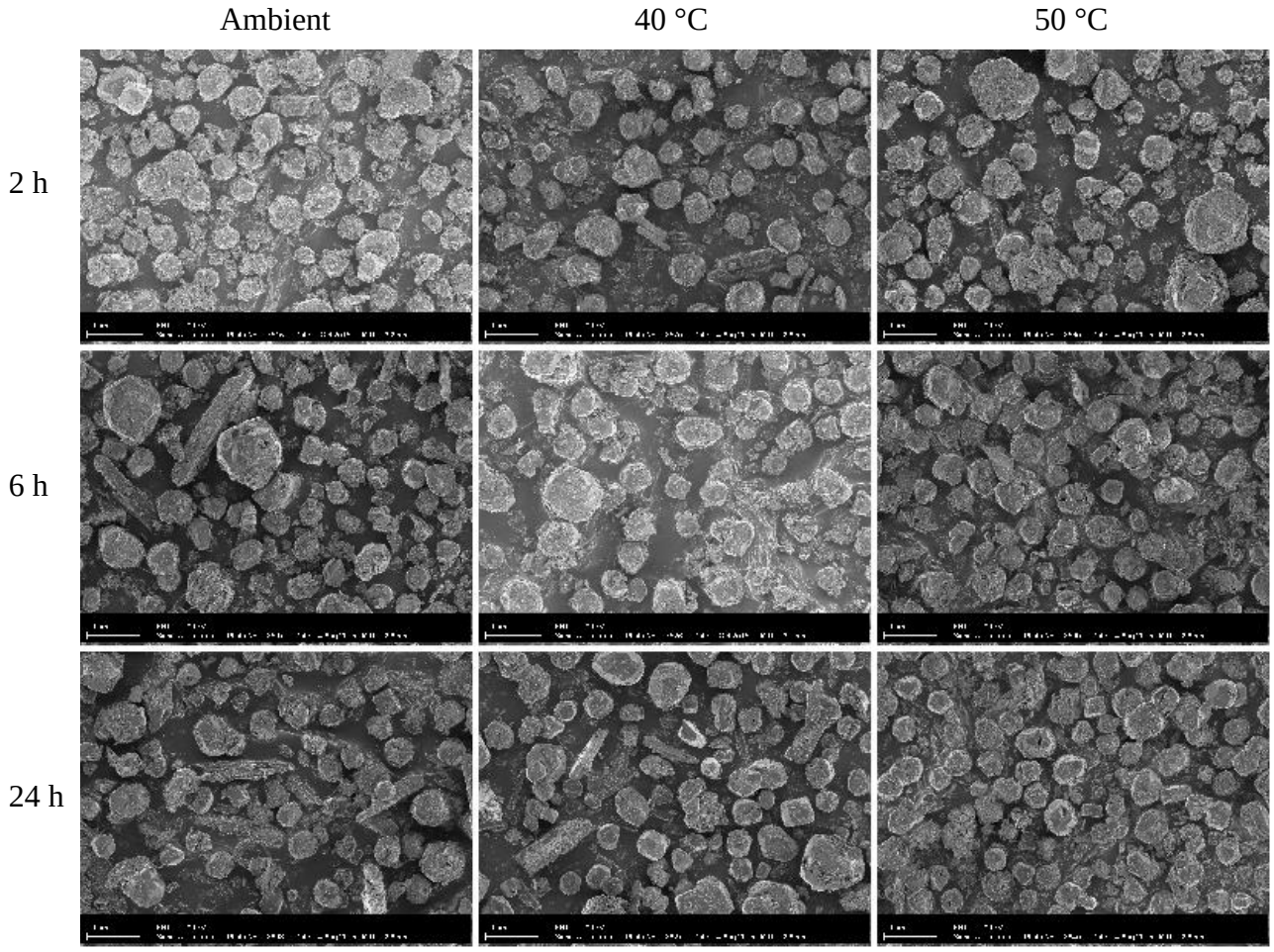

Figure 4-11: Scanning electron micrographs for benzoate uptake samples aged at different reaction conditions (resolution = 4 000)

The platelets formed in the benzoate uptake experiments are not as large as in the chloride uptake experiments (Figure 4-12, Figure 4-13, Figure 4-14, Figure 4-15 and Figure 4-16). The hexagonal platelets are also not very well-formed or crystalline. This phenomenon could be explained by the fact that Ca/Al LDHs sometimes appear in pseudo-hexagonal symmetries, due to the difference in size between the calcium and the aluminium ionic radii (Taylor, 1984).

At an aging time of 24 h at 40 °C, there are two new primary peaks. Upon visual inspection of the SEM images, this also appears to be accompanied by an increase in large, hexagonal

platelets that are more crystalline (Figure 4-15). For this reason, the new primary peak occurring when the samples are aged for 24 h could also be explained by the presence of a new crystalline morphology.

Finally, the SEM images for samples aged at 60 °C (Figure 4-13 and Figure 4-16) show some platelet formation. However, these crystalline structures were too sparse to appear in the XRD analyses.

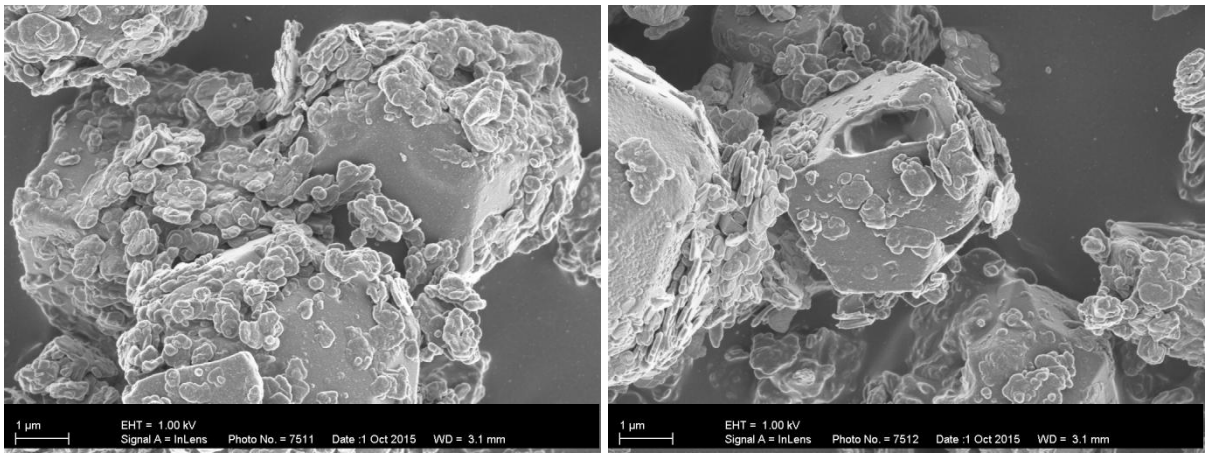

Figure 4-12: Scanning electron micrographs for benzoate uptake samples aged at 2 h, ambient temperature

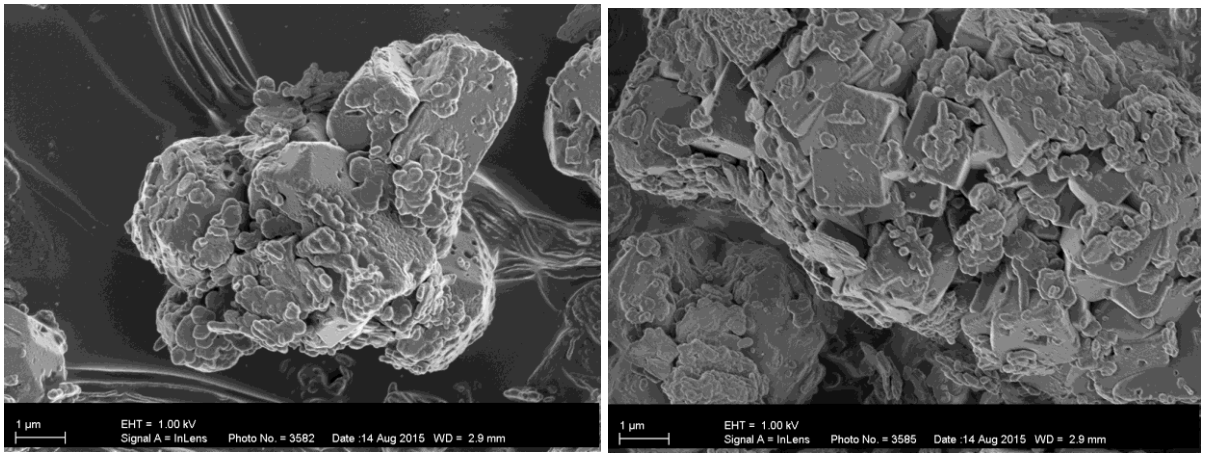

Figure 4-13: Scanning electron micrographs for benzoate uptake samples aged at 2 h, 60 °C

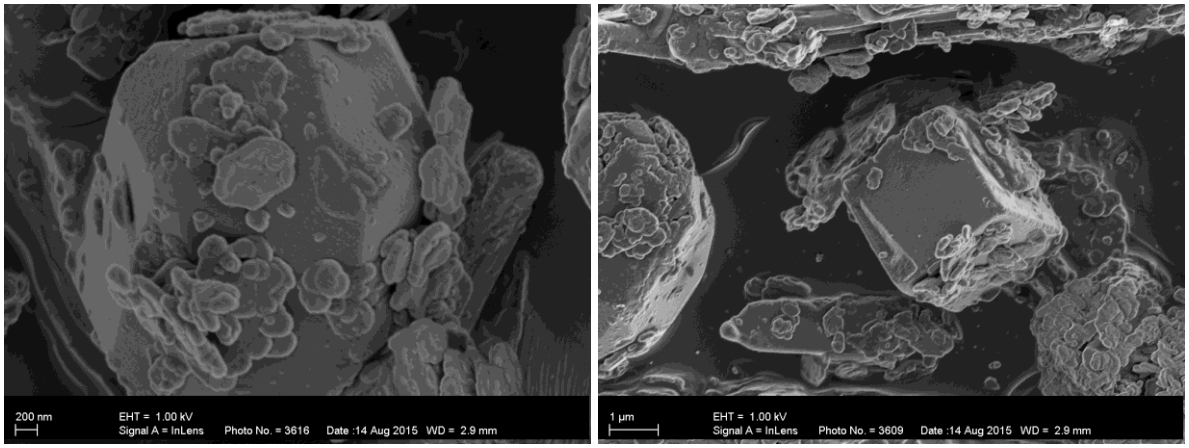

Figure 4-14: Scanning electron micrographs for benzoate uptake samples aged at 24 h, ambient temperature

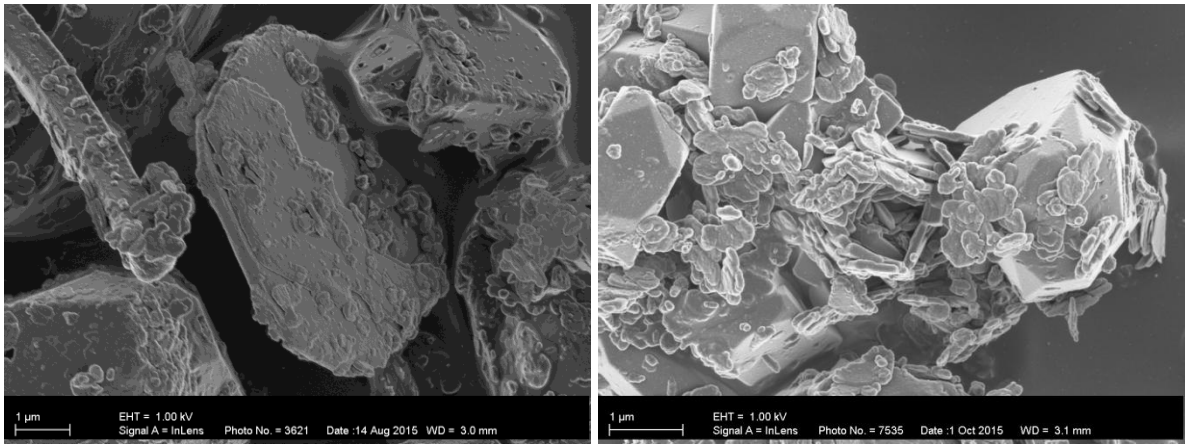

Figure 4-15: Scanning electron micrographs for benzoate uptake samples aged at 24 h, 40 °C

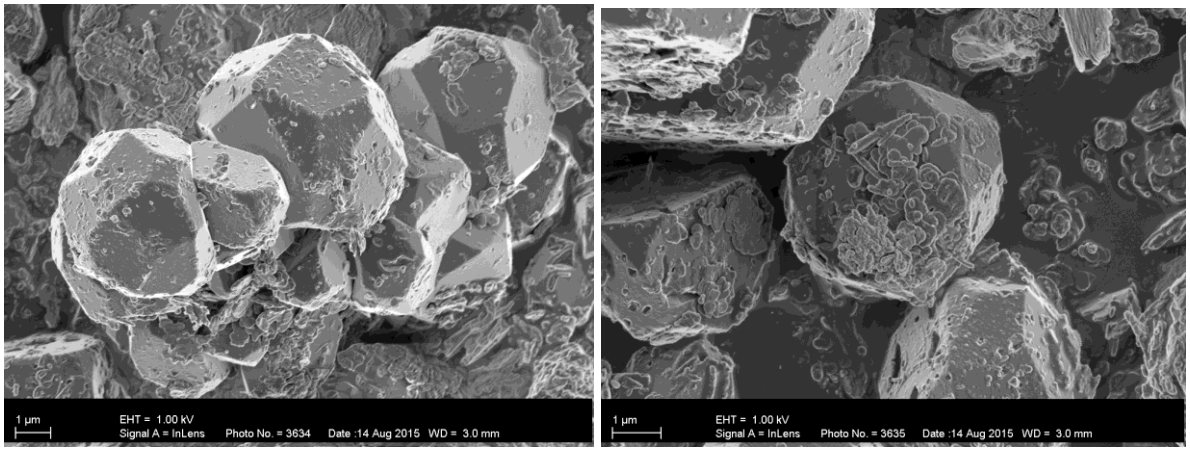

Figure 4-16: Scanning electron micrographs for benzoate uptake samples aged at 24 h, 60 °C

4.2 Different calcium sources

In the past, the novel synthesis method was only carried out using a pre-synthesised precursor (Van der Westhuizen, 2011; Van Graan, 2012), which contained both katoite [$Ca_3Al_2(OH)_{12}$] and portlandite [$Ca(OH)_2$]. Portlandite is needed in the precursor so that the more stable 2:1 Ca:Al LDH can be formed in the second step of the reaction. The extra mole of $Ca(OH)_2$ in the precursor was aged for 24 h, along with the katoite. In order to test the importance of the aging process on the portlandite, two different calcium sources were added to pure katoite. CaO and $Ca(OH)_2$ were chosen as the two calcium sources. The experiments were designed to test whether it is possible to add the extra calcium source in the second step of the reaction, if there is not enough portlandite in the precursor material.

Figure 4-17 shows the intercalation of benzoic acid using the 3 different calcium sources. When aged portlandite is used as the extra calcium source in combination with katoite, the new primary peak is very intense. The primary peak is a lot more intense than when fresh portlandite or calcium oxide was used.

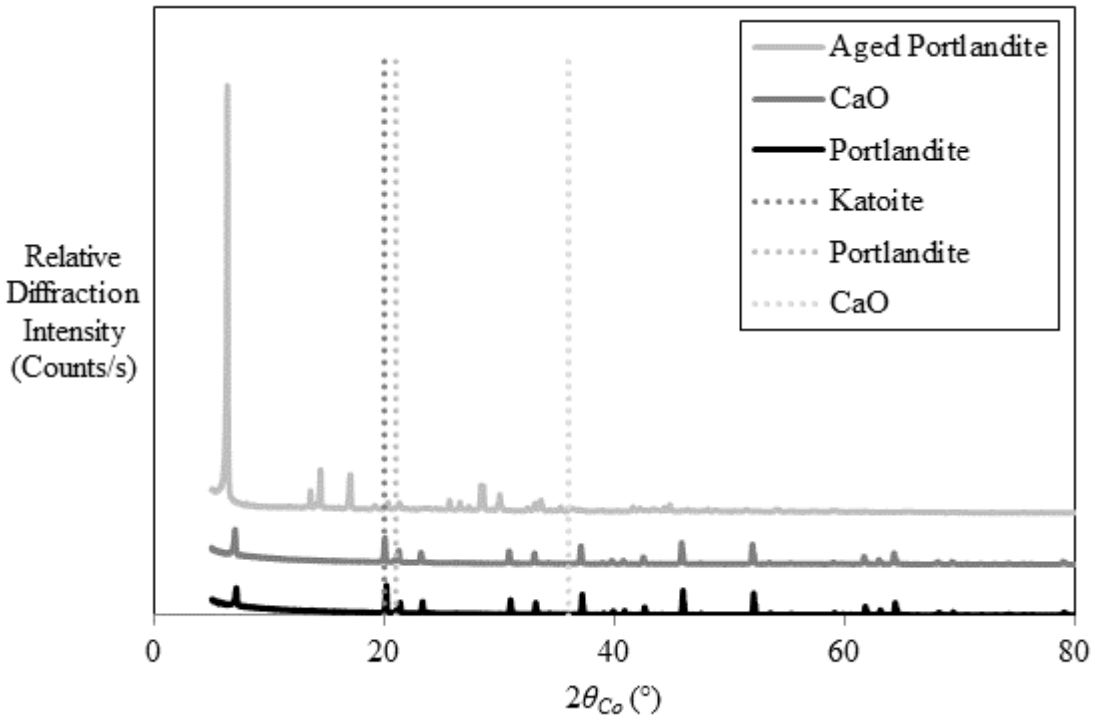

Figure 4-17: Impact of different calcium sources on the intercalation of benzoic acid

When calcium oxide was used, there is unreacted calcium hydroxide in the sample; however, there is no unreacted calcium oxide. This is due to the fact that calcium oxide converts to calcium hydroxide when it comes in contact with water, and this reaction is relatively rapid. When calcium hydroxide was added as the extra calcium source, there is also unreacted calcium hydroxide in the sample. Finally, the sample synthesised with aged portlandite has the least amount of unreacted katoite, indicating a higher conversion to a Ca/Al-benzoate LDH. For this reason, aged portlandite is the best calcium source to use when intercalating benzoic acid.

The same general trends can be seen for the intercalation of chloride (Figure 4-18). The only difference is the Ca/Al-benzoate primary peak is the most intense when aged portlandite is used, while the Ca/Al-chloride primary peak is the least intense when aged portlandite is used.

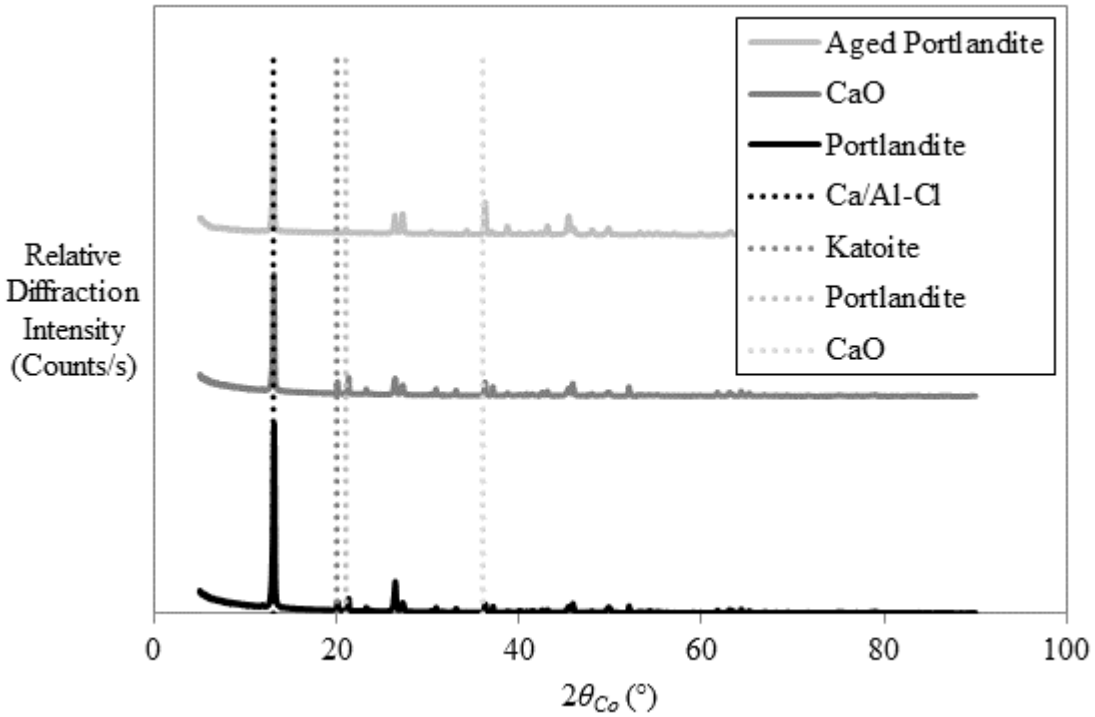

Figure 4-18: Impact of different calcium sources on the intercalation of hydrochloric acid

There appears to be unreacted calcium oxide in all three samples; however, this is due to the fact that the primary peak of CaO occurs at the same 2θ value as one of the hydrocalumite peaks. For both of the alternative calcium source samples, there is unreacted katoite also left

in the sample. When aged portlandite is used as the calcium source, however, there is almost no unreacted katoite or portlandite present in the sample. This indicates a higher reactivity of the calcium source when the portlandite is allowed to age with the katoite.

Adding fresh $Ca(OH)_2$ or CaO to the second step of the reaction, instead of using aged $Ca(OH)_2$ has little effect on the ability of the anion to intercalate. However, in the case of hydrochloric acid and benzoic acid, the amount of katoite left in the sample was less when using aged $Ca(OH)_2$; therefore, aged portlandite gives the highest conversion. For this reason, it is preferential to age the extra mole of calcium. However, if pure katoite is available, or there is excess katoite in the precursor, it is possible to supplement the extra mole of calcium with $Ca(OH)_2$ or CaO.

4.3 Top-down precursor titrations

4.3.1 Hydrochloric acid titration

Hydrochloric acid was the only inorganic acid tested in the titration experiments, and the results of the titration can be seen in Figure 4-19. The first obvious irregularity in the results is attributed to the fact that the first plateau carries on until a mole equivalent of 6. Since chloride is a monovalent anion, only 2 mol of chlorine is needed to intercalate between the layers of the LDH and fully convert the precursor to LDH material. This means that, according to the titration, excess chloride has been intercalated. Another explanation for this phenomenon is that the chloride ions have adsorbed onto the surface of the LDH.

The second obvious irregularity is the fact that HCl exhibits four plateaus instead of the expected three. The second plateau ends at a mole equivalent of 14, which is expected because all the hydroxides in the clay layers have then been neutralised. Ideally, hydrochloric acid should not exceed 6 mole equivalents because, according to Figure 4-19, the clay layers start breaking down after this point. This means that 3 times the correct stoichiometric amount of hydrochloric acid can be added to the precursor before the layers start to break down.

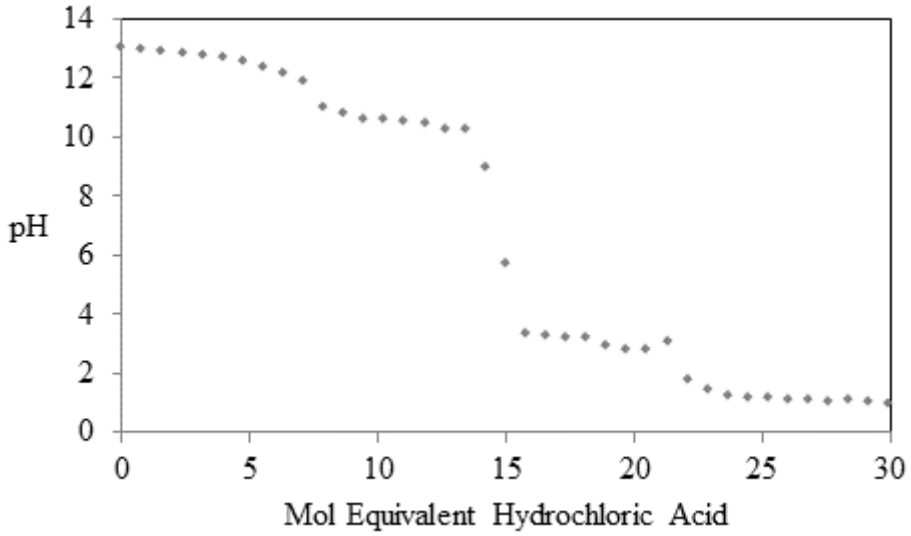

Figure 4-19: Top-down titration of hydrochloric acid

4.3.2 Benzoic acid titration

The benzoic acid titration graph shows 2 plateaus, the first of which occurs at a pH of roughly 12.5 (Figure 4-20). From the figure, it can be concluded that the pH of a Ca/Al-benzoate LDH is around 12.5. The first plateau drops after a mole equivalent of 2 benzoate anions have been added to the precursor mixture. Since benzoate is monovalent, these results are in line with what was expected.

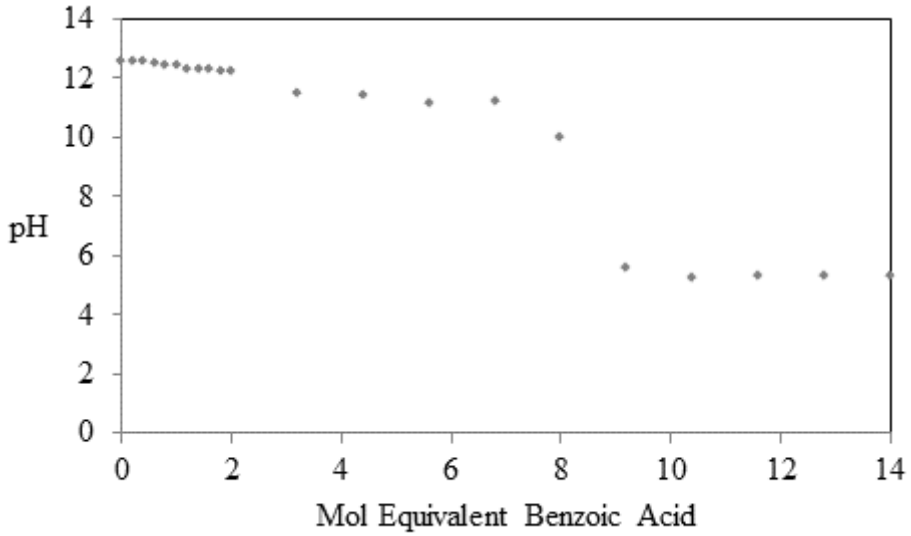

Figure 4-20: Top-down titration of benzoic acid

There is a second plateau that proceeds to a mole equivalent of 8. Since the second plateau represents the breaking down of the clay layers, the plateau is expected to end at a mole equivalent of 14. Since this is not the case, it could indicate that the clay layers did not break down entirely during the titration.

4.3.3 Ortho-substituted benzoic acid titrations

The curves for the titration of the ortho-substituted benzoic acid anions differ vastly (Figure 4-21).

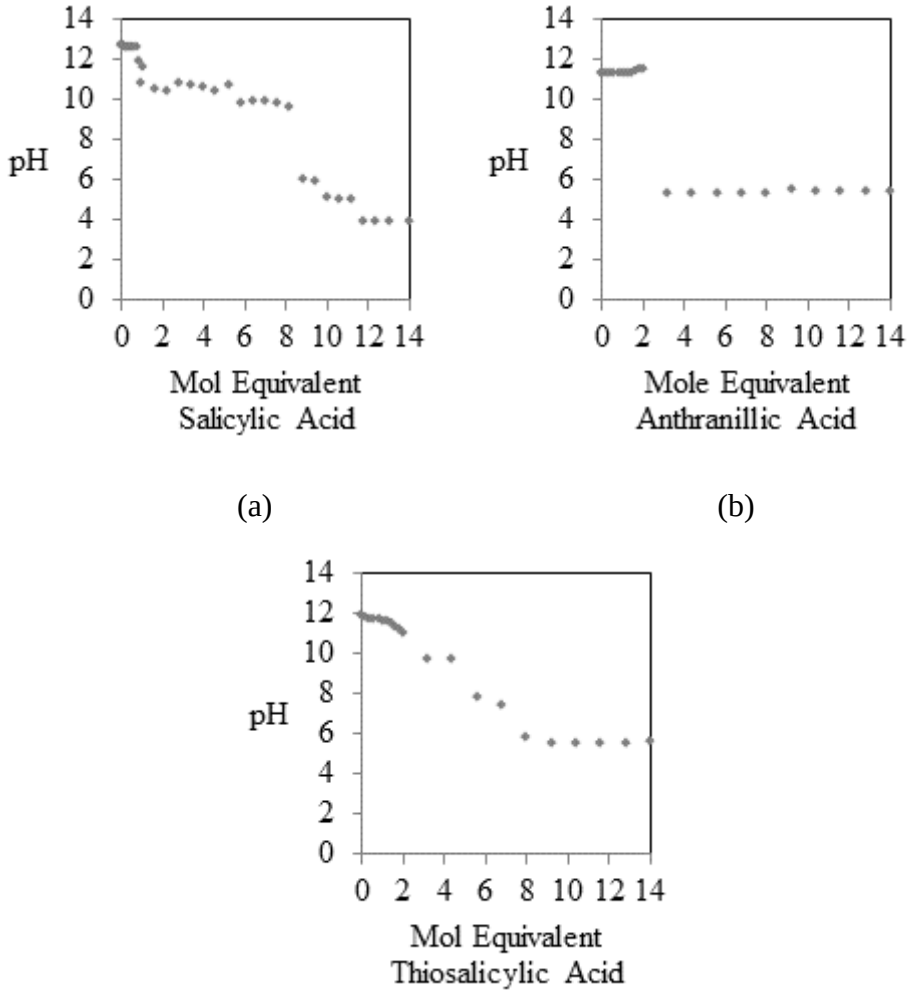

(a) (b)

(c)

Figure 4-21: Top-down titration curves of (a) salicylic acid, (b) anthranilic acid and (c) thiosalicylic acid

The first plateaus for anthranilic acid and thiosalicylic acid drop off at a mole equivalent of 2; however, the first plateau for salicylic acid drops off at a mole equivalent of 1. This could be because salicylic acid is considered a divalent anion at a pH above 13. For both salicylic acid and thiosalicylic acid, the second plateaus drop at a mole equivalent of 8. Once again, this could indicate the presence of layered material at a pH of approximately 5.

Finally, anthranilic acid has a unique titration curve in that it does not exhibit a second plateau before a mole equivalent of 14. This could indicate that none of the layered material was broken down during the titration.

4.3.4 Meta-substituted benzoic acid titrations

A similar phenomenon can be seen in Figure 4-22 when comparing the titration curves of salicylic acid and 3-hydroxybenzoic acid. There is a small plateau that drops after a mole equivalent of 1 has been added, and then a second slight drop in pH after 2 mole equivalents of 3-hydroxybenzoic acid has been added. This could suggest, once again, that 3-hydroxybenzoic acid is divalent at a pH above 12. For this reason, it only intercalates a mole equivalent of 1, before the pH drops sharply below 12. The 3-hydroxybenzoic acid then becomes monovalent, and therefore requires 2 mole equivalents to neutralise the clay layers. The second plateau continues until 9 mole equivalents were added, which is the same as salicylic acid.

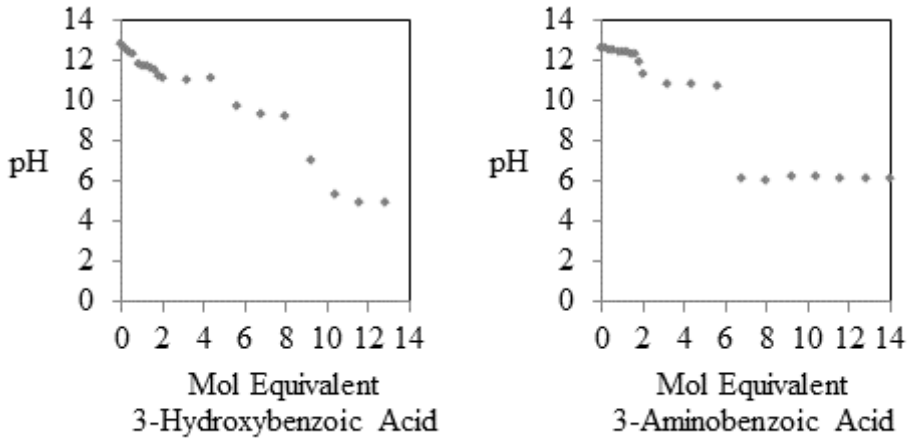

(a) (b)

Figure 4-22: Top-down titration of (a) 3-hydroxybenzoic acid and (b) 3-aminobenzoic acid

Unlike anthranilic acid, 3-aminobenzoic acid exhibits 2 very distinct plateaus. The first plateau ends after a mole equivalent of 2 mol 3-aminobenzoic acid has been added to the precursor. The second plateau, however, ends at a mole equivalent of 6.

4.3.5 Para-substituted benzoic acid titrations

The titration curve for 4-aminobenzoic acid looks similar to the curve of 3-aminobenzoic acid, as seen in Figure 4-23. There is only a slight difference in buffering pH values and the mole equivalent at which the second plateau ends. The second plateau for 4-aminobenzoic acid ends after a mole equivalent of 8 has been added to the solution, as opposed to 6.

The 4-hydroxybenzoic acid titration curve also resembles that of 3-hydroxybenzoic acid, except for the fact that the second small plateau continues until a mole equivalent of 4, instead of 2. The first small plateau reaches a mole equivalent of 1, which again could indicate the presence of a divalent anion at a high pH value. The fall of the pH from above 10 to approximately 6 is also a lot more gradual than with 3-hydroxybenzoic acid. This indicates a reduced ability of the LDH to buffer the anion.

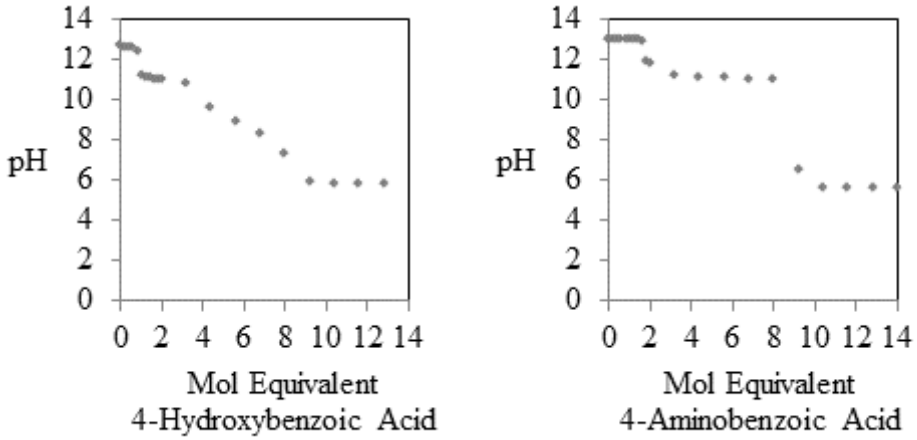

(a) (b)

Figure 4-23: Top-down titration of (a) 4-hydroxybenzoic acid and (b) 4-aminobenzoic acid

The pH of pure katoite in all the titrations was recorded as approximately 13. The fact that the precursor has an extremely high pH means that excess acid can be added to the precursor before the pH drops below 10. This is true even for a strong acid, like hydrochloric acid. For this reason, it is not essential to adjust the pH for most acid intercalation experiments.

4.4 Effect of substitution on intercalation

From the XRD data, it can be seen that the degree to which the anions intercalate and the optimum pH of intercalation varies between anions. The original XRD curves with peak identifications have been attached in Appendix A. A total of 3 runs (shown in Appendix B) were taken for each FTIR curve, and the average of all three runs was shown as the final FTIR pattern.

4.4.1 Benzoic acid intercalations

When benzoic acid was intercalated at a pH of 12.32 and 11.24, there is a new unidentified primary peak present on the XRD pattern to the left of the primary hydrocalumite peak (Figure 4-24). The new primary peak is more intense at the lower pH, and there is also no katoite present in the sample. This may be due to the fact that the amount of benzoic acid added to reach a pH of 12.32 was less than the stoichiometric amount required to fully react with the precursor to form an LDH.

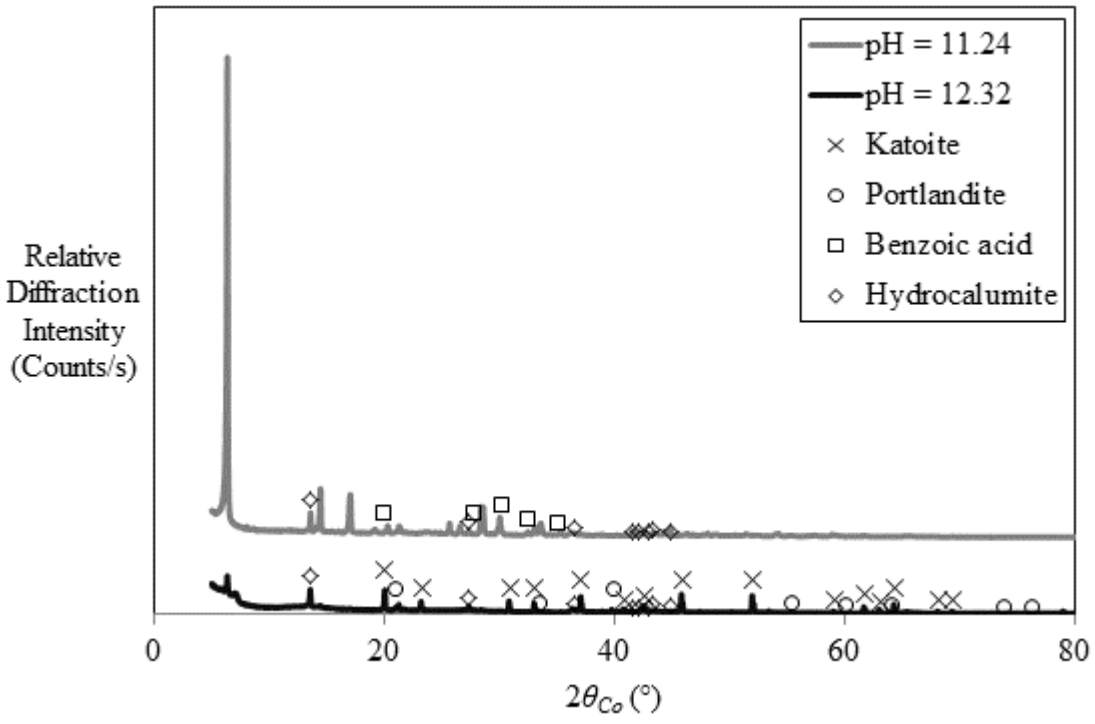

Figure 4-24: XRD patterns for benzoic acid intercalated at different pH values

At both pH values, there is a new primary peak at a 2θ value of 6.35°. This corresponds to a d_{003} spacing (d-spacing) of 16.16 Å, which is a significant increase in d-spacing from that of hydrocalumite. The thickness of a Ca/Al LDH layer is 2.02 Å (Rousselot *et al*, 2002), and according to Avogadro (*sa*), the height of the benzoate anion is 6.17 Å. For this reason, it can be concluded that benzoate intercalated in a bilayer configuration, as shown in Figure 4-25. At a pH of 11.24, there is also a new peak present at an angle of 30°, which corresponds to the primary peak of benzoic acid. This indicates that not all of the benzoic acid intercalated in the LDH at a lower pH. Both samples have a small amount of carbonate contamination in the form of hydrocalumite.

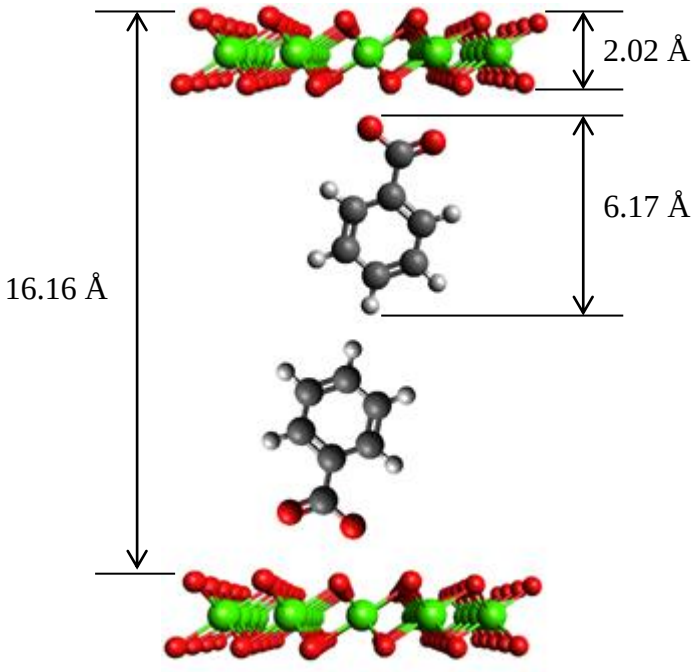

Figure 4-25: Configuration of benzoate in the interlayer

Up to a temperature of 110 °C, the mass loss indicated on the TGA curve can be attributed to the loss of free water. For the sample prepared at a pH of 12.32, there is 7 wt.% free water, while the sample prepared at a pH of 11.24 only contains 4 wt.% free water (Figure 4-26). Since the same amount of precursor was used for each sample, any extra mass loss above 110 °C is either attributed to excess unbound anion or excess water trapped in the interlayer. Above a temperature of 250 °C, all interlayer water has been eliminated; therefore, any difference in mass loss is attributed to a difference in anion content. Since the boiling point of

benzoic acid is approximately 250 °C (Perry & Green, 1999: 2 - 61), it can be assumed that above this temperature, all the free benzoic acid has evaporated from the sample.

From 250 °C to 800 °C, the sample aged at a pH of 12.32 loses 28 wt.%, while the sample aged at a pH of 11.24, loses 53 wt.% by weight. The increase in mass loss is due to the fact that there is more bound anion present in the lower pH sample. If the anion was intercalated in the correct stoichiometric ratio, the mass lost due to the LDH between 250 °C and 800 °C would be 53 wt.%, which corresponds to the results at a pH of 11.24. Due to the fact that all the katoite has reacted, the TGA analysis shows a full conversion to LDH.

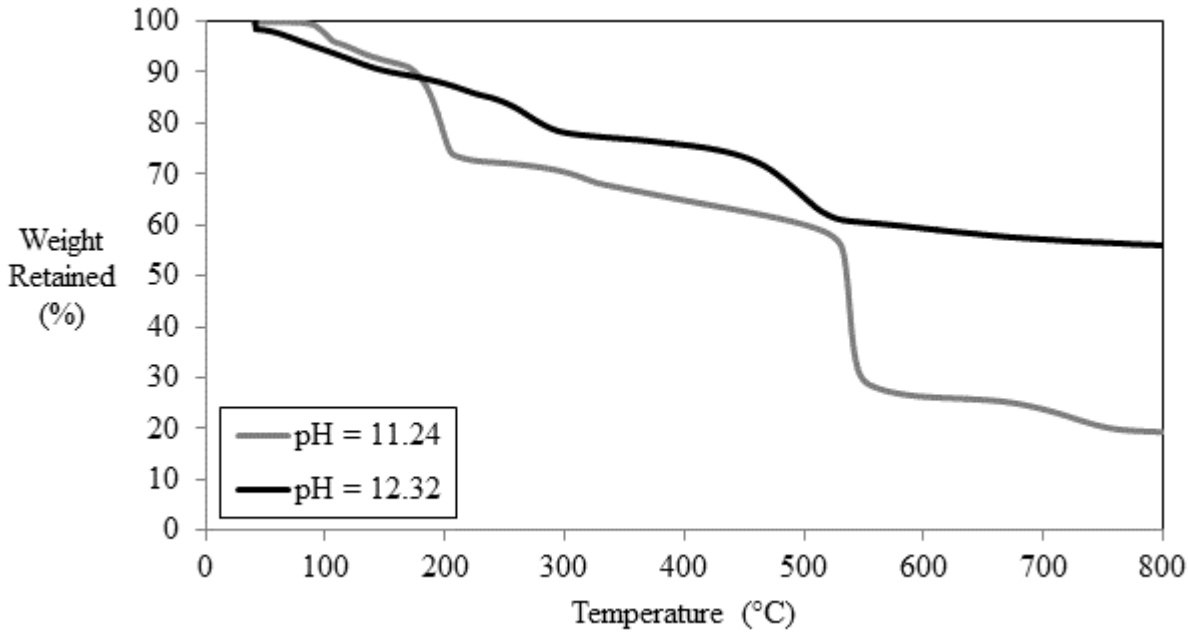

Figure 4-26: TGA curves for benzoic acid intercalated at different pH values

The FTIR curve of benzoate intercalated into a Ca/Al LDH at a pH of 11.24, as shown in Figure 4-27, is in line with the FTIR curves reported in literature (Matusinovic *et al*, 2008). The peaks present between 650 cm^{-1} and 720 cm^{-1} are associated with mono-substituted benzene (i.e. benzoic acid). There is a small peak present at 850 cm^{-1}, which is associated with M-O bonds; however, these bonds could also be due to the presence of katoite. The C-O bond band associated with alcohols can be seen at a wavelength of 1 030 cm^{-1}. The peaks from 1 435 cm^{-1} – 1 440 cm^{-1} and 1 600 cm^{-1} – 1 550 cm^{-1} are associated with the symmetrical and asymmetrical stretching of the COO^- group, which proves that benzoic acid is dissociated. Finally, the peaks present between 3 650 cm^{-1} and 2 650 cm^{-1} can be attributed

to the O-H and C-H stretching. All these peaks are more intense at a lower pH. This, once again, confirms that, even though benzoic acid intercalated at a pH of 12.32, there is more intercalated material present at a pH of 11.24. Even though the XRD pattern indicates the presence of katoite in the sample aged at a pH of 12.32, there are no katoite bands present in the FTIR graph.

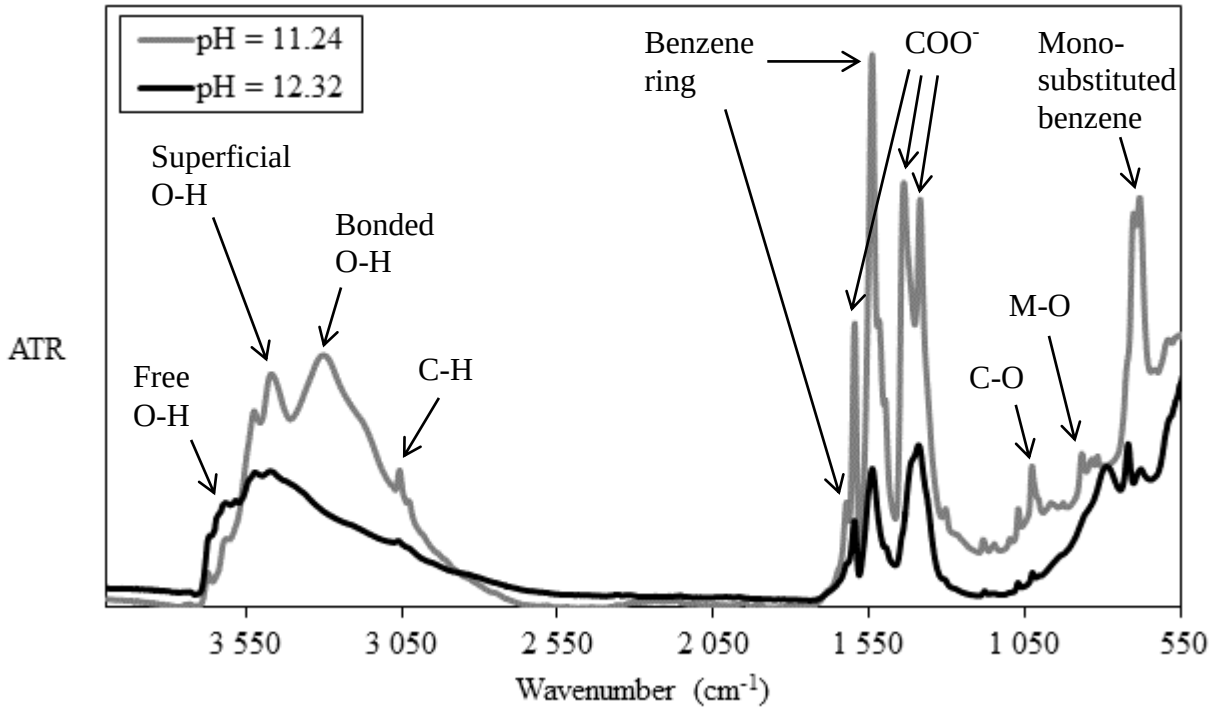

Figure 4-27: FTIR curves for benzoic acid intercalated at different pH values

4.4.2 Ortho-substituted benzoic acid intercalations

Unexpected results arise when intercalating salicylic acid at different concentrations (Figure 4-28). At a very low salicylic acid concentration (high pH), there is a new primary peak that occurs at a 2θ value of 9.50°. This corresponds to a d-spacing of 10.81 Å. This peak becomes even more intense at a higher salicylic acid concentration (pH = 11.11). However, there are two more peaks that occur at angles of 7.66° and 6.13°. These angles correspond to a new d-spacing of 13.40 Å and 16.74 Å.

The three new primary peaks could indicate that salicylic acid intercalates at 3 different configurations in the interlayer. For each different d-spacing, there is a different configuration

of salicylate in the interlayer (Figure 4-28). Using the calculated d-spacing from the XRD pattern, the 3 different configurations that were most likely present in the LDH samples are shown in Figure 4-29. When the d-spacing is 10.81 Å, salicylate can intercalate in a monolayer configuration, since the height of the salicylate anion is 6.18 Å (Avogadro, *sa*). This means that when the d-spacing increased to 13.40 Å, the salicylate anions must have an overlapping configuration, since there is not enough space for a bilayer. However, as the d-spacing increases to 16.74 Å, there is enough space for a bilayer configuration of salicylate anions. Finally, at a very low pH of 3.69, the salicylic acid peaks become dominant in the XRD pattern. This is because an excess of salicylic acid was added to reach a pH of 3.69, and the LDH was unable to accommodate the excess acid. There is, however, a new primary peak at 10.35°, which corresponds to a new d-spacing of 9.93 Å, which will incur an overlapping configuration. In the higher pH samples, there is carbonate contamination in the form of hydrocalumite. The hydrocalumite contamination becomes less with decreasing pH, since less carbon dioxide dissolves at a lower pH. However, the amount of unreacted katoite is greater at a lower pH.

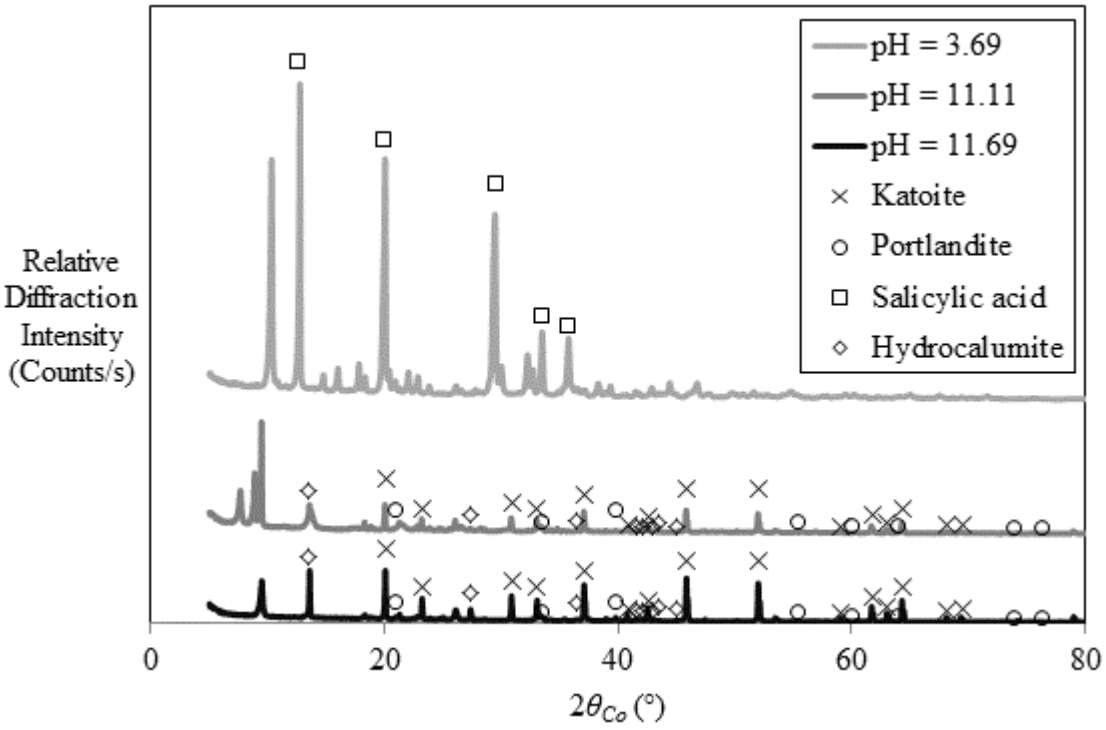

Figure 4-28: XRD patterns for salicylic acid intercalated at different pH values

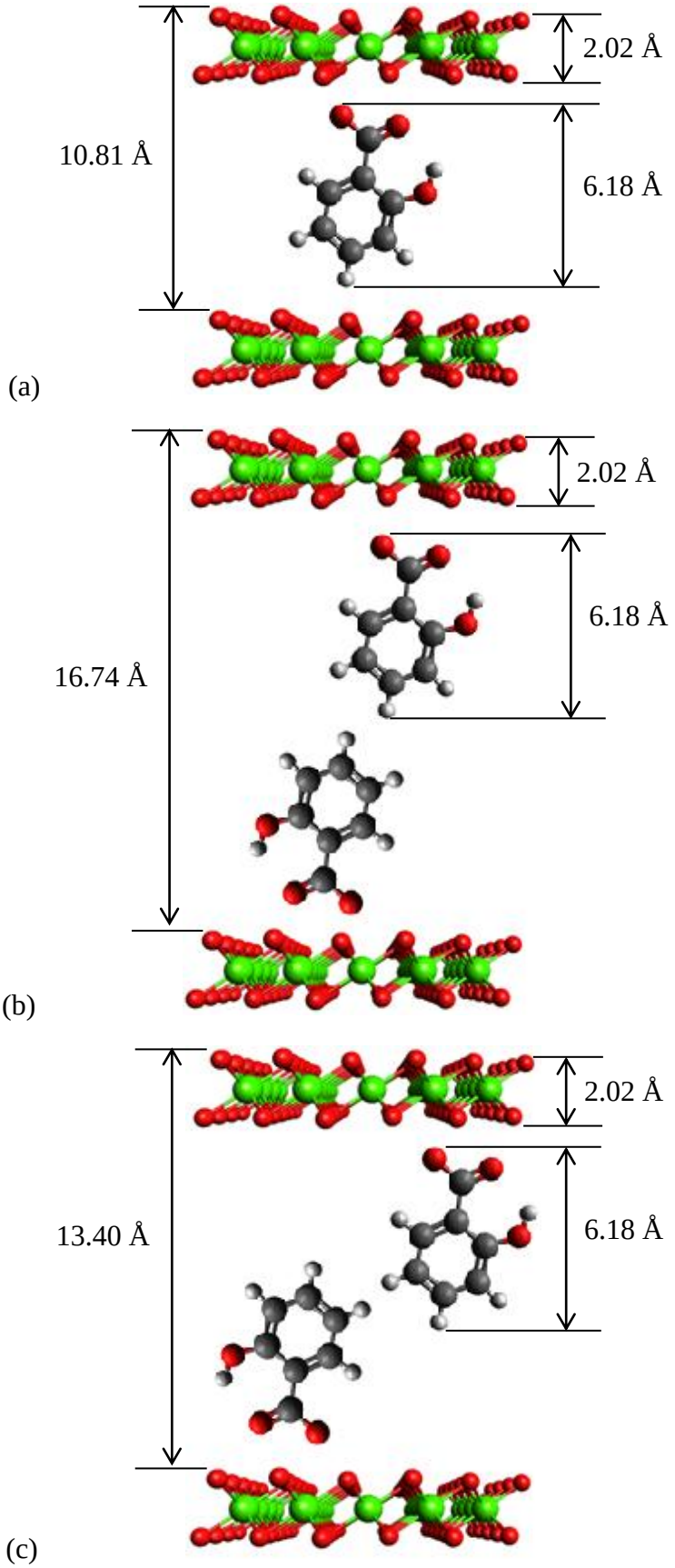

Figure 4-29: Salicylate in the interlayer: (a) monolayer (pH = 3.69, 11.11 and 11.69); (b) bilayer (pH = 11.11) and (c) overlapping (pH = 11.11) configuration

The XRD results indicate that there is no pure crystalline salicylic acid present in the sample at a pH of 11.11. However, there is a greater mass loss on the TGA curve than at a pH of 11.69 (Figure 4-30). At a pH of 11.69, there is only 1 wt.% extrinsic water, while at a pH of 11.11 and 3.69, the amount of extrinsic water is 4 wt.% and 5 wt.% respectively. At 250 °C, there is a higher mass loss at a pH of 11.69 than at a pH of 3.69. According to the FTIR (Figure 4-31), there is more salicylic acid present at a pH of 3.69. The boiling point of salicylic acid is 256 °C (Perry & Green, 1999: 2-73). The TGA curve indicates that there must be bound salicylic acid at a pH of 3.69, since the largest mass loss occurs at a temperature of approximately 500 °C. The mass losses between 250 °C and 800 °C at pH values of 11.69, 11.11 and 3.69 are 33 wt.%, 39 wt.% and 47 wt.% respectively. If the LDH was fully intercalated with salicylate, then the mass loss between 250 °C and 800 °C would be 55 wt.%. Therefore, none of the samples are fully intercalated.

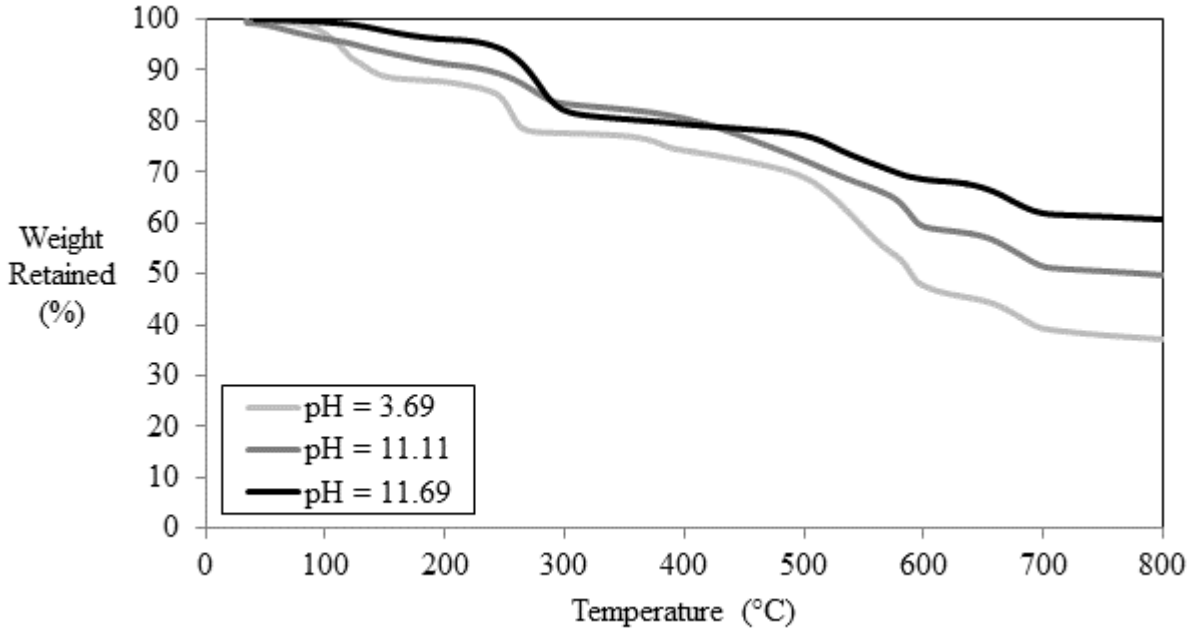

Figure 4-30: TGA curves for salicylic acid intercalated at different pH values

The FTIR curves for salicylic acid are very similar to that of benzoic acid (Figure 4-31). There are definite O-H and C-H bonds present between 2 600 cm^{-1} and 3 700 cm^{-1}. The only main difference is the presence of 1:2 substituted benzene ring bands, instead of the mono-substituted benzene ring bands. There is an increase of salicylate peak intensity with decreasing pH. The sharp characteristic peak at a wavelength of 3 650 cm^{-1} associated with

katoite is present at a pH of 11.69. The wide band between 2 750 cm^{-1} and 3 700 cm^{-1} is the most dominant at a pH of 11.11, indicating that there is more layered material present.

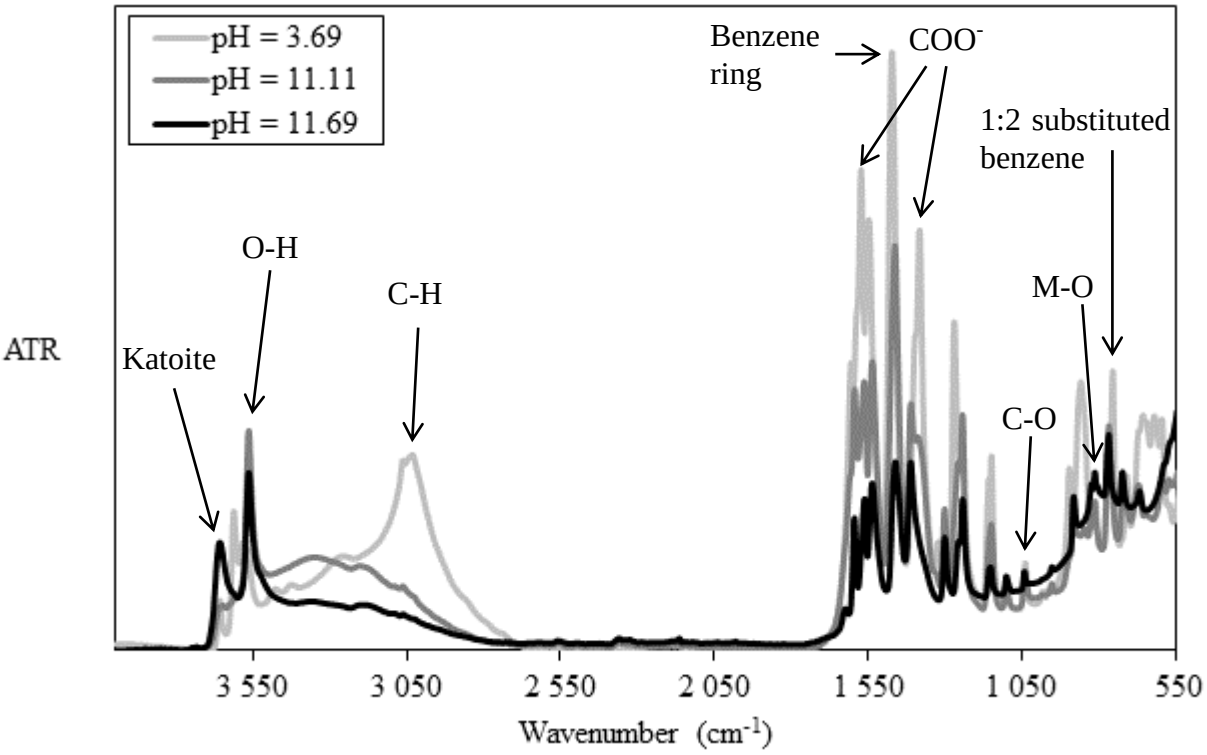

Figure 4-31: FTIR curves for salicylic acid intercalated at different pH values

Even though anthranilic acid had an irregular titration curve with only one plateau, the XRD analysis indicated that the anion intercalated at each pH value (Figure 4-32). There is a new primary peak that occurs at 7.22° for each pH. This 2θ value corresponds to a new d-spacing of 14.21 Å. Anthranilate has a maximum height of 6.13 Å (Avogadro, *sa*). The interlayer region is too large for a monolayer configuration and too small for a bilayer configuration if the anion intercalated upright. For this reason, anthranilate probably intercalated in an overlapping configuration. The other possibility is that anthranilate rotated so that the maximum width (5.64 Å) fits perfectly in the interlayer in a bilayer configuration (Figure 4-33). Due to steric hindrances of the anion, the latter configuration is unlikely.

The intensity of the primary peak decreases with decreasing pH, which indicates that less Ca/Al-anthranilate is present at a lower pH. This means that even though it is possible to form an intercalated LDH at a pH as low as 5.29, the optimum synthesis conditions are at a

pH above 11. However, the katoite and hydrocalumite peaks decrease at a lower pH. This means that the product is purer at a lower pH.

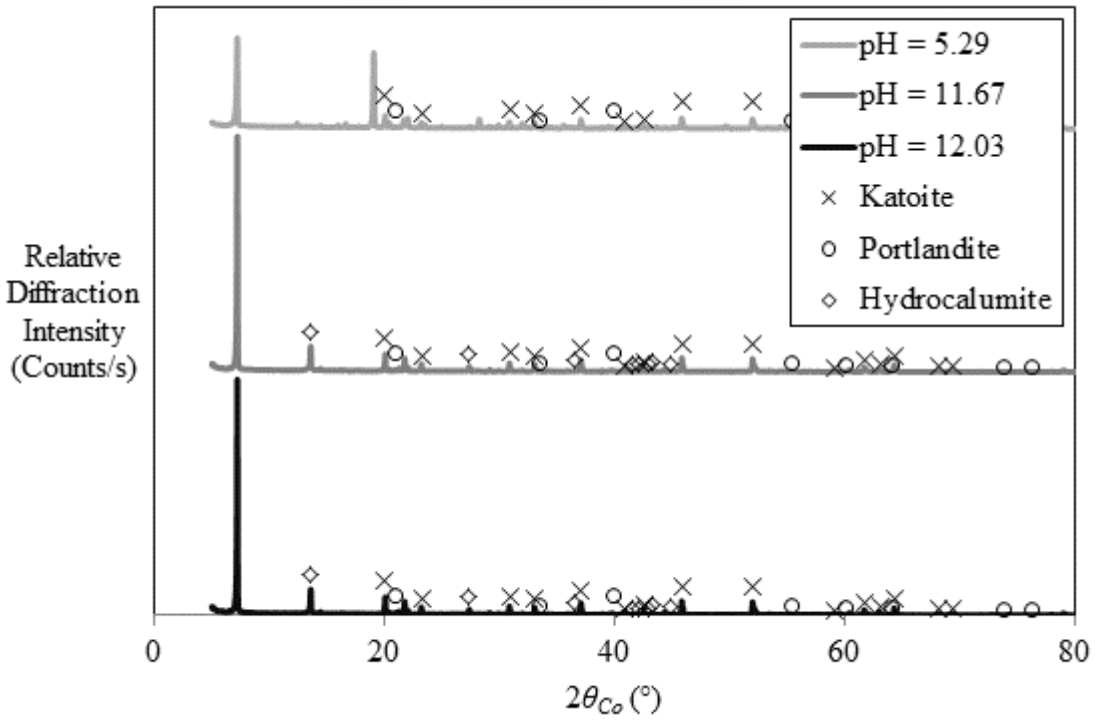

Figure 4-32: XRD pattern for anthranilic acid intercalated at different pH values

At each pH, there are only small pure crystalline anthranilic acid peaks present. The primary peak for anthranilic acid occurs at 28.21°. Therefore, any anthranilic acid or anthranilate present in the sample must be in the form of a complex, in the amorphous phase or intercalated between the layers of the LDH. Since the sample is not very amorphous, all the anthranilate added to the sample is in a new crystalline complex, or it was washed out in the filtration process. The latter explanation is highly unlikely, since the sample was only rinsed with water, and anthranilic acid is not water-soluble.

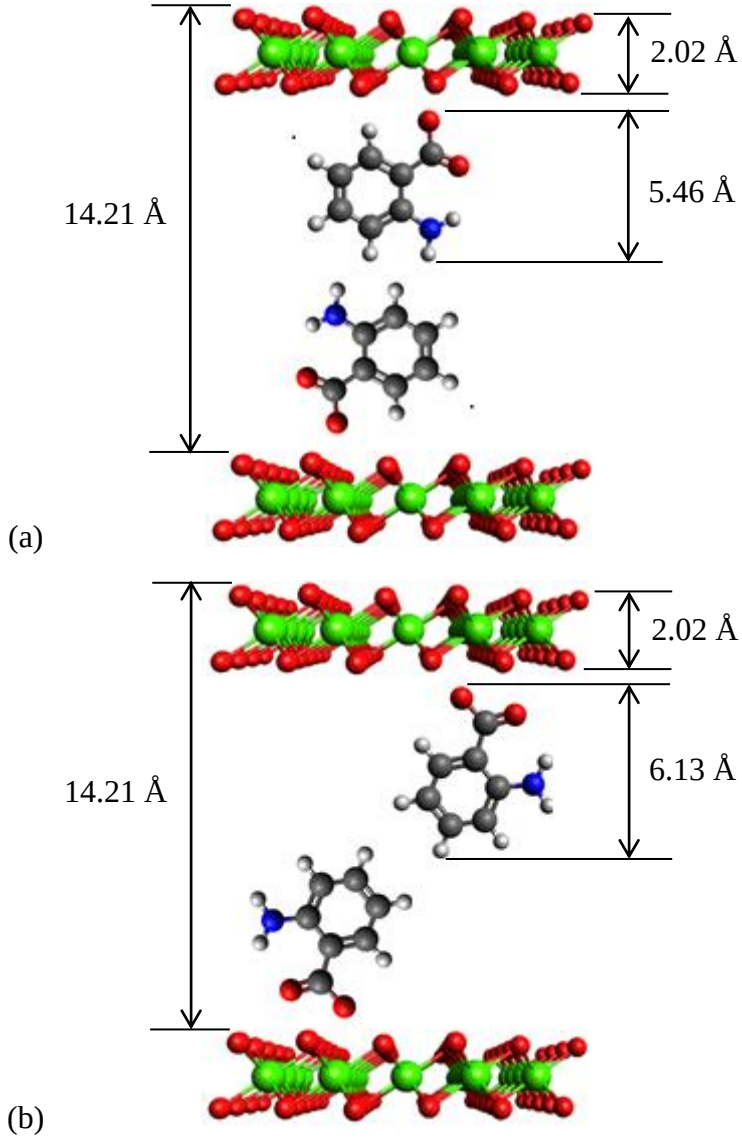

Figure 4-33: Anthranilate in the interlayer: (a) bilayer and (b) overlapping

The TGA and FTIR results are consistent with the XRD results, which can be seen in Figure 4-34 and Figure 4-35 respectively. At a pH of 12.03 and 11.67, the TGA and FTIR curves are almost identical for the two samples. The first mass loss at a temperature below 110 °C is the extrinsic water evaporating from the sample. The second mass loss step, occurring at approximately 250 °C is the evaporation of the intrinsic water and could also be due to the evaporation of unbound anthranilate. The final mass loss steps above 250 °C are attributed to the loss of the interlayer anion and the dehydroxylation of the sample. The largest difference between the three TGA curves is the sample aged at a pH of 5.29 has a major mass loss at a temperature of approximately 180 °C. The mass loss is most likely the loss of excess anion from the sample.

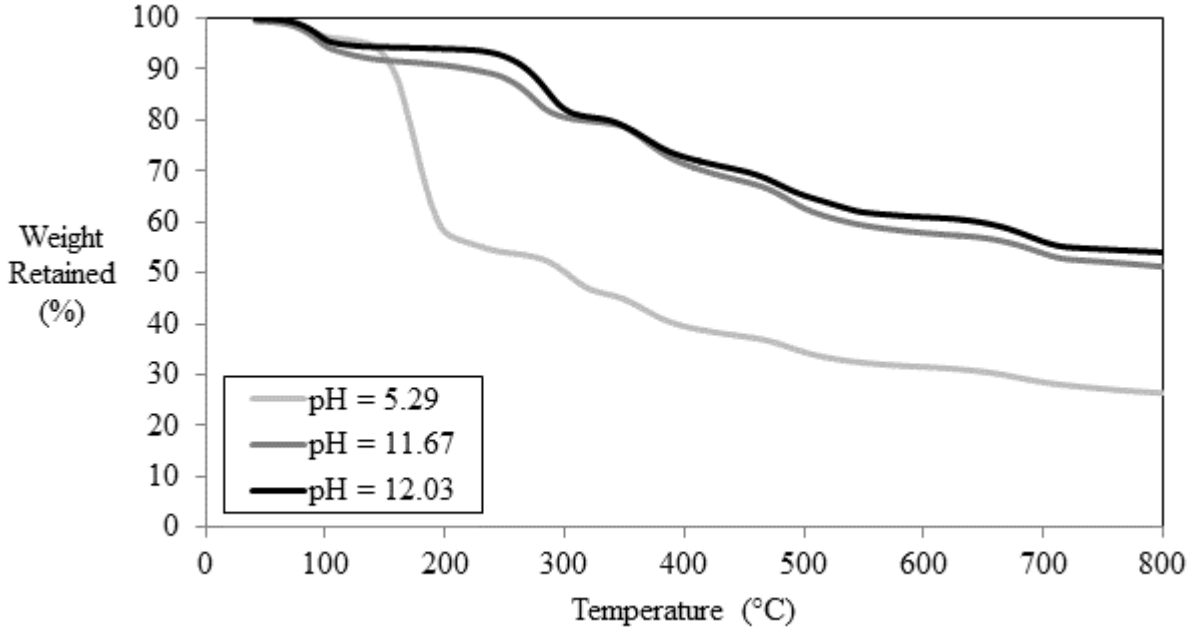

Figure 4-34: TGA curves for anthranilic acid intercalated at different pH values

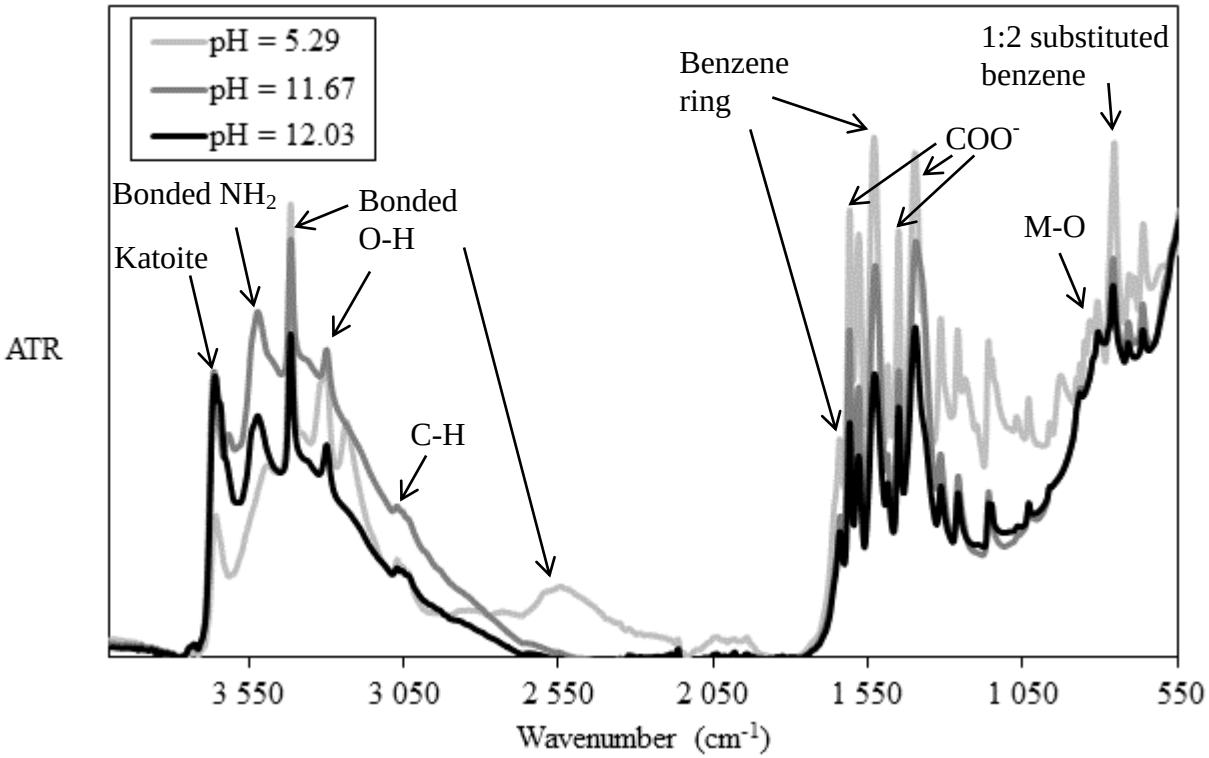

Figure 4-35: FTIR curves for anthranilic acid intercalated at different pH values

Between a temperature of 250 °C and 800 °C at pH values of 12.03 and 11.67, the samples lose 38 wt.% and 37 wt.% mass respectively. The sample at a pH of 5.29, on the other hand, loses 28 wt.%. This indicates that the samples intercalated at pH values of 12.03 and 11.67 have similar conversions, while the sample at a pH of 5.29 has a lower conversion. At full conversion, the mass loss would have been 55 wt.%; therefore, none of the samples have fully converted to LDH. At a pH of 5.29, there are more intense anthranilic acid bands in the FTIR curve. However, the decrease in O-H band intensities proves that even though there is still LDH in the sample, the amount of LDH has decreased.

Thiosalicylic acid did not intercalate as readily as the other organic anions. Furthermore, the crystallinity of the Ca/Al-thiosalicylate LDH was not as high as the other organically modified LDHs (Figure 4-36).

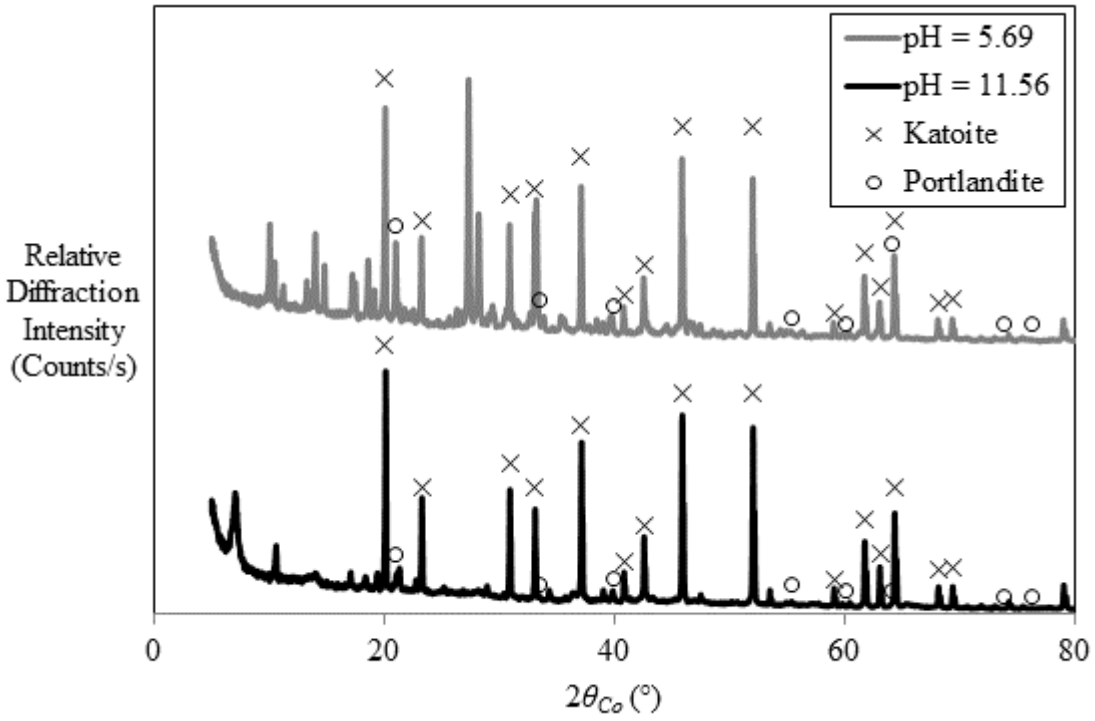

Figure 4-36: XRD patterns for thiosalicylic acid intercalated at different pH values

At a pH of 11.59 and 5.69, thiosalicylic acid only intercalated partially, and there is still a lot of unreacted katoite and portlandite in the sample. The peaks in the sample also do not correspond to the pure thiosalicylic XRD pattern. However, the sample does have large amounts of amorphous material present, meaning that thiosalicylic acid might be present in

an amorphous form. The different peaks that are present at different pH values indicate that thiosalicylic acid intercalates at different orientations depending on the pH. The broad primary reflection occurs at an angle of 7.00°. This corresponds to a d-spacing of 14.66 Å. Thiosalicylate has a height of 6.15 Å and a width of 5.01 Å (Figure 4-37); therefore, the anion most probably intercalated in one of the two ways proposed for anthranilate (Figure 4-33).

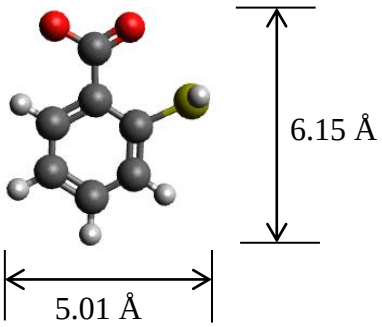

Figure 4-37: Dimensions of thiosalicylate (Avogadro, *sa*)

Figure 4-38 shows the TGA curves of thiosalicylic acid. These curves are not characteristic of an LDH material. The first mass loss is well-defined; however, both have very gradual mass losses after the first bulk mass loss. All the mass lost after the first bulk mass loss can be attributed to the loss of the organic species from the sample and dehydroxylation.

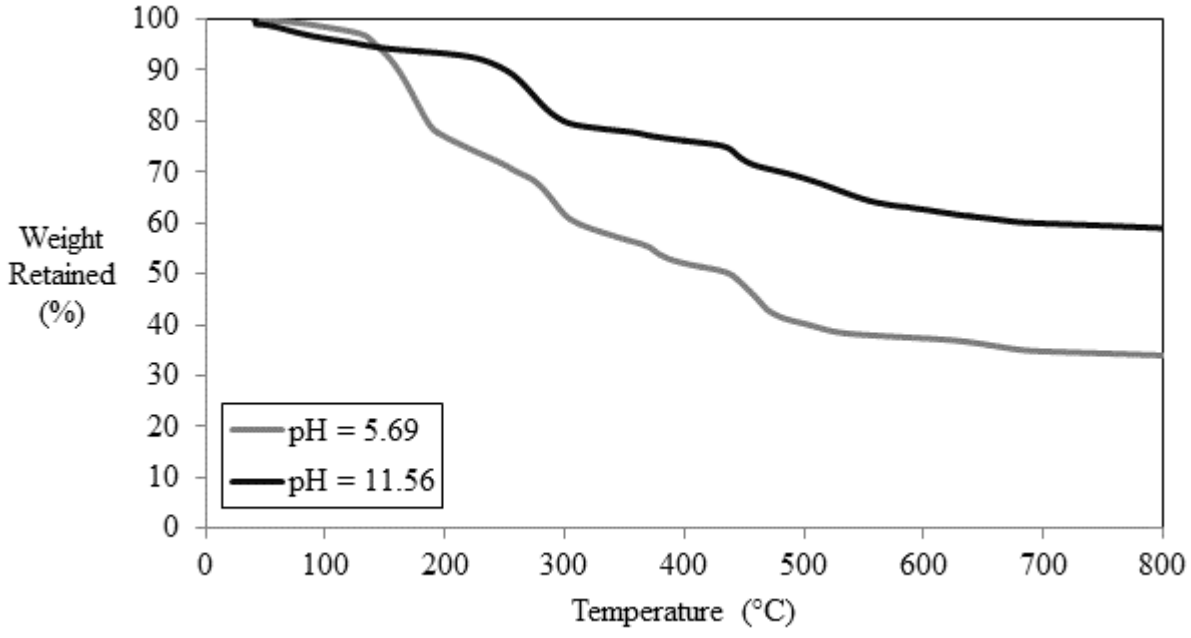

Figure 4-38: TGA curves for thiosalicylic acid intercalated at different pH values

There is definitely thiosalicylic acid in both samples, as seen on the FTIR pattern (Figure 4-39). Both the TGA curve and the FTIR pattern support the fact that there is more thiosalicylic acid present in the sample at a pH of 5.69. The thiosalicylic acid bands on the FTIR pattern are distinctly present at a pH of 11.56; however, they are more intense at the lower pH. These bands could be from the small amount of thiosalicylic acid that intercalated, or it could be present in the amorphous phase of the samples. Even though the FTIR does indicate some LDH material at a pH of 11.56, the peaks are not as clear as with the other anions. The wide O-H band is not present at a pH of 5.96, which indicates that the layered structure was broken apart at a low pH. There is, however, more thiosalicylate anion present in the sample. At a pH of 11.59, there is also a distinct sharp katoite band present at 3 650 cm^{-1}. Once again, this concludes that thiosalicylic acid does not intercalate as readily as the other organic anions.

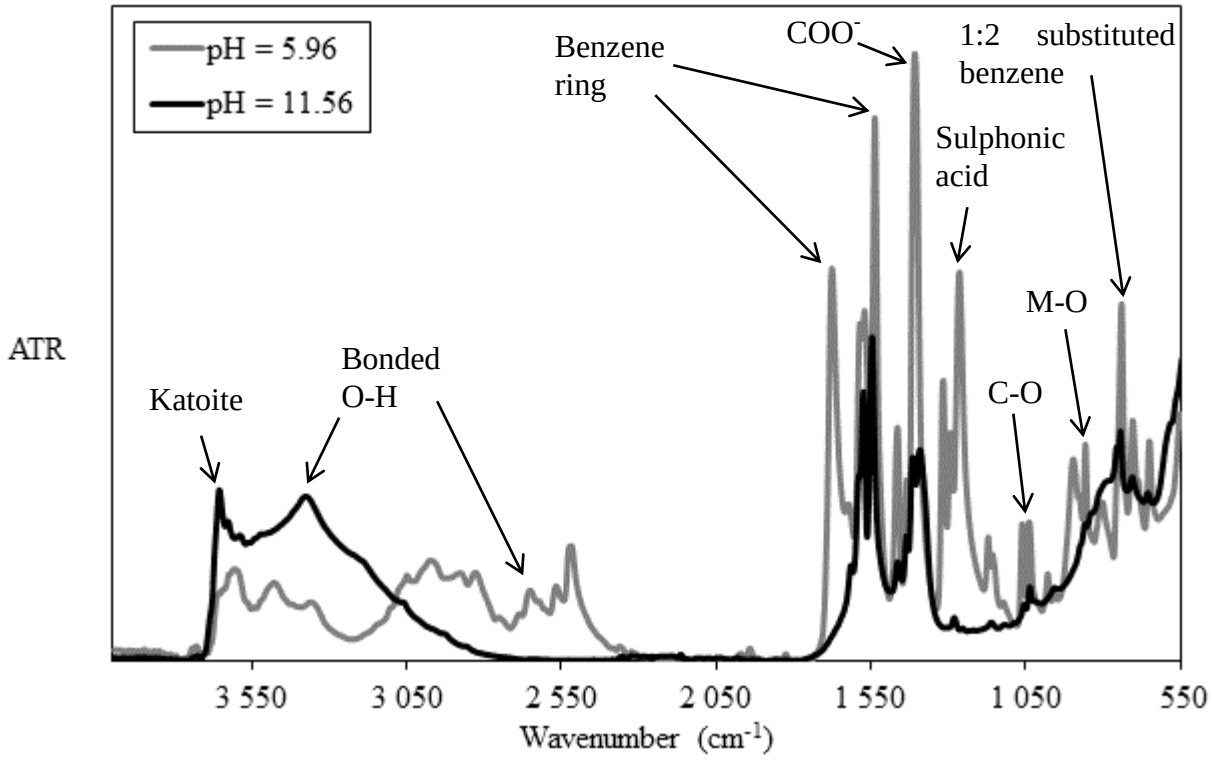

Figure 4-39: FTIR curves for thiosalicylic acid intercalated at different pH values

4.4.3 Meta-substituted benzoic acid intercalations

The XRD patterns for 3-hydroxybenzoic acid intercalated at different pH values are shown in Figure 4-40. At a pH above 12, the anion did not intercalate to a large extent, even though there is a peak starting to form at a 2θ value of 11.83°. When more 3-hydroxybenzoic acid is added to reach a pH of 11.12, there is a clear new peak at 11.83°. This corresponds to a new d-spacing of 8.68 Å. This means that 3-hydroxybenzoate did not intercalate upright, as shown in Figure 4-41. The anion most probably intercalated at a 90° angle to the molecule shown in Figure 4-41. The anion definitely intercalated in a monolayer configuration. At a pH of 4.98, there is a distinctive new peak at 10.60°, which corresponds to a d-spacing of 9.69 Å. 3-Hydroxybenzoic acid would, once again, have intercalated in a monolayer configuration. Since the d-spacing is slightly larger than the previous d-spacing, 3-hydroxybenzoic acid could have intercalated upright, as indicated in Figure 4-41. The peak at 11.83° has disappeared entirely at a pH of 4.98. None of the peaks in the XRD patterns correspond to those of pure crystalline 3-hydroxybenzoic acid, proving that if 3-hydroxybenzoic acid is present in the sample, it must either be in the amorphous phase, in a new complex or between the layers of the LDH.

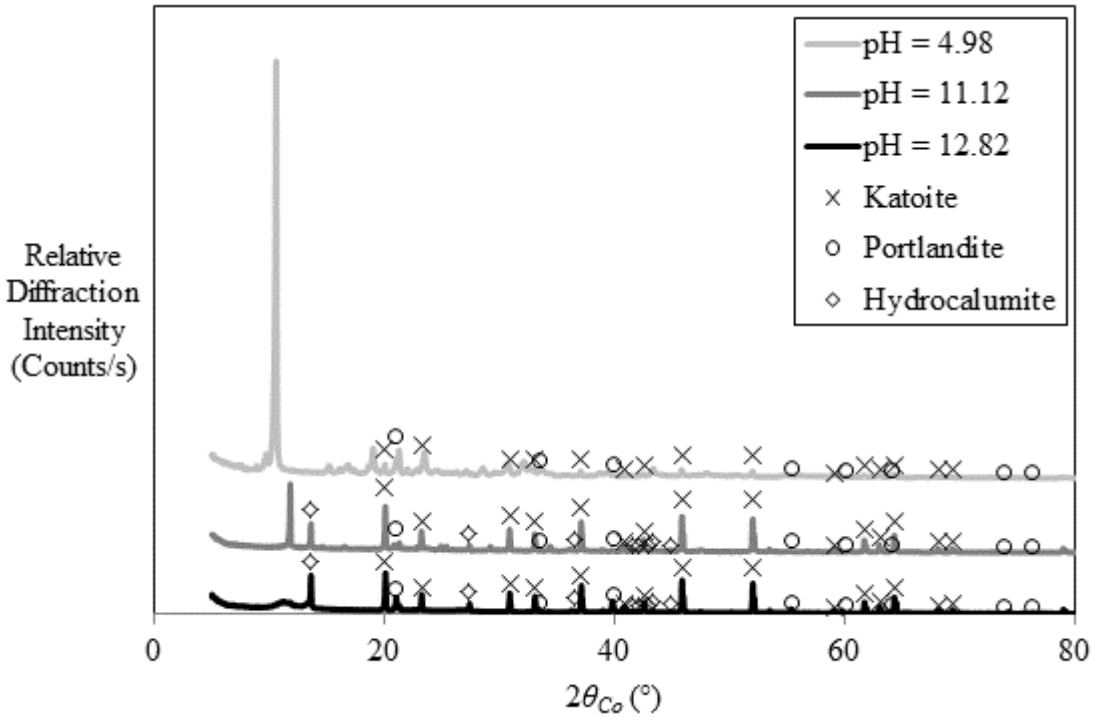

Figure 4-40: XRD patterns for 3-hydroxybenzoic acid intercalated at different pH values

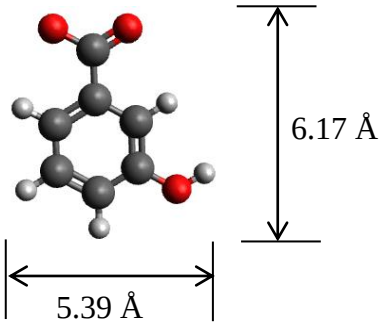

Figure 4-41: Dimensions of 3-hydroxybenzoate (Avogadro, *sa*)

The TGA curves for 3-hydroxybenzoic acid at a pH of 12.82 and 11.12 are almost identical (Figure 4-42). The mass loss between 250 °C and 800 °C for both samples is approximately 25 wt.%, which is less than the fully-intercalated mass loss of 55 wt.%. For the sample aged at a pH of 4.98, there is a significant increase in mass loss at a temperature of around 250 °C. This mass loss is most likely attributed to an increase in unbound anion. Between 250 °C and 800 °C, the sample aged at a pH of 4.98 loses 35 wt.% of its mass. This indicates an increase in bound 3-hydroxybenzoate in the sample, supporting the results in the XRD pattern.

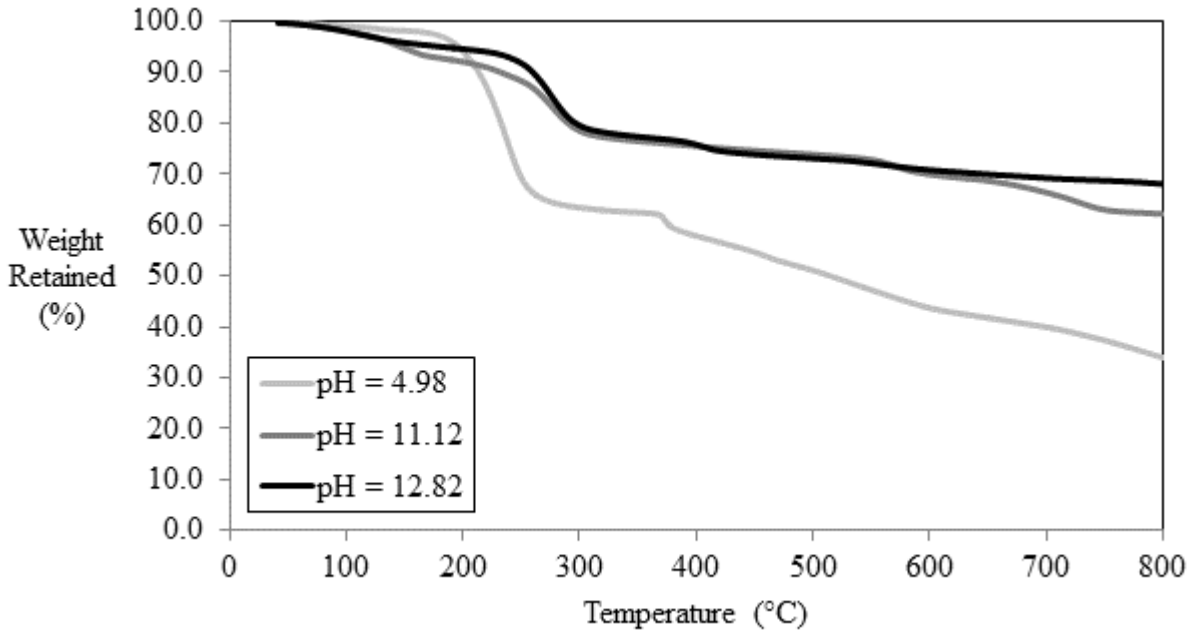

Figure 4-42: TGA curves for 3-hydroxybenzoic acid intercalated at different pH values

The FTIR curves for pH values of 11.12 and 12.82 are also almost completely identical, except for one peak at 2 500 cm^{-1} (Figure 4-43). The extra peak could be associated with O-H

bonds, indicating more layered material in the sample. The FTIR curves also indicate the presence of 3-hydroxybenzoic acid in the sample, with bands that occur between 650 cm^{-1} and 950 cm^{-1}. However, there is only one mass loss on the TGA curves. This indicates that either the water loss and dehydroxylation steps occur simultaneously, or it indicates that there is no layered material present in the sample. Analysis of the XRD curves for the two pH values suggests that the former argument seems the most likely. Both FTIR curves show unreacted katoite in the samples. The 3-hydroxybenzoate peaks are more intense at a pH of 4.98.

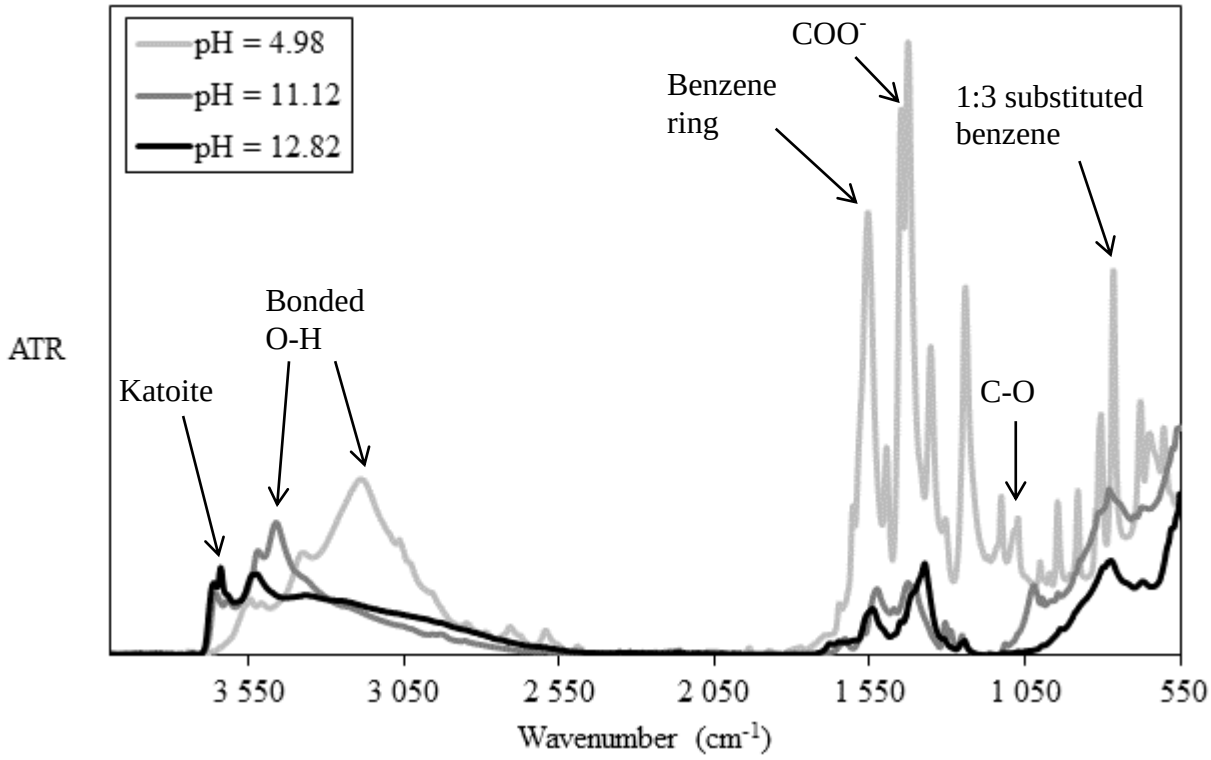

Figure 4-43: FTIR curves for 3-hydroxybenzoic acid intercalated at different pH values

There is a definite shift of the primary peak to a 2θ value of 7.32 when intercalating 3-aminobenzoic acid at a low and a high pH (Figure 4-44). This corresponds to a new d-space of 14.02 Å, which is 0.2 Å smaller than the d-spacing of anthranilate-intercalated Ca/Al LDH. Due to the similarity of their dimensions (Figure 4-45), the two anions intercalated at similar orientations (Figure 4-33). In both samples, there was no unreacted 3-aminobenzoic acid present in the crystal phase. There is very little amorphous material in the sample; therefore, all 3-aminobenzoic acid in the sample must be in a new crystalline complex. As with anthranilic acid, it is possible to intercalate 3-aminobenzoic acid at a pH as low as 4.98;

however, decreasing the pH disintegrates part of the LDH. For this reason, it is recommended to keep the pH above 10. Once again, for both anions, the amount of katoite and hydrocalumite at a lower pH is less than at a higher pH. For this reason, a low pH value can be used to synthesise samples with higher purity.

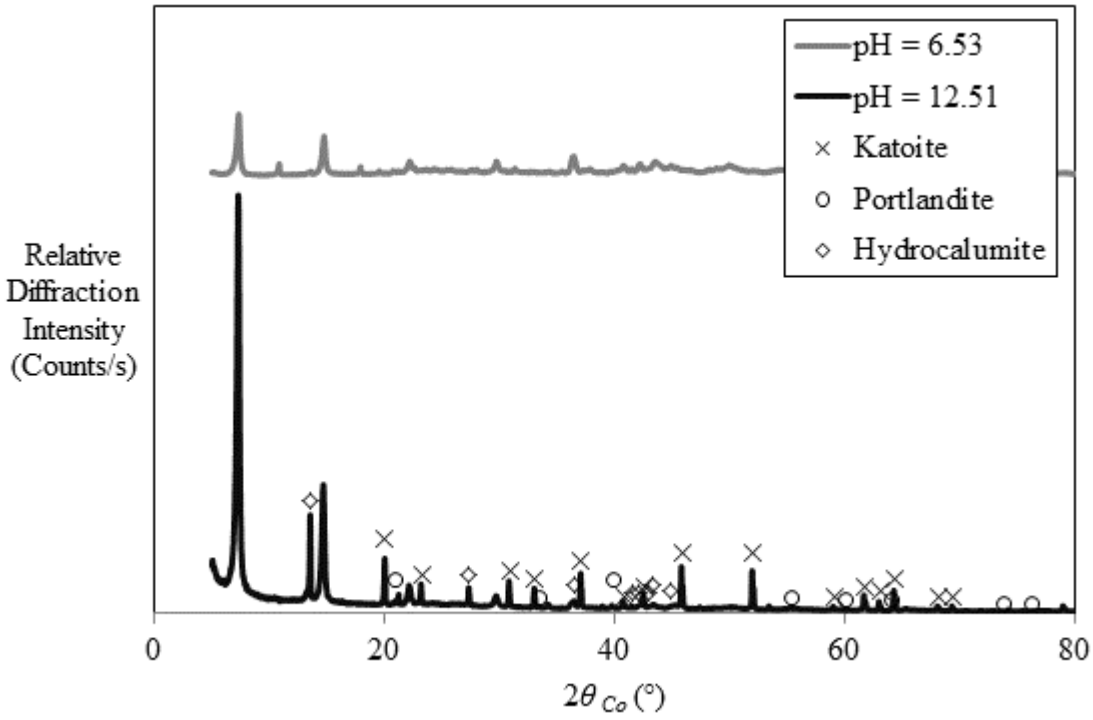

Figure 4-44: XRD patterns for 3-aminobenzoic acid intercalated at different pH values

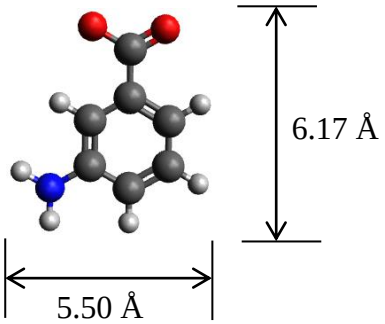

Figure 4-45: Dimensions of 3-aminobenzoate (Avogadro, *sa*)

There is almost no difference between the TGA and FTIR curves for 3-aminobenzoic acid intercalated at the 2 different pH values (Figure 4-46 and Figure 4-47 respectively). This contrasts the XRD results, which shows a massive difference in crystallinity between the two pH values. According to the XRD results, there should be more LDH present at the higher

pH. Both samples lose roughly 25 wt.% of their mass between 250 °C and 800 °C. If the sample was fully intercalated, there would have been a 55 wt.% mass loss.

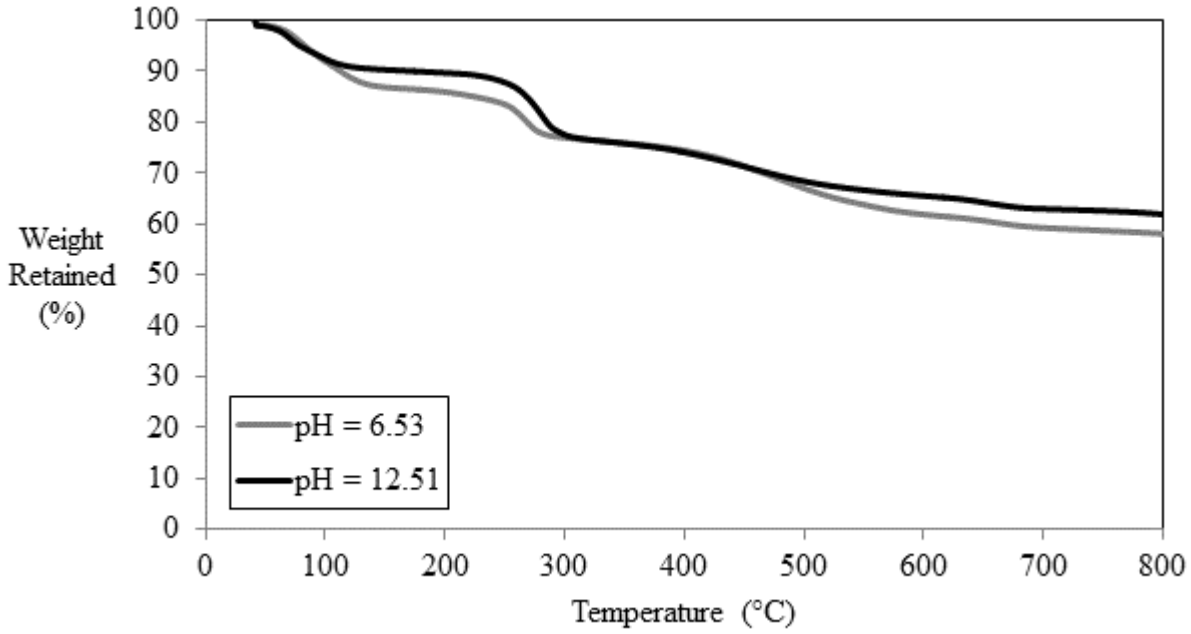

Figure 4-46: TGA curves for 3-aminobenzoic acid intercalated at different pH values

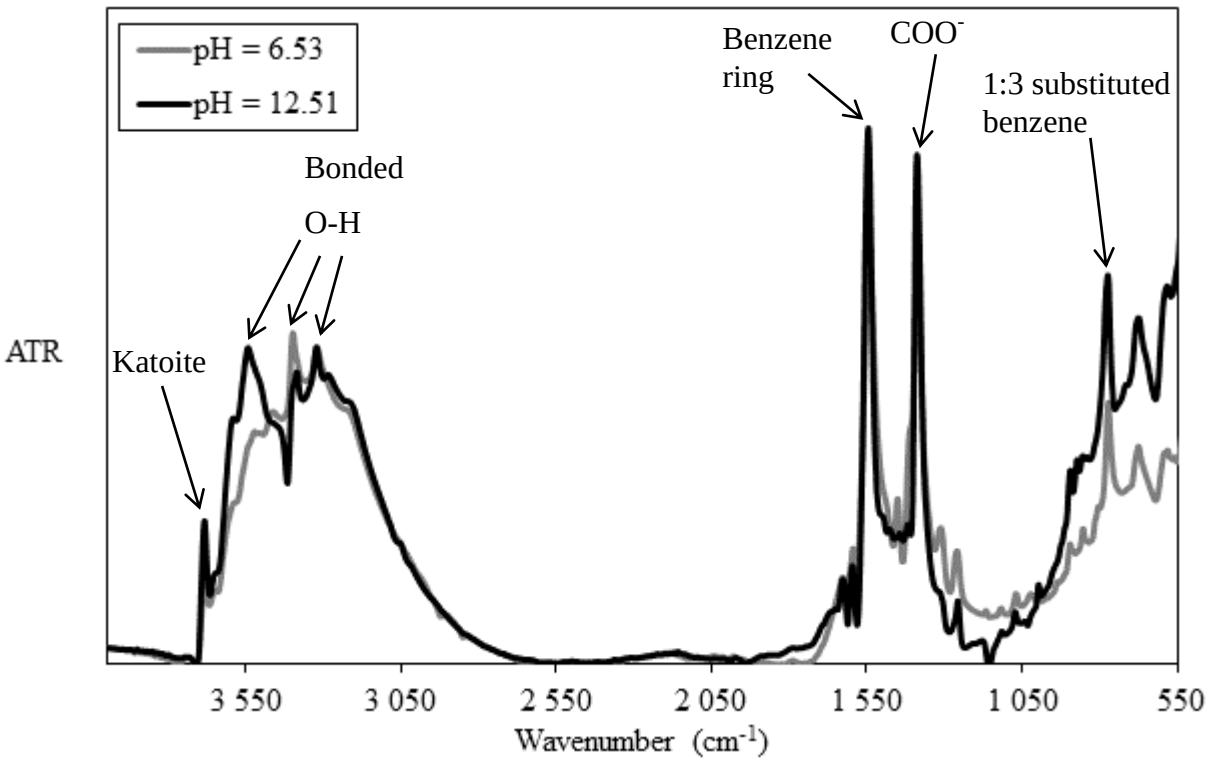

Figure 4-47: FTIR curves for 3-aminobenzoic acid intercalated at different pH values

The FTIR curves support the idea that there is still 3-aminobenzoic acid present in the sample. However, there are no peaks present in the XRD that correspond to pure crystalline 3-aminobenzoic acid. Both samples have high levels of crystallinity, which leads to the conclusion that most of the 3-aminobenzoic acid must have formed a new complex, and could be intercalated between the layers of the LDH.

4.4.4 Para-substituted benzoic acid intercalations

As seen from Figure 4-48, the intercalation of 4-hydroxybenzoic acid was not as successful as the other organic acids. At a pH of 12.26, there is a new primary peak, which is also very amorphous. The only crystalline peaks at the high pH are hydrocalumite and precursor peaks. The new amorphous peak corresponds to a new d-spacing of 8.37 Å ($2\theta = 12.37°$). The dimensions of 4-hydroxybenzoate are shown in Figure 4-49. The height of the anion is 7.12 Å. For this reason, the anion must have intercalated horizontally, or at an angle.

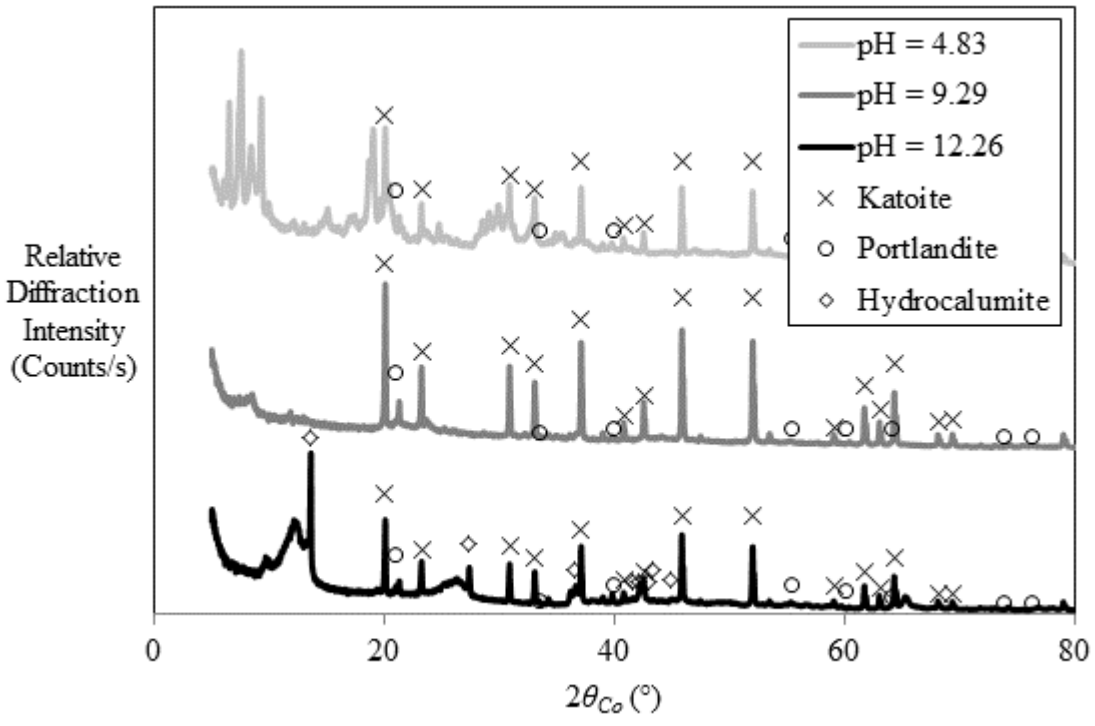

Figure 4-48: XRD patterns for 4-hydroxybenzoic acid intercalated at different pH values

At a pH of 9.29, there is almost only precursor materials left in the crystalline phase. Finally, at a pH of 4.83 there are several new crystalline peaks, none of which are associated with

pure crystalline 4-hydroxybenzoic acid. The crystalline peaks are between 6.52° and 9.29°; therefore, the new interlayer space varies between 15.74 Å and 11.05 Å.

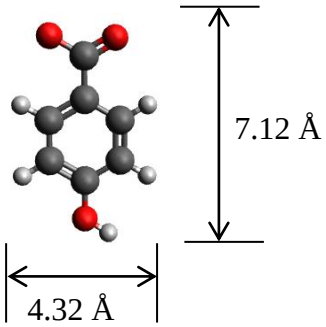

Figure 4-49: Dimensions of 4-hydroxybenzoate (Avogadro, *sa*)

Since the intercalation was unsuccessful at a pH of 9.29, no further analyses were performed on the sample. According to the TGA curve (Figure 4-50), there is a lot more anion present at a pH of 4.83 than 12.26. The large mass loss at a pH of 4.83 below 300 °C is due to water and unbound 4-hydroxybenzoic acid. Between 250 °C and 800 °C, the sample aged at a pH of 12.26 loses 19 wt.% of its mass, while the sample aged at a pH of 4.83 loses 46 wt.% of its mass. At full conversion, the mass loss between these temperatures would be 55 wt.%. For this reason, the conversion at a high pH is extremely low.

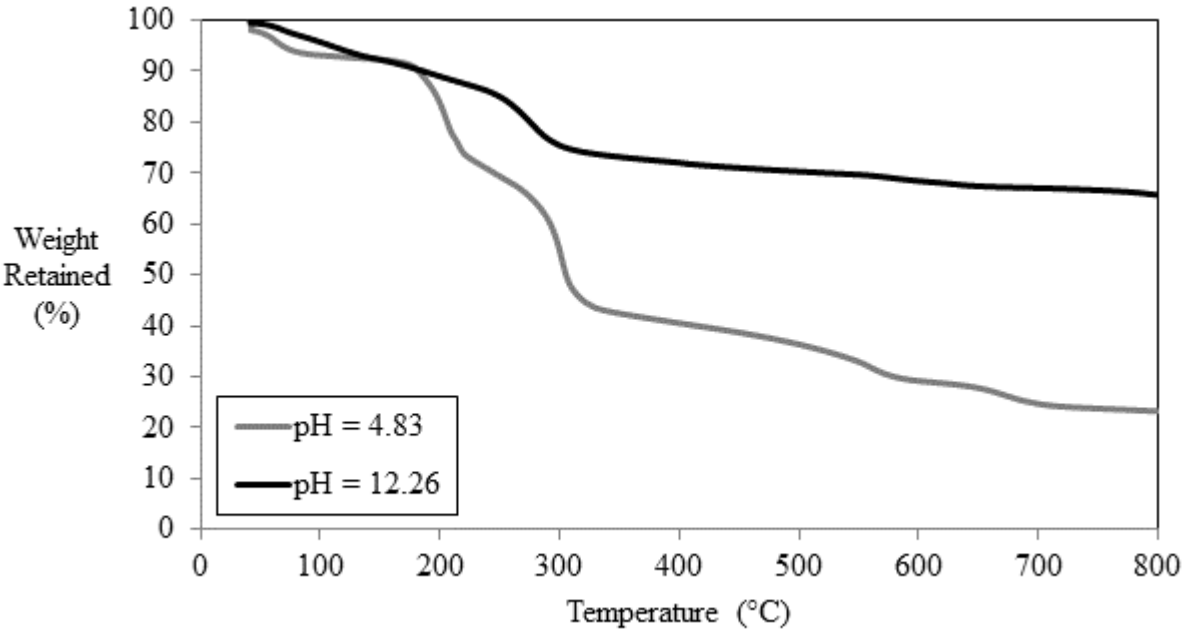

Figure 4-50: TGA curves for 4-hydroxybenzoic acid intercalated at different pH values

The FTIR results support this fact (Figure 4-51), as there are very weak OH and 4-hydroxybenzoate bands. The TGA curve at a pH of 4.83 shows the more distinctive 2 bulk mass losses that is characteristic of LDHs, which agrees with the FTIR results. There are stronger LDH and anion bands at a pH of 4.83. This indicates that the intercalation of 4-hydroxybenzoic acid is more successful at a lower pH.

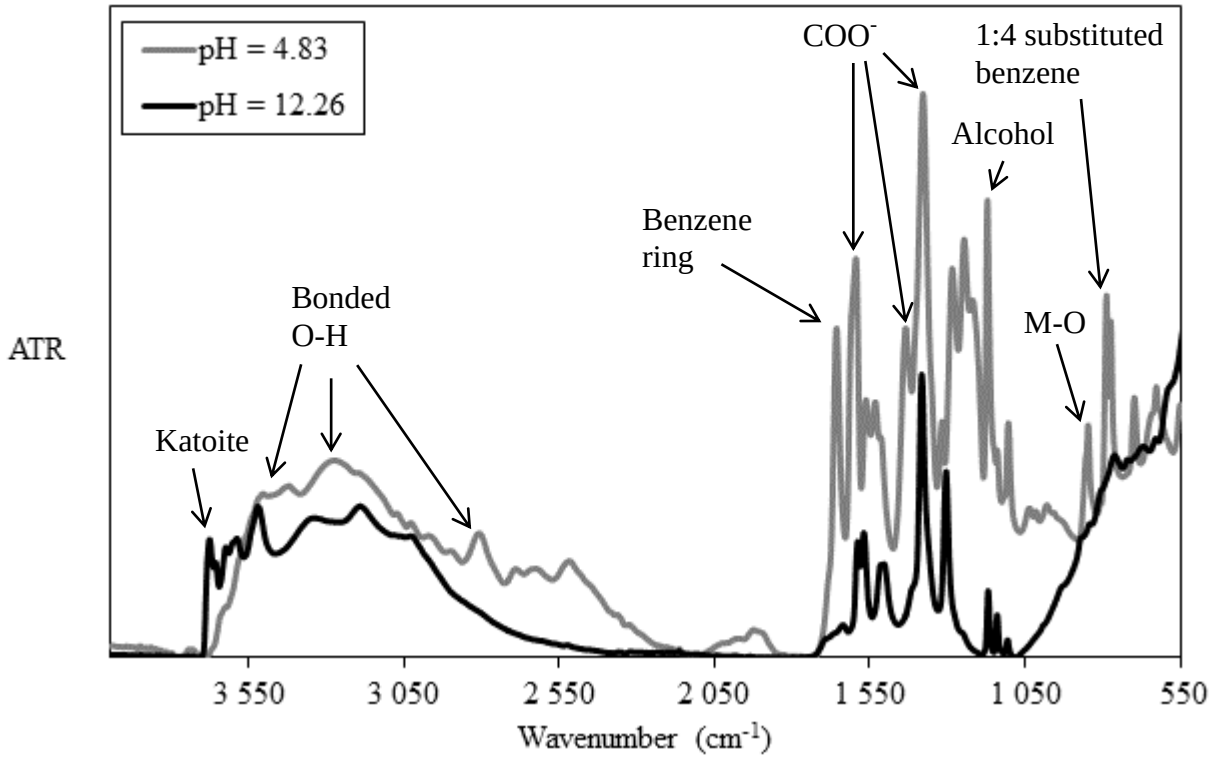

Figure 4-51: FTIR curves for 4-hydroxybenzoic acid intercalated at different pH values

4-Aminobenzoic acid was intercalated at 2 different pH values. The XRD patterns for these two samples can be seen in Figure 4-52. As with anthranilic acid and 3-aminobenzoic acid, both pH values have a new primary peak, which decrease with decreasing pH. The crystalline peaks for 4-aminobenzoic acid are not present in either of the samples.

The new primary peak at a 2θ of 7.42° corresponds to a new d-spacing of 13.83 Å. The d-spacing of 13.83 Å of the new Ca/Al-4-aminobenzoate LDH suggests that the anion intercalated in an overlapping configuration. This is due to the fact that the height of the anion is 7.12 Å and the width is 4.32 Å, as shown in Figure 4-53 (Avogadro, *sa*).

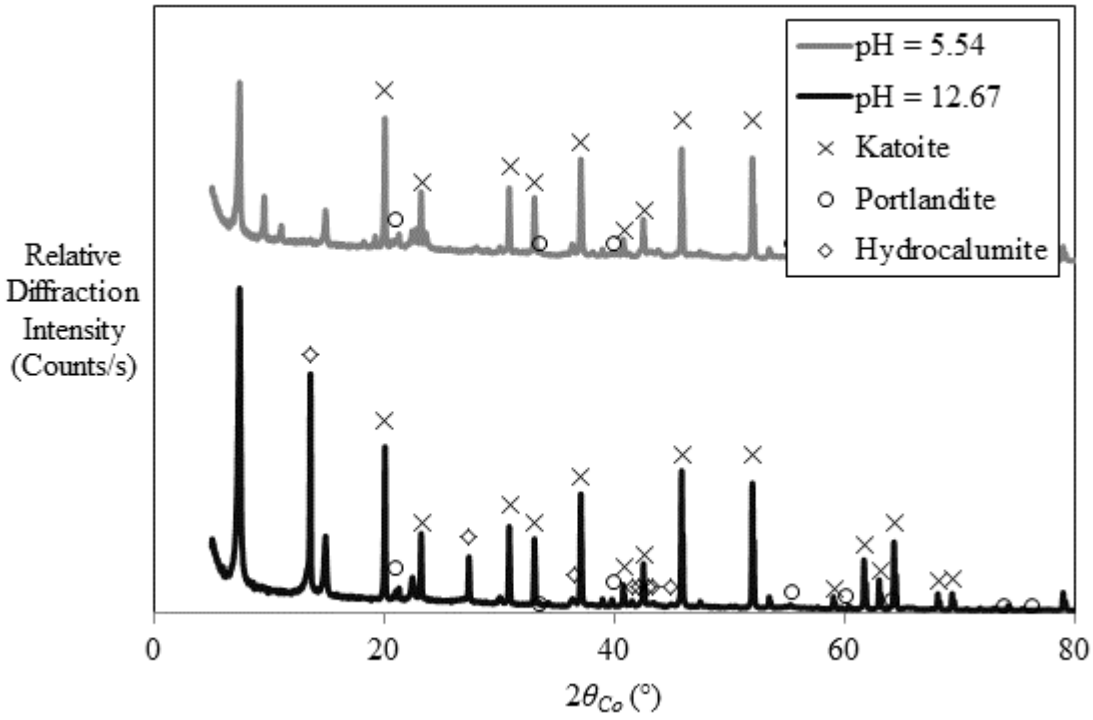

Figure 4-52: XRD patterns for 4-aminobenzoic acid intercalated at different pH values

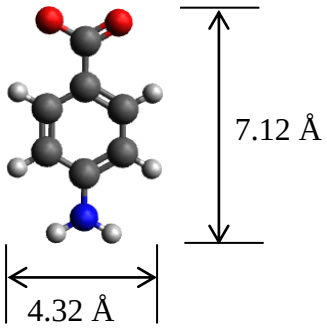

Figure 4-53: Dimensions of 4-aminobenzoate (Avogadro, *sa*)

Even though the XRD pattern shows a decrease in LDH material, the TGA curves for both samples look almost identical (Figure 4-54). Both of the samples lose approximately 28 wt.% by mass between 250 °C and 800 °C, while a fully-intercalated LDH would have lost 55 wt.%. For this reason, neither sample intercalated to a large extent. This supports the XRD results, which show ample unreacted katoite. The FTIR patterns, on the other hand, differ drastically (Figure 4-55), with more anion being present at a pH of 5.54. There are sharp new bands between 3 550 cm^{-1} and 3 000 cm^{-1} present at a lower pH, which are not present at the higher pH, indicating more bonded hydroxides. There is also distinctly more organic anion present at a lower pH.

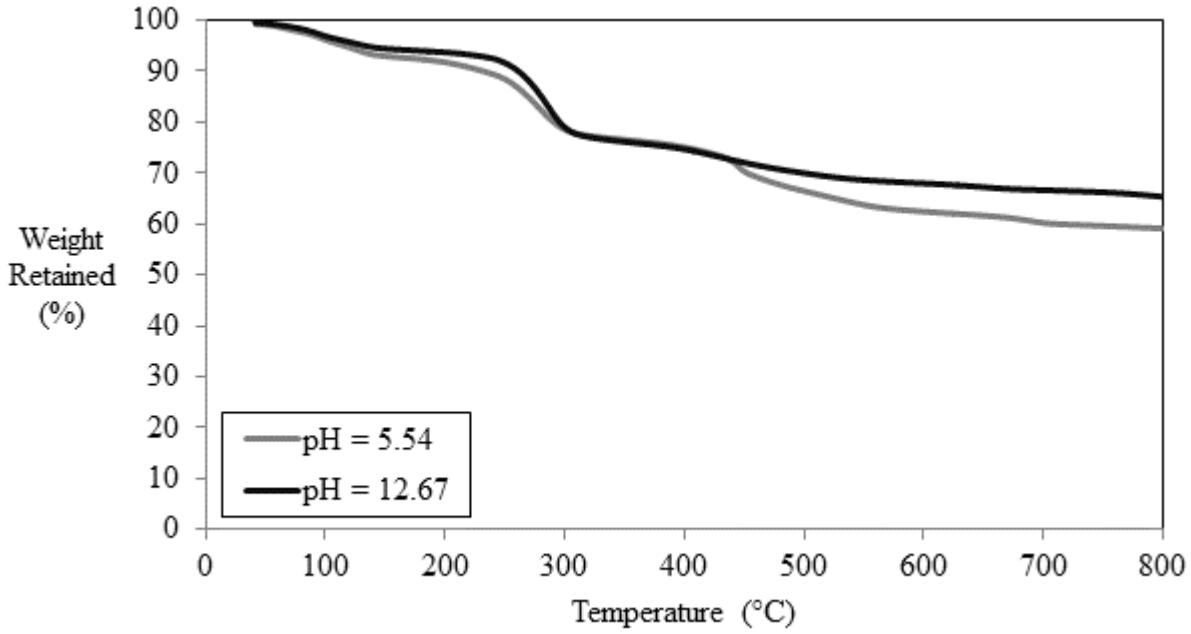

Figure 4-54: TGA curves for 4-aminobenzoic acid intercalated at different pH values

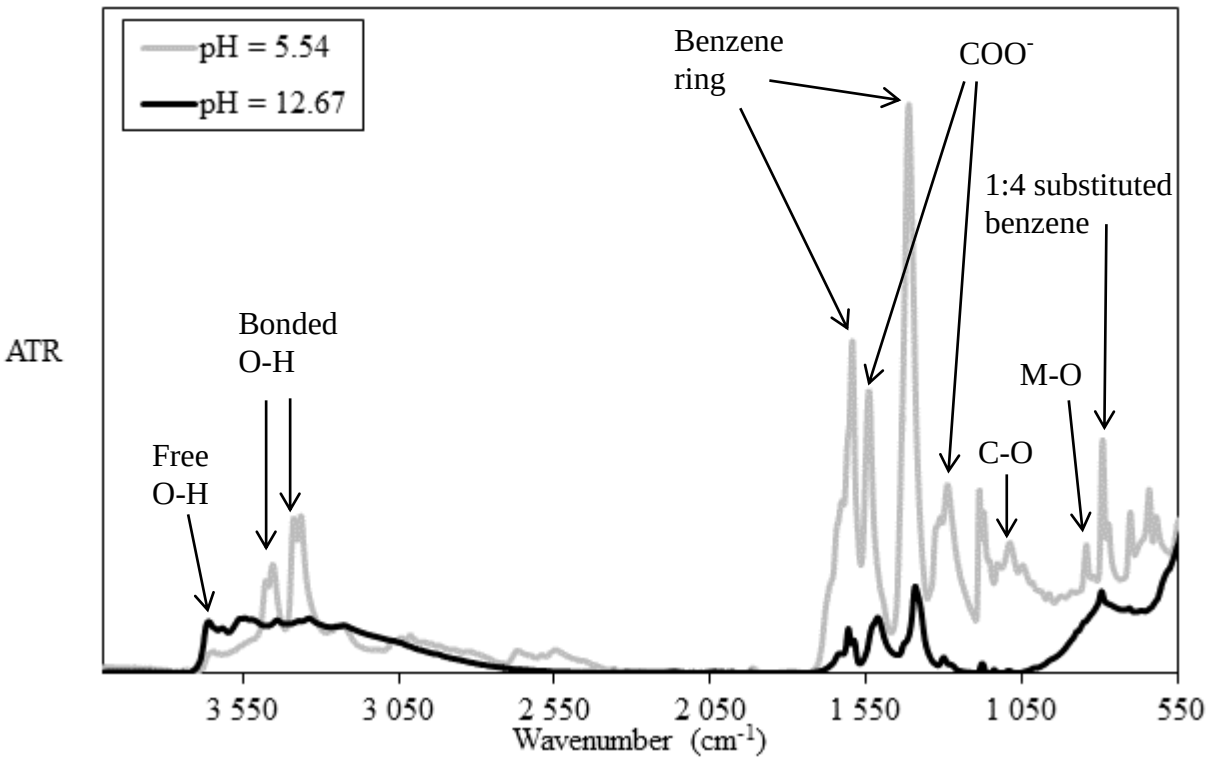

Figure 4-55: FTIR curves for 4-aminobenzoic acid intercalated at different pH values

4.4.5 Effect of substitution on intercalation

Overall, the type of functional group present on the benzoic acid aromatic ring seems to have a larger effect on intercalation than the orientation of the substitution. The hydroxyl group substituted benzoic acids intercalate at different orientations at different pH values. They are also a lot more difficult to intercalate than the amine substituted benzoic acids.

The amine groups seem to intercalate at the same orientation at each different pH. This is because the d-spacing of the newly formed primary peak does not vary between pH values. The only difference between the different pH values is the intensity of the primary peak, which decreases with decreasing pH. This shows that less intercalated materials are present at a lower pH.

Finally, thiosalicylic acid was the most difficult anion to intercalate. This could be due to the bulky thiol side group present in the anion.

4.5 Effect of anion acid strength and solubility on intercalation

4.5.1 Intercalation of weak acids with low solubility

All the organic anions tested in Section 4.4 were weak acids that have low solubility in water. The results show a general trend that organic acids intercalate more readily at higher pH values, yet they can still be intercalated at a lower pH. This phenomenon could be explained by the fact that the organic acids are more stable between the layers than in water, creating a driving force that holds the clay layers together.

4.5.2 Intercalation of strong acids with high solubility

Three strong, inorganic acids were tested at different pH values: hydrochloric acid, nitric acid and sulphuric acid. The first strong acid that was tested was hydrochloric acid, which was intercalated at 4 different pH values (Figure 4-56).

Below a pH of 10, the clay layers disintegrated. The only crystalline peak remaining is that of sodium chloride (NaCl) at 36.90°. The rest of the sample was washed out, and a small amount of the sample was present in the amorphous phase. To get to a pH 13.00, sodium hydroxide was added to the solution. It is likely that this resulted in the intercalation of hydroxide ions between the layers of the clay and explains the new primary peak at 13.59° at a pH of 13.00 (Figure 4-56). This corresponds to a d-spacing of 7.56 Å, which is almost identical to that of hydrocalumite. This is due to the fact that the carbonate and hydroxide anions are similar sizes when intercalated flat between the layers of an LDH. To reach a pH of 11.11, hydrochloric acid was added to the solution. This initialised the formation of a new primary peak slightly to the left of the primary hydrocalumite peak. The new peak occurs at 13.08°, which corresponds to a new d-spacing of 7.86 Å.

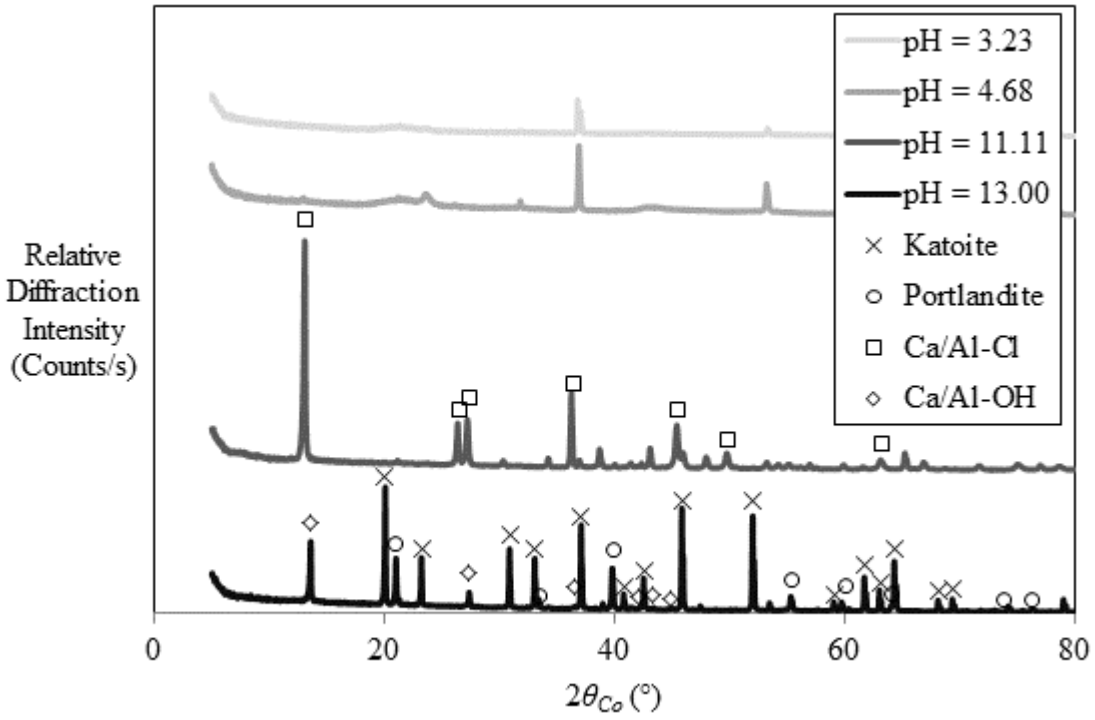

Figure 4-56: XRD patterns for hydrochloric acid intercalated at different pH values

The chloride ion only intercalated at the higher pH value (Figure 4-56). For this reason, only these two samples were tested using TGA and FTIR. At a pH of 13.00, there was almost no extrinsic water, while at a pH of 11.11, there is a 15 wt.% mass loss due to extrinsic water. There is more intrinsic water at a pH of 13.00. Approximately 20 wt.% of the sample is intrinsic water, while at a pH of 11.11, only 10 wt.% of the sample is intrinsic water. The

final mass loss is attributed to the release of the anion, which is more abundant in the sample at a pH of 11.11. This shows that the TGA curve supports the results shown in the XRD pattern (Figure 4-57). The same is true of the FTIR pattern (Appendix B-20 and Appendix B-21). According to the XRD results, the sample synthesised at 11.11 is almost pure hydrocalumite. However, if this was the case, the mass loss between 250 °C and 800 °C would have been 36 wt.%. The mass loss is, however, 21 wt.%. The rest of the impurities are, therefore, present in the amorphous phase.

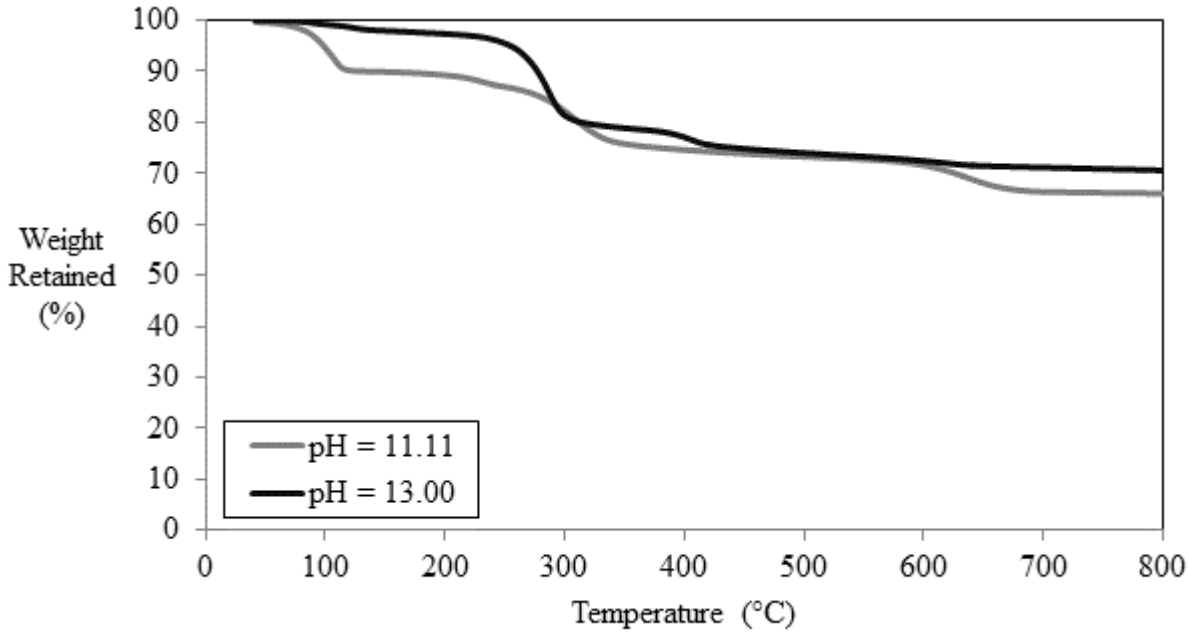

Figure 4-57: TGA curves for hydrochloric acid intercalated at different pH values

Nitric acid is unable to intercalate at a low pH. When excess nitric acid was added to the solution, the solution became transparent and no precipitate remained. At low pH values, the crystalline species in the sample had broken down almost entirely, and only amorphous compounds remained (Figure 4-58). At a high pH, however, nitric acid intercalated to a large degree. Nitrate-intercalated calcium/aluminium LDH ($Ca_4Al_2(OH)_{12}(NO_3)_2 \cdot 4H_2O$) has been identified in the XRD pattern. It was possible to identify all the crystalline phases in the Ca/Al-nitrate sample with XRD; therefore, the FTIR graphs have been attached in Appendix B-28 and Appendix B-29.

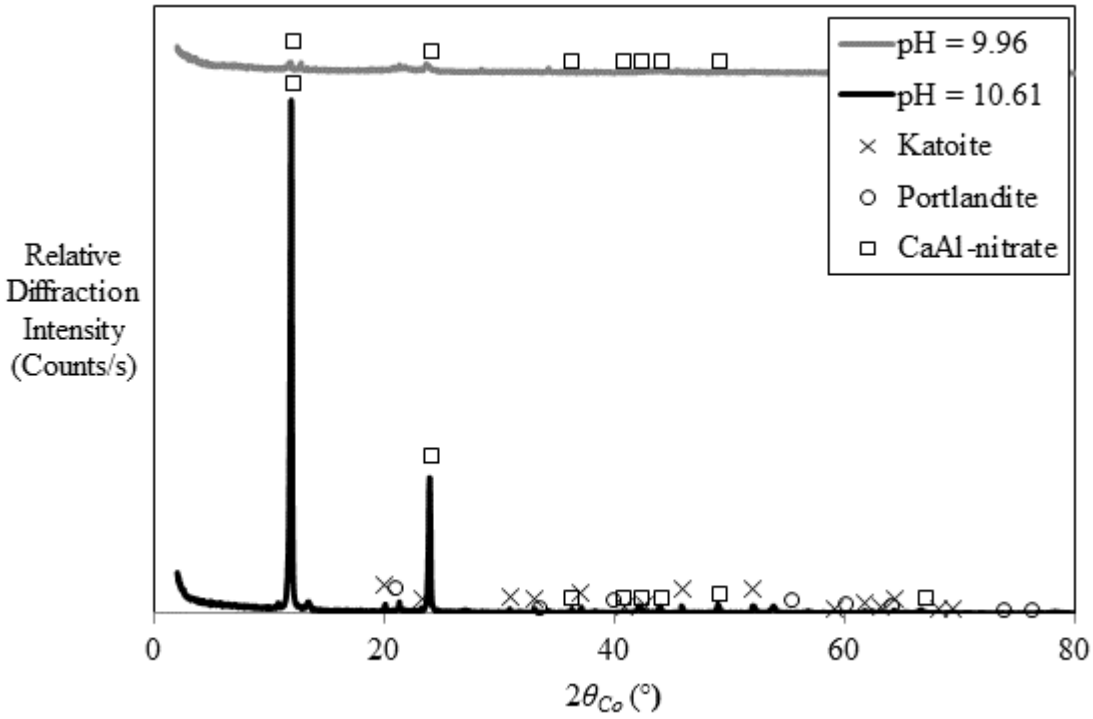

Figure 4-58: XRD patterns for nitric acid intercalated at different pH values

The TGA curves for nitric acid intercalated at two different pH values do not differ vastly, even though the XRD pattern shows a more crystalline species at a high pH (Figure 4-59).

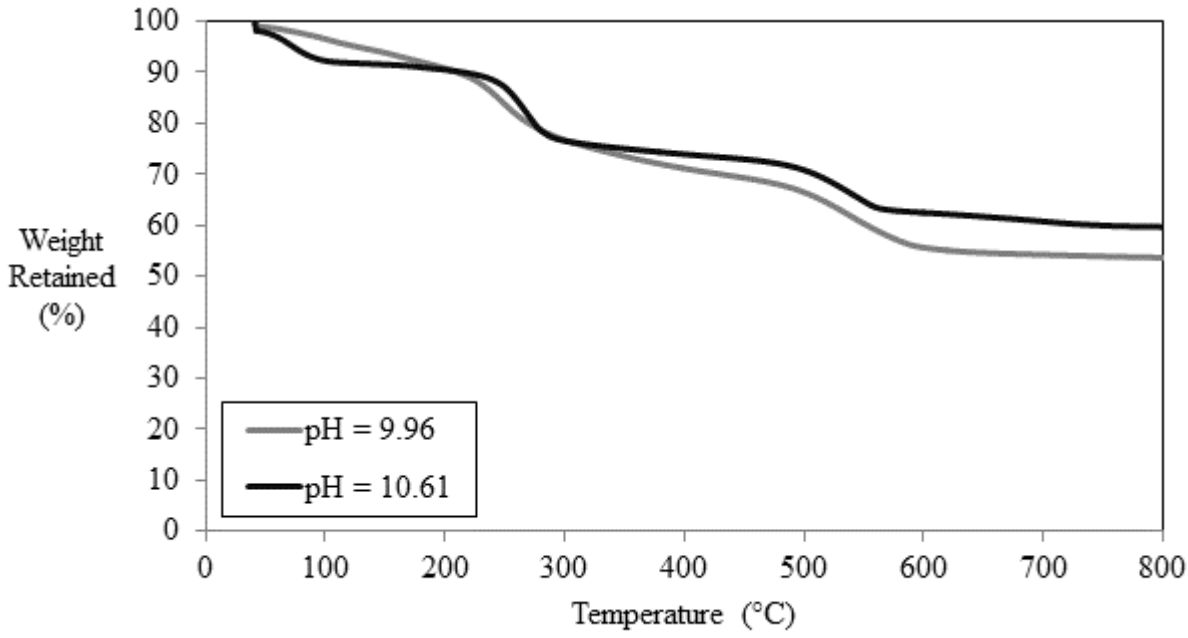

Figure 4-59: TGA curves for nitric acid intercalated at different pH values

The mass loss between 250 °C and 800 °C is greater at a pH of 9.96 than 10.61, indicating a larger degree of intercalation at a lower pH. Even at a pH of 9.96, the mass loss between these temperatures is only 30 wt.%. If the conversion was complete, the mass loss would be 43 wt.%.

When attempting to intercalate sulphate at a high pH, the dominant phases in the sample are unreacted precursor and Ca/Al-sulphate LDH (Figure 4-60). At a pH of 9.90, the sulphate reacts with the calcium in the sample to form calcium sulphate hydrate. This species has a primary peak that occurs at the same 2θ value as hydrocalumite. Finally, at a low pH, there were only two crystalline phases identified: calcium sulphate hydrate and aluminium hydroxide. As with hydrochloric acid and nitric acid, sulphuric acid instantly breaks down the LDH structure when the pH drops to a low pH. Unlike nitric acid, however, there is a new crystalline phase formed between sulphuric acid and calcium from the precursor. This means that, even though the LDH was broken down, the sample did not wash through the filter completely. The TGA results (Appendix C-1) show that at a pH of 11.66, there is a mass loss of 10 wt.% between 250 °C and 800 °C. This is lower than the fully-intercalated 37 wt.% expected, meaning that the conversion is low.

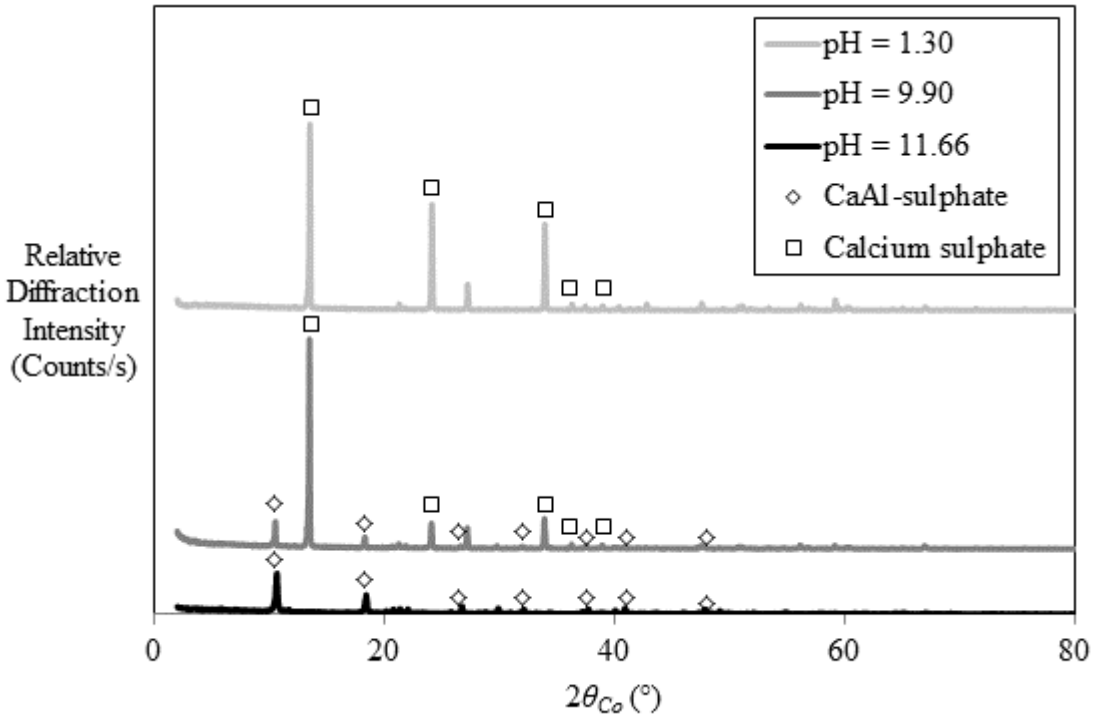

Figure 4-60: XRD patterns for sulphuric acid intercalated at different pH values

In general, strong, soluble acids break down the clay layers at a pH below 10. Unlike the acids with low solubility tested in Section 4.4, the soluble, strong acids have a large driving force to dissociate in water. This means that there is little driving force for the clay layers to remain intact as soon as the pH drops below the stability pH of the LDH layers.

4.5.3 Intercalation of weak acids with high solubility

There was a definite difference between intercalating strong and weak acids at different pH values. All the weak acids with low solubility were able to intercalate at a low pH, whereas the strong, soluble acids could not. The question then arises whether the strength or the solubility of the acids has a major influence on the intercalation. For this reason, 4 weak, soluble acids were tested and intercalated at different pH values. These acids were: citric acid, acetic acid, thioglycolic acid and carbonic acid.

The XRD patterns for citric acid intercalated at different pH values are shown in Figure 4-61. As seen from the figure, citric acid had difficulty intercalating at each pH value.

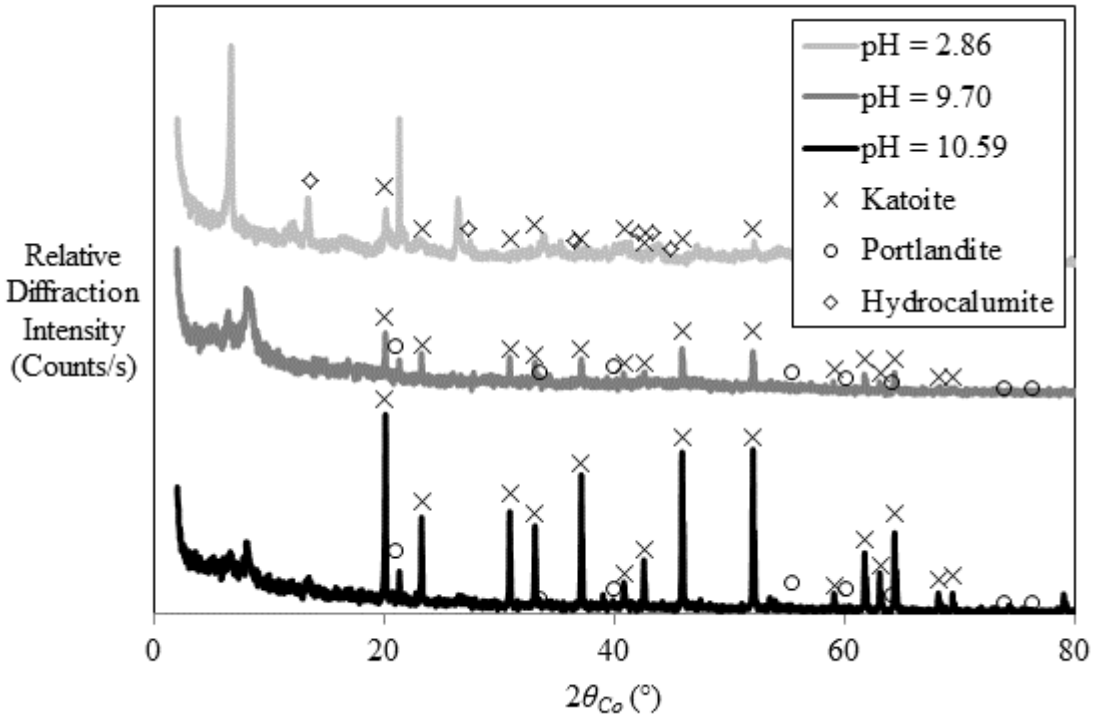

Figure 4-61: XRD patterns for citric acid intercalated at different pH values

An interesting phenomenon occurred at the lower pH value, since the mixture of citric acid with the precursor started at a pH of 3.32, after which the pH dropped to 2.86 when the mixture was left to react for 2 days. The pK_a value for the first carboxylic acid dissociation is 3.13; therefore, it is highly unlikely that this result is accurate. At a pH of 10.59 and 9.70 all three of the carboxylic acid groups on the citric acid molecule are said to be dissociated. This would mean that citric acid is a trivalent anion at a high pH. The anion may struggle to intercalate due to the repulsive forces caused by the third carboxylic acid group. Since the intercalation of citric acid was not successful and yielded a very amorphous product, no further tests were performed.

Acetic acid intercalated to a larger extent than citric acid (Figure 4-62). At a high pH, there is a new peak to the left of the primary hydrocalumite peak. This peak is at 9.51° and 9.46° at a pH of 12.61 and 11.50 respectively. Both of these peaks correspond to a new d-spacing of approximately 10.8 Å. A new primary peak forms as the pH is decreased through the addition of excess acetic acid. This primarily is attributed to the presence of calcium acetate in the sample, as indicated on the XRD pattern.

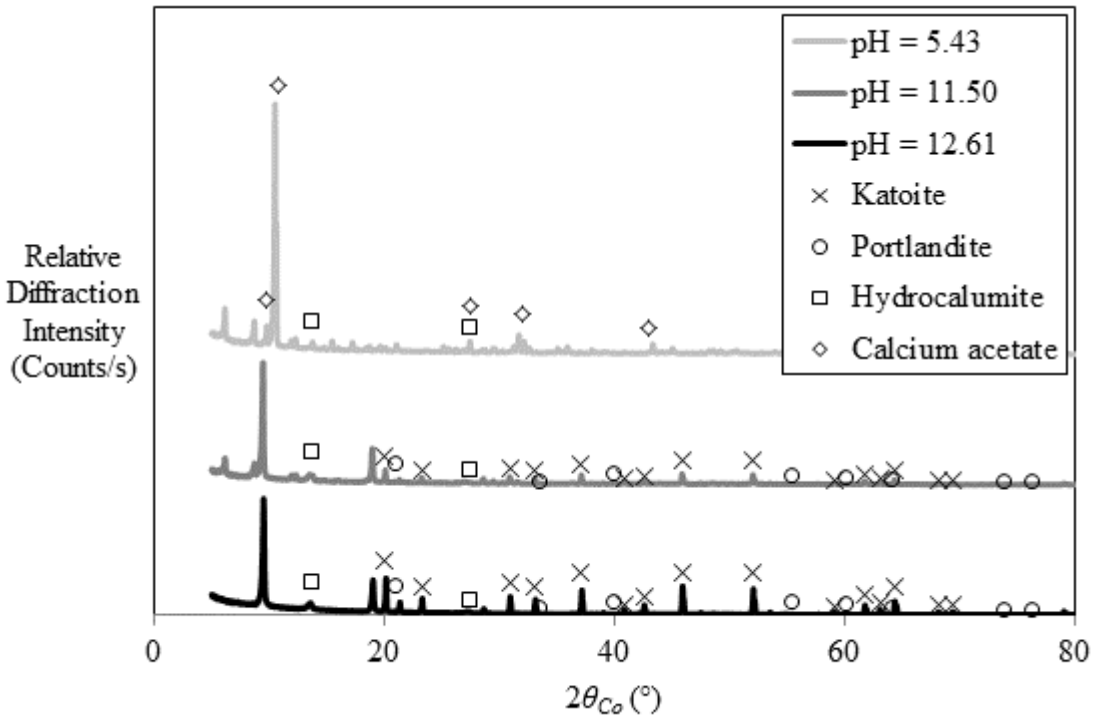

Figure 4-62: XRD patterns for acetic acid intercalated at different pH values

The dimensions of the acetate anion are shown in Figure 4-63. The maximum height of the acetate anion is 3.38 Å, which indicates that acetate could have intercalated in a bilayer configuration. However, even a bilayer configuration does not justify the d-spacing of 10.8 Å. The large d-spacing could be due to the presence of interlayer water or due to repulsive forces between the acetate anions in the interlayer.

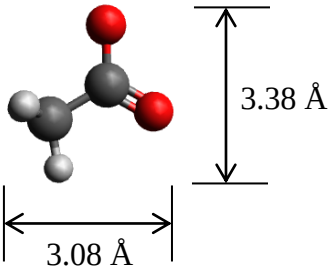

Figure 4-63: Dimensions of acetate (Avogadro, *sa*)

The TGA curves confirm the XRD results (Figure 4-64). There are two different phases present at a pH of 12.61 and 5.43. At the highest pH, there is only one major mass loss step at approximately 250 °C. The lowest pH sample has two distinct mass loss steps at approximately 400 °C and 650 °C. At the intermediate pH, all three of the mass loss steps are present, indicating a mixture of the phases present at the high and the low pH.

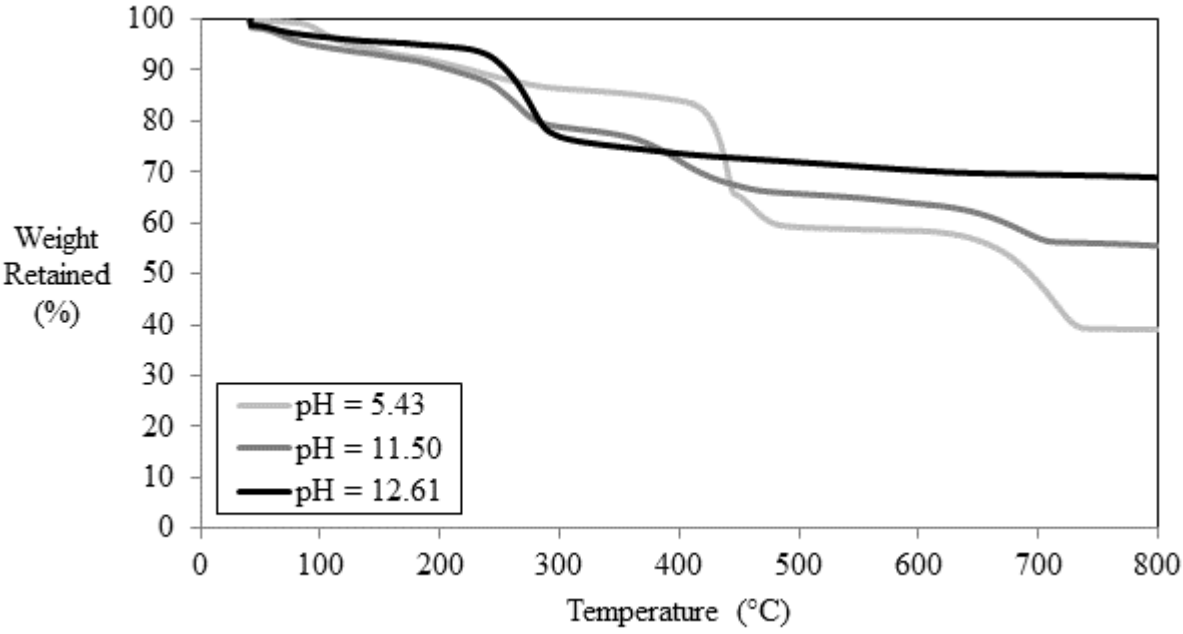

Figure 4-64: TGA curves for acetic acid intercalated at different pH values

At a pH of 5.43, there is an increase in mass loss between 250 °C and 800 °C, which can be attributed to the increase in bound acetate in the form of calcium acetate. The FTIR pattern (Figure 4-65), shows that there is more acetic acid present at the lower pH, but there is less LDH material present, due to the decrease in the O-H band.

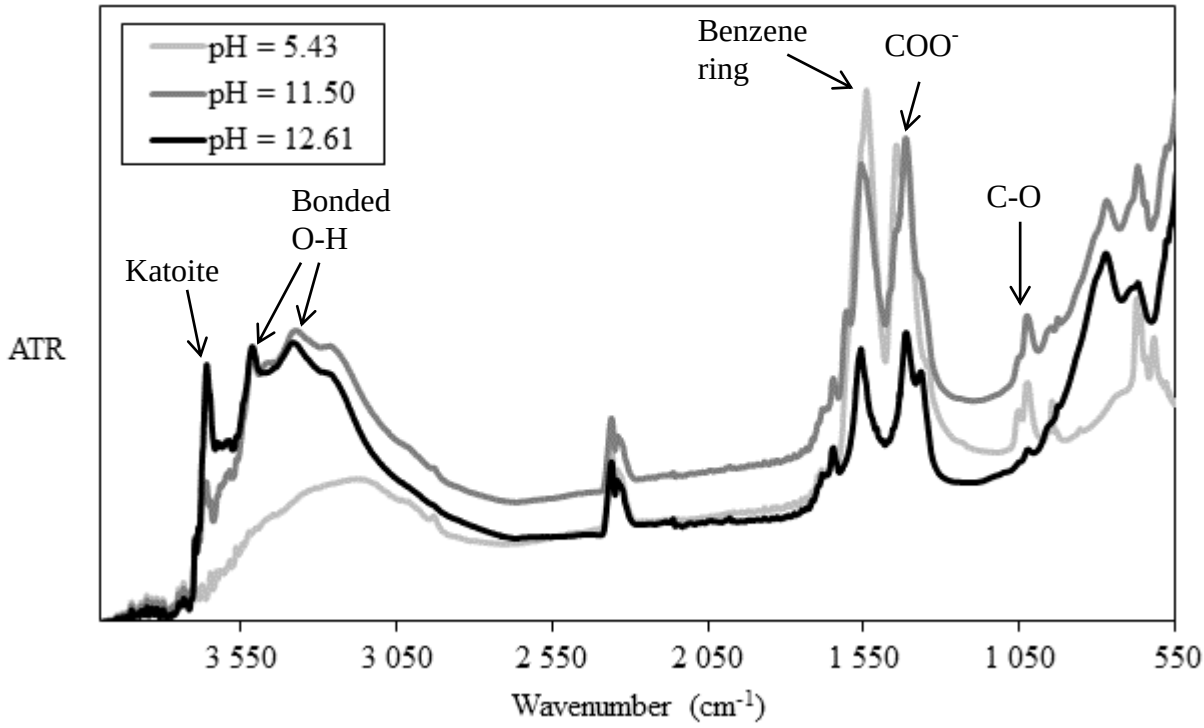

Figure 4-65: FTIR curves for acetic acid intercalated at different pH values

Thioglycolic acid was unable to intercalate at a low pH. As seen from Figure 4-66, there is no layered material left at a low pH. It is clear from the XRD analyses that there is no new primary peak at a pH of 4.41 and 5.27; therefore, no new LDH formed. All the samples are extremely amorphous, including the sample intercalated at a pH of 10.88. There is, however, a slight new primary peak at an angle of 4.86°, which corresponds to a d-spacing of 21.11 Å.

The TGA graph for the sample intercalated at a pH of 10.88 is attached in Appendix C-2. The analysis shows no bulk mass loss steps, indicating that there is no LDH present in the sample. For this reason, FTIR analysis was not performed on the thioglycolic acid samples.

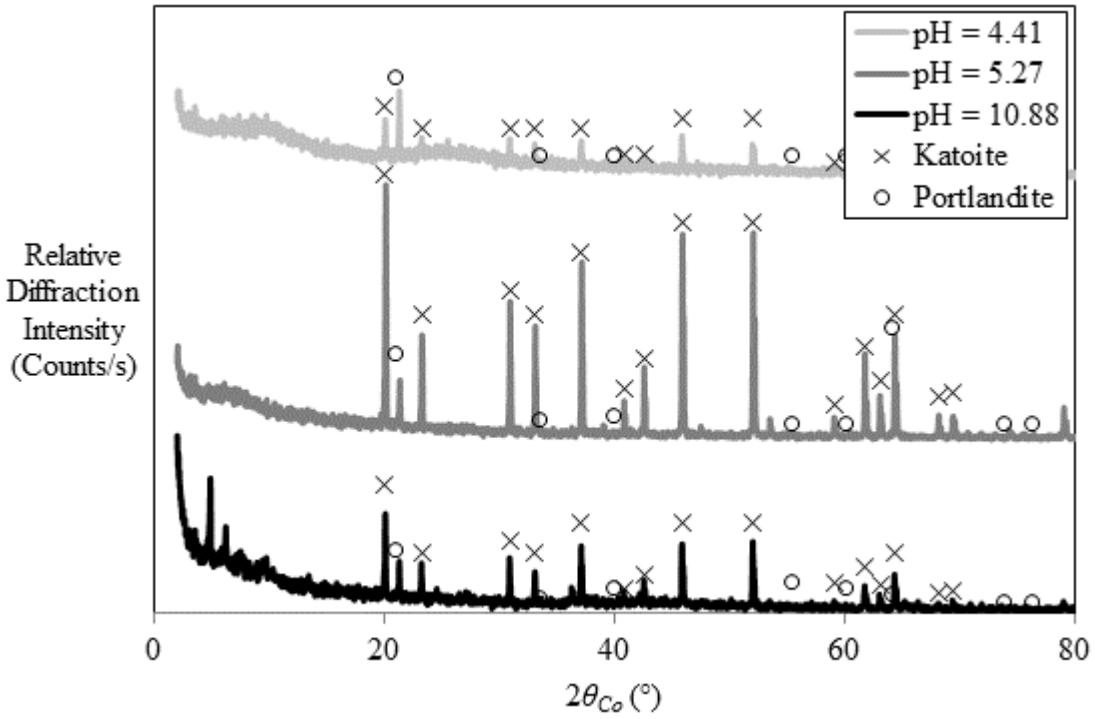

Figure 4-66: XRD patterns for thioglycolic acid intercalated at different pH values

Carbonic acid was the final weak, soluble acid intercalated at different pH values. When intercalating carbonate in a Ca/Al LDH, the LDH dissociates as soon as the pH drops below 10, as seen in Figure 4-67. In turn, calcium carbonate forms. The calcium carbonate also breaks down as the pH decreases further to a pH of 8.82, and the sample becomes more amorphous. This indicates that calcium carbonate is more stable than hydrocalumite at a pH below 10, and a more stable amorphous phase is formed when the pH is dropped even further. For this reason, hydrocalumite synthesis cannot be carried out below a pH of 10. Katoite was only present in small quantities in all three samples, indicating a high conversion.

There is approximately 10 wt.% water in the hydrocalumite sample at a pH of 12.62, as seen from the TGA graph (Figure 4-68). The final bulk mass loss for all 3 species is most probably due to calcium carbonate, since the amount is at a maximum at a pH of 9.05. Between 250 °C and 800 °C, the sample aged at a pH of 12.62 only loses 22 wt.%. Theoretically, a fully-intercalated LDH would lose 39 wt.%.

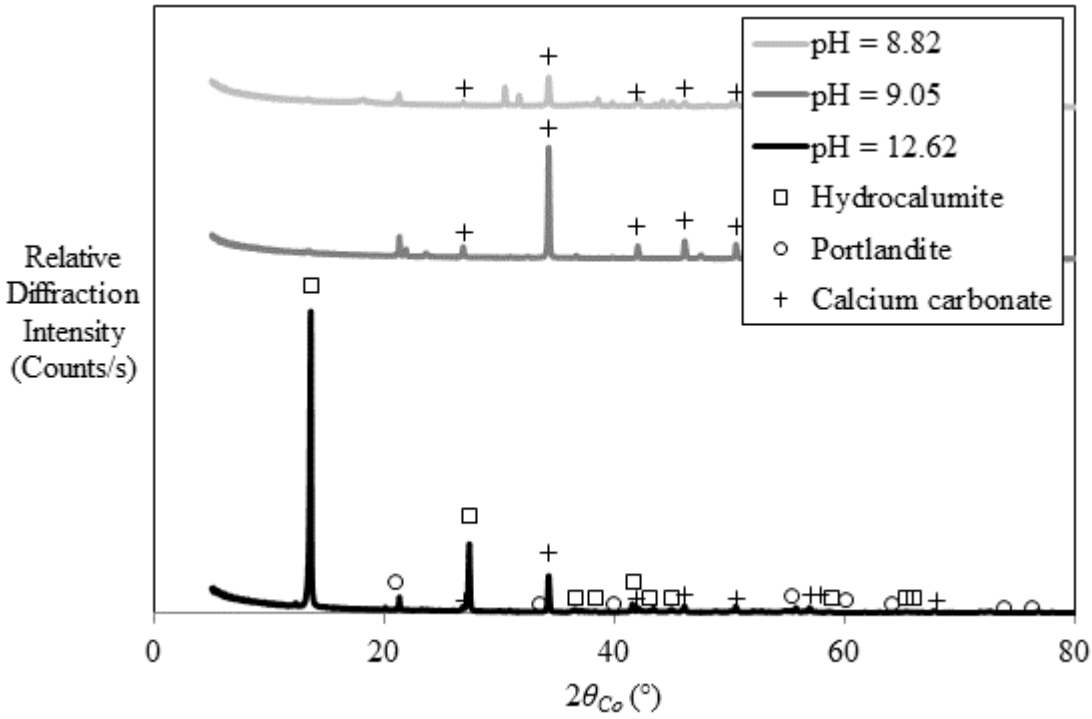

Figure 4-67: XRD patterns for carbonic acid intercalated at different pH values

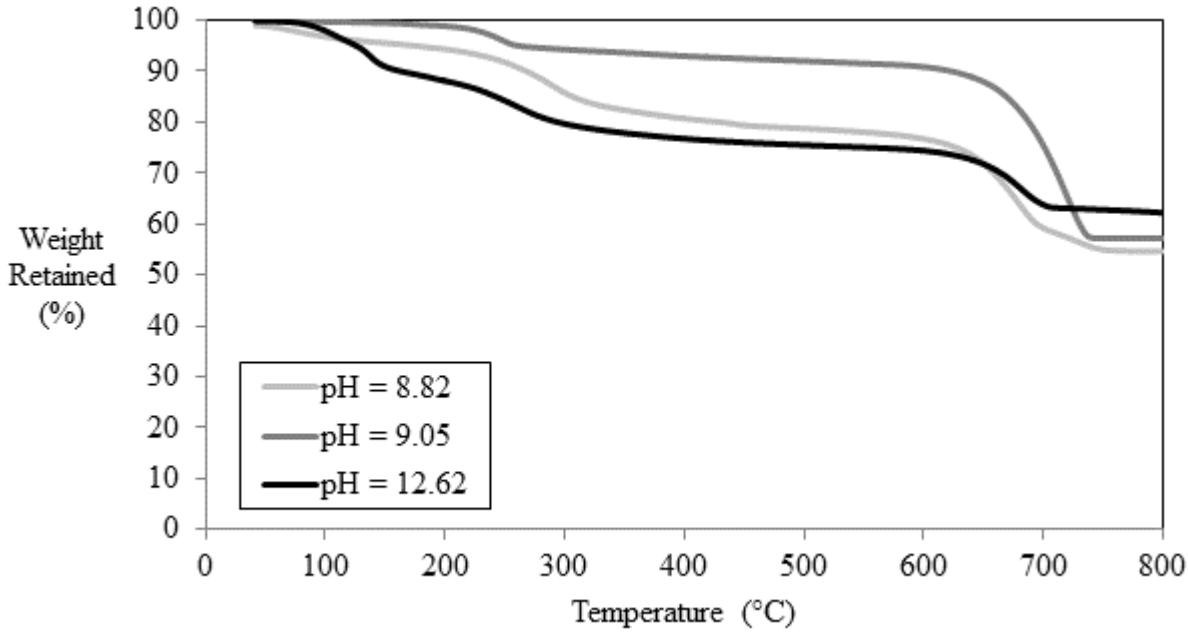

Figure 4-68: TGA curves for carbonic acid intercalated at different pH values

The FTIR curves (Figure 4-69) support the XRD and TGA results. The wide hydroxide bands decrease in intensity with decreasing pH, which indicates that less layered material is present as the pH decreases.

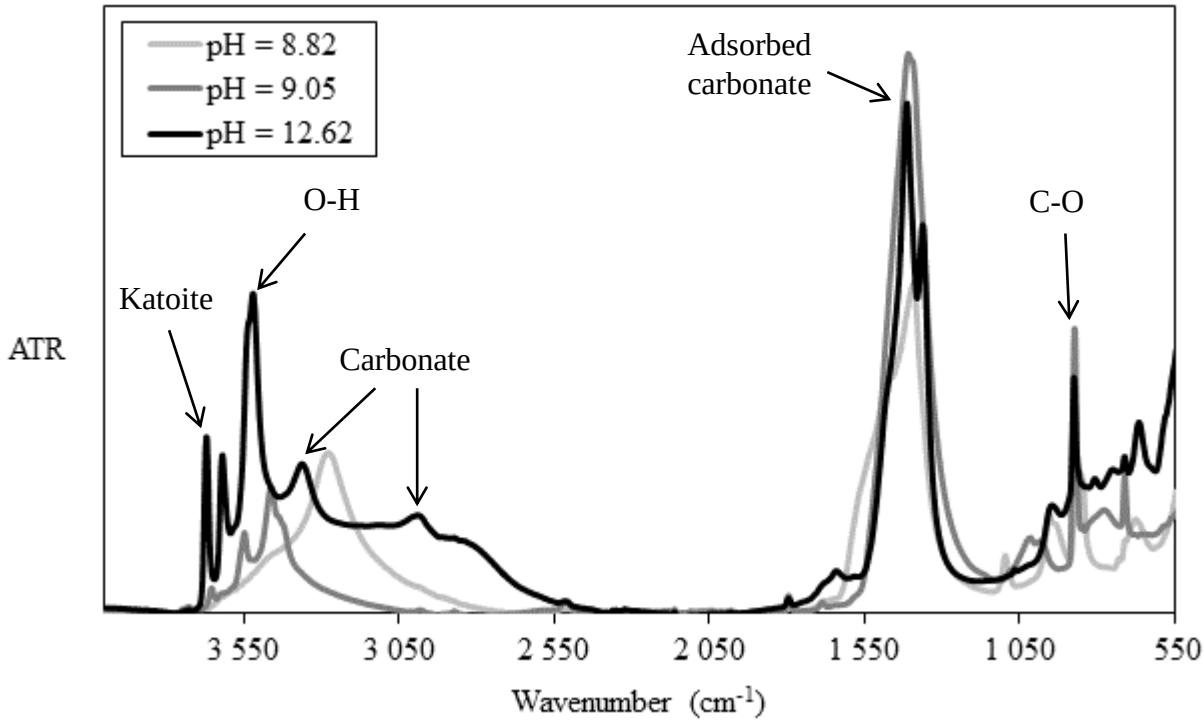

Figure 4-69: FTIR curves for carbonic acid intercalated at different pH values

4.6 Synthesis methods comparison

The results of benzoic acid intercalation using the precursor method versus two traditional synthesis methods, namely reconstruction and co-precipitation, are as shown in Figure 4-70. Nitrate salts of calcium and aluminium were used in the co-precipitation experiments; therefore, nitrate intercalated between the layers of the LDH, as indicated on the XRD pattern. This implies that nitrate is more stable in the interlayer than benzoate. There is a new primary peak slightly to the left of the primary Ca/Al-nitrate peak when using the co-precipitation method, which could be attributed to a horizontally-intercalated benzoate anion. However, the peak is more likely due to the presence of two nitrate orientations between the layers. Due to the higher stability of the nitrate ion in the interlayer, co-precipitation is the least effective synthesis method.

The reconstruction method shows similar results to the precursor method when intercalating benzoate; however, the sample is more crystalline when the precursor method was used. The new primary peak for the reconstruction method occurs at the same angle as the new primary

peak for the precursor method. The similarity between these two methods is expected, since the reconstruction method makes use of mixed metal oxides, while the precursor method essentially makes use of mixed metal hydroxides.

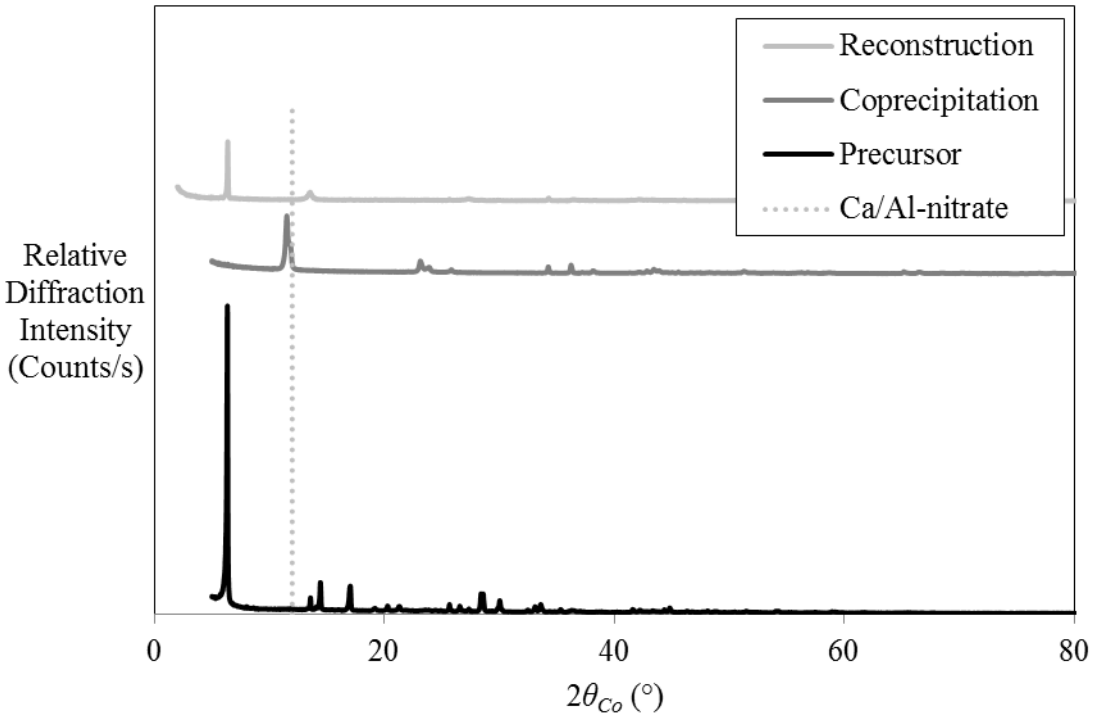

Figure 4-70: Benzoate intercalation using different synthesis methods

The reconstruction method is the most ineffective method to use when intercalating salicylate (Figure 4-71). The peak present at 10.9° for the reconstruction method is the primary peak for calcium salicylate trihydrate. The other two peaks present to the left of the primary calcium salicylate trihydrate could be the primary peak of Ca/Al-salicylate in which the salicylate is oriented at 2 different orientations.

In the co-precipitation experiment, there is a nitrate-intercalated Ca/Al LDH present; however, there is also a new unidentified primary peak, attributed to a Ca/Al-salicylate LDH. The new primary peak is at the same angle as the new primary peak in the precursor synthesis method, meaning that salicylate intercalates at the same angle with both methods. The precursor method, however, is less effective than the co-precipitation method when intercalating salicylate. Even though there is nitrate contamination in the co-precipitation

method, the conversion to Ca/Al-salicylate is still higher compared to the precursor method experiment.

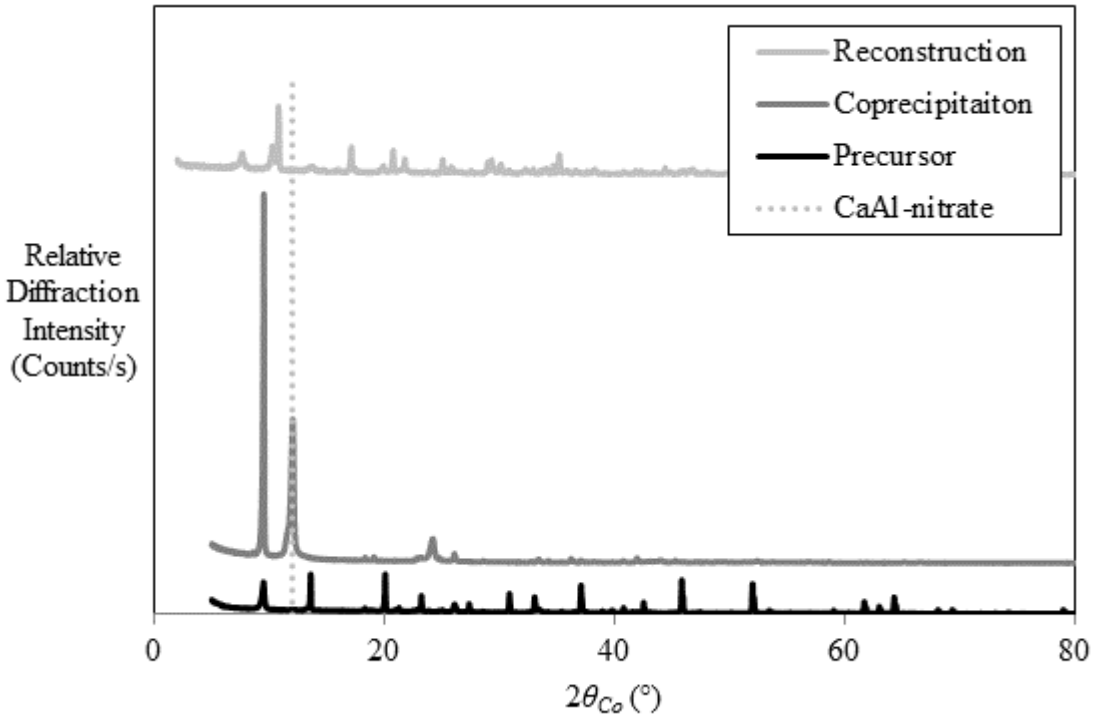

Figure 4-71: Salicylate intercalation using different synthesis methods

The results for anthranilate intercalated with 3 different synthesis methods (Figure 4-72) were similar to that of benzoate (Figure 4-70). The co-precipitation method was unsuccessful because nitrate is more stable in the interlayer than anthranilate. The reconstruction method and the precursor method, on the other hand, were both successful. In both methods, the anion intercalated at the same orientation, however, the precursor method produced a more crystalline material. In the precursor method, there is still a small amount of unreacted katoite, while the reconstruction method has minimal crystalline impurities.

The same results were seen when intercalating 3-aminobenzoic acid (Figure 4-73). The co-precipitation method yielded a Ca/Al-nitrate LDH, with a small Ca/Al-3-aminobenzoate peak starting to form at the same angle as the precursor and reconstruction methods. Both the reconstruction method and the precursor method were successful when intercalating 3-aminobenzoic acid; however, the precursor method yielded a product with higher

crystallinity. The sample prepared by the precursor method still contains crystalline impurities in the form of unreacted katoite.

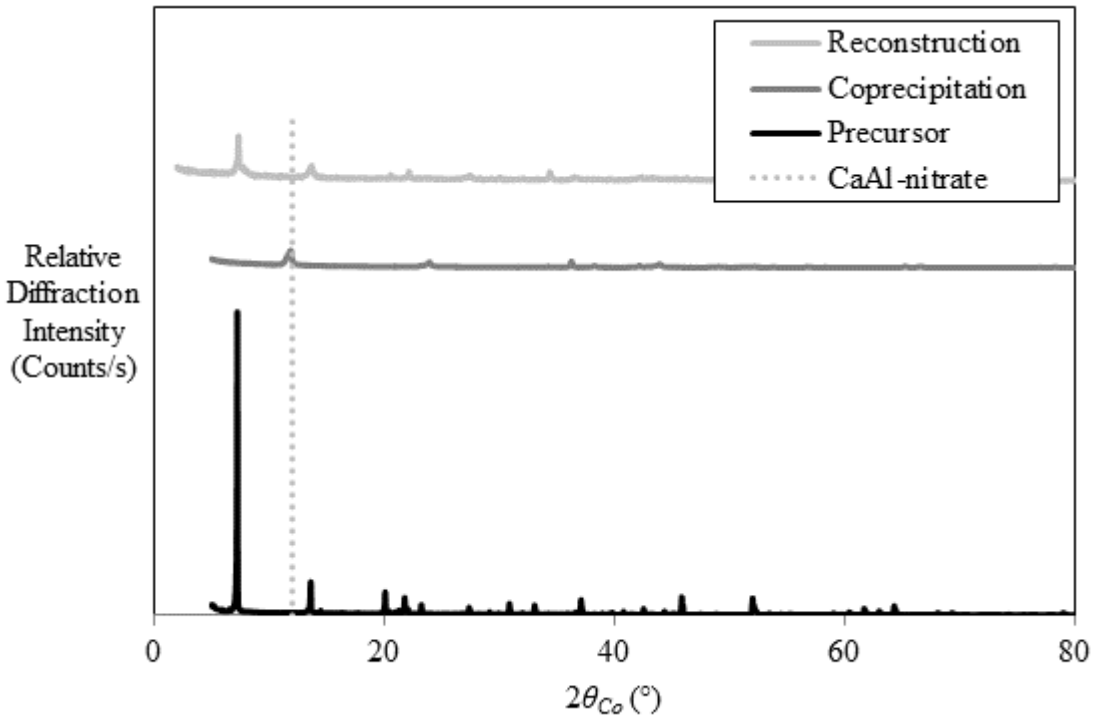

Figure 4-72: Anthranilate intercalation using different synthesis methods

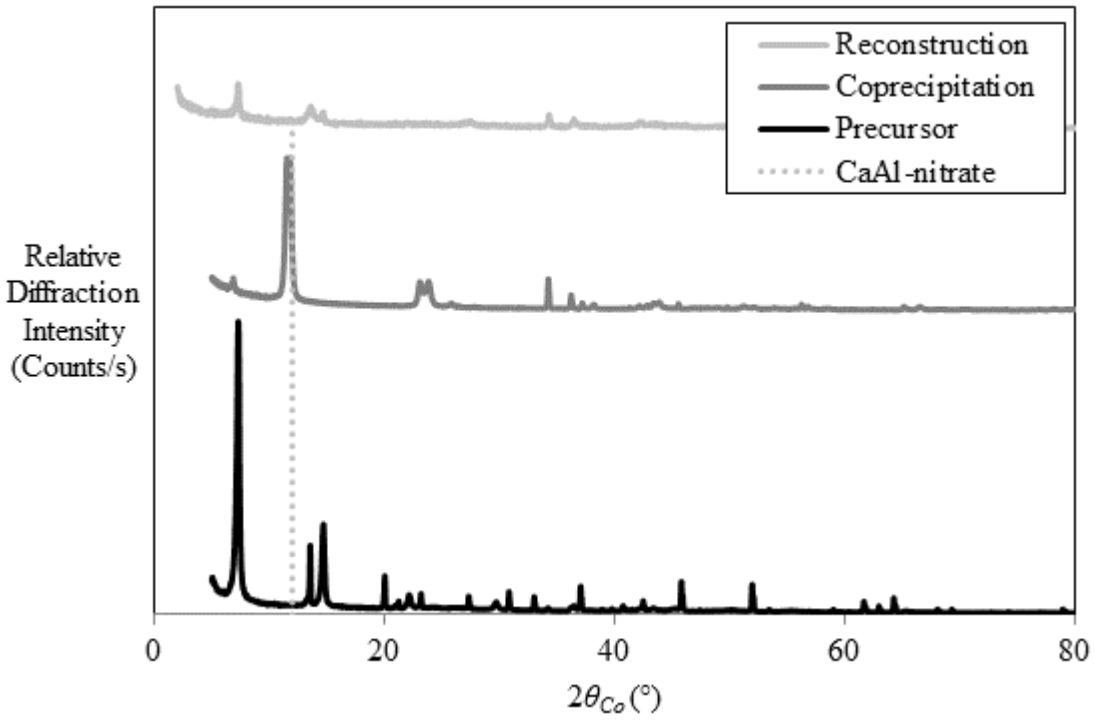

Figure 4-73: 3-Aminobenzoate intercalation using different synthesis methods

Finally, 4-aminobenzoate did not successfully intercalate using the co-precipitation method (Figure 4-74). This indicates that nitrate is more stable in the interlayer of a Ca/Al LDH than 4-aminobenzoate. Both the precursor and the reconstruction methods were successful when intercalating 4-aminobenzoate; however, the orientation of the anion varies between the two methods.

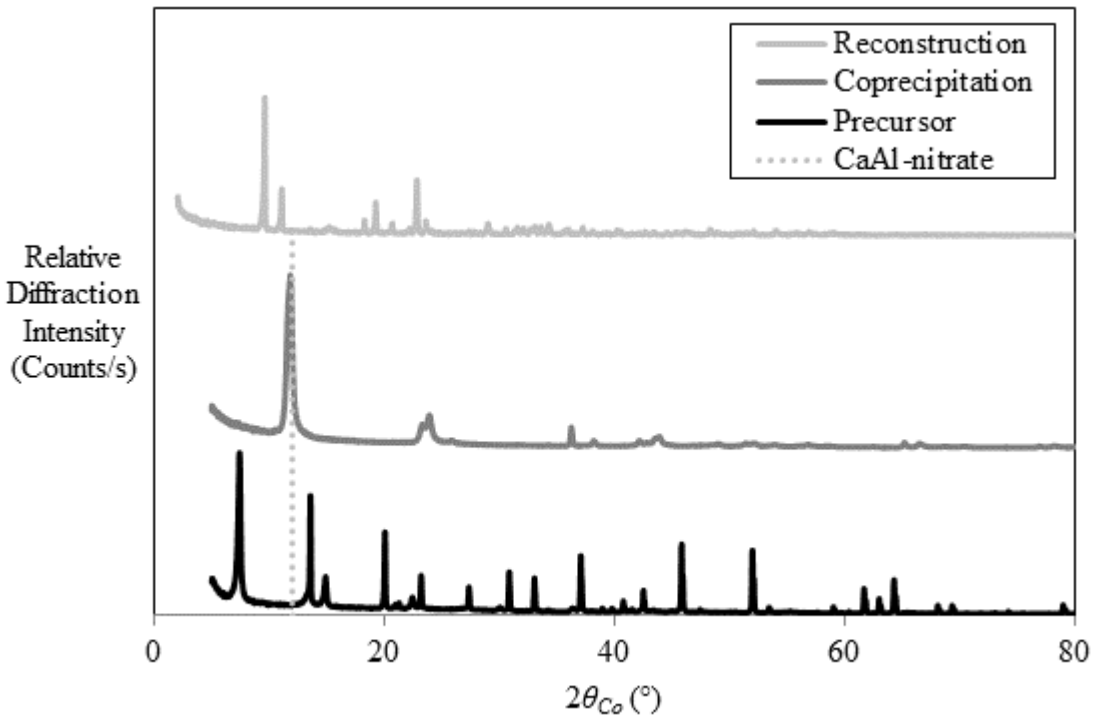

Figure 4-74: 4-Aminobenzoate intercalation using different synthesis methods

Overall, the precursor method produces organically modified LDHs that are comparable, and in some cases superior, in quality to those produced in the traditional synthesis methods. The anions behave differently when using different synthesis methods. In general, the co-precipitation method is the least effective method. This is due to the stability of the nitrate ion in the interlayer, which competes for the interlayer space with the organic anions. In all cases, Ca/Al-nitrate formed. Only salicylic acid seemed equally stable in the interlayer.

The reconstruction method, on the other hand, showed similar results to the precursor method; however, the precursor method produced LDH materials that were more crystalline. The reconstruction method is also one of the most expensive synthesis methods. The

calcination step in the reconstruction method adds considerably to the cost of production of the LDH. For this reason, if the two methods produce similar final products, the precursor method is the most economical.

5. Conclusions and Recommendations

When compared to traditional synthesis methods, the novel precursor method has an obvious cost advantage. The novel method also produces organically modified Ca/Al LDHs that have comparable or higher quality than those synthesised with the reconstruction method. Co-precipitation with nitrates, on the other hand, produces more nitrate-intercalated LDH than organic-modified LDH. This indicates that nitrate is more stable in the interlayer than most of the organic anions. For this reason, the novel synthesis method is preferential to the two traditional synthesis methods when synthesising organically modified hydrocalumites. However, it is recommended that inorganic anions also be tested for the various methods, in order to determine whether the novel synthesis method is adequate when intercalating inorganic anions.

When the precursor mixture is wetted in a beaker that is left open to air at different times and temperatures, the maximum conversion occurs at a temperature of 60 °C after 6 h. The maximum conversion is approximately 15 wt.%, indicating a slow conversion from precursor to hydrocalumite. For this reason, if 85 wt.% purity is sufficient in the product, the reaction vessel does not need to be sealed from air. Since there is very little carbon dioxide in air, it is not necessary to replace the air in the vessel with nitrogen. As long as the vessel is sealed the amount of carbonate present to intercalate will be negligible.

The intercalation of chloride ions was most effective when the precursor mixture was aged with hydrochloric acid for 12 h at 40 °C. There was, however, no obvious trend when intercalating chloride using the novel synthesis method. The conversion increased with increasing aging time, and the decreased at specific reaction conditions. The same was true for temperature. Samples that have a sudden drop in conversion also have a considerable increase in amorphous material. This could indicate that samples aged for extended periods of time or at elevated temperatures form a new, more stable amorphous phase.

Unlike chloride, benzoate showed more distinct trends when intercalating using the novel synthesis method. There was a general increase in conversion with increasing reaction time and decreasing temperatures. At 60 °C, the benzoate did not intercalate when aged for 2 h to 24 h. When left to age for 24 h, two new primary peaks were present on the XRD pattern.

This indicates that benzoate either intercalated at 2 different orientations or that two different crystalline symmetries were present in the sample. A smaller d-spacing was favoured at higher temperatures.

In the past, the precursor material had been synthesised in such a way that katoite and portlandite were present in the correct stoichiometric ratio to form a 2:1 Ca:Al LDH. However, if pure katoite is available, an extra mole of calcium can be added in the second step of the reaction in the form of CaO or $Ca(OH)_2$. Before reacting to form an LDH, CaO is converted to $Ca(OH)_2$ via a fast reaction. For this reason, there is no difference between using CaO or $Ca(OH)_2$ as a calcium source in the second step of the reaction. Adding the extra mole of calcium to the second step of the reaction does not affect the ability of the anion to intercalate.

Benzoic acid rings with the same functional groups substituted on the ortho-, meta- and para-positions behave similarly. The interaction of the anion with the precursor mixture differs when different functional groups are present. Hydroxyl-substituted benzoate rings are divalent at a high pH and monovalent at a low pH. For this reason, salicylic acid, 3-hydroxybenzoic acid and 4-hydroxybenzoic acid intercalate at different orientations when intercalated at different pH values. Amine-substituted benzoic acids intercalate at the same orientation regardless of pH. The only difference is that the amount of intercalated-LDH decreases with decreasing pH. This was true for amine-substituted benzoic acids. Finally, thiosalicylic acid did not intercalate to a high degree even at a high pH, which is most likely due to the bulky thiol group.

In general, it is more beneficial to intercalate LDHs at a pH above 10. Due to the pH of the precursor, the pH will remain above 10 for most anions, even when the correct stoichiometric amount of acid is added to fully convert the katoite to a Ca/Al LDH. The solubility of the anion has the biggest impact on whether the anion intercalates at a low pH. Soluble anions instantly break down the LDH at a pH below 10. However, anions with low solubility tend to keep the layered structure at pH values as low as 5. For this reason, anions with low solubility can be intercalated without monitoring the pH. However, extra care should be taken when intercalating soluble anions. The pH in these situations should be monitored closely to make sure that it does not drop below 10.

Thioglycolic acid and citric acid did not intercalate at any pH. At a high pH, all three carboxylate groups of citric acid are dissociated, making citric acid a trivalent anion. The repulsion of the third dissociated carboxylate group may prevent the anions from intercalating. As with thiosalicylic acid, the bulky thiol group on thioglycolic acid may have prevented intercalation of the anion.

There are several factors affecting intercalation that have not been studied. It is recommended that the following factors also be investigated:

- Mixing efficiency
- Boiled vs. non-boiled water
- Size of anion

For a more detailed understanding of why weak, soluble acids break down the layered structure, titrations with these acids can also be performed. The most important factor to test would be the final properties of the intercalated LDH materials when used in their intended applications.

6. References

Abu-Bakr, M (1997), "Complexation equilibria between copper (II) and thiosalicylic acid. Spectrophotometric determination of copper in non-ferrous alloys" *Monatshefte für Chemie*, *128*, 563–570.

Aisawa, S, Higashiyama, N, Takahashi, S, Hirahara, H, Ikematsu, D, Kondo, H, Nakayama, H and Narita, E (2007), "Intercalation behavior of L-ascorbic acid into layered double hydroxides" *Applied Clay Science*, *35*(3), 146–154.

Aisawa, S, Hirahara, H, Uchiyama, H, Takahashi, S and Narita, E (2002), "Synthesis and thermal decomposition of Mn-Al layered double hydroxides" *Journal of Solid State Chemistry*, *167*, 152–159.

Allmann, R (1968), "The crystal structure of pyroaurite" *Acta Crystallographica*, *24*(7), 972–977.

Allmann, R (1970), "Doppelschichtstrukturen mit brucitaehnlichen schichtionen $[Me(II)_{1-x}Me(III)_x(OH)_2]^{x+}$" *Chimia*, *24*(3), 99–108.

Anon (*sa*), "Dissociation Constants Of Organic Acids And Bases" http://www.zirchrom.com/organic.html [2015, October 13].

Assarsson, G (1931), "Untersuchungen über Calciumaluminate. I. Kristallisation der Calciumaluminatlösungen bei 20°C" *Zeitschrift für anorganische und allgemeine Chemie*, *200*(1), 385 – 401.

Auerbach, SM, Carrado, KA and Dutta, PK (2004), *Handbook of Layered Materials*, Marcel Dekker, Inc., New York.

Avogadro (*sa*), "Avogradro version 1.1.1."

Boclair, JW and Braterman, PS (1999), "Layered double hydroxide stability. 1. Relative stabilities of layered double hydroxides and their simple counterparts" *Chemistry of Materials, 11,* 298–302.

Bontchev, RP, Liu, S, Krumhansl, JL, Voigt, J and Nenoff, TM (2003), "Synthesis, characterization, and ion exchange properties of hydrotalcite $Mg_6Al_2(OH)_{16}(A)^x(A')^{-x}.4H_2O$ (A, A′= Cl^-, Br^-, I^-, and NO^{3-}, 2>x >0) derivatives" *Chemistry of Materials, 15*(19), 3669–3675.

Brindley, GW and Kikkawa, S (1980), "Thermal behavior of hydrotalcite and of anion-exchange forms of hydrotalcite" *Clays and Clay Minerals, 28*(2), 87–91.

Brown, G and Gastuche, MC (1967), "Mixed magnesium-aluminium hydroxides. II. Sturcture and structural chemistry of synthetic hydroxycarbonates and related minerals and compounds" *Clay Minerals, 7,* 193–201.

Buttler, F, Dent Glasser, L and Taylor, H (1959), "Studies on $4CaO•Al_2O_3•13H_2O$ and the related natural mineral hydrocalumite" *Journal of the American Ceramic Society, 42*(3), 121–126.

Campos-Molina, MJ, Santamarıa-Gonzalez, J, Merida-Robles, J, Moreno-Tost, R, Albuquerque, MCG, Bruque-Gamez, S, Rodrıguez-Castellon, E, Jimenez-Lopez, A and Maireles-torres, P (2010), "Base catalysts derived from hydrocalumite for the transesterification of sunflower oil" *Energy Fuels, 24,* 979–984.

Cantrell, DG, Gillie, LJ, Lee, AF and Wilson, K (2005), "Structure-reactivity correlations in MgAl hydrotalcite catalysts for biodiesel synthesis" *Applied Catalysis A: General, 287,* 183–190.

Carlino, S (1997), "The intercalation of carboxylic acids into layered double hydroxides: a critical evaluation and review of the different methods" *Solid State Ionics, 98,* 73–84.

Cartwright, JHE, Checa, AG, Gale, JD, Gebauer, D and Sainz-Díaz, CI (2012), "Calcium carbonate polyamorphism and its role in biomineralization: how many amorphous calcium carbonates are there?" *Angewandte Chemie*, *51*(48), 11960–11970.

Cavani, F, Trifiro, F and Vaccari, A (1991), "Hydrotalcite-type anionic clays: preparation, properties and applications" *Catalysis Today*, *11*, 173–301.

Clause, O, Gazzano, M, Trifiro′, F, Vaccari, A and Zatorski, L (1991), "Preparation and thermal reactivity of nickel/chromium and nickel/aluminium hydrotalcite-type precursors" *Applied Catalysis*, *73*(2), 217–236.

Clearfield, A, Kieke, M, Kwan, J, Colon, JL and Wang, R-C (1991), "Intercalation of dodecyl sulfate into layered double hydroxides" *Journal of Inclusion Phenomena and Molecular Recognition in Chemistry*, *11*(4), 361–378.

Cota, I, Ramírez, E, Medina, F, Sueiras, JE, Layrac, G and Tichit, D (2010), "New synthesis route of hydrocalumite-type materials and their application as basic catalysts for aldol condensation" *Applied Clay Science*, *50*(4), 498–502.

Dinnebier, R and Billinge, S (2008), *Powder Diffraction: Theory and Practice*, RCS Publishing, UK.

Duan, X, Li, D, Lv, Z, Lin, Y and Xu, X (2008), "Clean method for preparing layered double hydroxides",*US Patent 2008/0170978 A1*, assigned to Beijing University of Chemical Technology, US.

Dudek, B, Kustrowski, P, Białas, A, Natkanski, P, Piwowarska, Z, Chmielarz, L, Kozak, M and Michalik, M (2012), "Influence of textural and structural properties of Mg-Al and Mg-Zn-Al containing hydrotalcite derived oxides on Cr(VI) adsorption capacity" *Materials Chemistry and Physics*, *132*, 929–936.

Feitknecht, W and Buser, H (1951), "Über den Bau der plättchenförmigen Calcium-Aluminiumhydroxysalze" *Helvetica Chemica Acta*, *34*(1), 128–142.

Feitknecht, W and Gerber, M (1942), "Zur kenntnis der Doppelhydroxyde und basisehen Doppelsalze. III. Über Magnesium-Aluminiumdoppelhydroxyd" *Helvetica Chimica Acta*, *25*(1), 131–137.

Fogg, AM and O'Hare, D (1999), "Study of the intercalation of lithium salt in gibbsite using time-resolved in situ X-ray diffraction" *Chemistry of Materials*, *11*(7), 1771–1775.

Forano, C, Costantino, U, Prevot, V and Taviot-Gueho, C (2013), *Handbook of Layered Materials*, 2nd edition. Elsevier Ltd, UK.

Forano, C, Hibino, T, Leroux, F and Taviot-Gueho, C (2006), *Handbook of Layered Materials*, F Annabi-Bergaya, B Theng and G Lagaly (Eds.) Elsevier Ltd, UK.

Frondel, C (1941), "Constitution and polymorphism of the pyroaurite and sjogrenite groups" *American Minerologist*, *26*, 295–315.

Frunza, L, Schonhals, A, Frunza, S, Parvulescu, VI, Cojocaru, B, Carriazo, D, Martın, C and Rives, V (2007), "Rotational fluctuations of water confined to layered oxide materials: nonmonotonous temperature dependence of relaxation times" *Journal of Physical Chemistry*, *111*(24), 5166–5175.

Giacovazzo, C, Monaco, H, Artioli, G, Viterbo, D, Ferraris, G, GGilli, Zanotti, G and Catti, M (2002), *Fundamentals of Crystallography*, 2nd edition, C Giacovazzo (Ed.) Oxford University Press, UK.

Goh, K, Lim, T and Dong, Z (2008), "Application of layered double hydroxides for removal of oxyanions: a review" *Water Research*, *42*, 1343–1368.

Guo, Q and Tian, J (2013), "Removal of fluoride and arsenate from aqueous solution by hydrocalumite via precipitation and anion exchange" *Chemical Engineering Journal*, *231*, 121–131.

Harris, D (2007), *Quantitative Chemical Analysis*, 7th edition, W.H. Freeman and Company, New York.

Hwang, S, Han, Y and Choy, J (2001), "Intercalation of functional organic molecules with pharmaceutical , cosmeceutical and nutraceutical functions into layered double hydroxides and zinc basic salts" *Bulletin of the Korean Chemical Society*, *22*(9), 1019–1022.

Kumar, PP, Kalinichev, AG and Kirkpatrick, RJ (2006), "Hydration, swelling, interlayer structure, and hydrogen bonding in organolayered double hydroxides: insights from molecular dynamics simulation of citrate-intercalated hydrotalcite." *The journal of physical chemistry B*, *110*(9), 3841–4.

Li, Y, Hou, W and Zhu, W (2007), "Adsorption of cationic starch on aluminum magnesium hydrotalcite-like compound" *Colloids and Surfaces A: Physicochemical and Engineering Aspects*, *303*, 166–172.

Lombardo, GM, Pappalardo, GC, Costantino, F, Costantino, U and Sisani, M (2008), "Thermal effects on mixed metal (Zn/Al) layered double hydroxides: direct modeling of the X-ray powder diffraction line shape through molecular dynamics simulations" *Chemistry of Materials*, *20*(17), 5585–5592.

Lopez-Salinas, E, Serrano, MEL, Jacome, MAC and Secora, IS (1996), "Characterization of synthetic hydrocalumite-type $[Ca_2Al(OH)_6]NO_3.mH_20$: effect of the calcination temperature" *Journal of Porous Materials*, *2*, 291–297.

Madejova, J (2003), "FTIR techniques in clay mineral studies" *Vibrational Spectroscopy*, *31*, 1–10.

Mandal, S and Mayadevi, S (2008), "Adsorption of fluoride ions by Zn–Al layered double hydroxides" *Applied Clay Science*, *40*, 54–62.

Matusinovic, Z, Marko, R, Sipusic, J and Macan, J (2008), "Polymer nanocomposite materials based on polystyrene and a layered aluminate filler" *Polymer Engineering and Science*, *48*(10), 2027–2032.

Meyn, M, Beneke, K and Lagaly, G (1990), "Anion-exchange reactions of layered double hydroxides" *Inorganic Chemistry*, *29*(26), 5201–5207.

Miyata, S (1980), "Physio-chemical properties of synthetic hydrotalcites in relation to composition" *Clays and Clay Minerals*, *28*(1), 50–56.

Miyata, S (1983), "Anion-exchange properties of hydrotalcite-like compounds" *Clays and Clay Minerals*, *31*(4), 305–311.

Miyata, S (1975), "The synthesis of hydrotalcite-like compounds and their structures and physio-chemical properties" *Clays and Clay Minerals*, *23*, 369–375.

Miyata, S and Kumura, T (1973), "Synthesis of new hydrotalcite like compounds and their physio-chemical properties" *Chemistry Letters*, 843–848.

Miyata, S and Okada, A (1982), "Hydrotalcites having a hexagonal needle-like crystal structure and process for production thereof" ,*US Patent 4,351,814*, assigned to Kyowa Chemical Industry Co., Ltd., US.

Mylius (1933), "Calcium aluminate hydrates and their double salts" *Acta Academiae Aboensis*, *7*(3), 147.

Newman, SP and Jones, W (1998), "Synthesis, characterization and applications of layered double hydroxides containing organic guests" *New Journal of Chemistry*, *22*(2), 105–115.

Niazi, M and Mollin, J (1987), "Dissociation constants of some amino acid and pyridinecarboxylic acids in ethanol-H_2O mixtures" *Bulletin of the Chemical Society of Japan*, *60*(7), 2605–2610.

Nicolet (*sa*), "Infrared Correlation Chart" http://ftirsearch.com/ [2015, August 15].

Okamoto, K, Iyi, N and Sasaki, T (2007), "Factors affecting the crystal size of the MgAl-LDH (layered double hydroxide) prepared by using ammonia-releasing reagents" *Applied Clay Science*, *37*, 23–31.

Othman, MR, Helwani, Z, Martunus and Fernando, WJN (2009), "Synthetic hydrotalcites from different routes and their application as catalysts and gas adsorbents: a review" *Applied Organometallic Chemistry*, *23*, 335–346.

Passaglia, E and Rinaldi, R (1984), "Katoite, a new member of the $Ca_3Al_2(SiO4)_3$-$Ca_3Al_2(SiO4)_3(OH)_{12}$ series and a new nomenclature for the hydrogrossular group of minerals" *Bulletin de Mineralogie*, *107*, 605–618.

Pecharsky, V and Zavalij, P (2009), *Fundamentals of Powder Diffraction*, 2nd edition, Springer, New York.

Perry, RH and Green, DW (1999), *Perry's Chemical Engineers' Handbook*, 7th edition, McGraw-Hill, New York.

Rapin, JP, Walcarius, A, Lefevre, G and François, M (1999), "A double-layered hydroxide, $3CaO.Al_2O_3.CaI_2.10H_2O$" *Acta Crystallographica Section C Crystal Structure Communications*, *55*(12), 1957–1959.

Reich, HJ (2012), "pKa's of inorganic and oxo-acids" http://www.chem.wisc.edu/areas/reich/pkatable/index.htm [2015, October 13].

Reichle, WT (1986), "Synthesis of anionic clay minerals (mixed metal hydroxides, hydrotalcite)" *Solid State Ionics*, *22*, 135–141.

Rives, V (2002), "Characterisation of layered double hydroxides and their decomposition products" *Materials Chemistry and Physics*, *75*, 19–25.

Roberts, M (1957), "New calcium aluminate hydrates" *Journal of Applied Chemistry*, *7*, 543–546.

Rousselot, I, Taviot-gueho, C, Leroux, F, Leone, P, Palvadeau, P and Besse, J (2002), "Insights on the structural chemistry of hydrocalumite and hydrotalcite-like materials: investigation of the series $Ca_2M^{3+}(OH)_6Cl_2H_2O$ (M^{3+}: Al^{3+}, Ga^{3+}, Fe^{3+}, and Sc^{3+}) by X-ray powder diffraction" *Journal of Solid State Chemistry*, *167*, 137–144.

Roy, DM, Roy, R and Osborn, E (1953), "The system MgO-Al_2O_3-H_2O and influence of carbonate and nitrate ions on the phase equilibria" *American Journal of Science*, *251*, 337–361.

Sánchez-Cantú, M, Pérez-Díaz, LM, Tepale-Ochoa, N, González-Coronel, VJ, Ramos-Cassellis, ME, Machorro-Aguirre, D and Valente, JS (2013), "Green synthesis of hydrocalumite-type compounds and their evaluation in the transesterification of castor bean oil and methanol" *Fuel*, *110*, 23–31.

Sato, T, Fujita, H, Endo, T, Shimada, M and Tsunashima, A (1988), "Synthesis of hydrotalcite-like compounds and their physio-chemical properties" *Reactivity of Solids*, *5*, 219–228.

Sato, T, Wakabayashi, T and Shimada, M (1986), "Adsorption of various anions by magnesium aluminum oxide ($Mg_{0.7}Al_{0.3}O_{1.15}$)" *Industrial & Engineering Chemistry Product Research and Development*, *25*(1), 89–92.

Sauerwein, R, Reimer, A, Edenharter, L, Sorgalla, M and Wehner, W (2011), "Calcium carbonate hydroxodialuminates comprising a hexagonal platelet-shaped crystal habit", *US Patent 7,919,066*, assigned to Nabaltec, US.

Scheckel, KG, Scheinost, AC, Ford, RG and Sparks, DL (2000), "Stability of layered Ni hydroxide surface precipitates — A dissolution kinetics study" *Geochimica et Cosmochimica Acta*, *64*(16), 2727–2735.

Shumaker, JL, Crofcheck, C, Tackett, SA, Santillan-Jimenez, E, Morgan, T, Ji, Y, Crocker, M and Toops, TJ (2008), "Biodiesel synthesis using calcined layered double hydroxide catalysts" *Applied Catalysis B: Environmental*, *82*(1-2), 120–130.

Stanimirova, TS, Vergilov, I, Kirov, G and Petrova, N (1999), "Thermal decomposition products of hydrotalcite-like compounds: low-temperature metaphases" *Journal of Materials Science, 34,* 4153–4161.

Tauler, R, Marques, R and Casassas, E (1998), "Multivariable curve resolution applied to three way trilinear data: study of a spectrofluorimetric acid-base titration of salicylic acid at three excitation wavelengths" *Journal of Chemometrics, 12,* 55–75.

Taylor, H (1969), "Segregation and cation-ordering in sjögrenite and pyroaurite" *Mineralogical Magazine, 37*(2), 287–342.

Taylor, H (1973), "Crystal structures of some double hydroxide minerals" *Mineralogical Magazine, 39,* 377–389.

Taylor, RM (1984), "The rapid formation of crystalline double hydroxy salts and other compounds by controlled hydrolysis" *Clay Minerals, 19,* 591–603.

Tilley, C, Megaw, D and Hey, M (1934), "Hydrocalumite ($4CaO.Al_2O_3.12H_20$), a new mineral from Scawt Hill, Co. Antrim." *Mineralogical Magazine, 23*(146), 607–615.

Vaccari, A (1998), "Preparation and catalytic properties of cationic and anionic clays" *Catalysis Today, 41,* 53–71.

Van der Pol, A, Mojet, BL, van de Ven, E and de Boer, E (1994), "Ordering of intercalated water and carbonate anions in hydrotalcite. An NMR study" *The Journal of Physical Chemistry, 98*(15), 4050–4054.

Van der Westhuizen, F (2011), "The green engineering of layered double hydroxides," Report, Department of Chemical Engineering, University of Pretoria, Pretoria.

Van Graan, M (2012), "Layered double hydroxide synthesis for utilisation as catalysts," Report, Department of Chemical Engineering, University of Pretoria, Pretoria.

Vaysse, C, Guerlou-Demourgues, L, Demourgues, A and Delmas, C (2002), "Thermal behavior of oxometalate (Mo,W)-intercalated layered double hydroxides: study of the grafting phenomenon" *Journal of Solid State Chemistry*, *167*, 59–72.

Venter, HP (2013), "Optimisation of the synthesis of Mg-Al-CO_3 LDH and the partial substitution of Mg/Ca-based LDHs," Masters Thesis, Department of Chemical Engineering, University of Pretoria, Pretoria.

Vieille, L, Rousselot, I, Leroux, F, Besse, J and Taviot-Gue, C (2003), "Hydrocalumite and its polymer derivatives. 1. Reversible thermal behavior of Friedel's salt: a direct observation by means of high-temperature in situ powder X-ray Diffraction" *Chemistry of Materials*, *15*, 4361–4368.

Vucelic, M, Moggridge, GD and Jones, W (1995), "Thermal properties of terephthalate- and benzoate-intercalated LDH" *The Journal of Physical Chemistry*, *99*(20), 8328–8337.

Wen, X, Yang, Z, Yan, J and Xie, X (2015), "Green preparation and characterization of a novel heat stabilizer for poly(vinyl chloride)–hydrocalumites" *RSC Advances*, *5*(40), 32020–32026.

Williams, GR and O'Hare, D (2006), "Towards understanding, control and application of layered double hydroxide chemistry" *Journal of Materials Chemistry*, *16*(30), 3065–3074.

Xu, S, Chen, Z, Zhang, B, Yu, J, Zhang, F and Evans, DG (2009), "Facile preparation of pure CaAl-layered double hydroxides and their application as a hardening accelerator in concrete" *Chemical Engineering Journal*, *155*, 881–885.

Yun, SK and Pinnavaia, TJ (1995), "Water content and particle texture of synthetic hydrotalcite-like layered double hydroxides" *Chemistry of Materials*, *7*, 348–354.

Zhang, WH, Guo, XD, He, J and Qian, ZY (2008), "Preparation of Ni(II)/Ti(IV) layered double hydroxide at high supersaturation" *Journal of the European Ceramic Society*, *28*(8), 1623–1629.

Zhang, Y, Wang, J, Liu, X, Gao, P, Gong, C and Lei, L (2015), "A green route to synthesize layered double hydroxides" *Environmental Progress & Sustainable Energy*, *34*(1), 234–239.

7. Appendices

Appendix A: XRD Results

A-1: XRD graph for Ca/Al-carbonate synthesis at 2 h (ambient temperature)

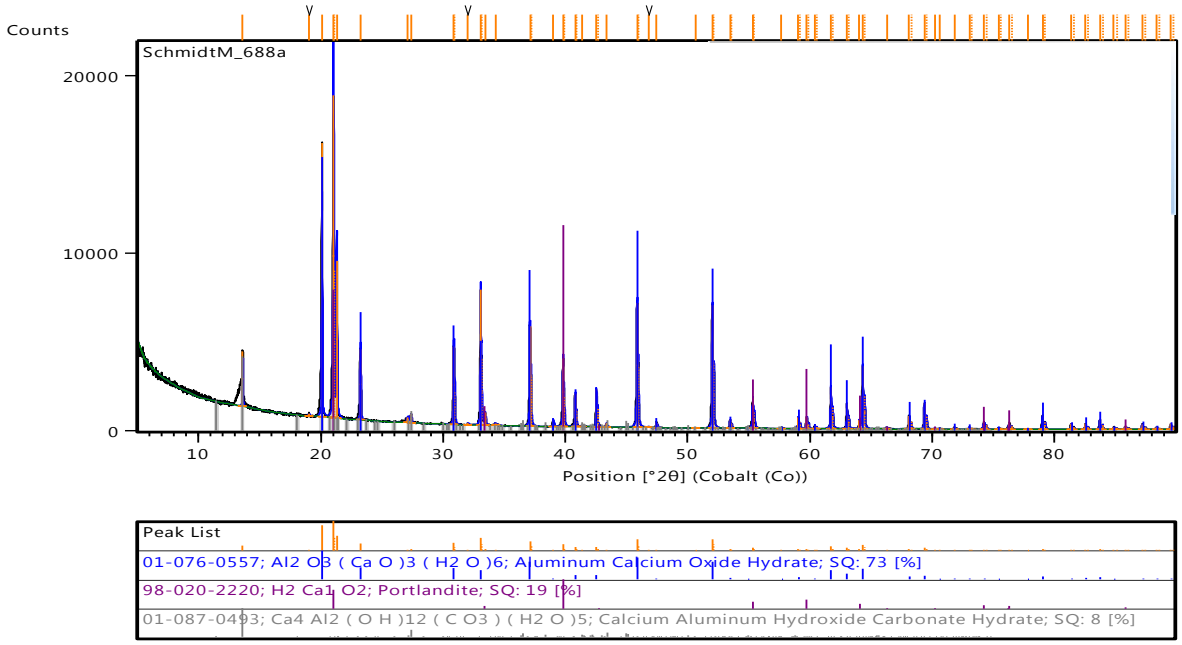

A-2: XRD graph for Ca/Al-carbonate synthesis at 2 h (40 °C)

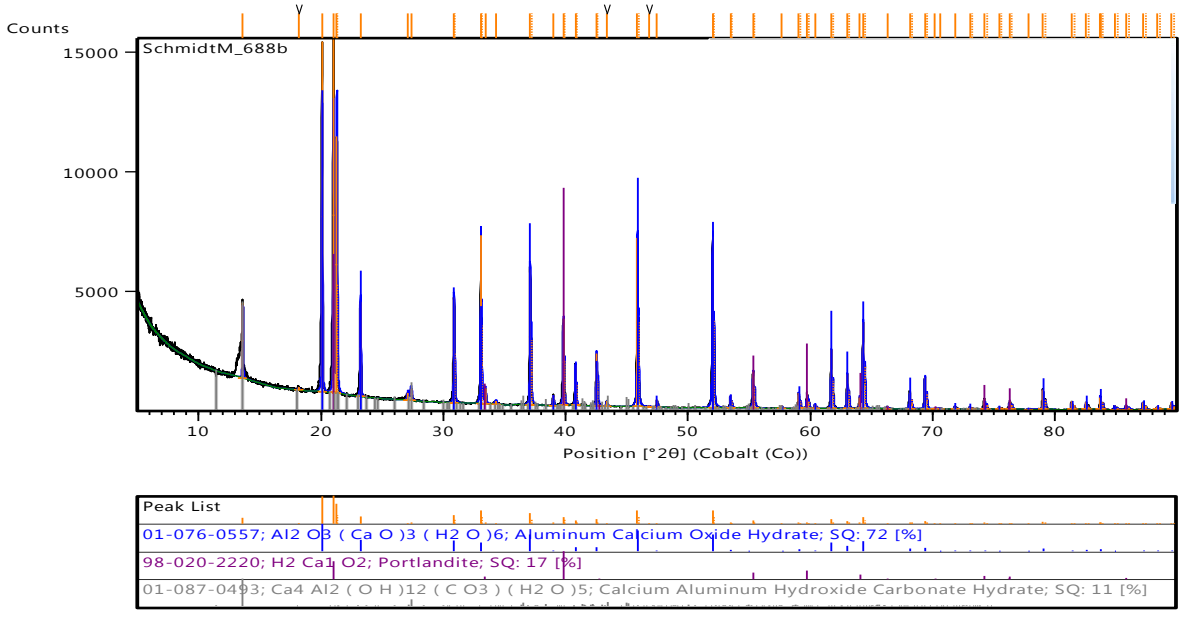

A-3: XRD graph for Ca/Al-carbonate synthesis at 2 h (60 °C)

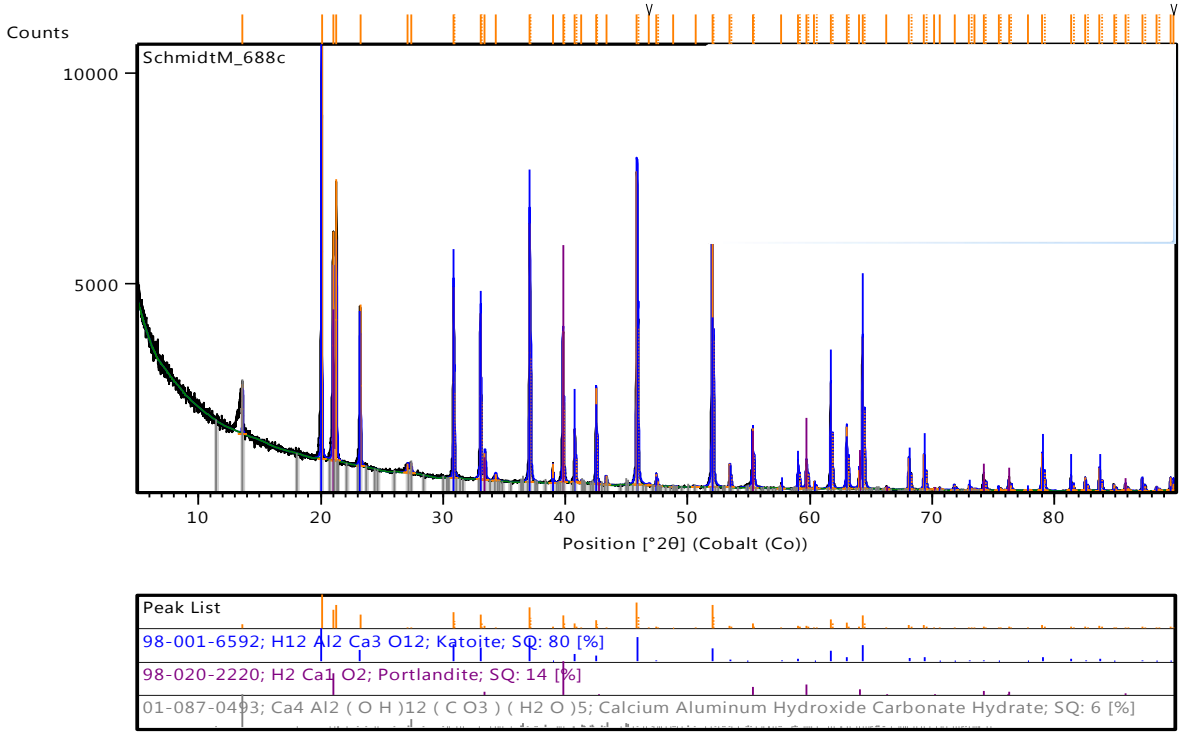

A-4: XRD graph for Ca/Al-carbonate synthesis at 2 h (80 °C)

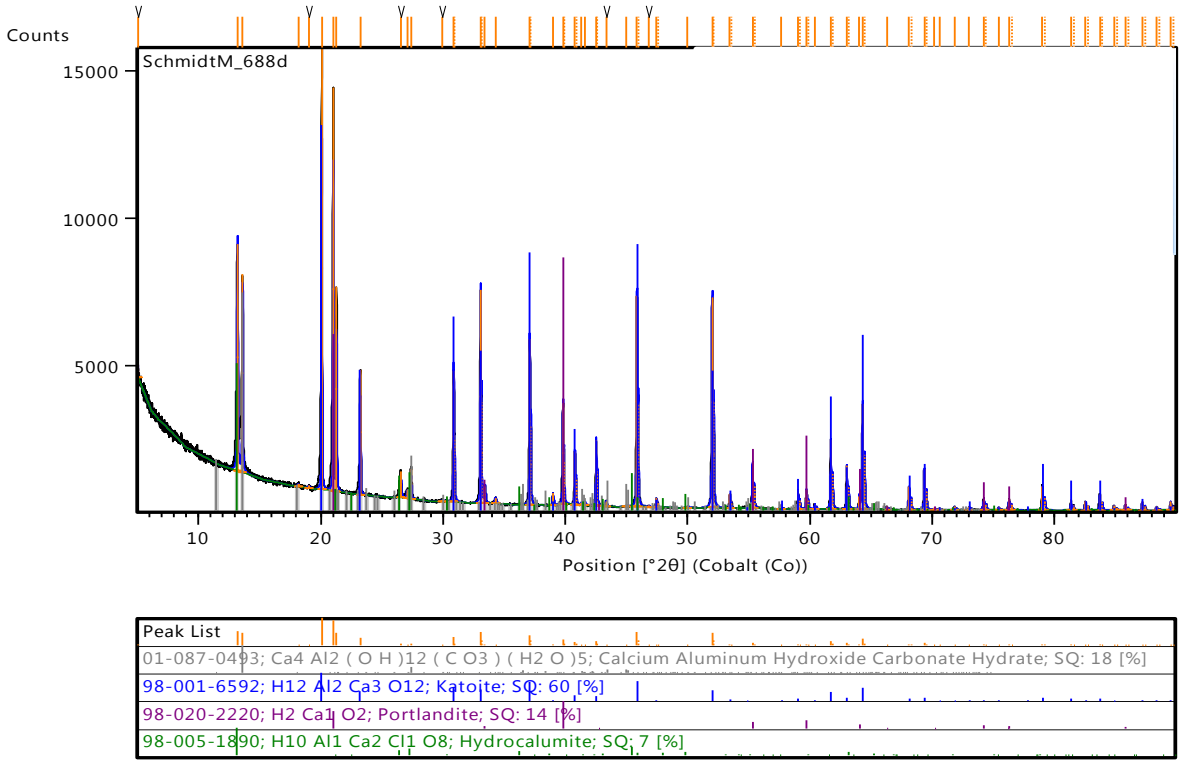

A-5: XRD graph for Ca/Al-carbonate synthesis at 6 h (ambient temperature)

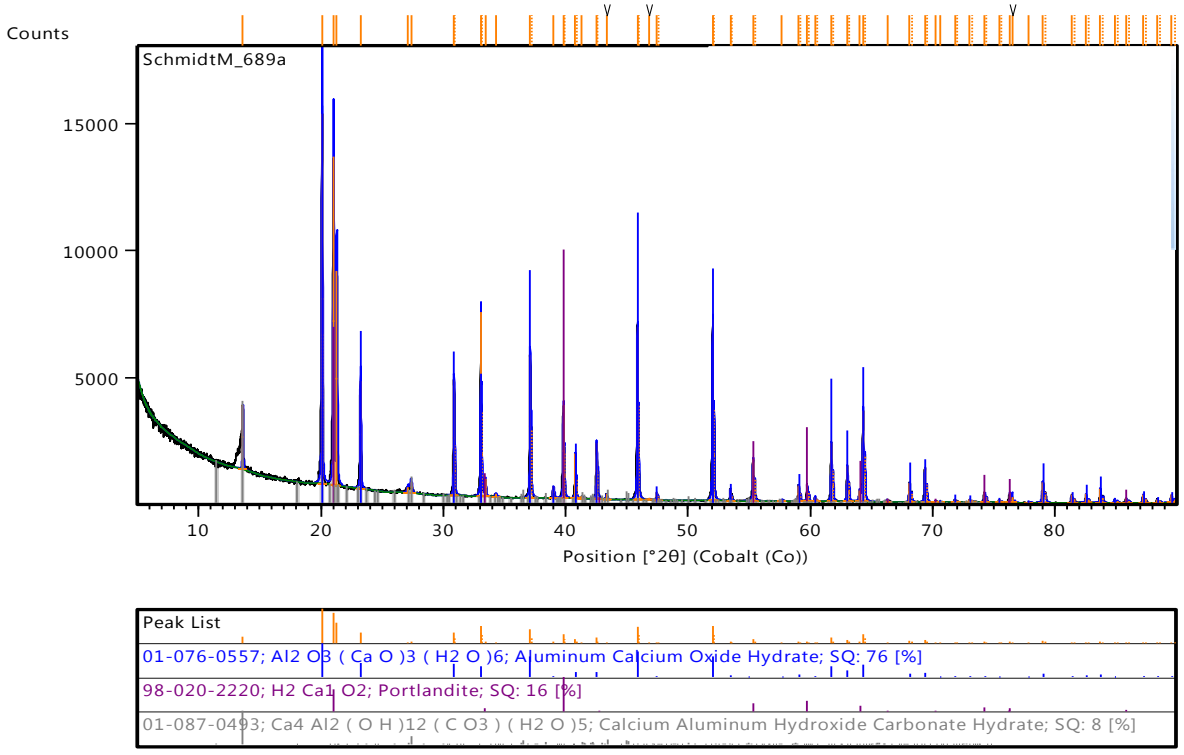

A-6: XRD graph for Ca/Al-carbonate synthesis at 6 h (40 °C)

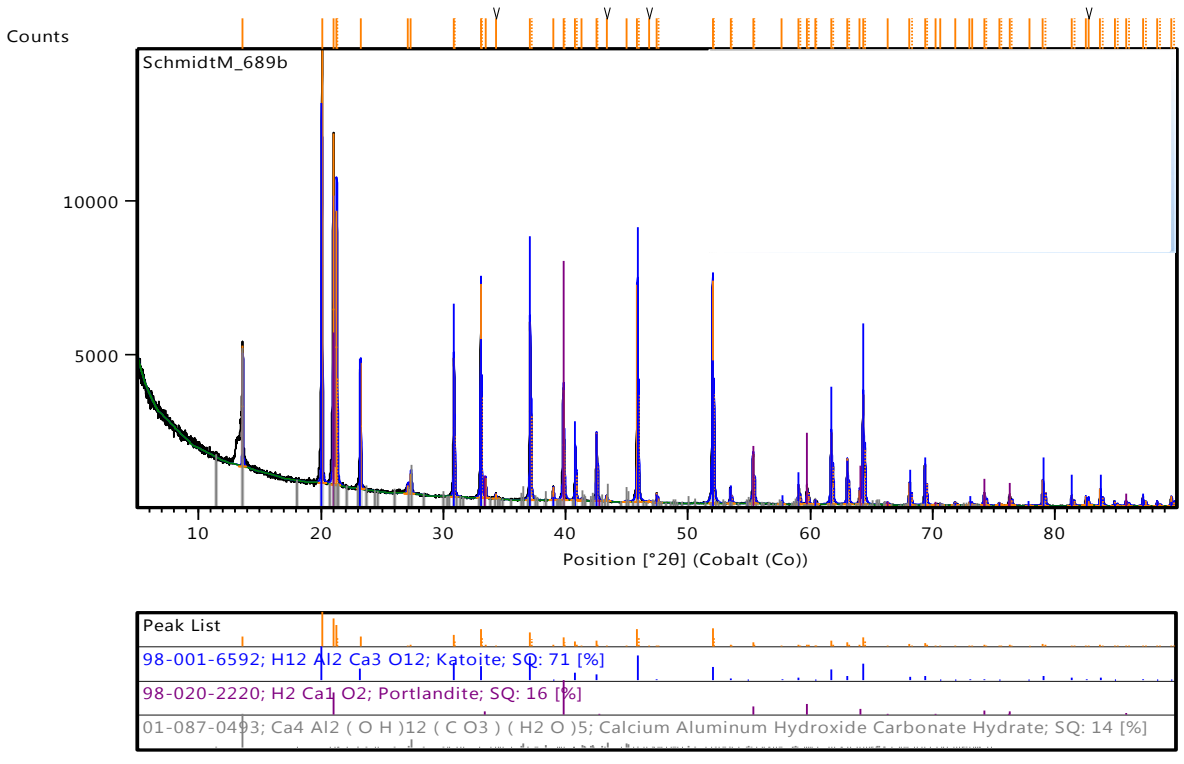

A-7: XRD graph for Ca/Al-carbonate synthesis at 6 h (60 °C)

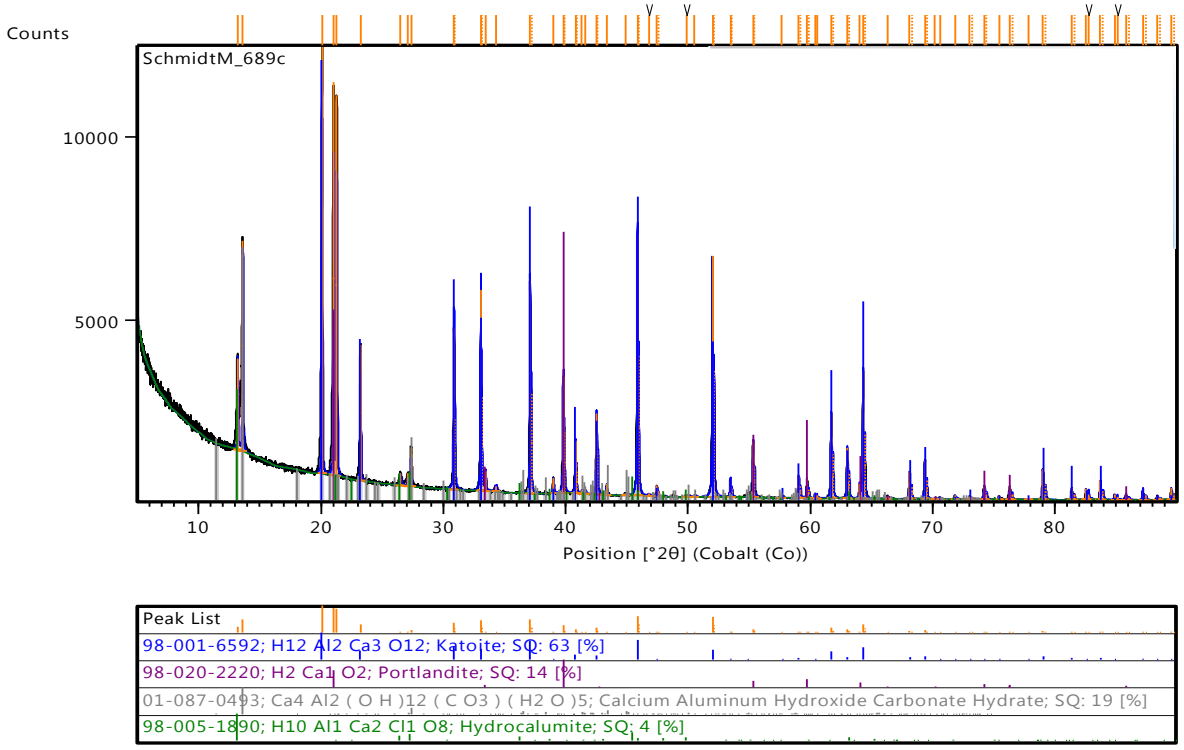

A-8: XRD graph for Ca/Al-carbonate synthesis at 6 h (80 °C)

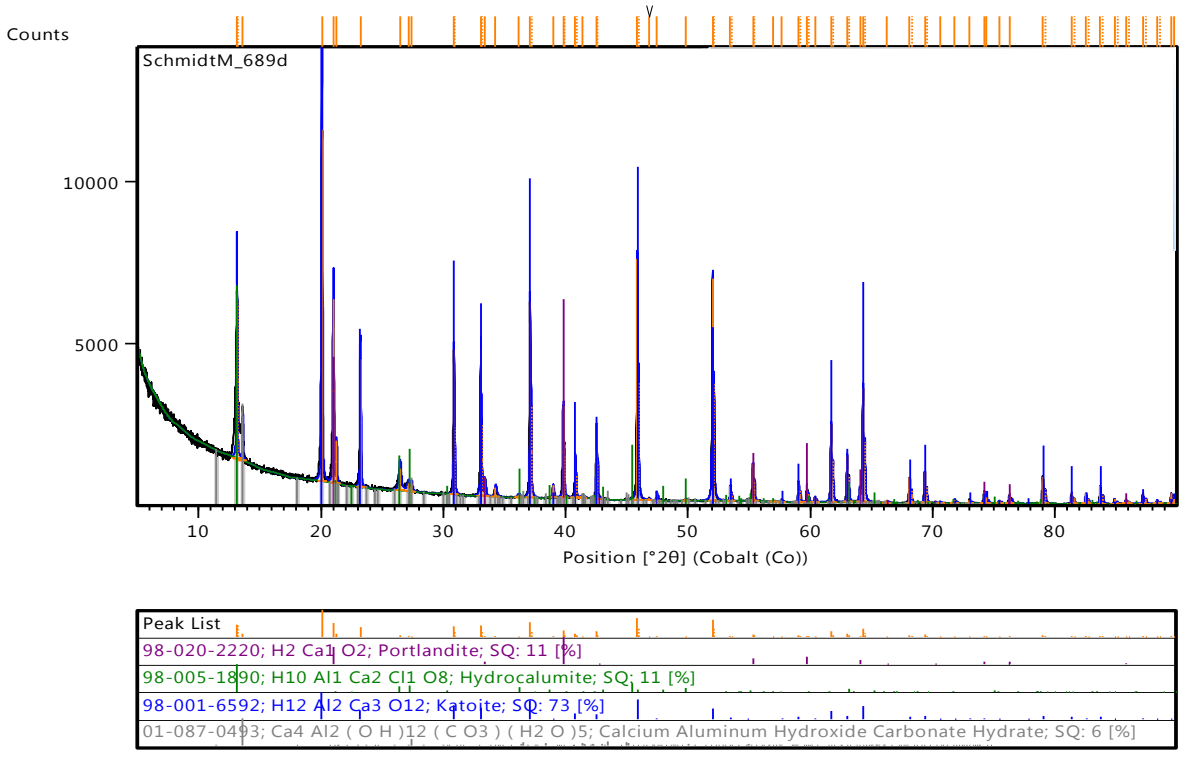

A-9: XRD graph for Ca/Al-carbonate synthesis at 12 h (ambient temperature)

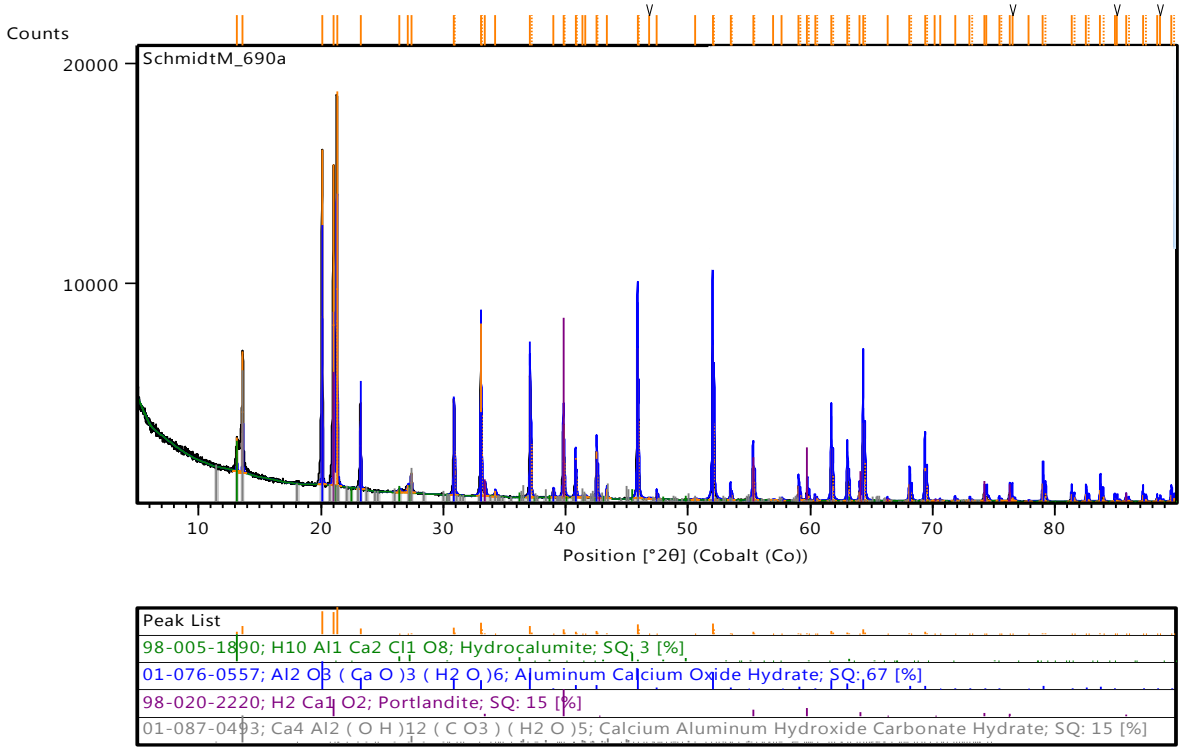

A-10: XRD graph for Ca/Al-carbonate synthesis at 12 h (40 °C)

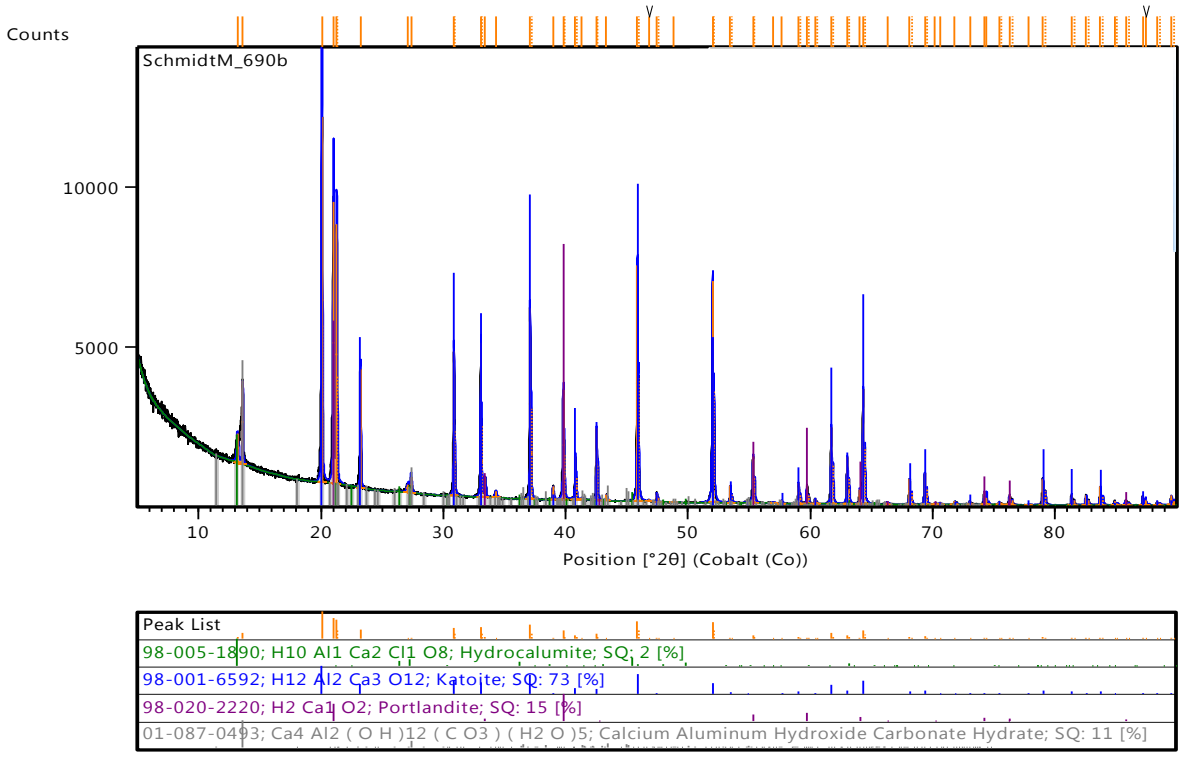

A-11: XRD graph for Ca/Al-carbonate synthesis at 12 h (60 °C)

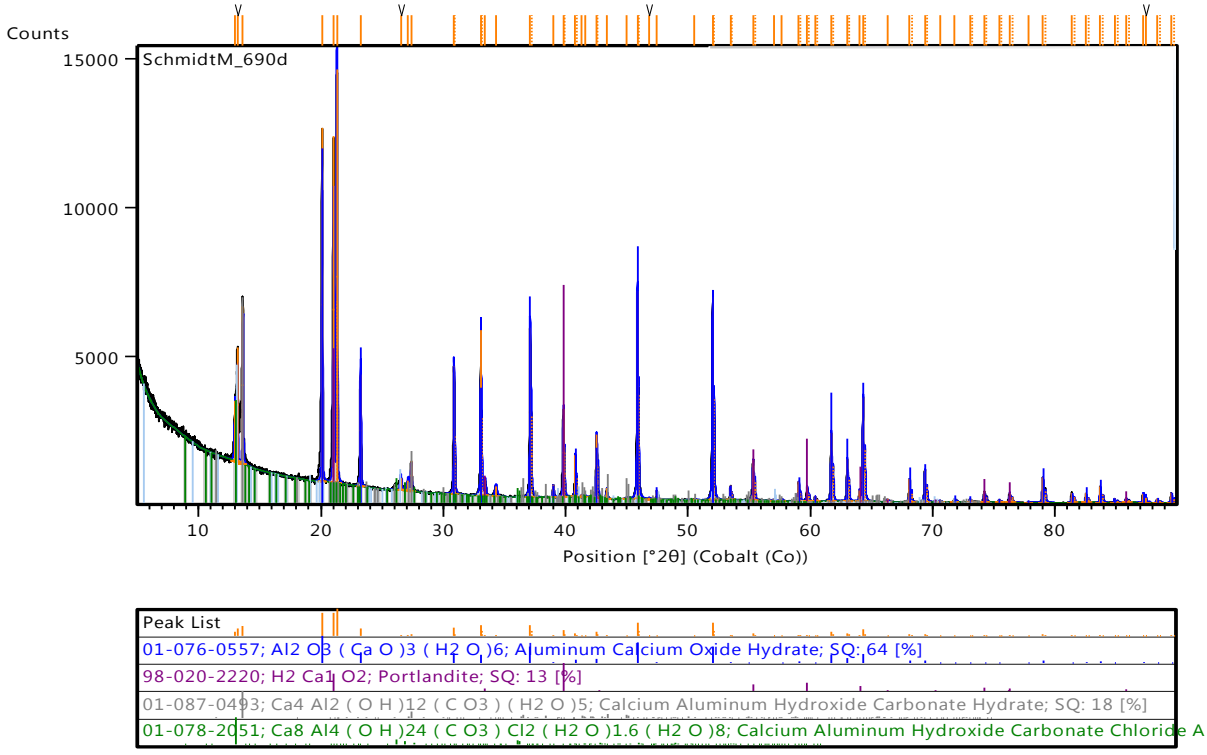

A-12: XRD graph for Ca/Al-carbonate synthesis at 24 h (ambient temperature)

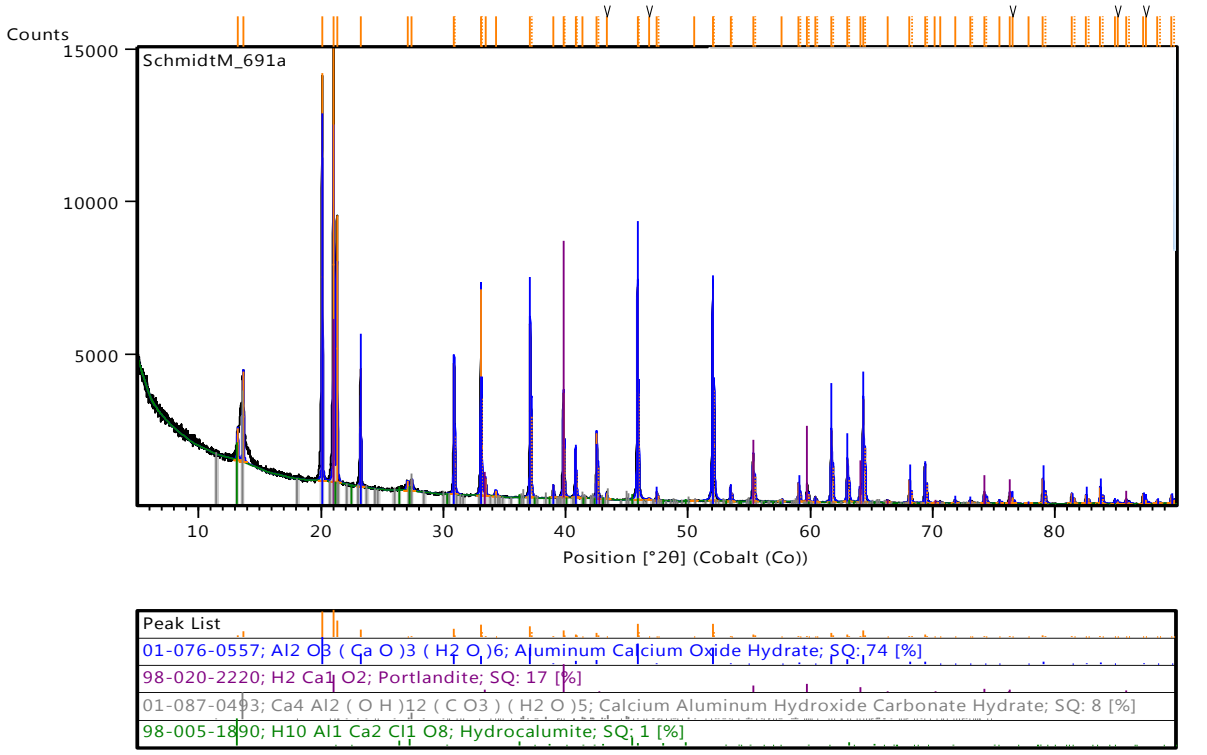

A-13: XRD graph for Ca/Al-carbonate synthesis at 24 h (40 °C)

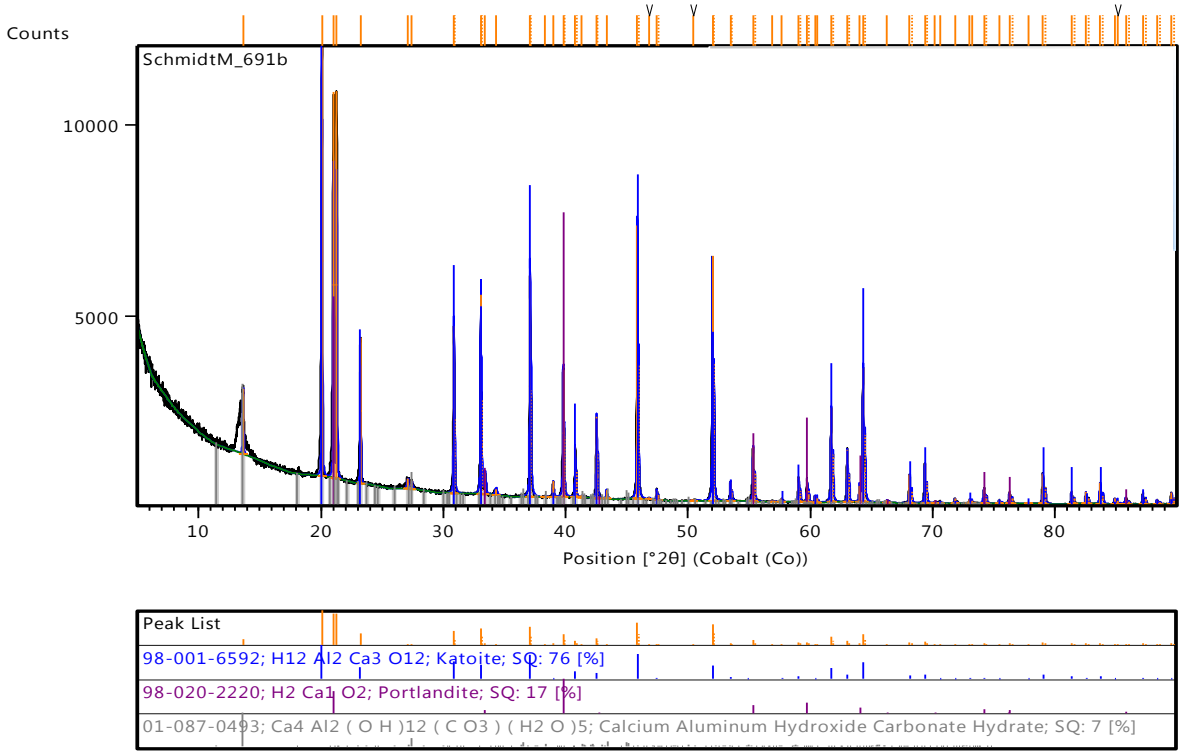

A-14: XRD graph for Ca/Al-carbonate synthesis at 24 h (60 °C)

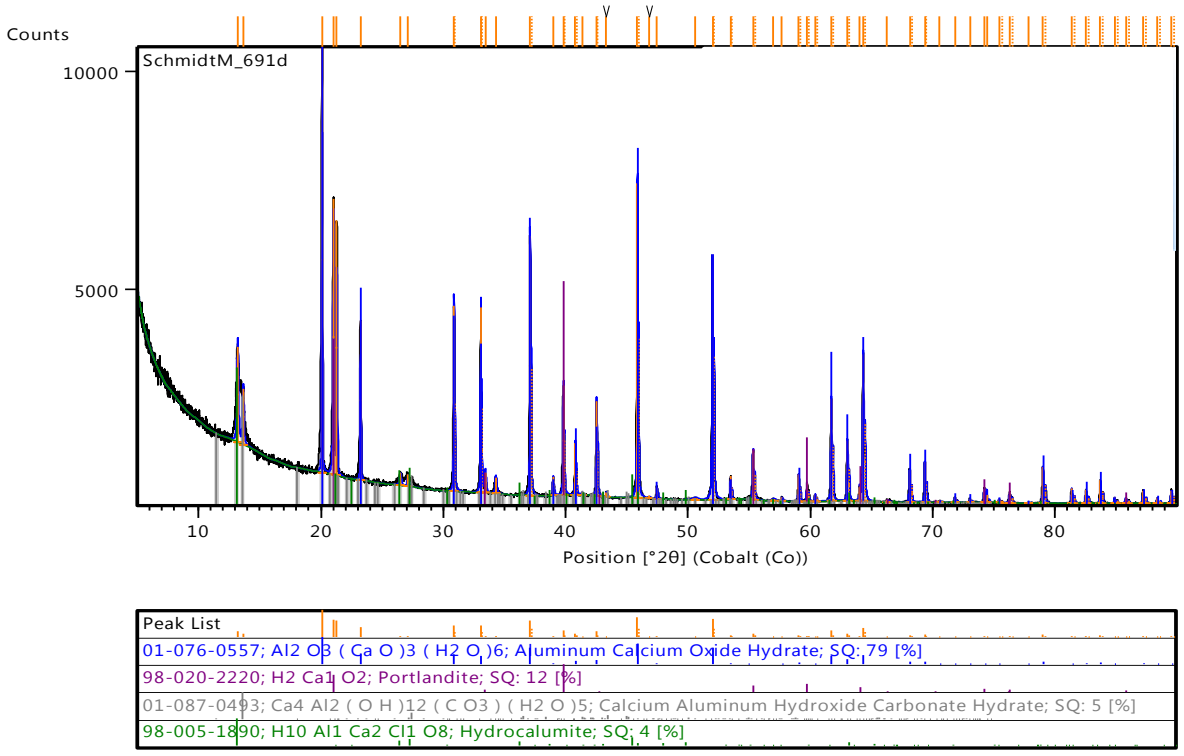

A-15: XRD graph for Ca/Al-chloride synthesis at 2 h (ambient temperature)

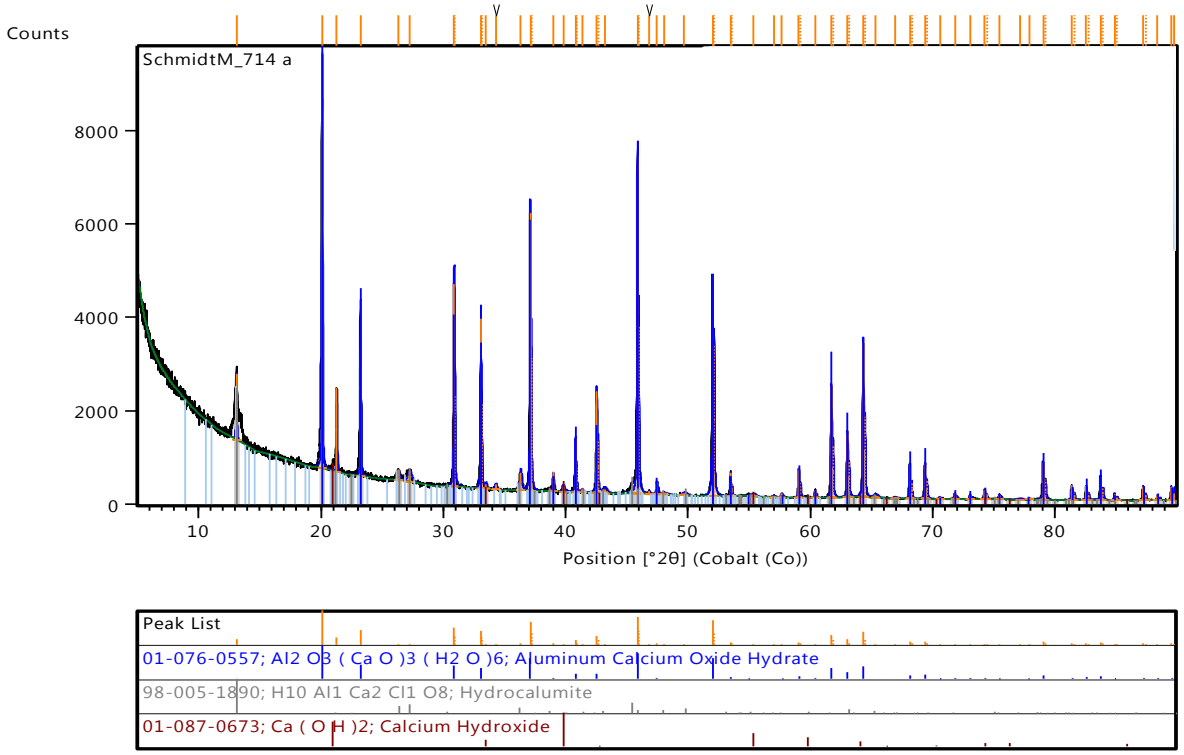

A-16: XRD graph for Ca/Al-chloride synthesis at 2 h (40 °C)

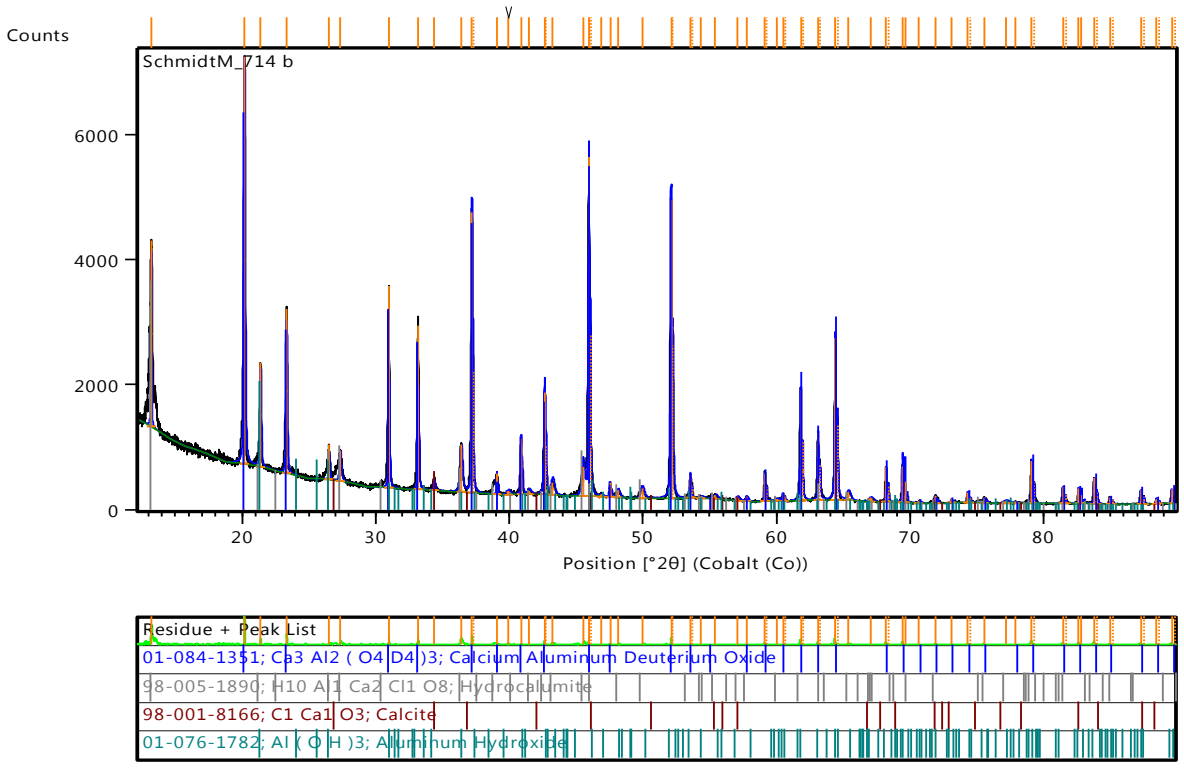

A-17: XRD graph for Ca/Al-chloride synthesis at 2 h (50 °C)

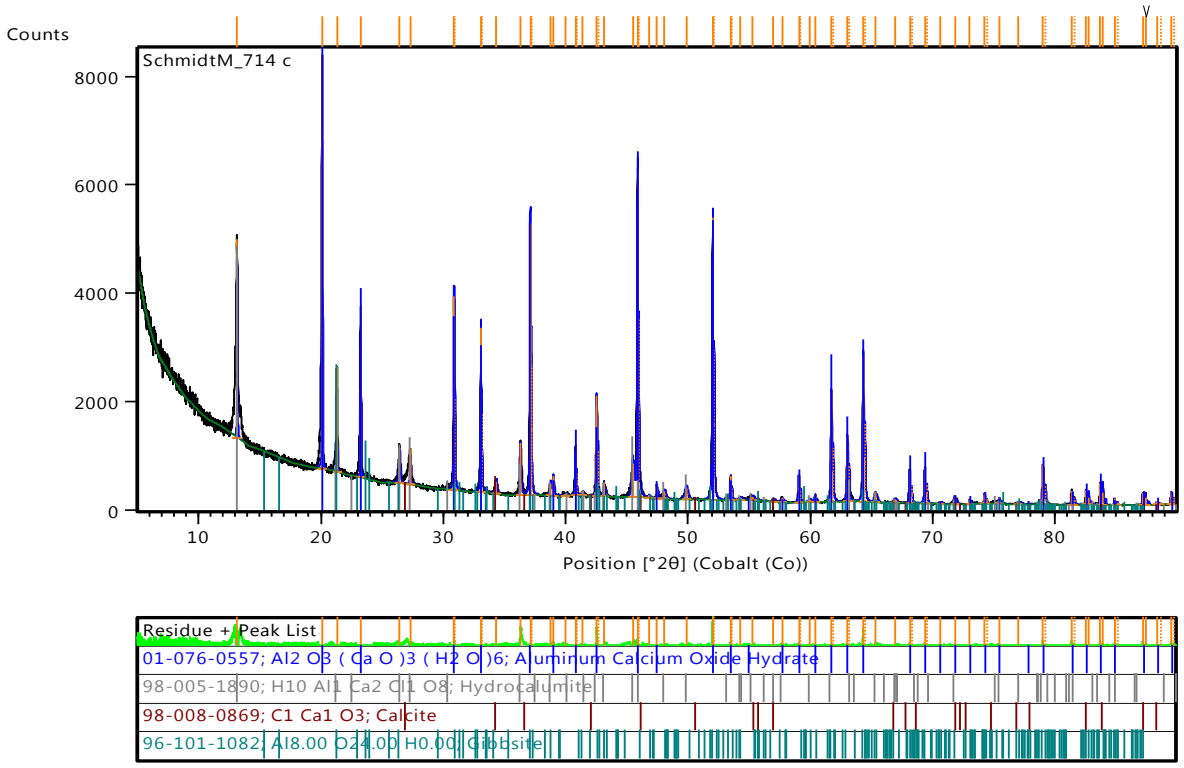

A-18: XRD graph for Ca/Al-chloride synthesis at 2 h (60 °C)

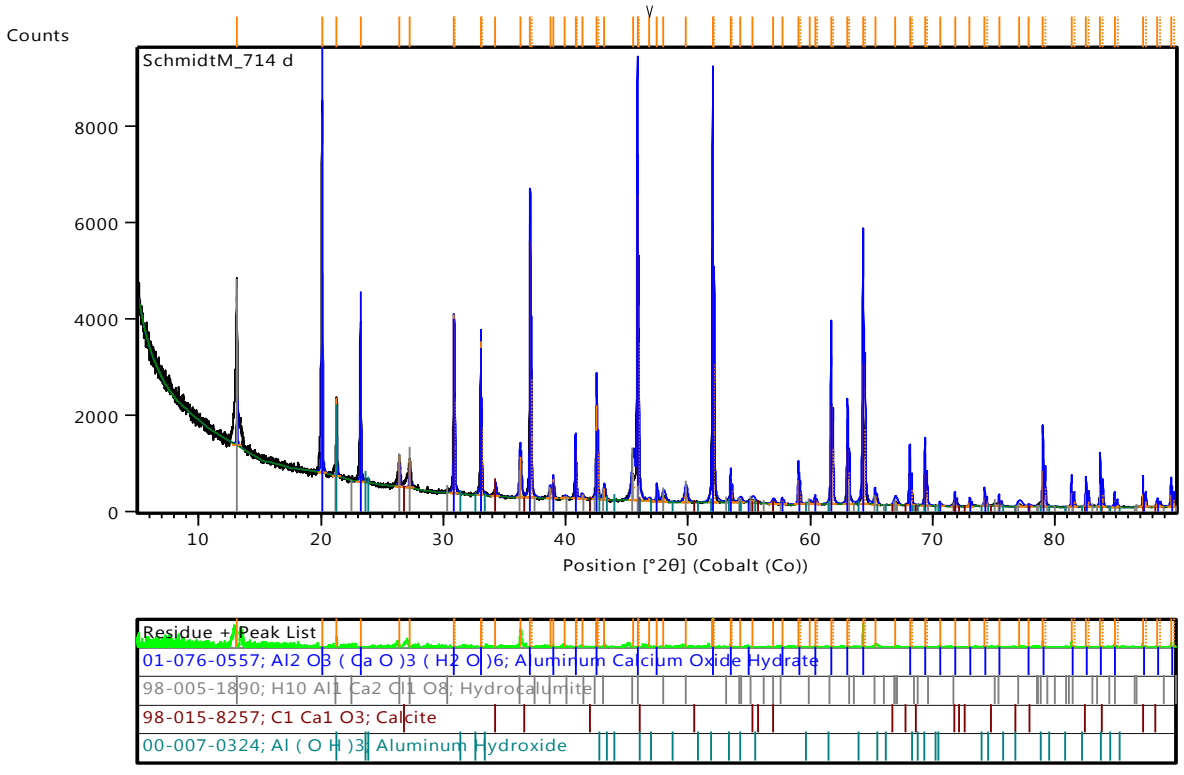

A-19: XRD graph for Ca/Al-chloride synthesis at 6 h (ambient temperature)

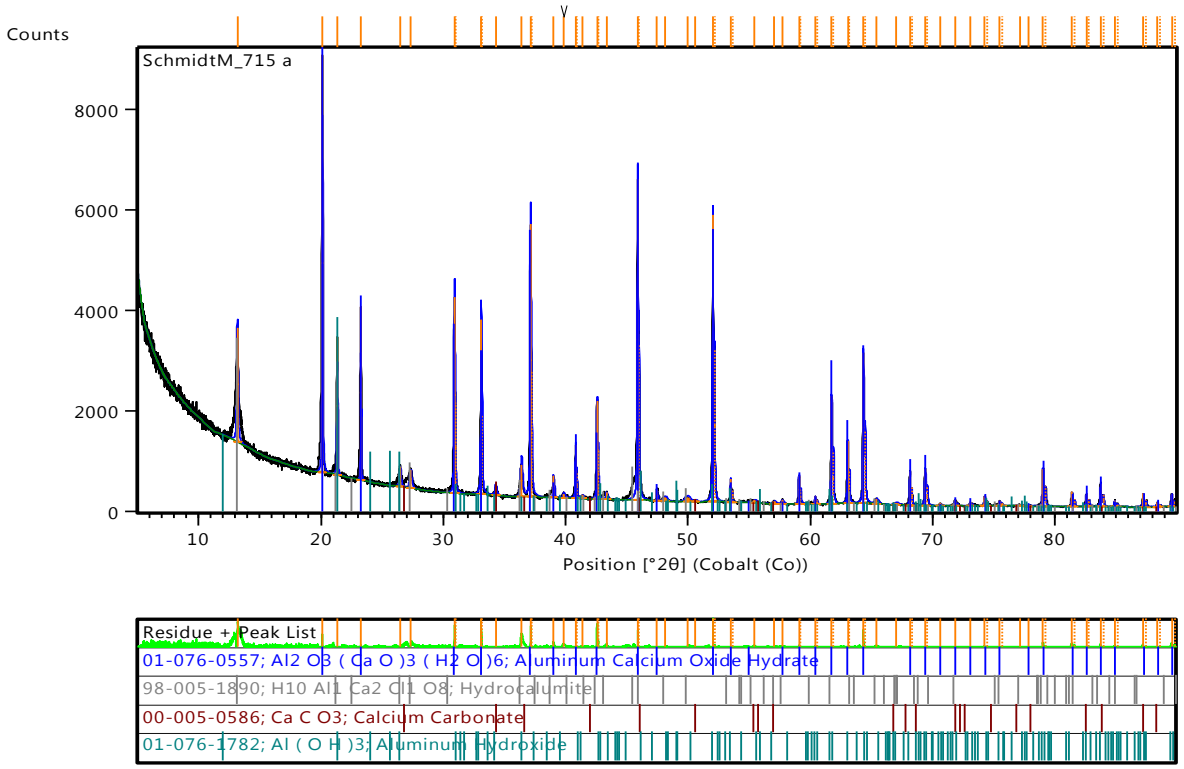

A-20: XRD graph for Ca/Al-chloride synthesis at 6 h (40 °C)

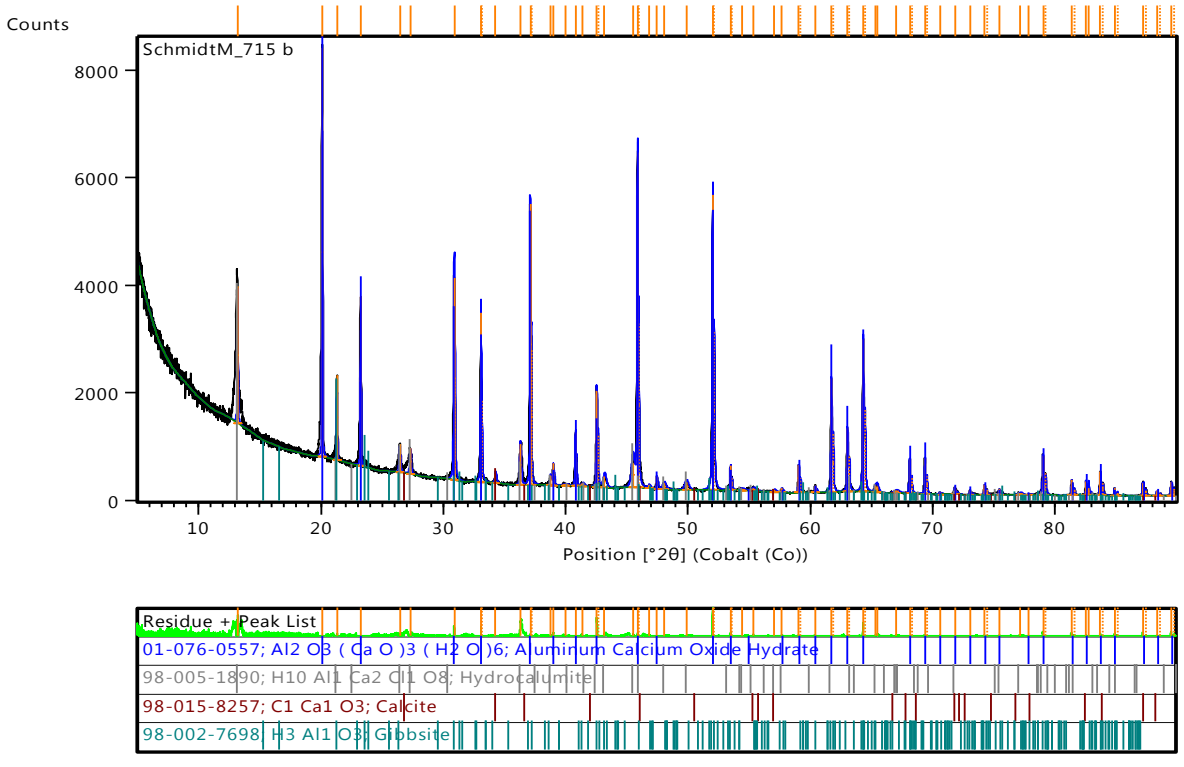

A-21: XRD graph for Ca/Al-chloride synthesis at 6 h (50 °C)

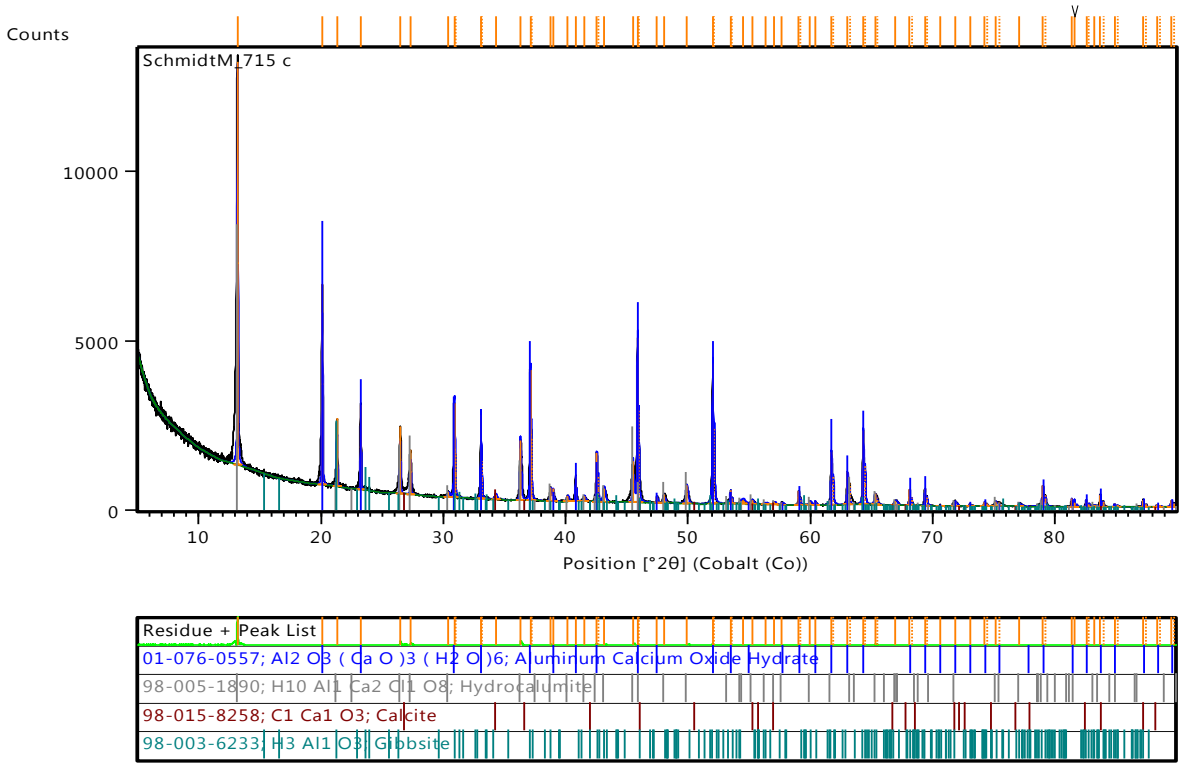

A-22: XRD graph for Ca/Al-chloride synthesis at 6 h (60 °C)

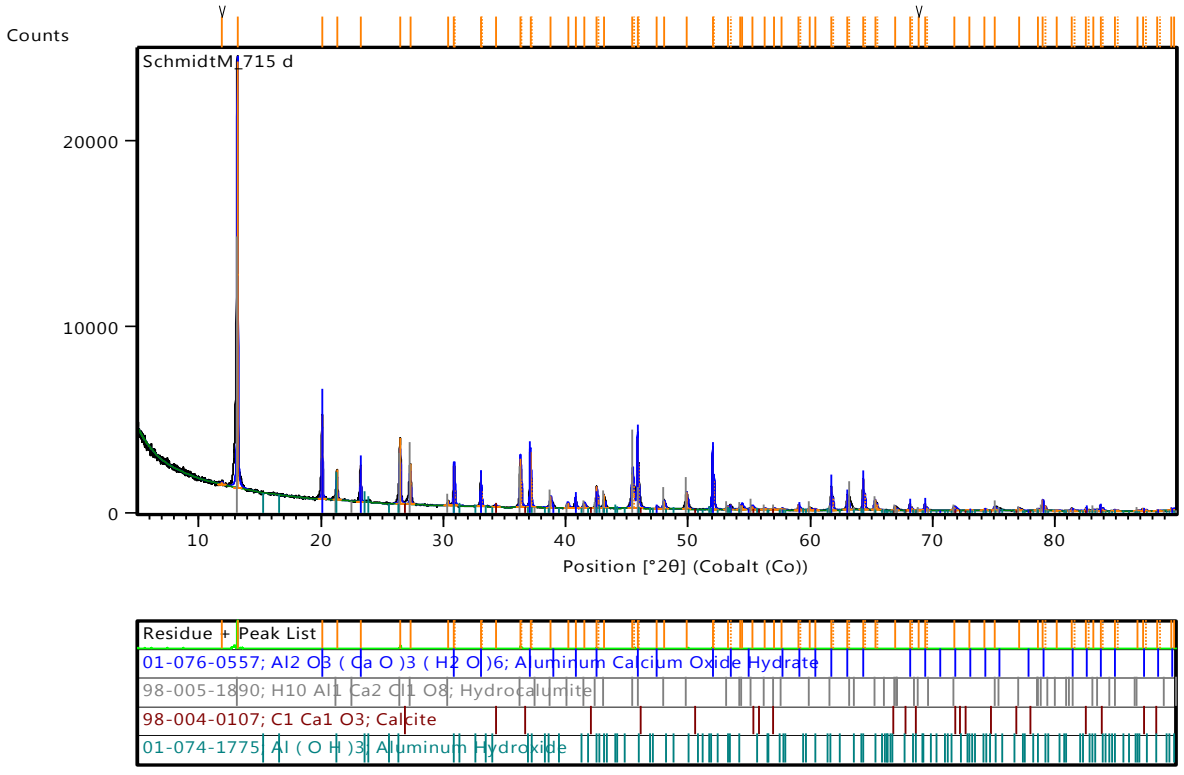

A-23: XRD graph for Ca/Al-chloride synthesis at 12 h (ambient temperature)

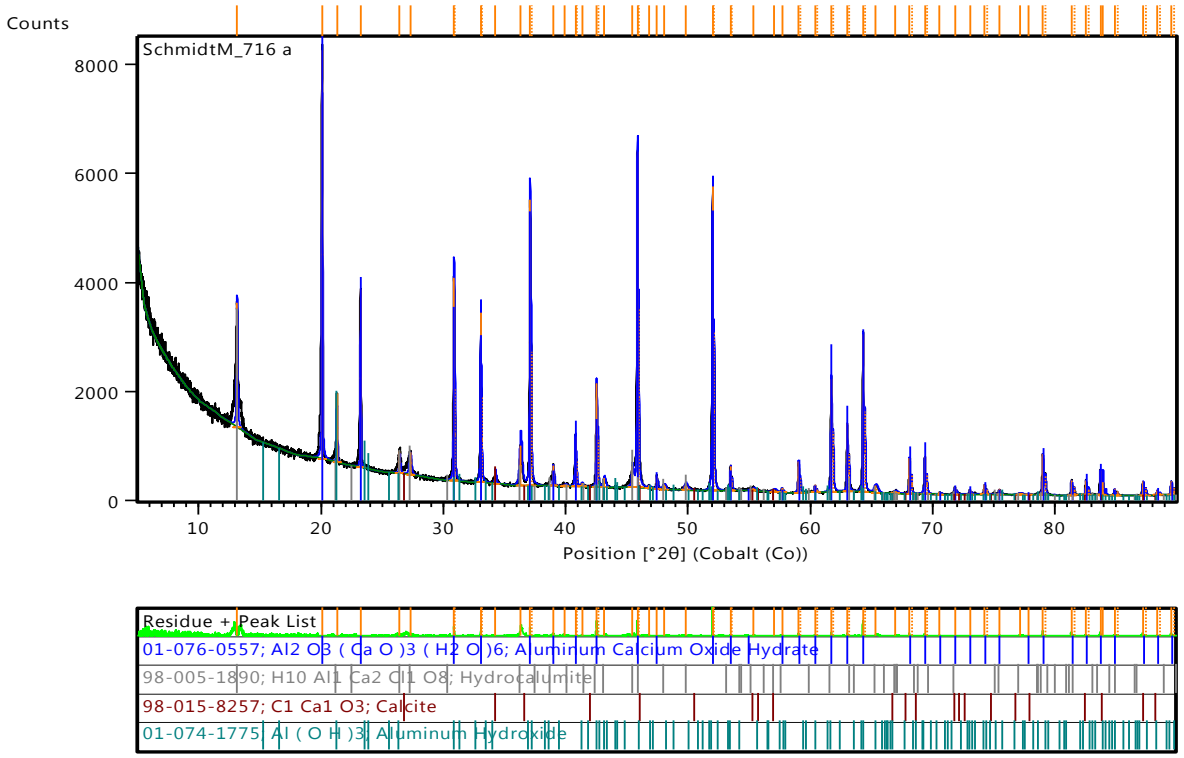

A-24: XRD graph for Ca/Al-chloride synthesis at 12 h (40 °C)

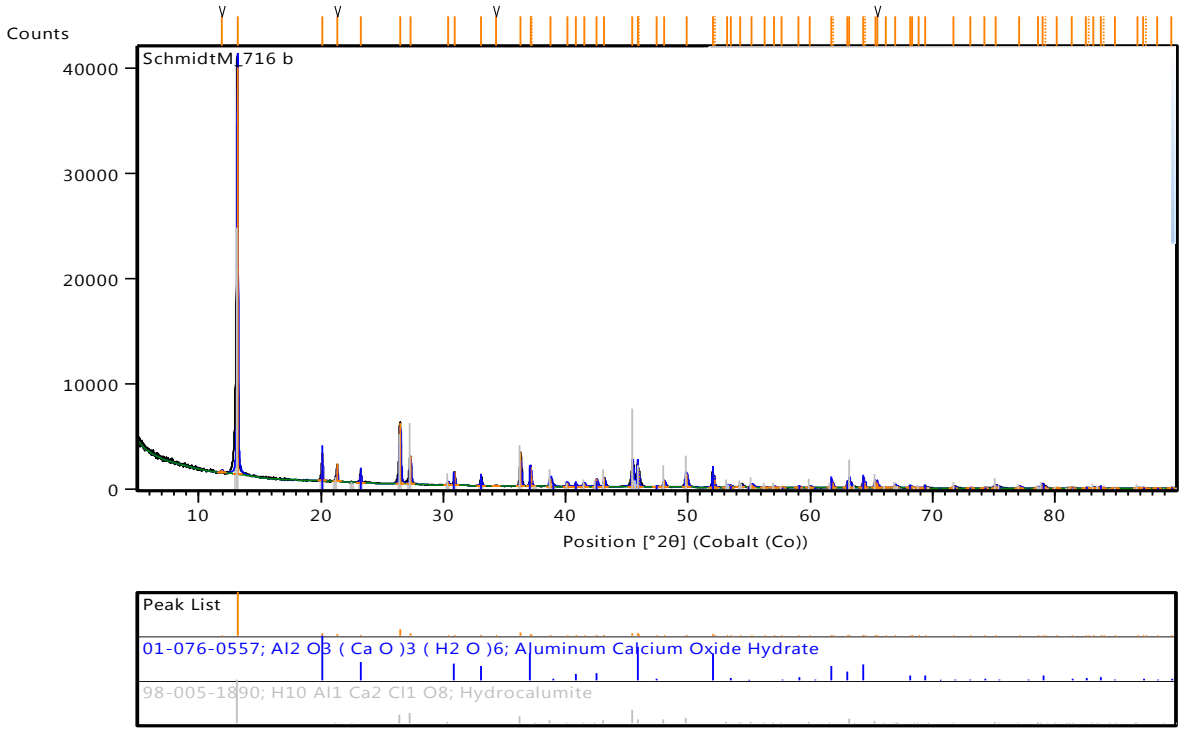

A-25: XRD graph for Ca/Al-chloride synthesis at 12 h (50 °C)

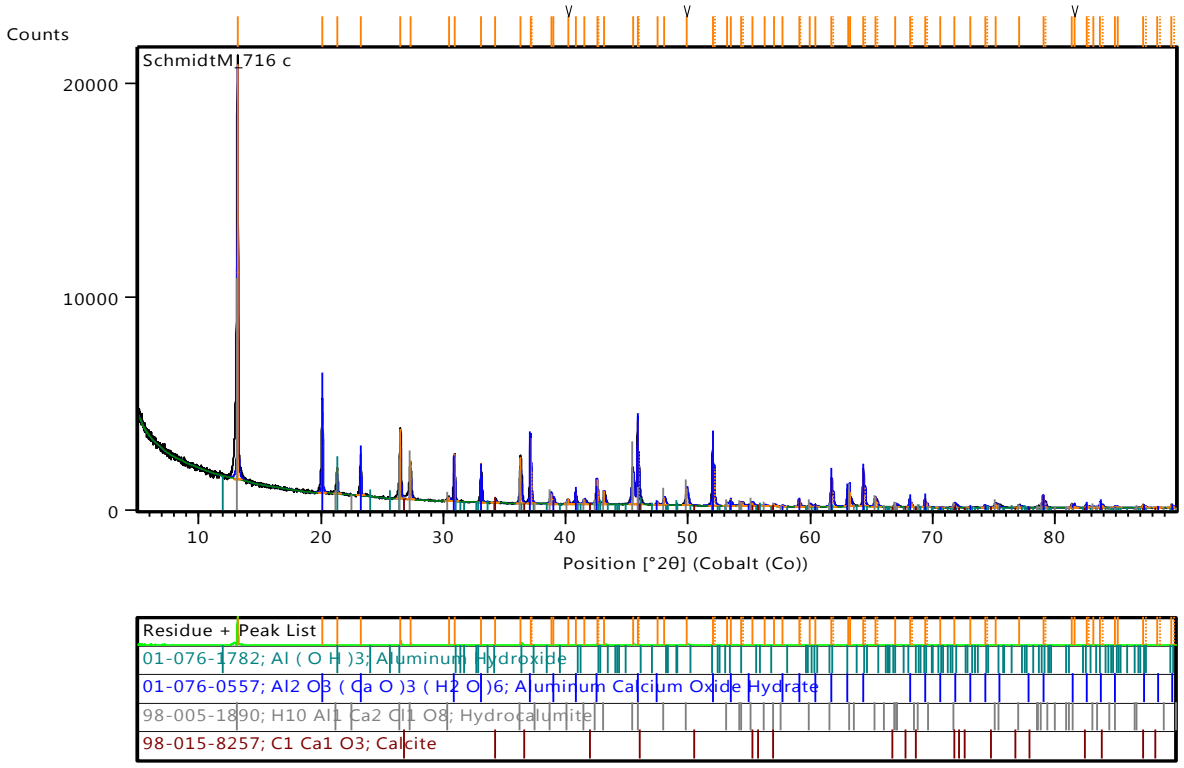

A-26: XRD graph for Ca/Al-chloride synthesis at 12 h (60 °C)

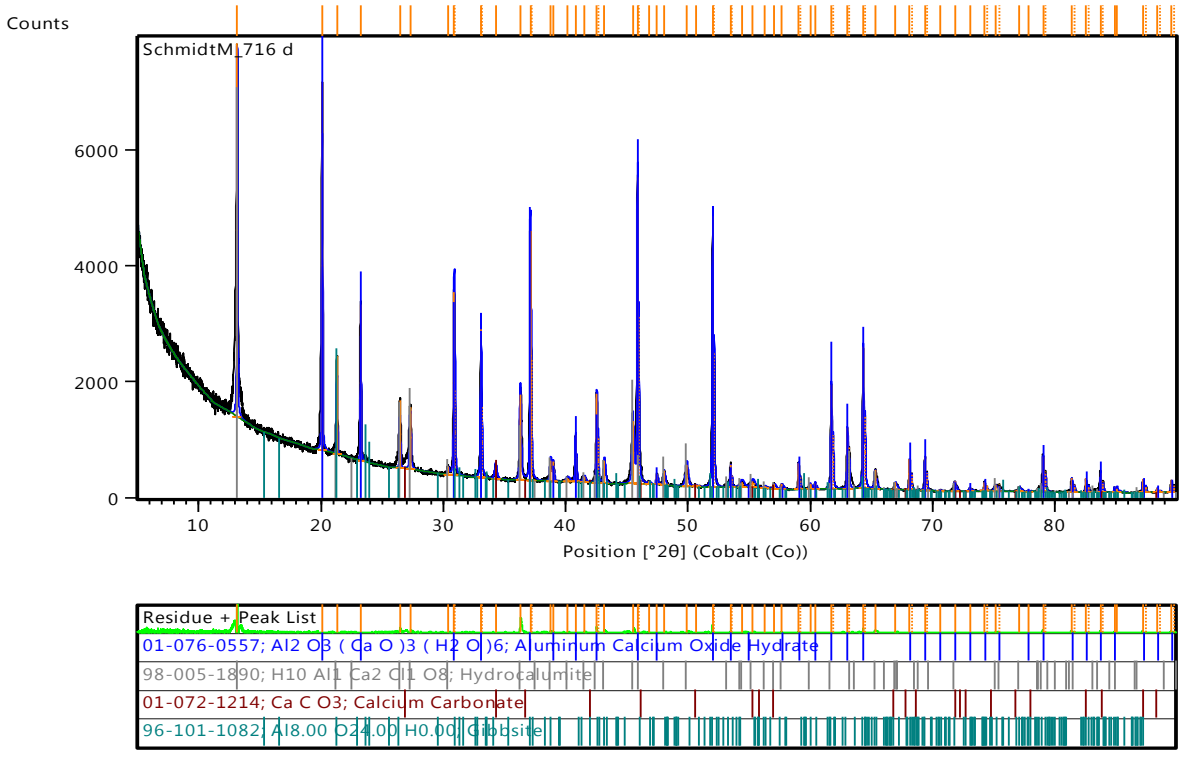

A-27: XRD graph for Ca/Al-chloride synthesis at 24 h (ambient temperature)

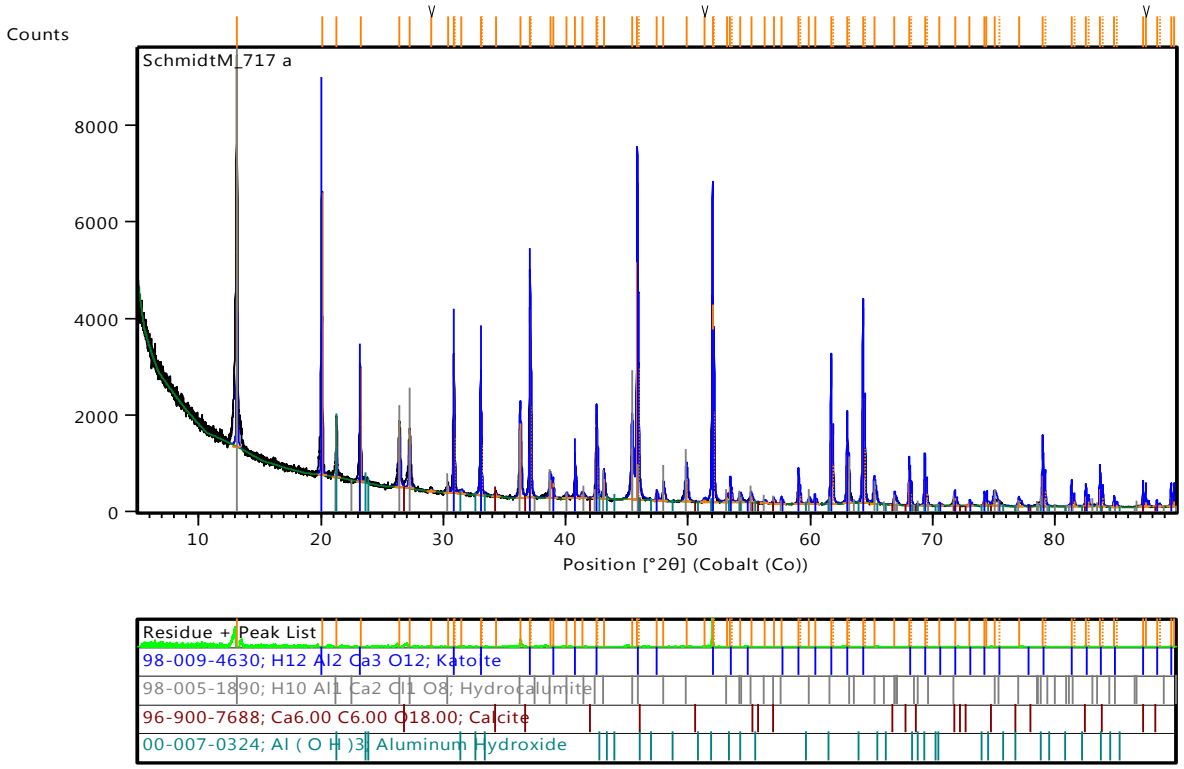

A-28: XRD graph for Ca/Al-chloride synthesis at 24 h (40 °C)

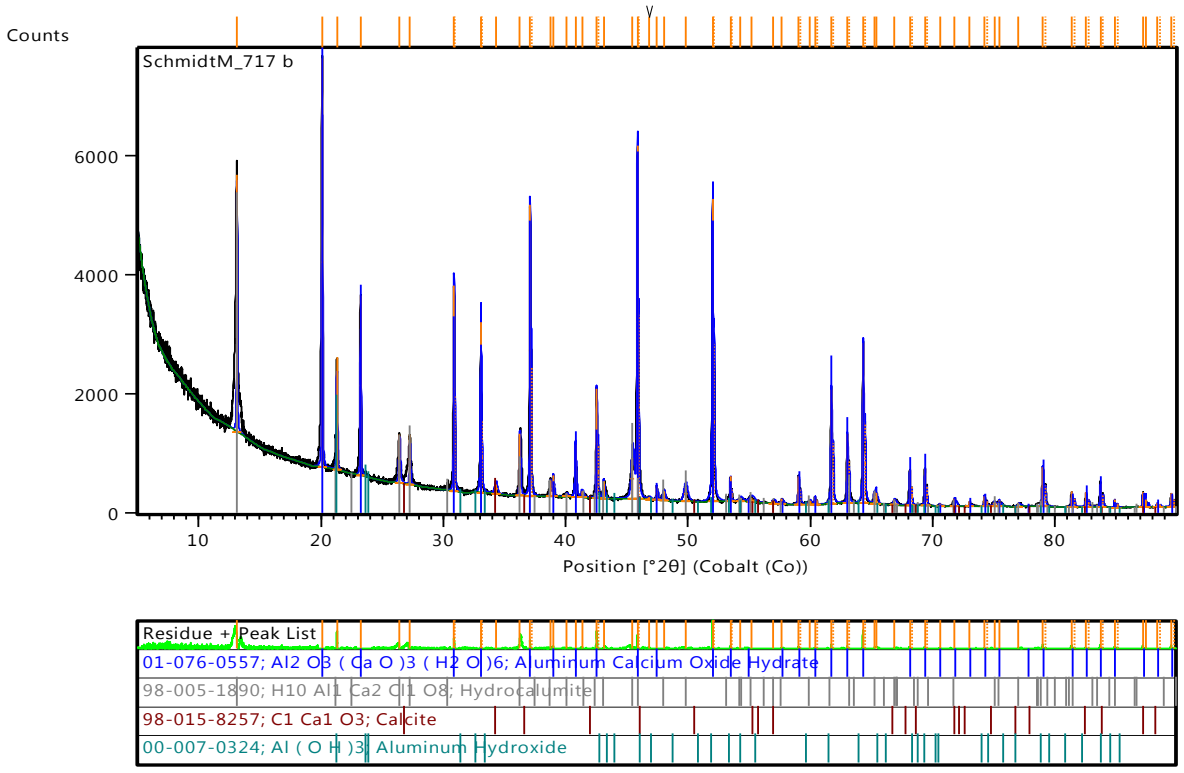

A-29: XRD graph for Ca/Al-chloride synthesis at 24 h (50 °C)

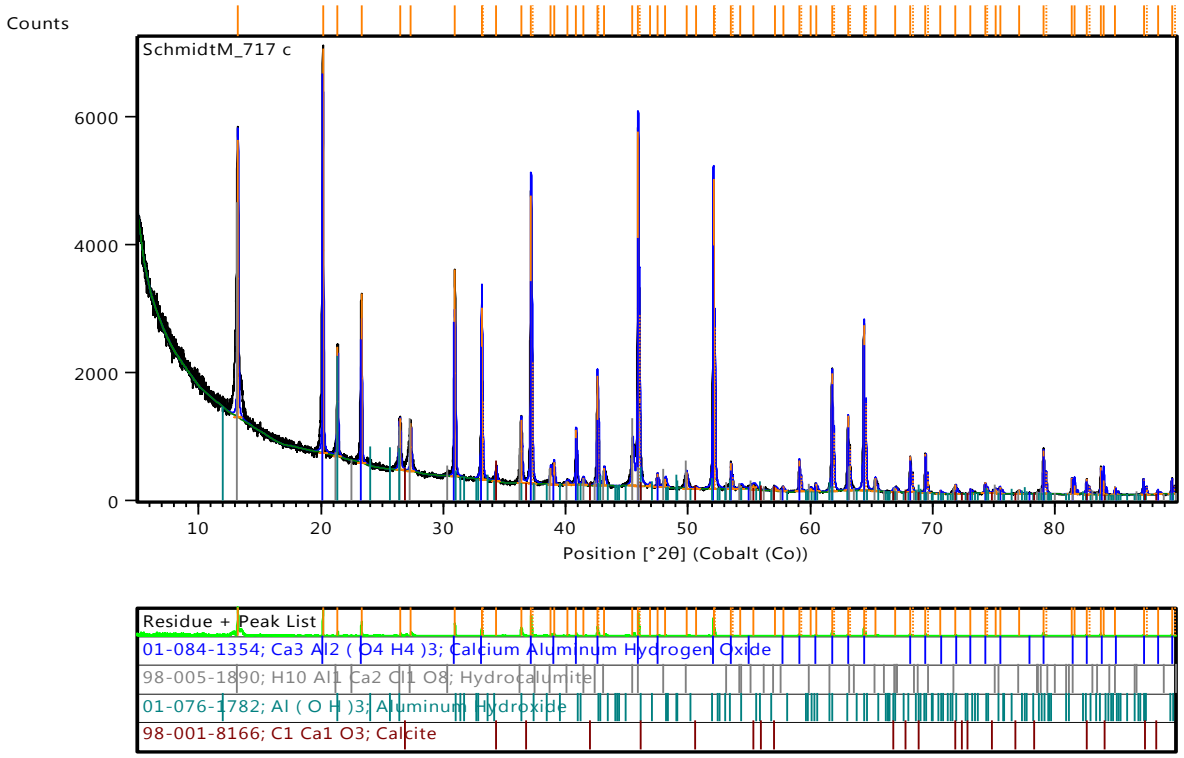

A-30: XRD graph for Ca/Al-chloride synthesis at 24 h (60 °C)

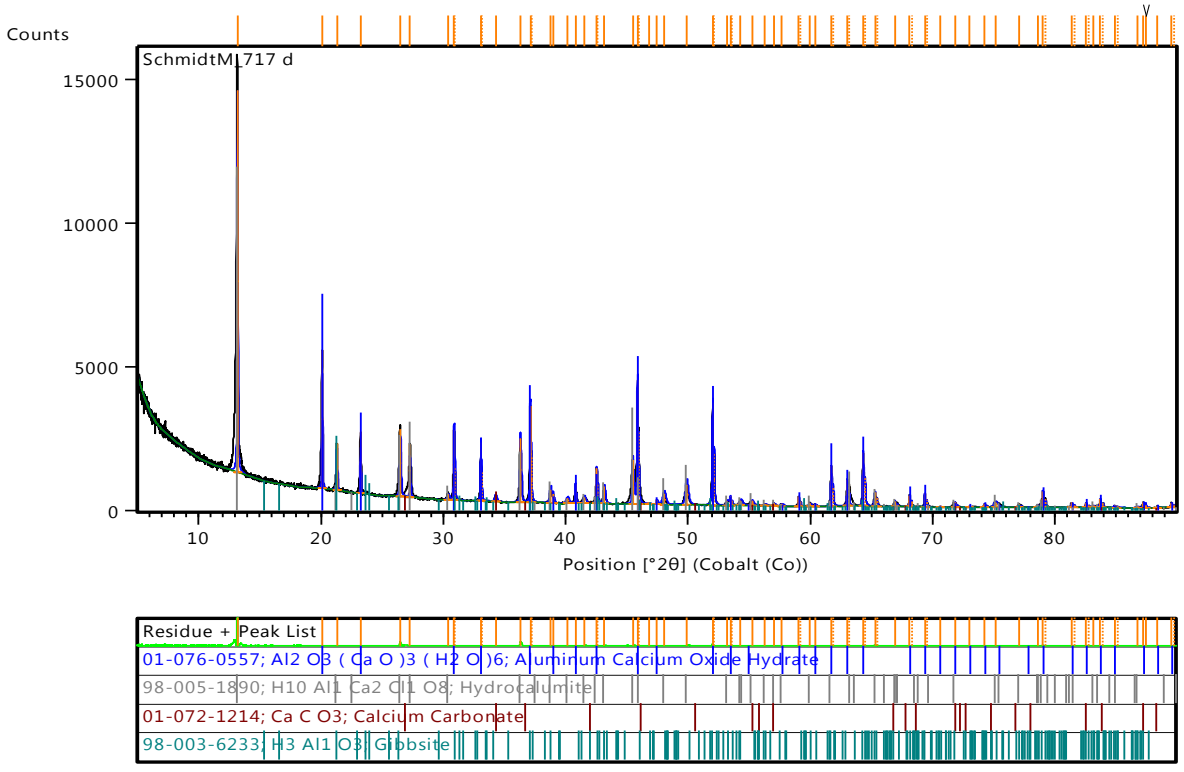

A-31: XRD graph for Ca/Al-benzoate synthesis at 2 h (ambient temperature)

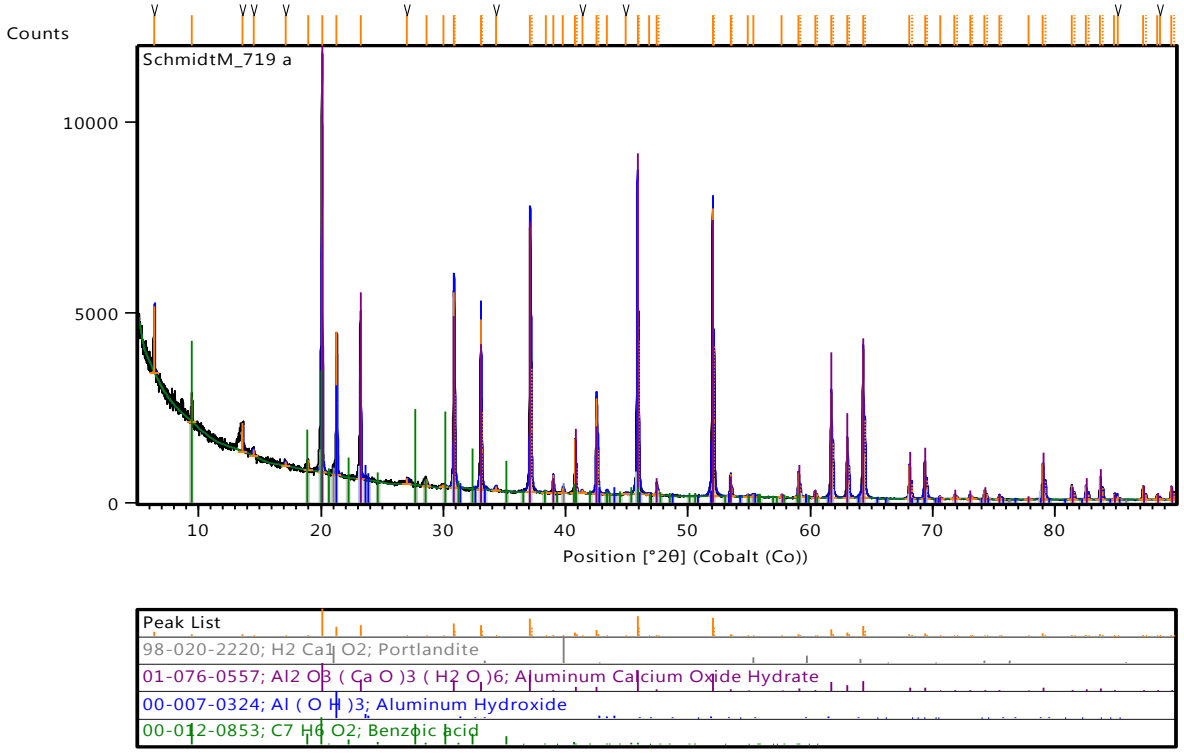

A-32: XRD graph for Ca/Al-benzoate synthesis at 2 h (40 °C)

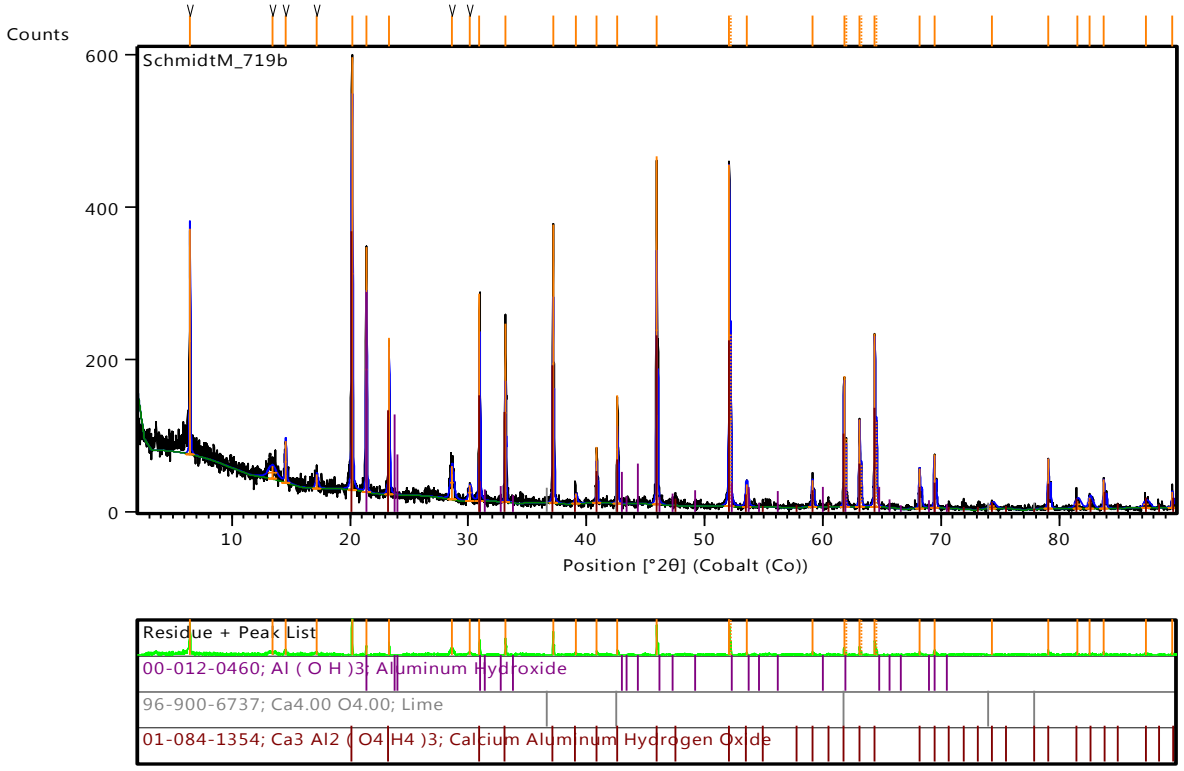

A-33: XRD graph for Ca/Al-benzoate synthesis at 2 h (50 °C)

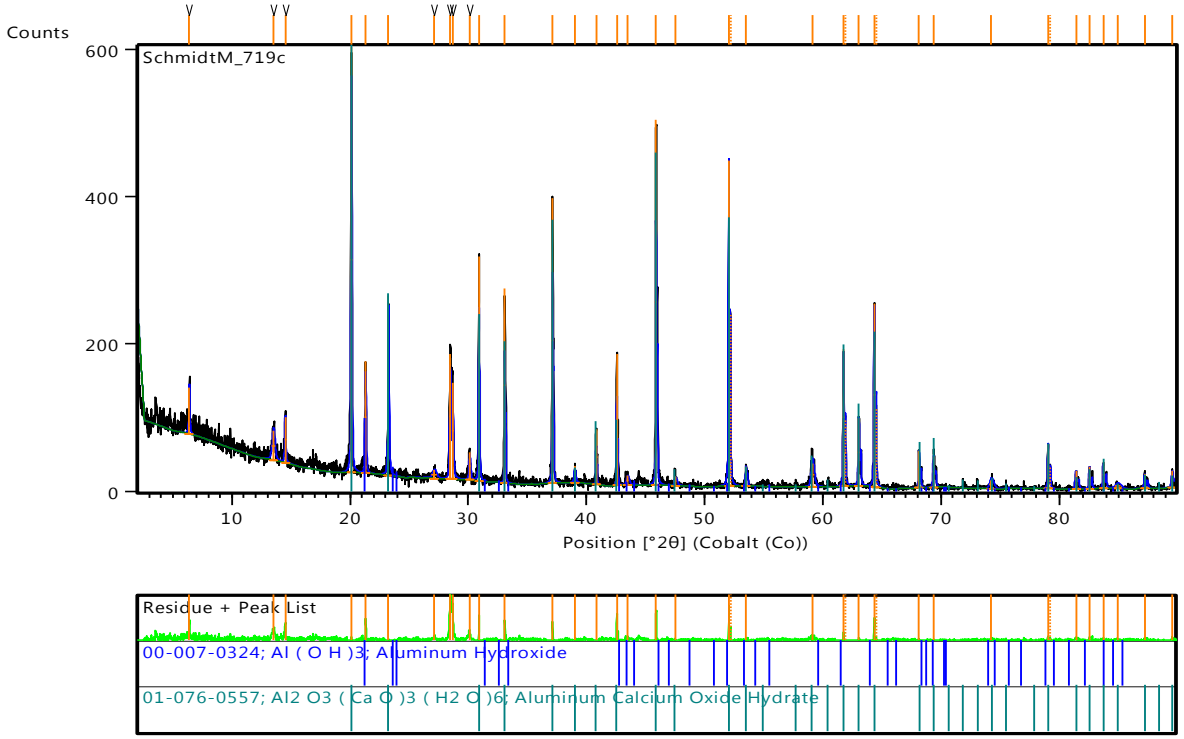

A-34: XRD graph for Ca/Al-benzoate synthesis at 2 h (60 °C)

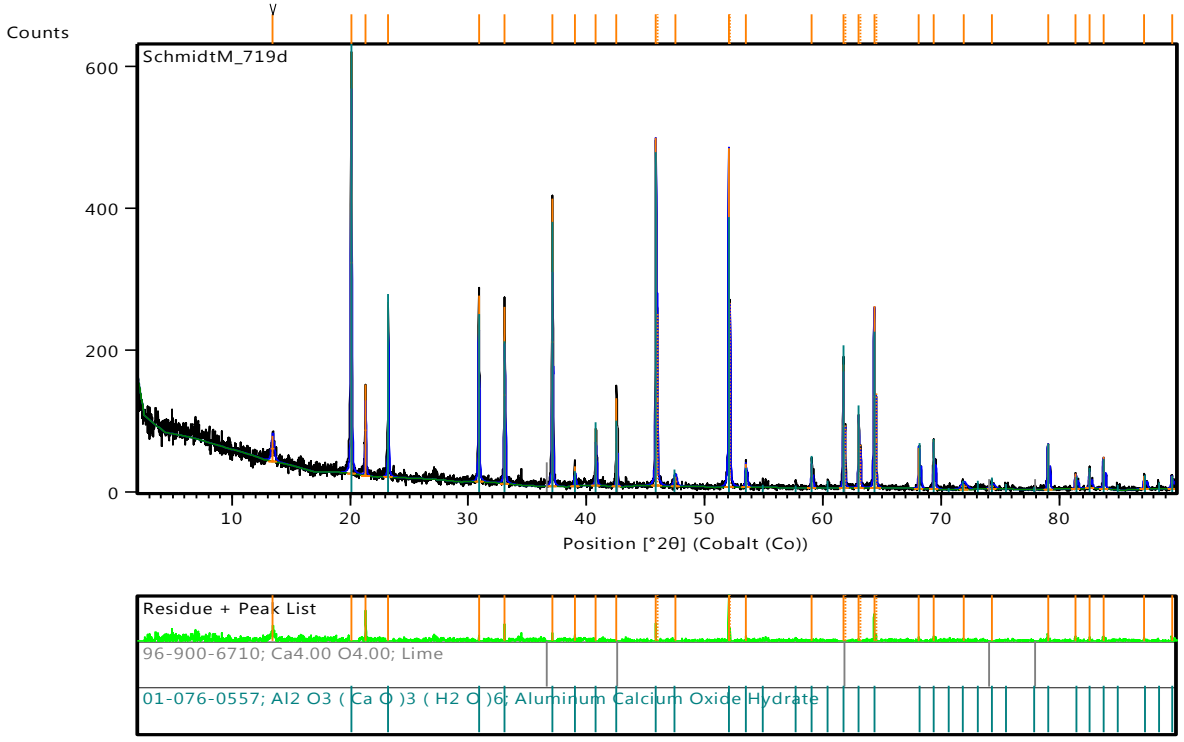

A-35: XRD graph for Ca/Al-benzoate synthesis at 6 h (ambient temperature)

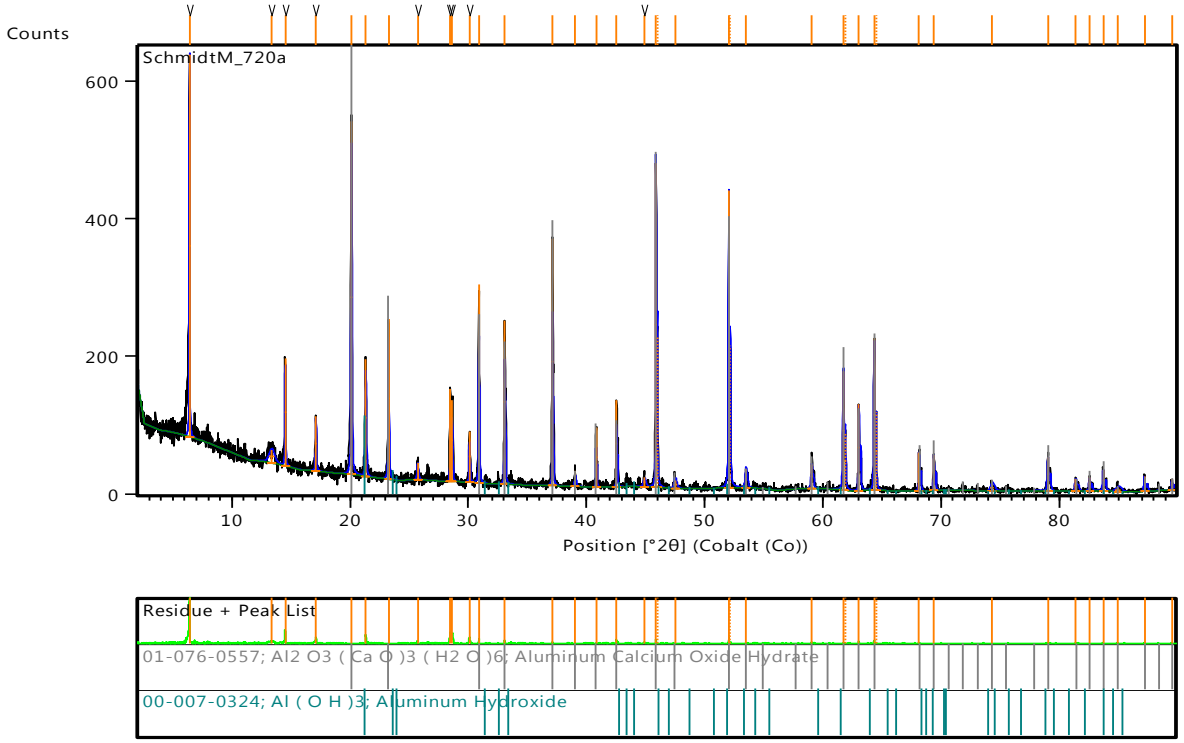

A-36: XRD graph for Ca/Al-benzoate synthesis at 6 h (40 °C)

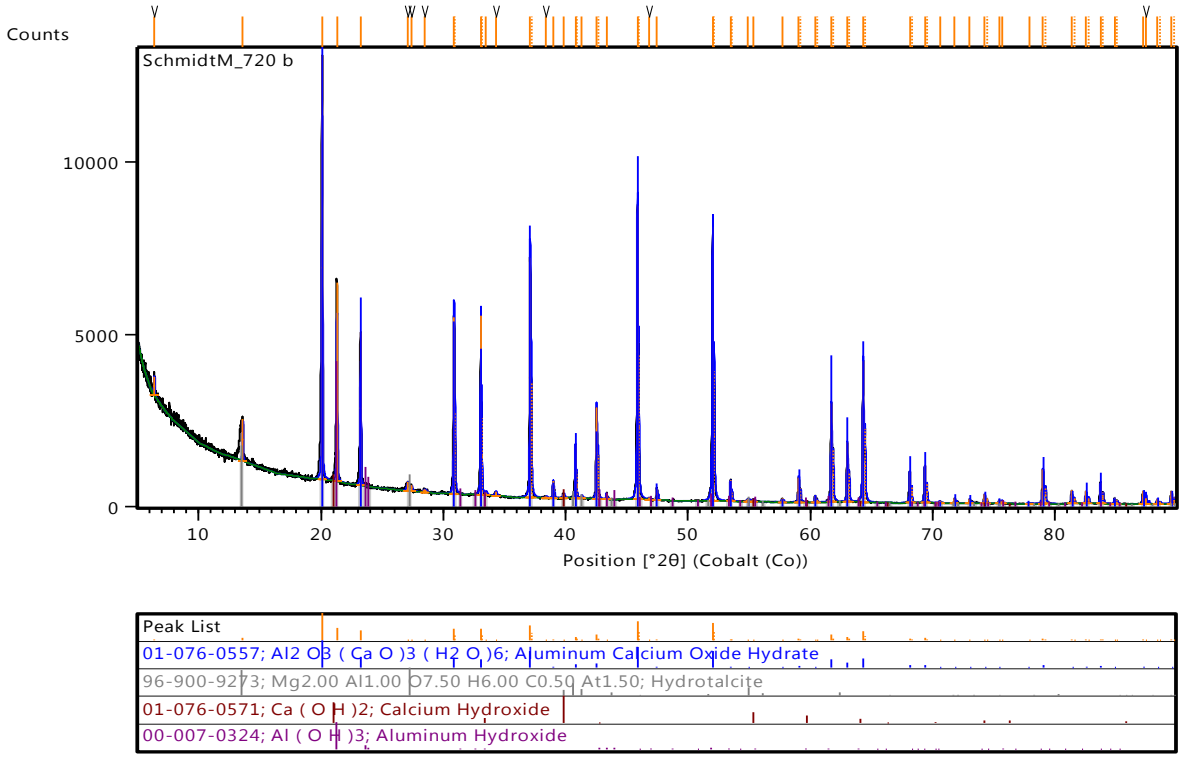

A-37: XRD graph for Ca/Al-benzoate synthesis at 6 h (50 °C)

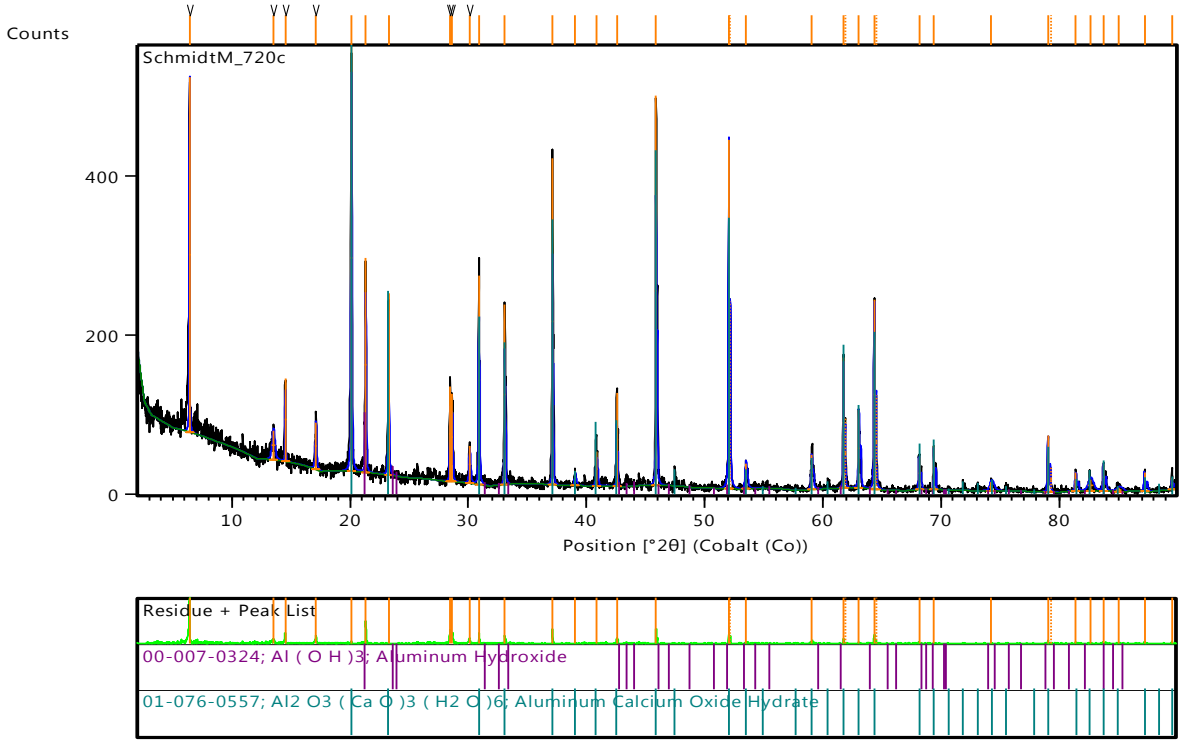

A-38: XRD graph for Ca/Al-benzoate synthesis at 6 h (60 °C)

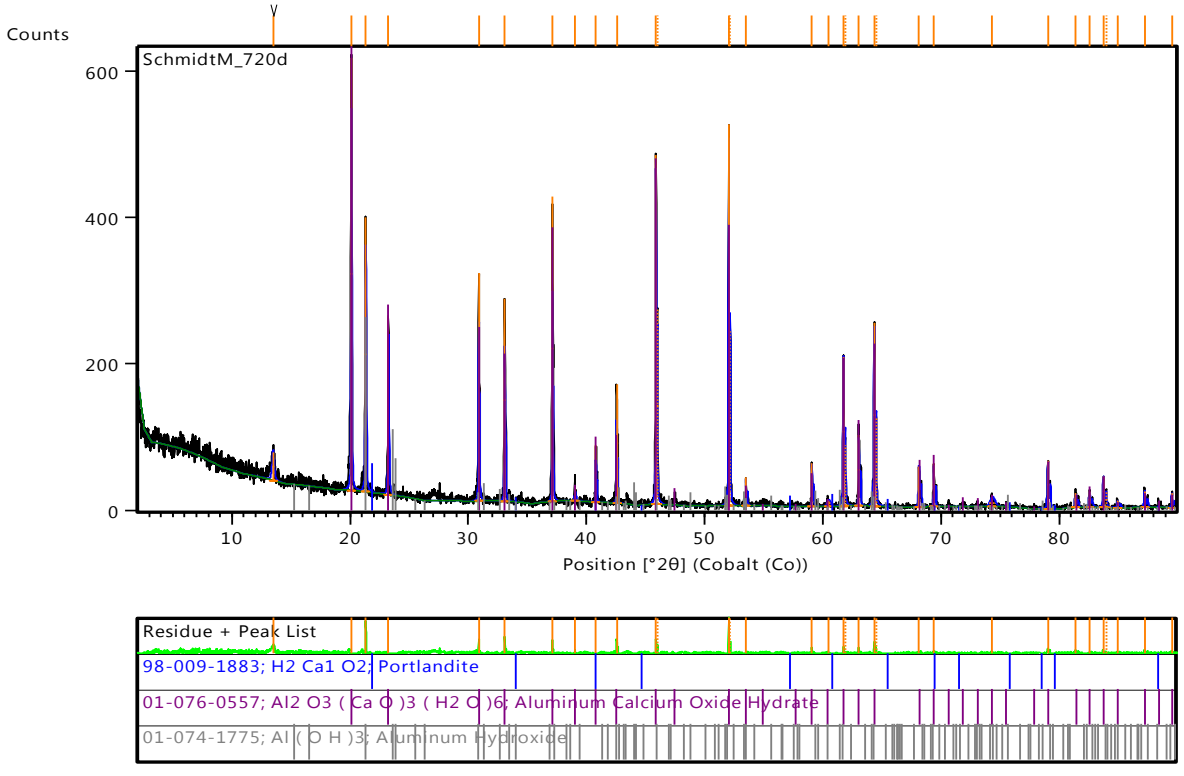

A-39: XRD graph for Ca/Al-benzoate synthesis at 12 h (ambient temperature)

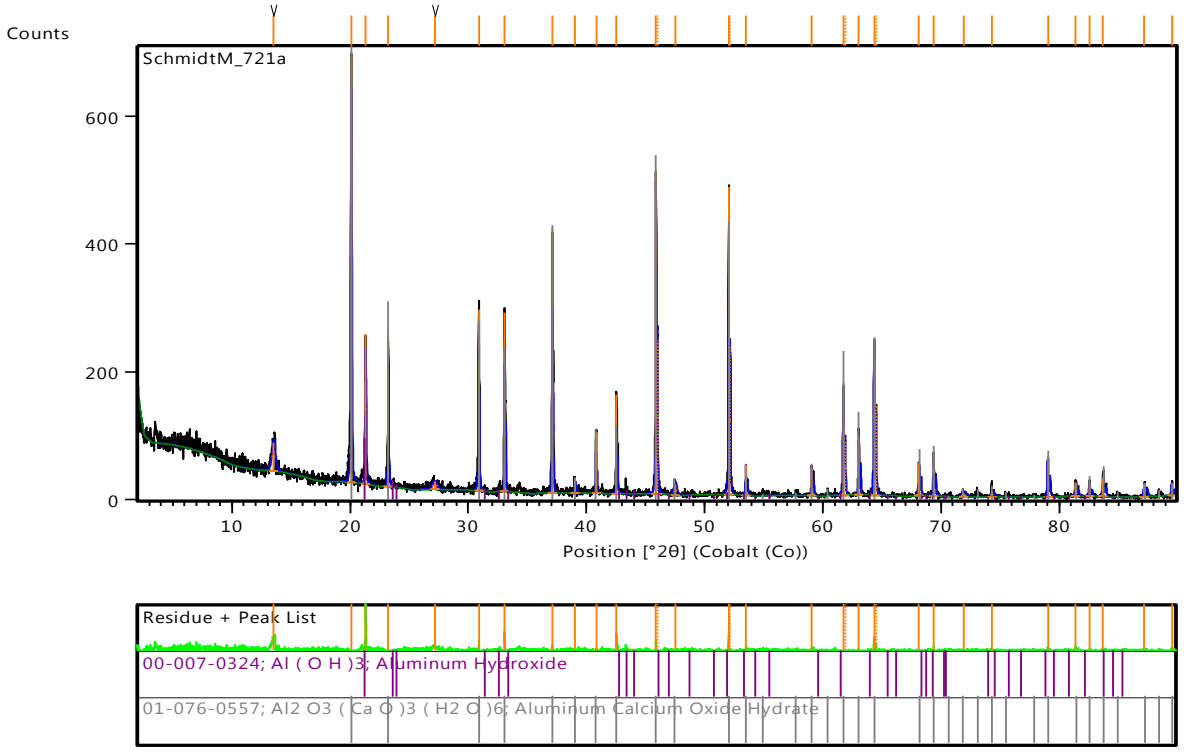

A-40: XRD graph for Ca/Al-benzoate synthesis at 12 h (40 °C)

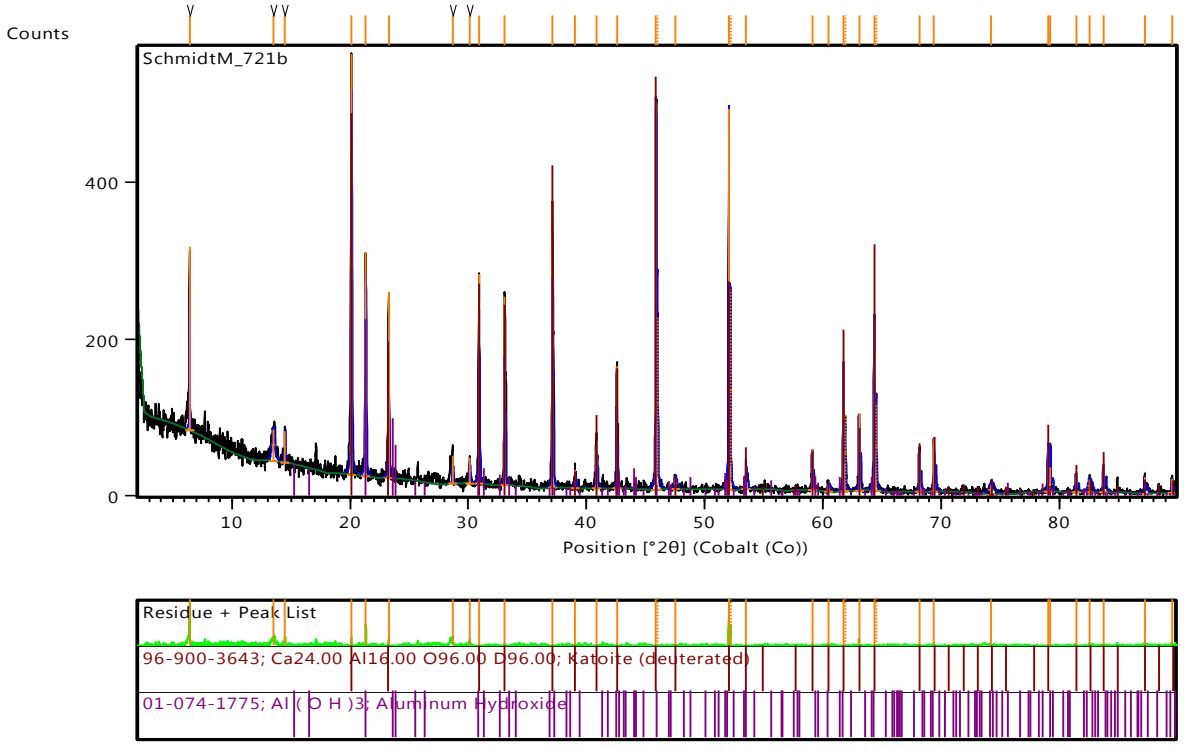

A-41: XRD graph for Ca/Al-benzoate synthesis at 12 h (50 °C)

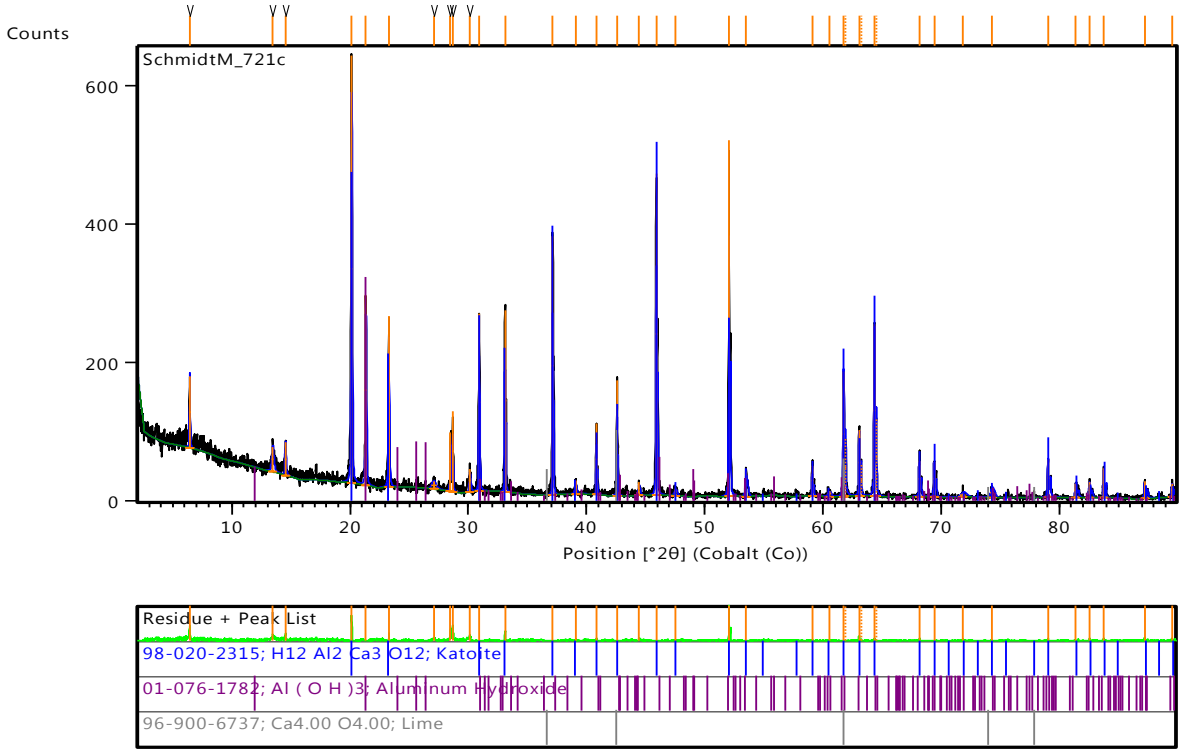

A-42: XRD graph for Ca/Al-benzoate synthesis at 12 h (60 °C)

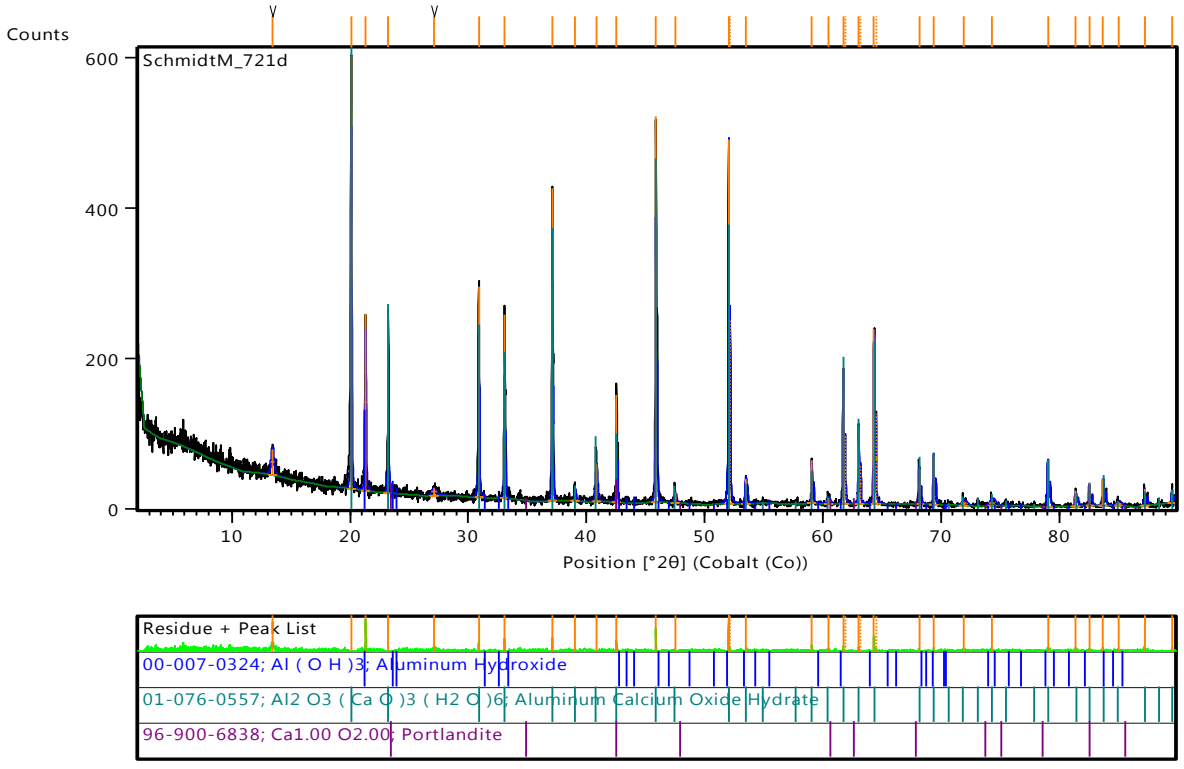

A-43: XRD graph for Ca/Al-benzoate synthesis at 24 h (ambient temperature)

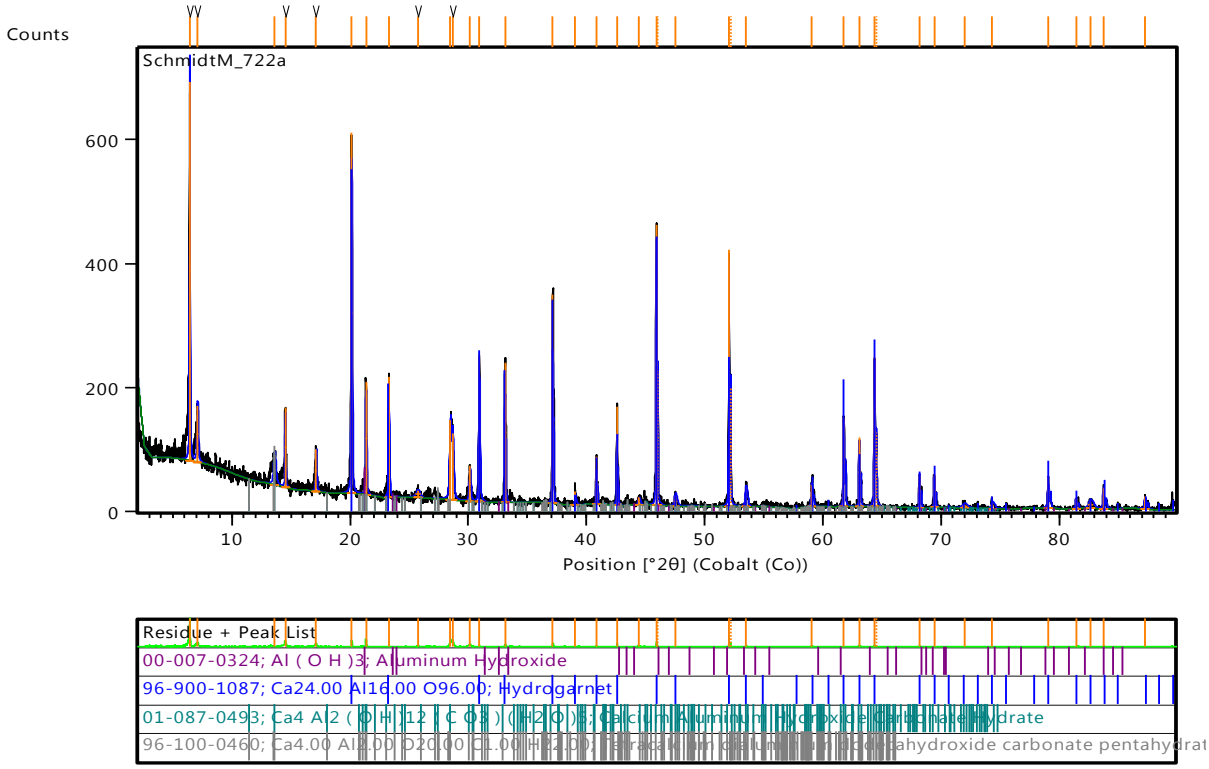

A-44: XRD graph for Ca/Al-benzoate synthesis at 24 h (40 °C)

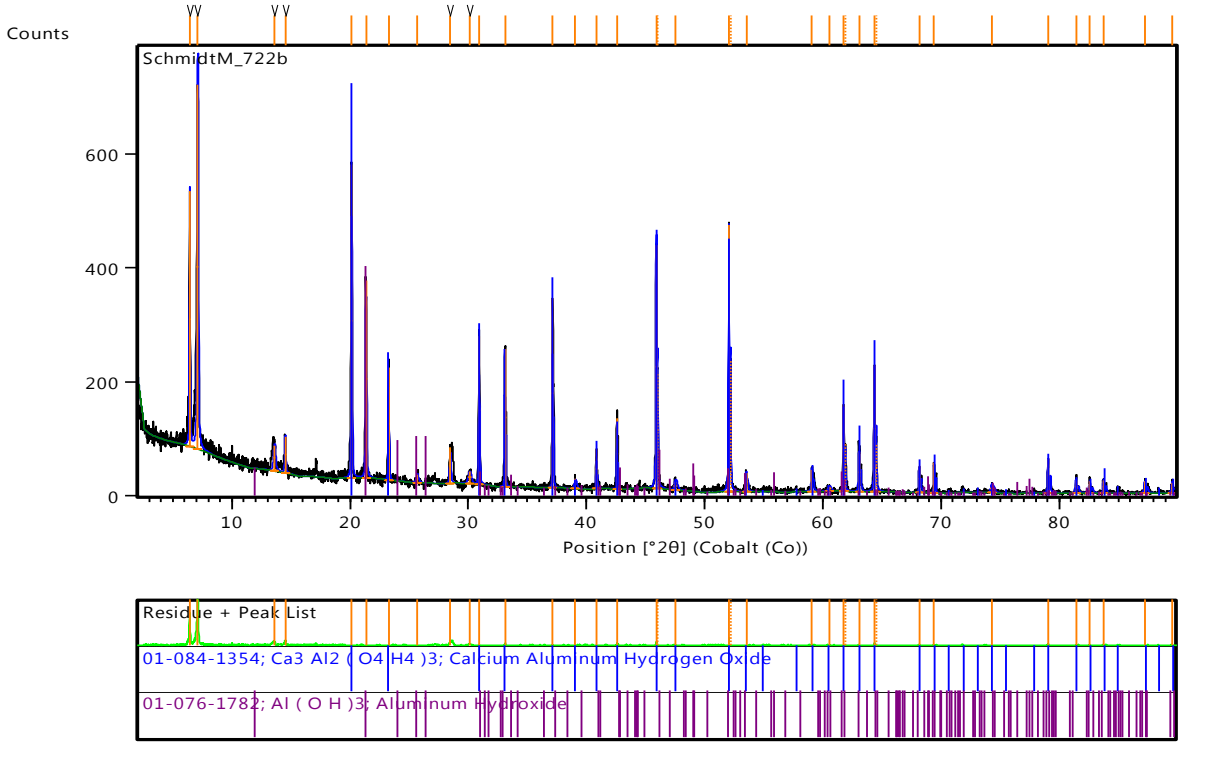

A-45: XRD graph for Ca/Al-benzoate synthesis at 24 h (50 °C)

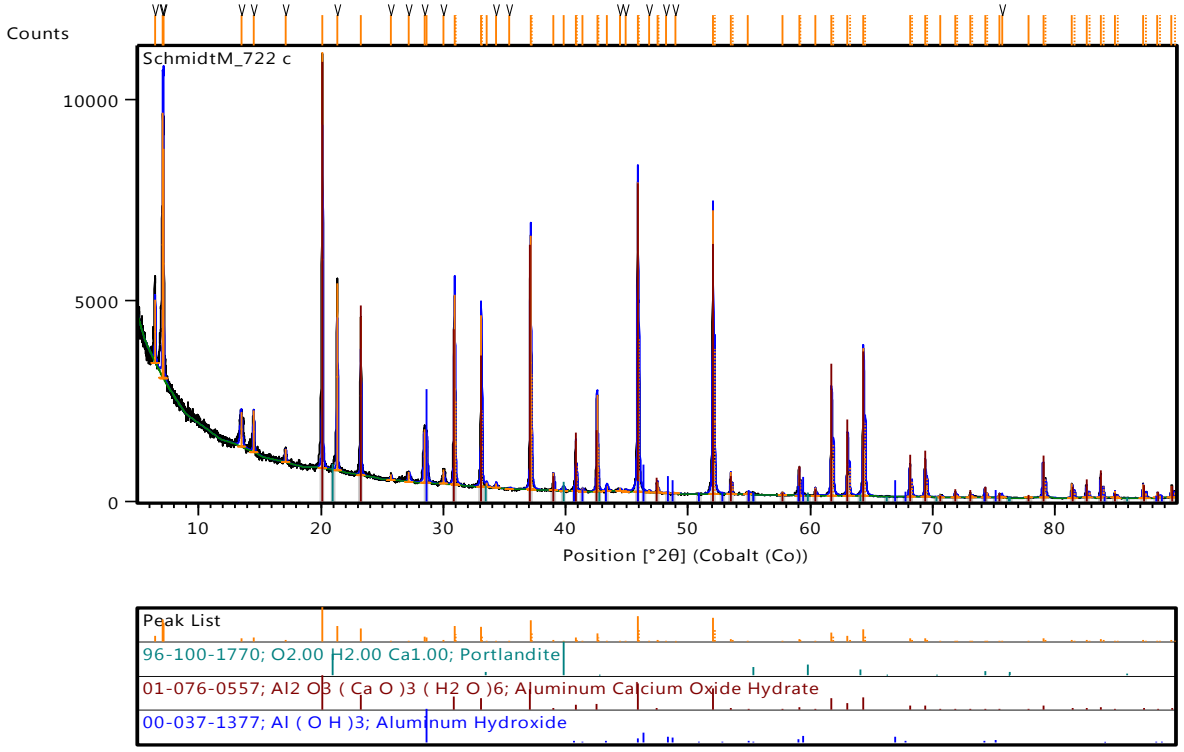

A-46: XRD graph for Ca/Al-benzoate synthesis at 24 h (60 °C)

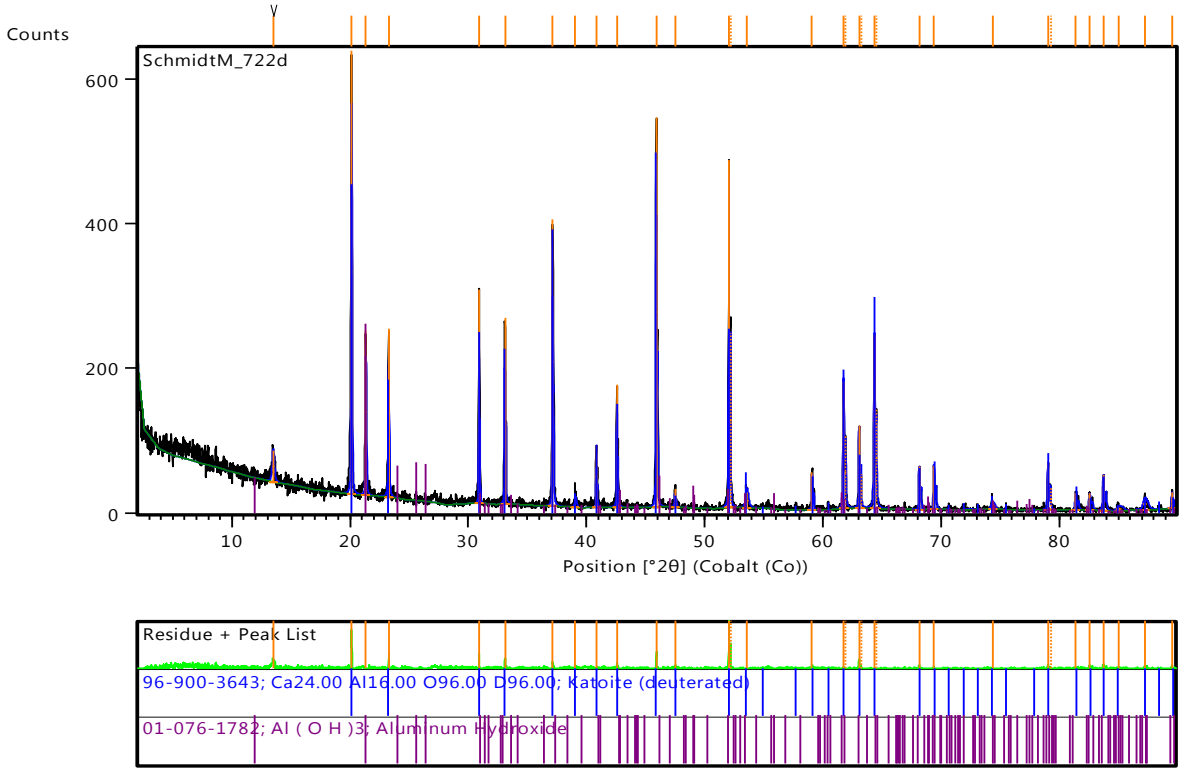

A-47: XRD graph for Ca/Al-benzoate synthesis with CaO calcium source

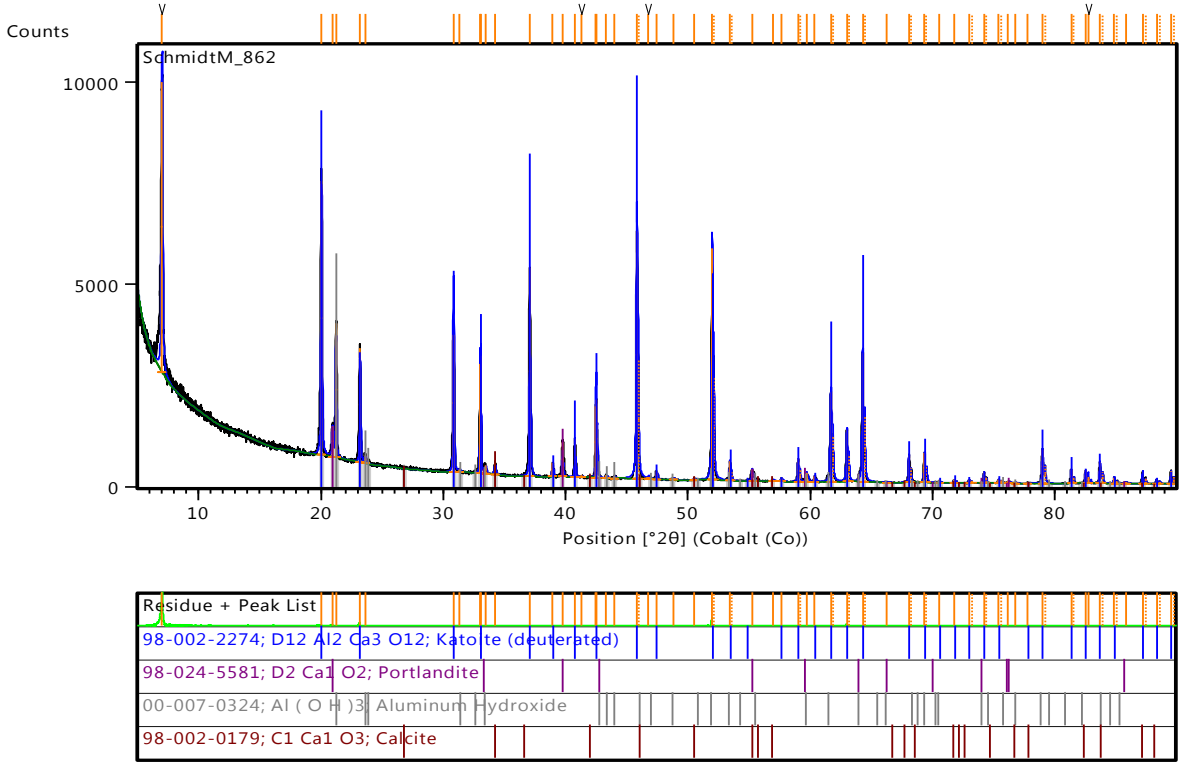

A-48: XRD graph for Ca/Al-benzoate synthesis with $Ca(OH)_2$ calcium source

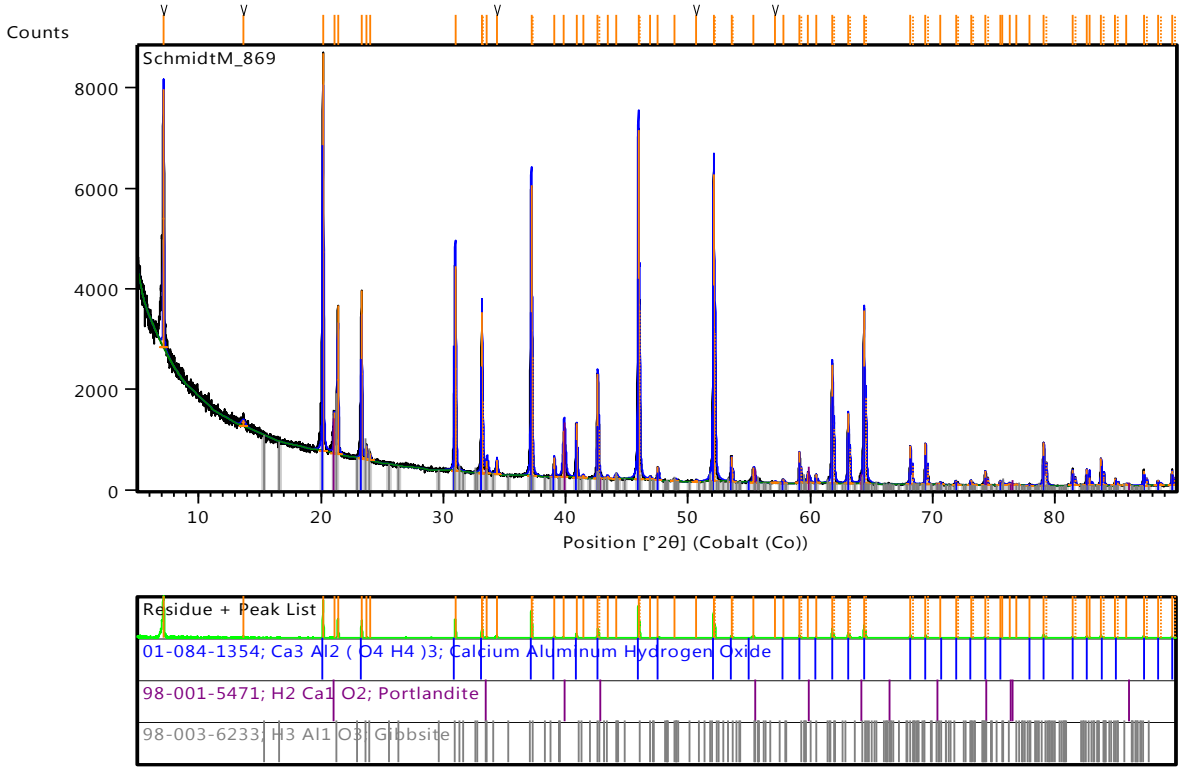

A-49: XRD graph for Ca/Al-chloride synthesis with CaO calcium source

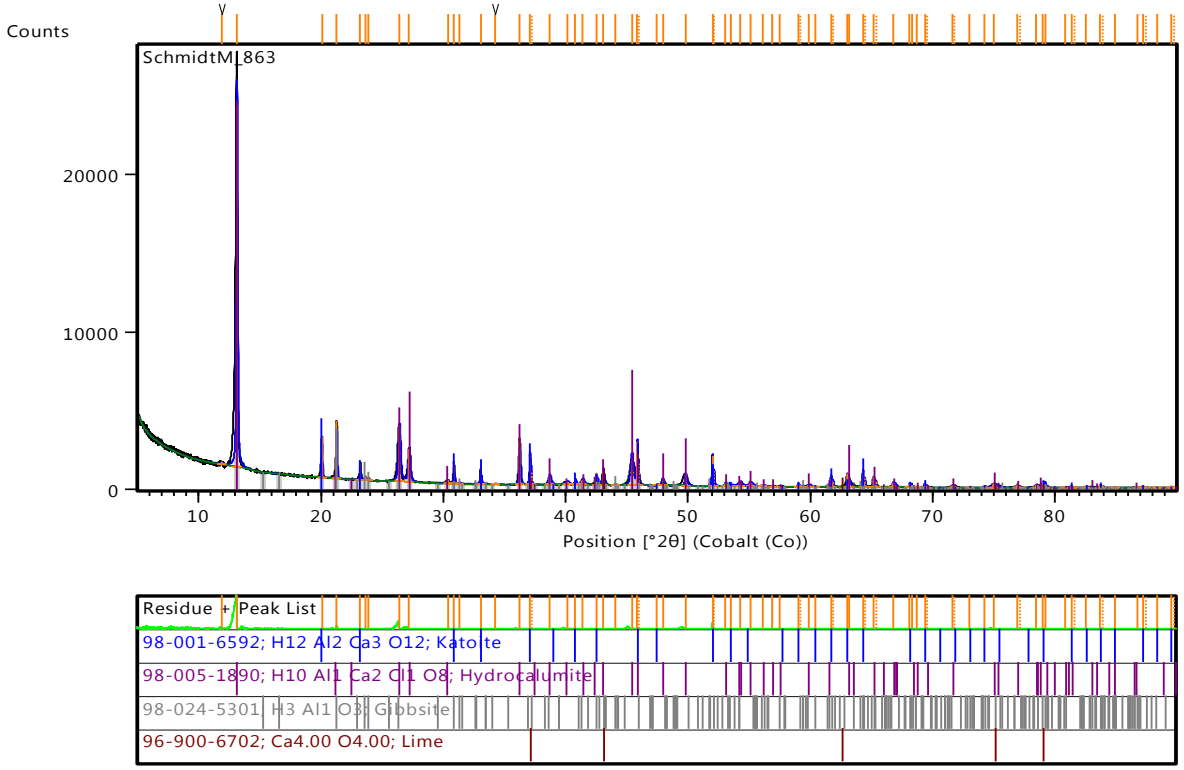

A-50: XRD graph for Ca/Al-chloride synthesis with $Ca(OH)_2$ calcium source

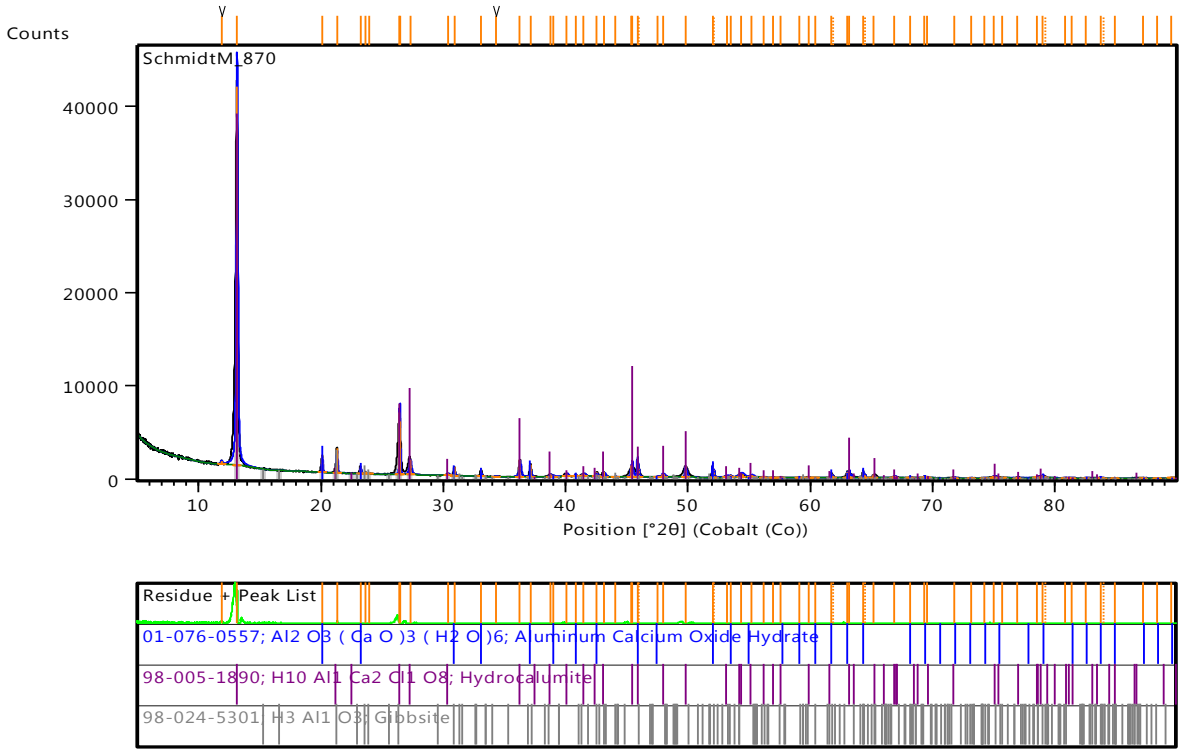

A-51: XRD graph for Ca/Al-benzoate synthesis (pH = 12.32)

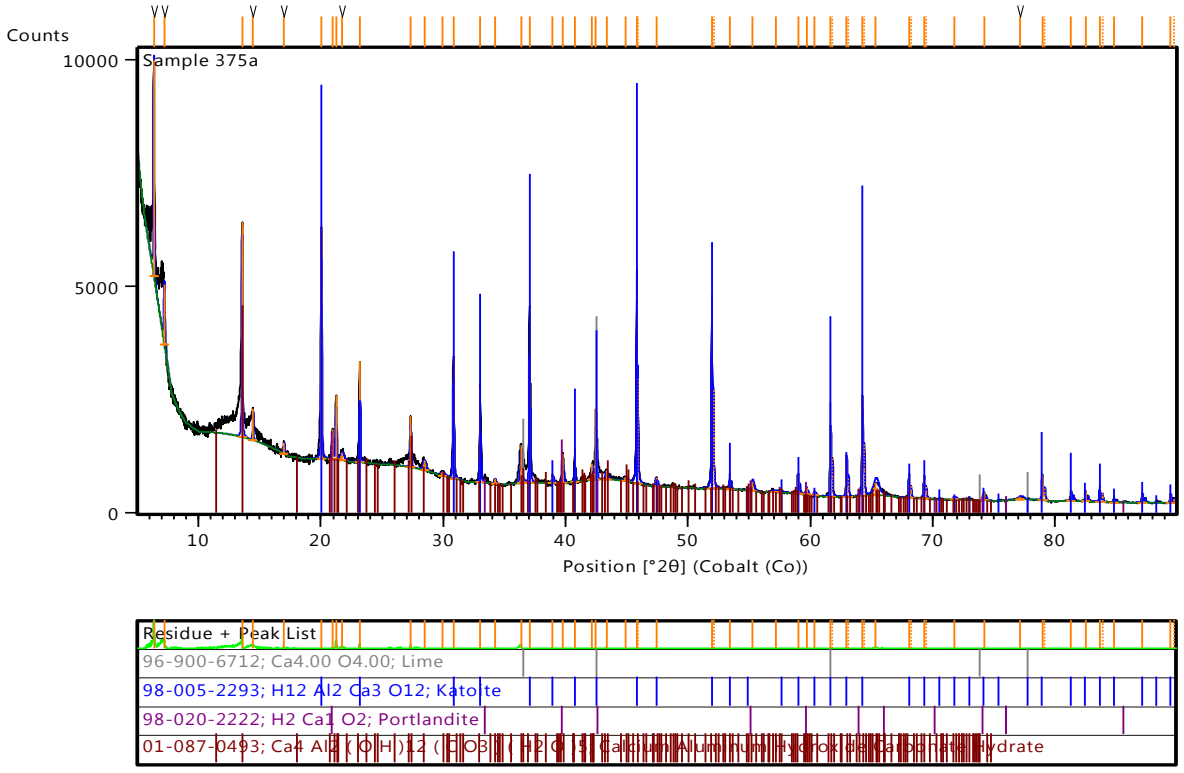

A-52: XRD graph for Ca/Al-benzoate synthesis (pH = 11.24)

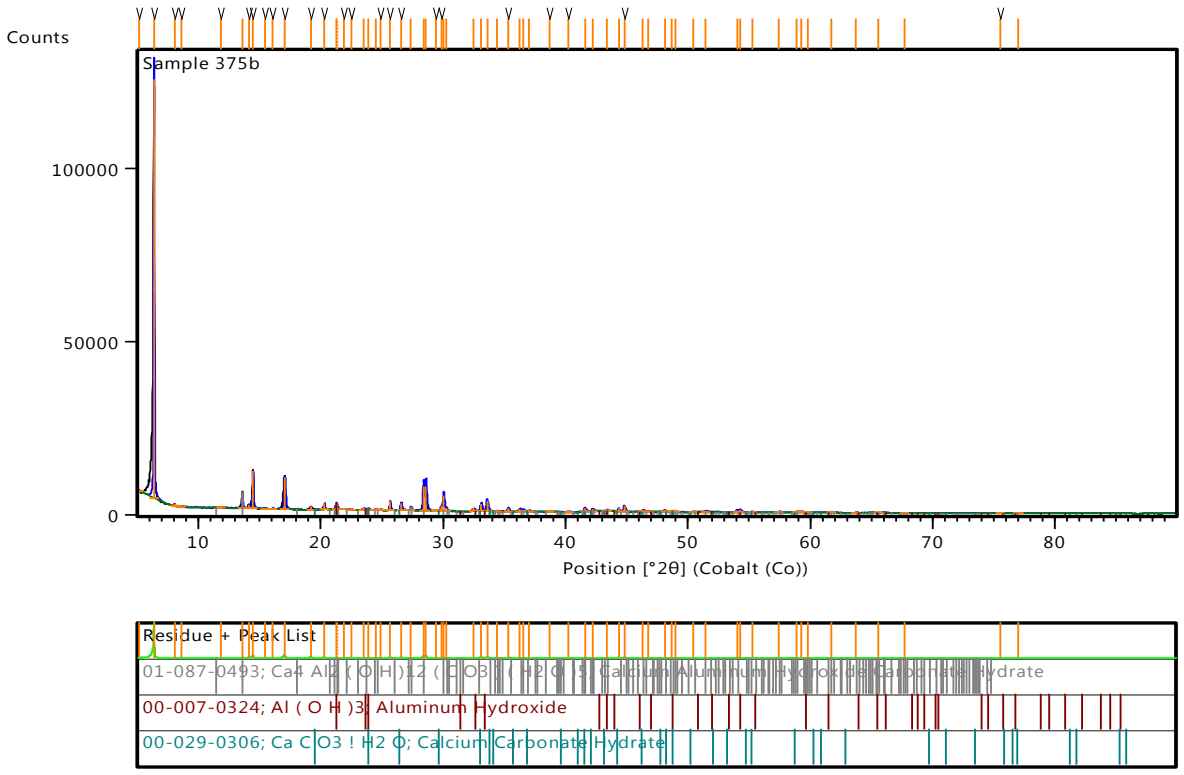

A-53: XRD graph for Ca/Al-salicylate synthesis (pH = 11.69)

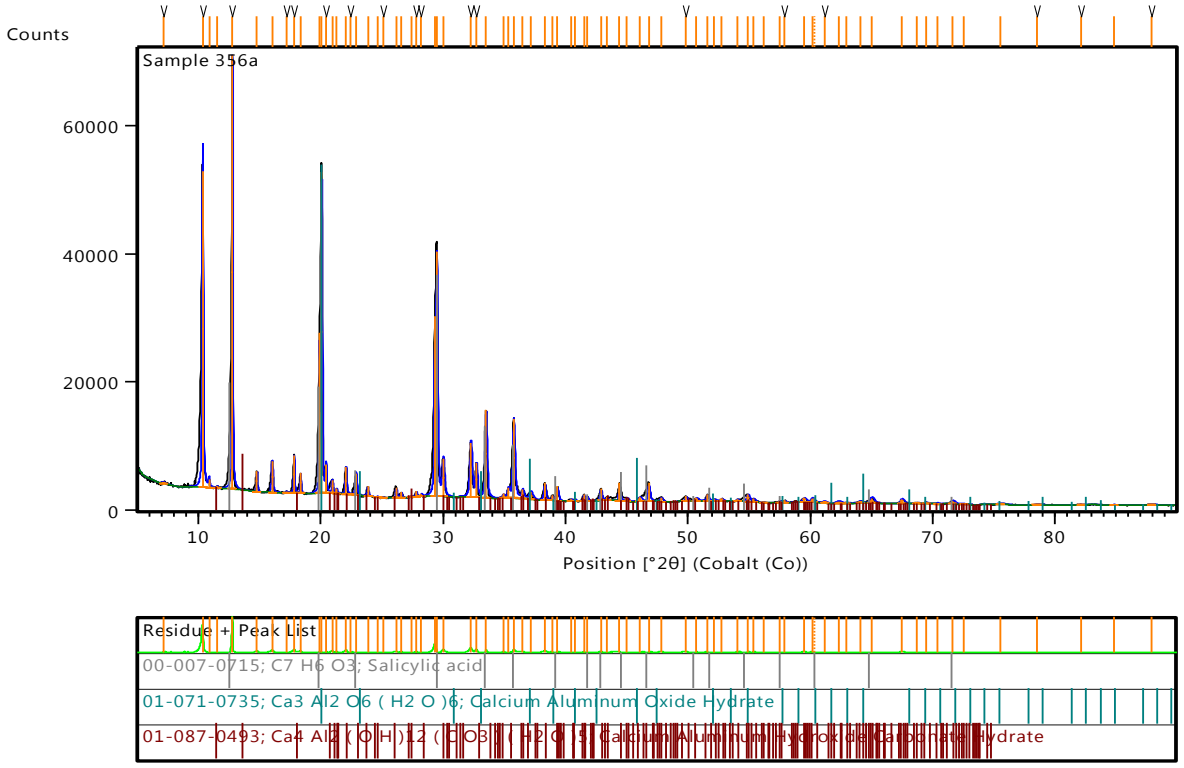

A-54: XRD graph for Ca/Al-salicylate synthesis (pH = 11.11)

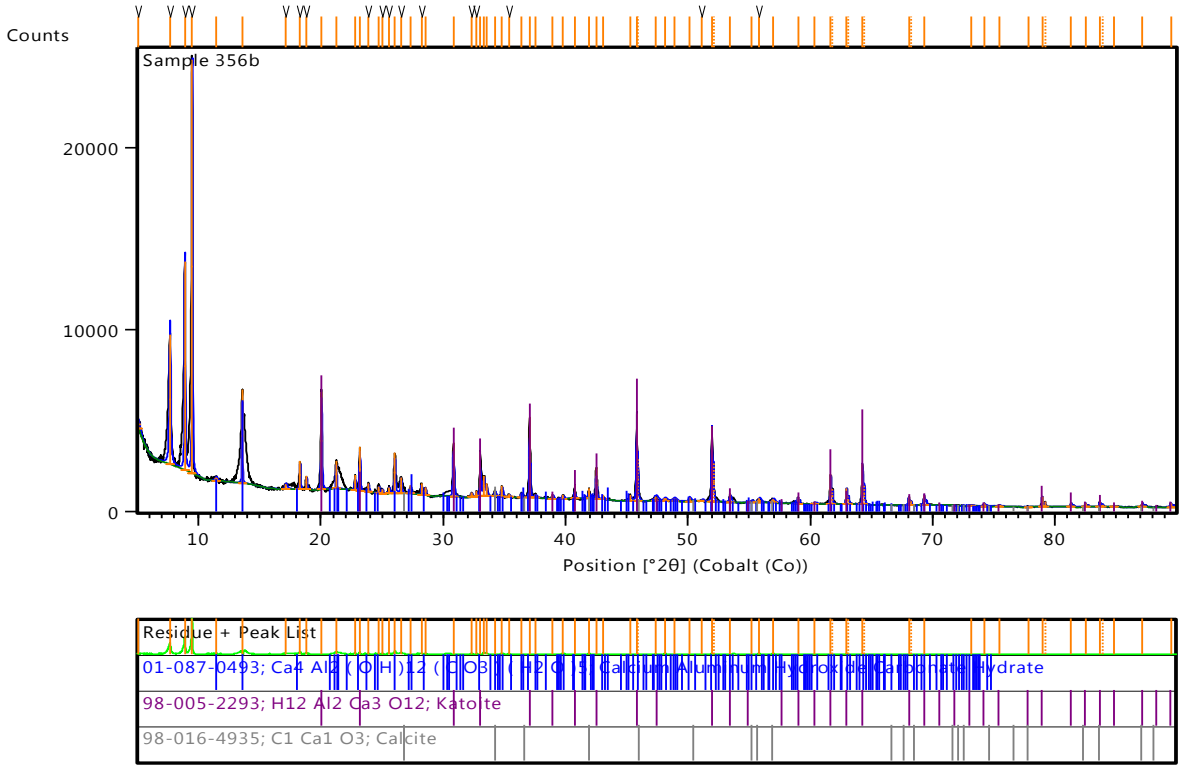

A-55: XRD graph for Ca/Al-salicylate synthesis (pH = 3.69)

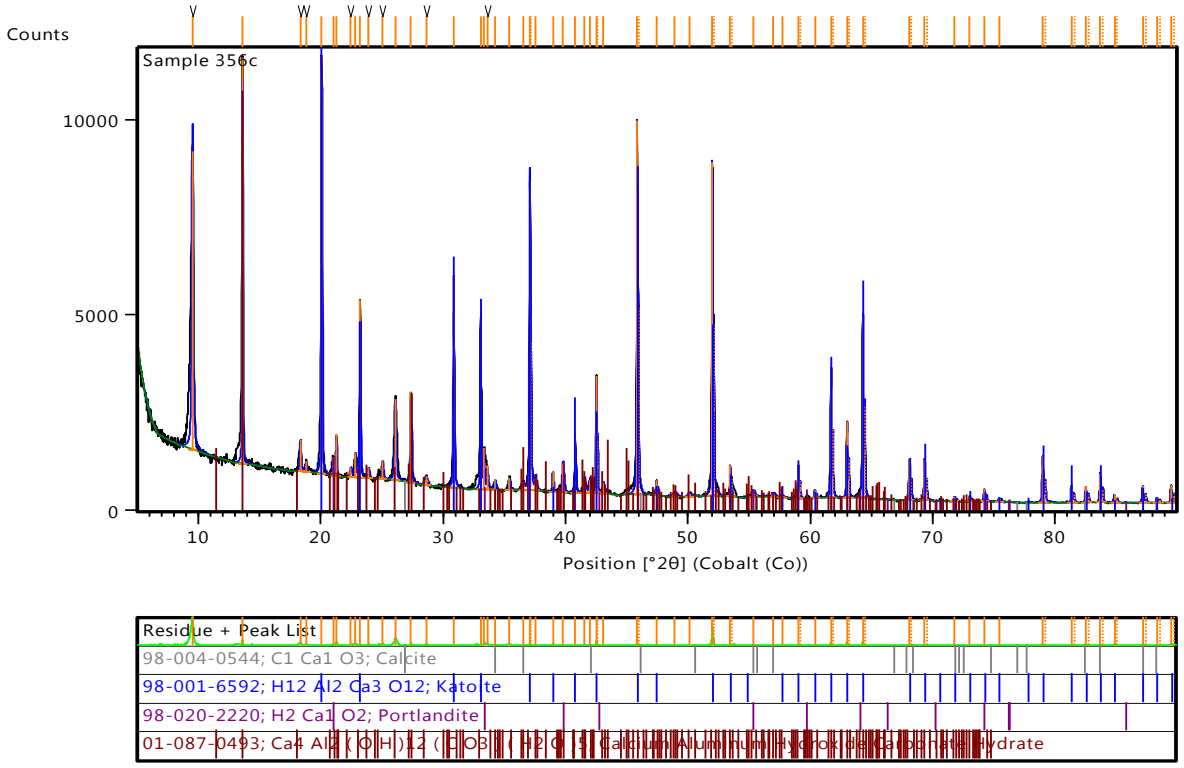

A-56: XRD graph for Ca/Al-anthranilate synthesis (pH = 12.03)

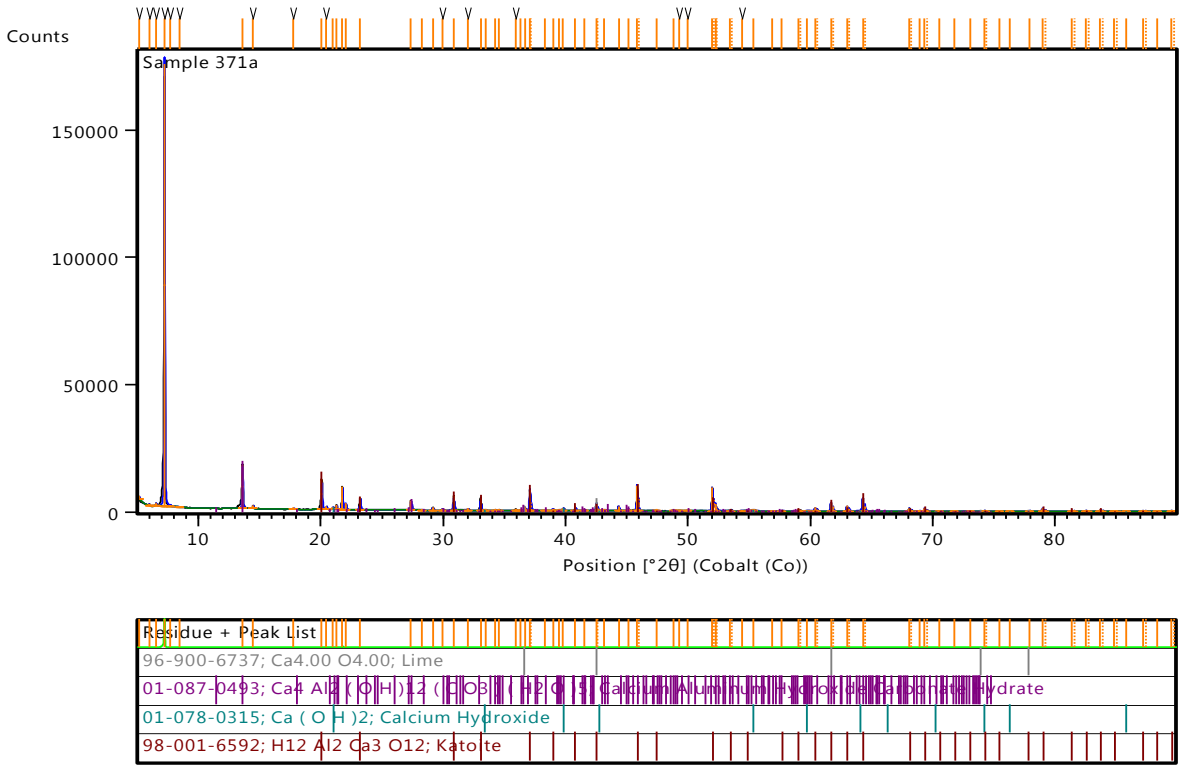

A-57: XRD graph for Ca/Al-anthranilate synthesis (pH = 11.67)

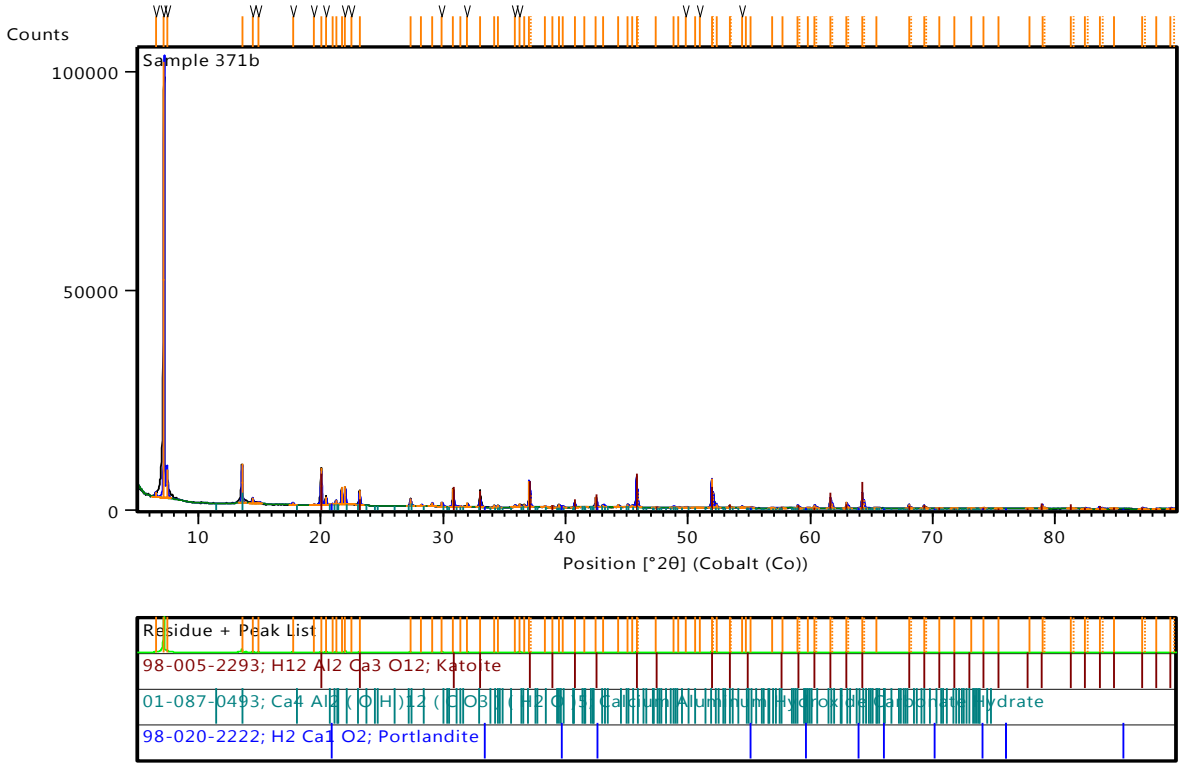

A-58: XRD graph for Ca/Al-anthranilate synthesis (pH = 5.29)

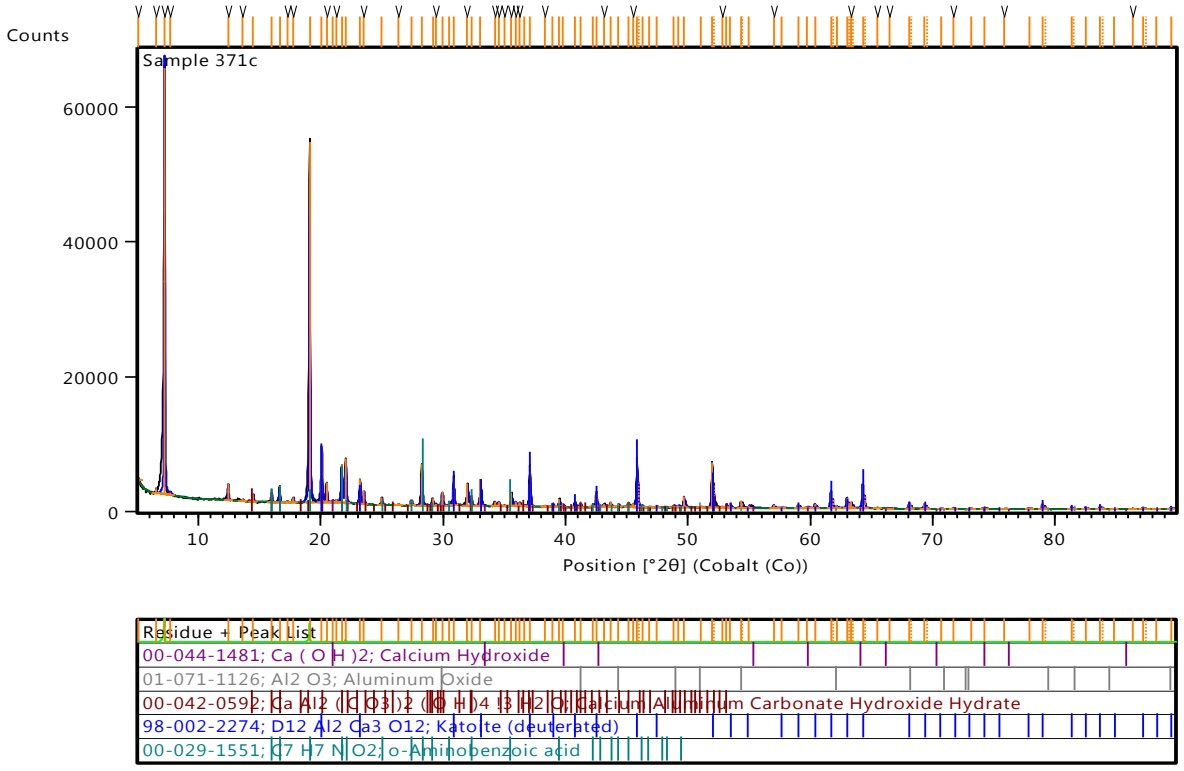

A-59: XRD graph for Ca/Al-thiosalicylate synthesis (pH = 11.56)

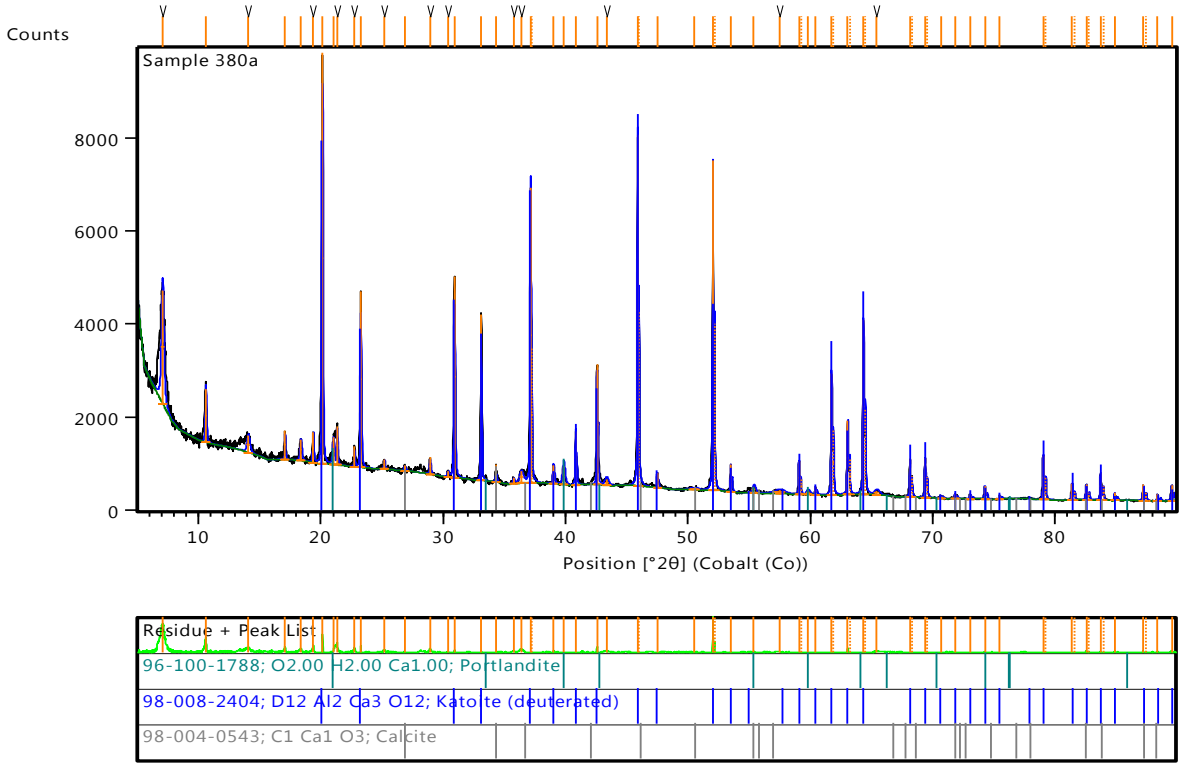

A-60: XRD graph for Ca/Al-thiosalicylate synthesis (pH = 5.69)

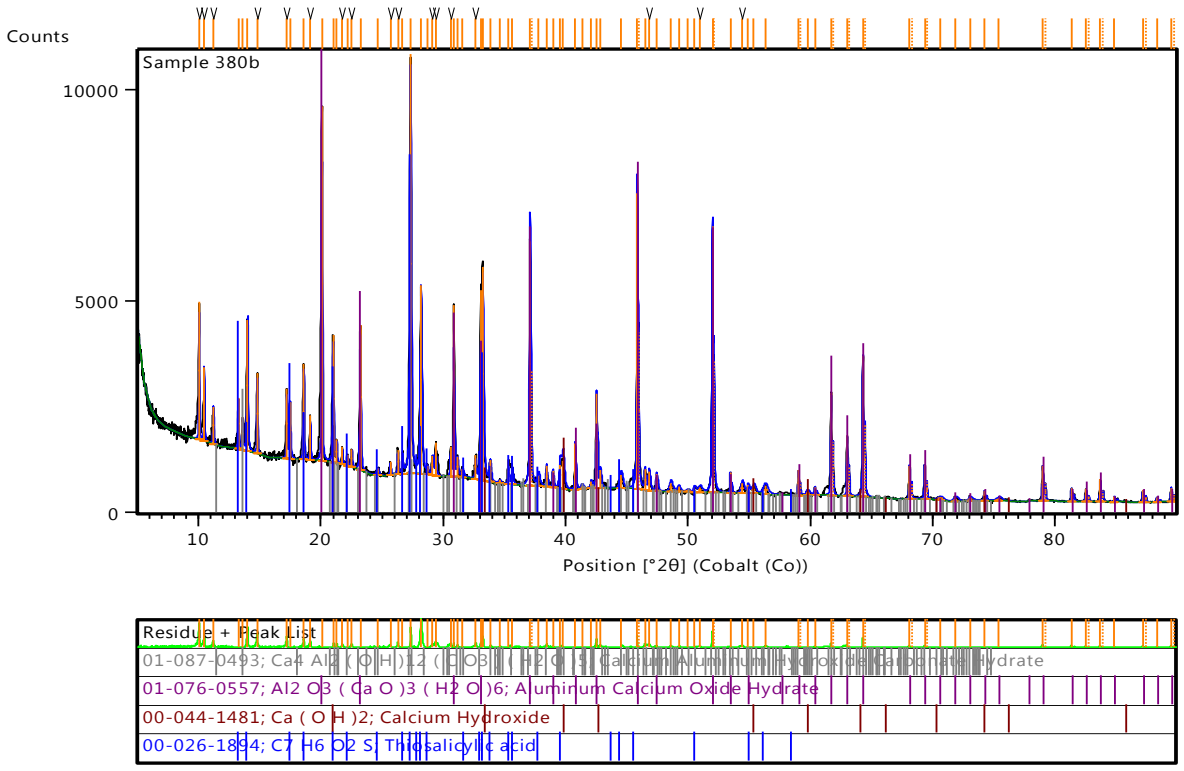

A-61: XRD graph for Ca/Al-3-hydroxybenzoate synthesis (pH = 12.82)

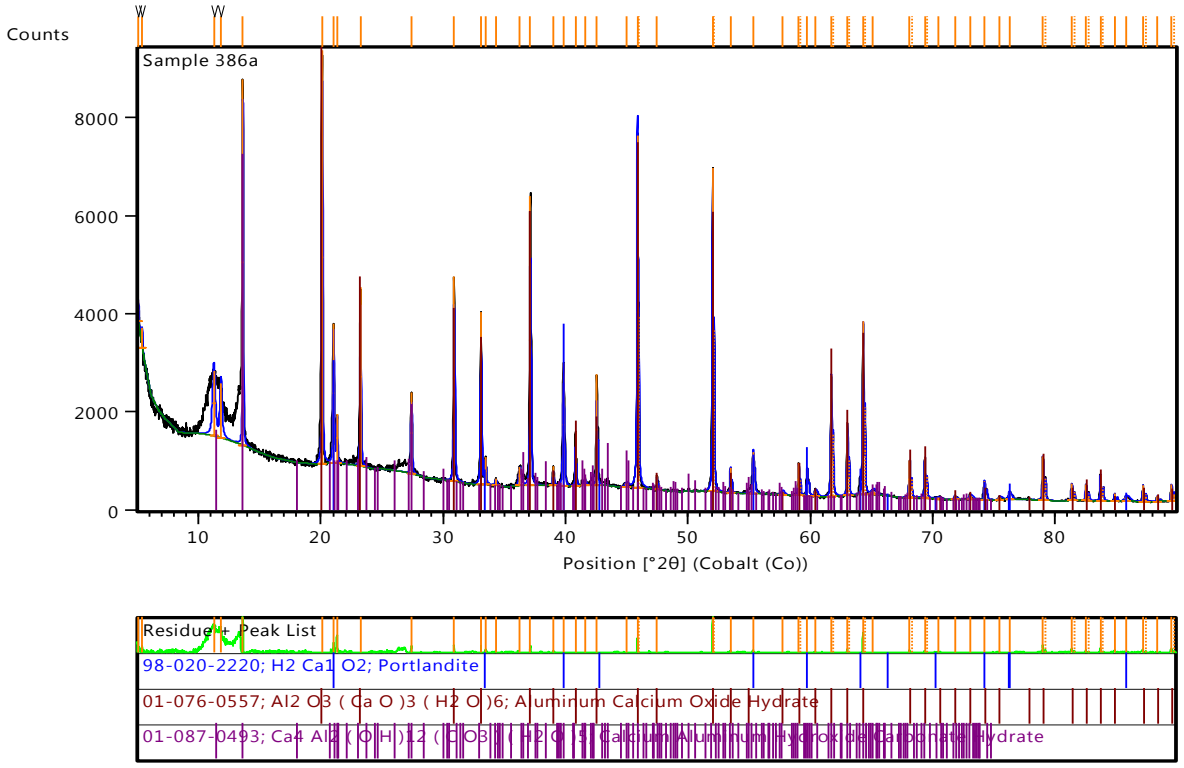

A-62: XRD graph for Ca/Al-3-hydroxybenzoate synthesis (pH = 11.12)

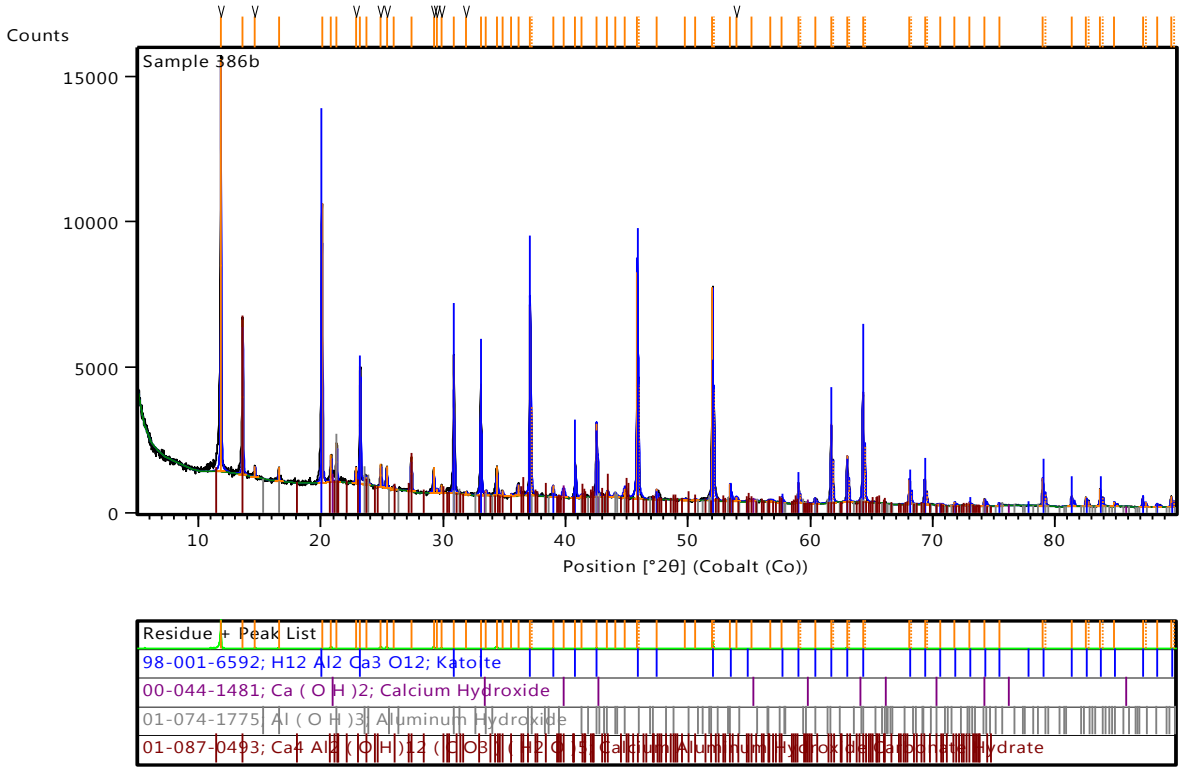

A-63: XRD graph for Ca/Al-3-hydroxybenzoate synthesis (pH = 4.98)

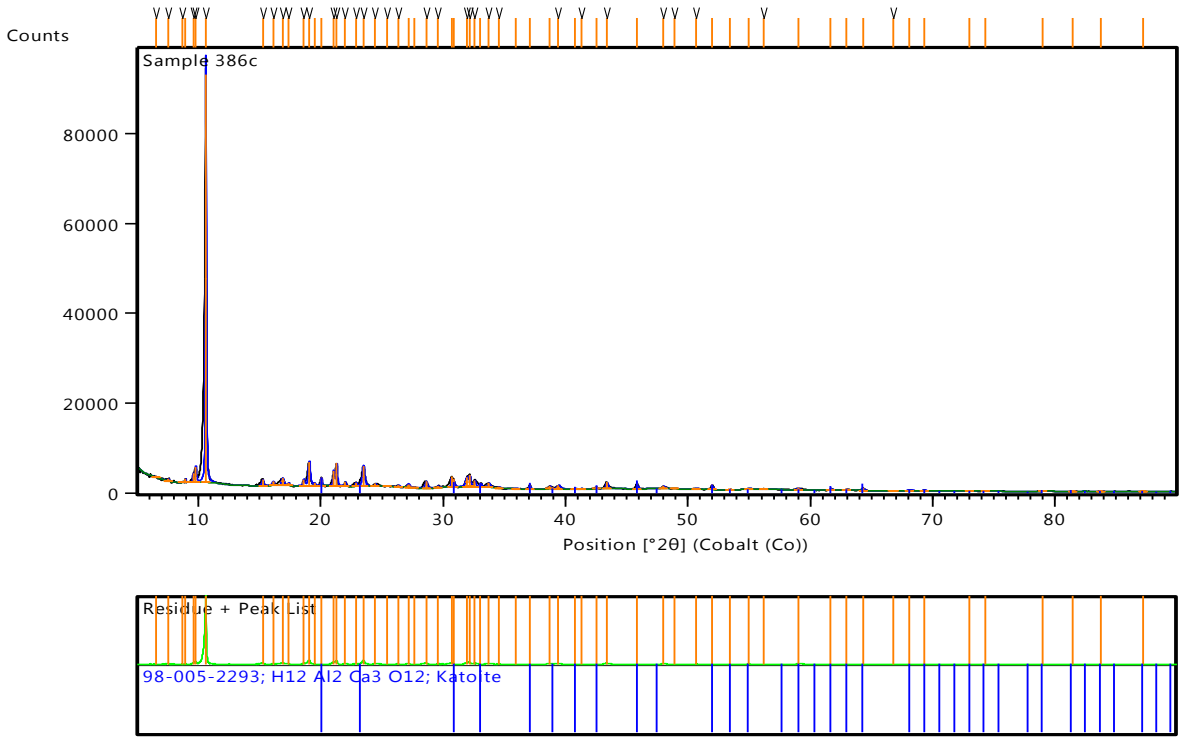

A-64: XRD graph for Ca/Al-3-aminobenzoate synthesis (pH = 12.50)

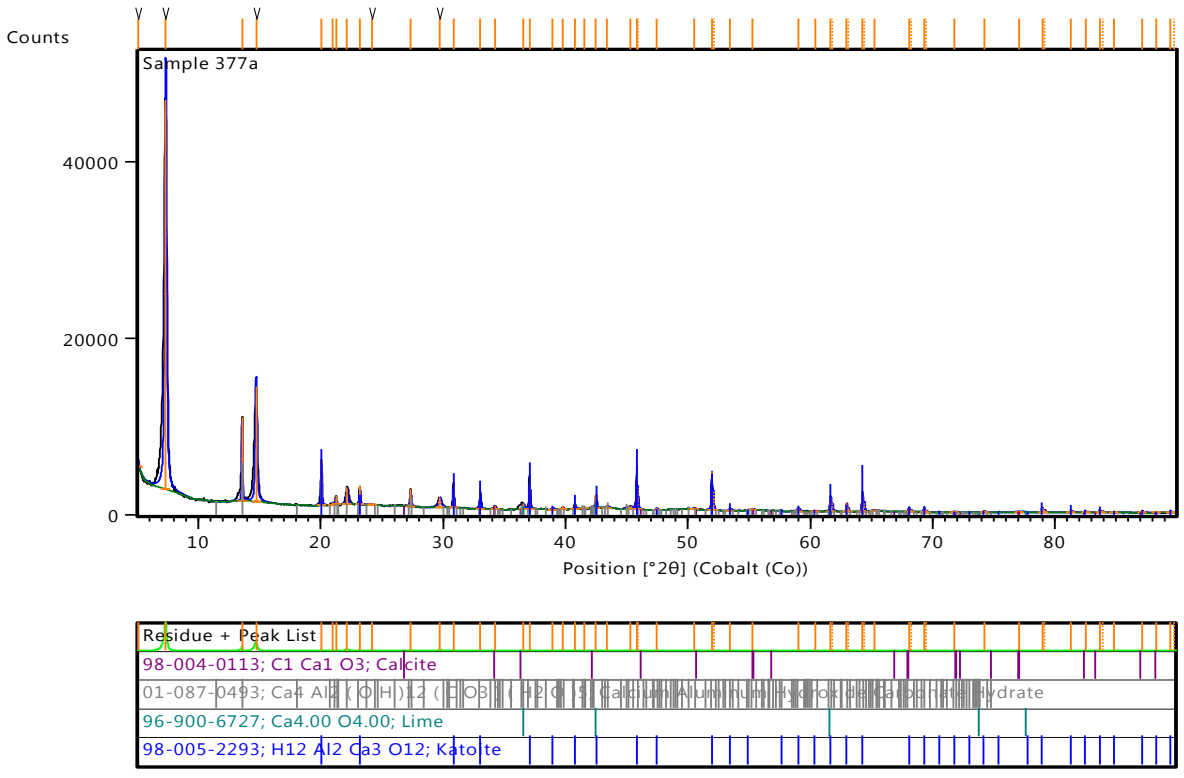

A-65: XRD graph for Ca/Al-3-aminobenzoate synthesis (pH = 5.30)

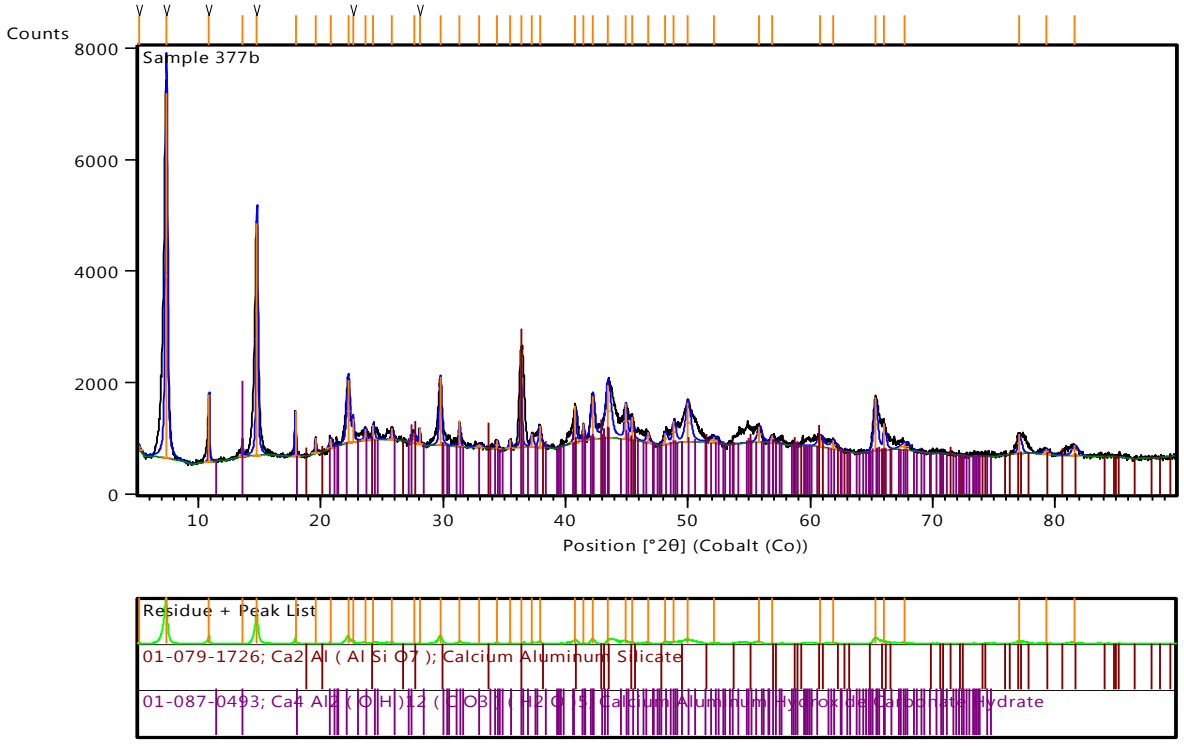

A-66: XRD graph for Ca/Al-4-hydroxybenzoate synthesis (pH = 12.26)

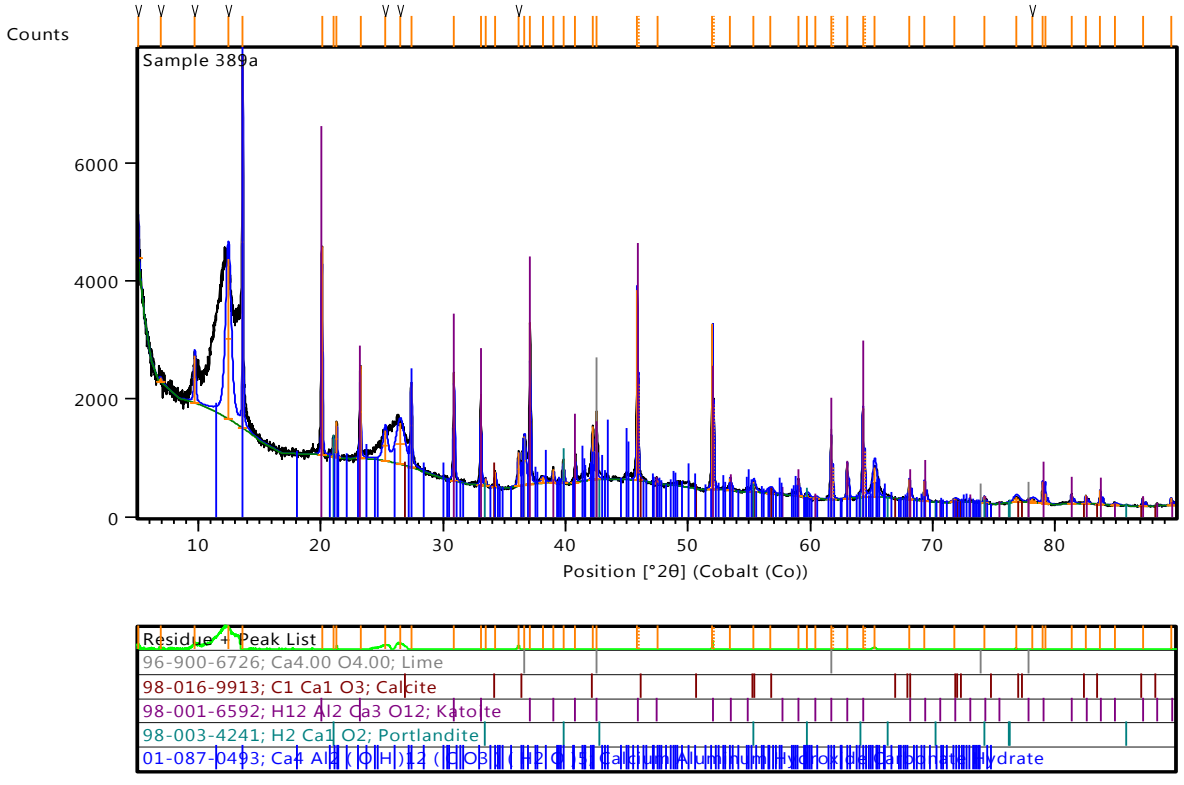

A-67: XRD graph for Ca/Al-4-hydroxybenzoate synthesis (pH = 9.29)

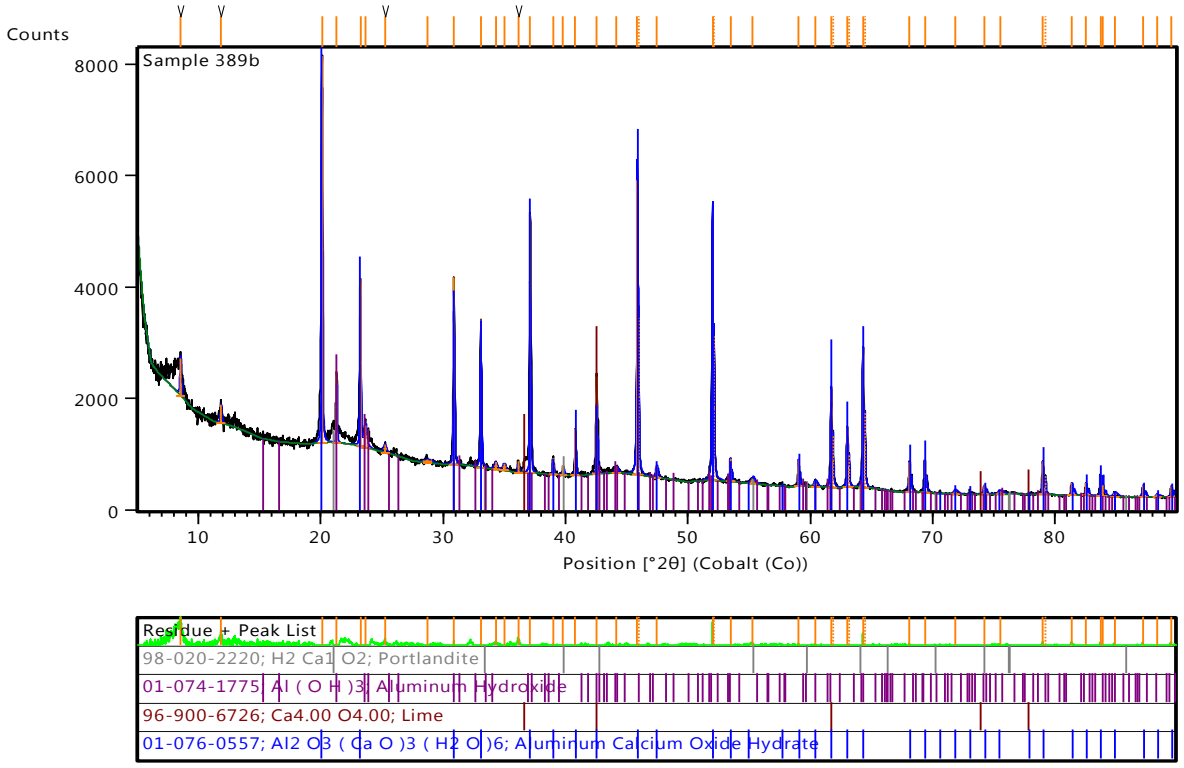

A-68: XRD graph for Ca/Al-4-hydroxybenzoate synthesis (pH = 4.83)

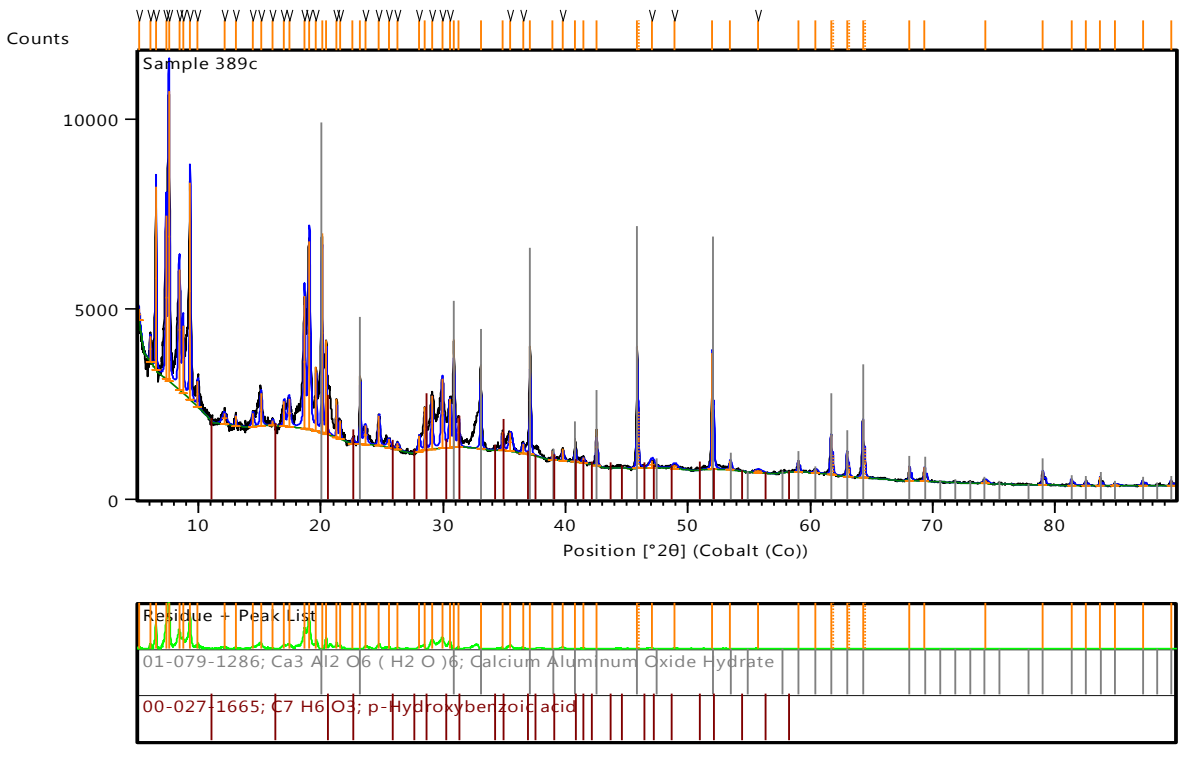

A-69: XRD graph for Ca/Al-4-aminobenzoate synthesis (pH = 12.67)

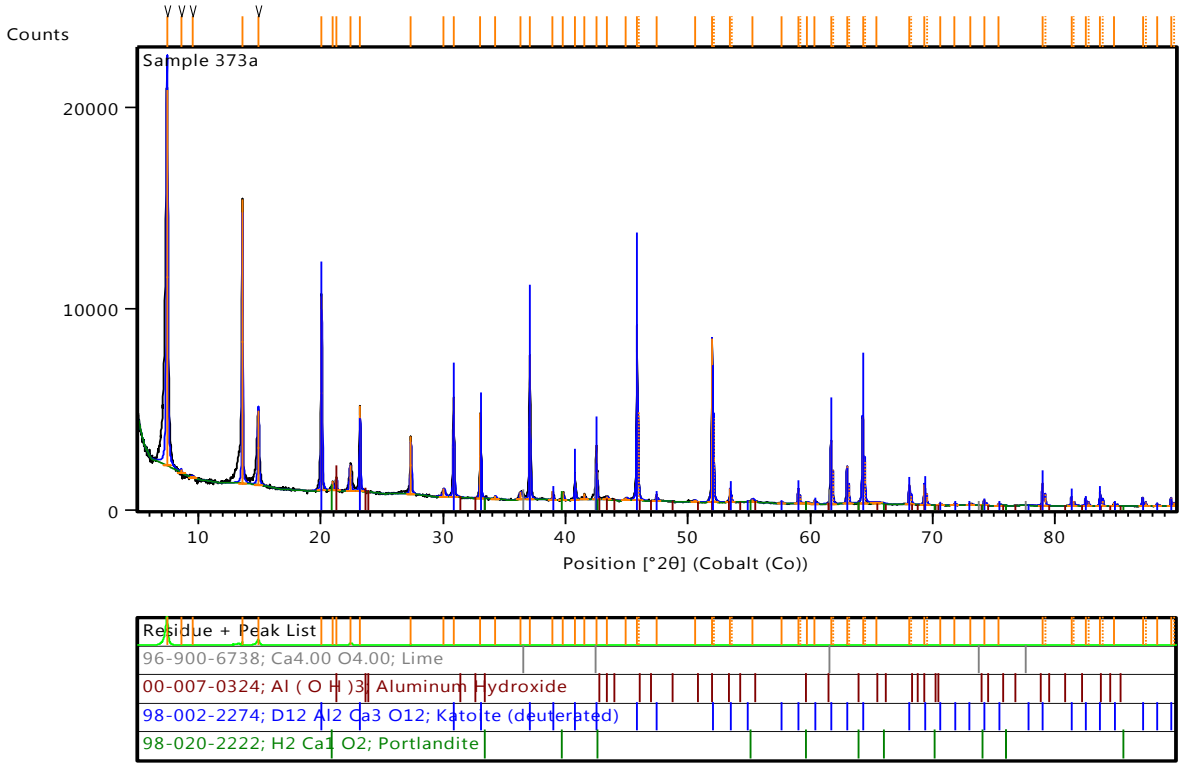

A-70: XRD graph for Ca/Al-4-aminobenzoate synthesis (pH = 5.54)

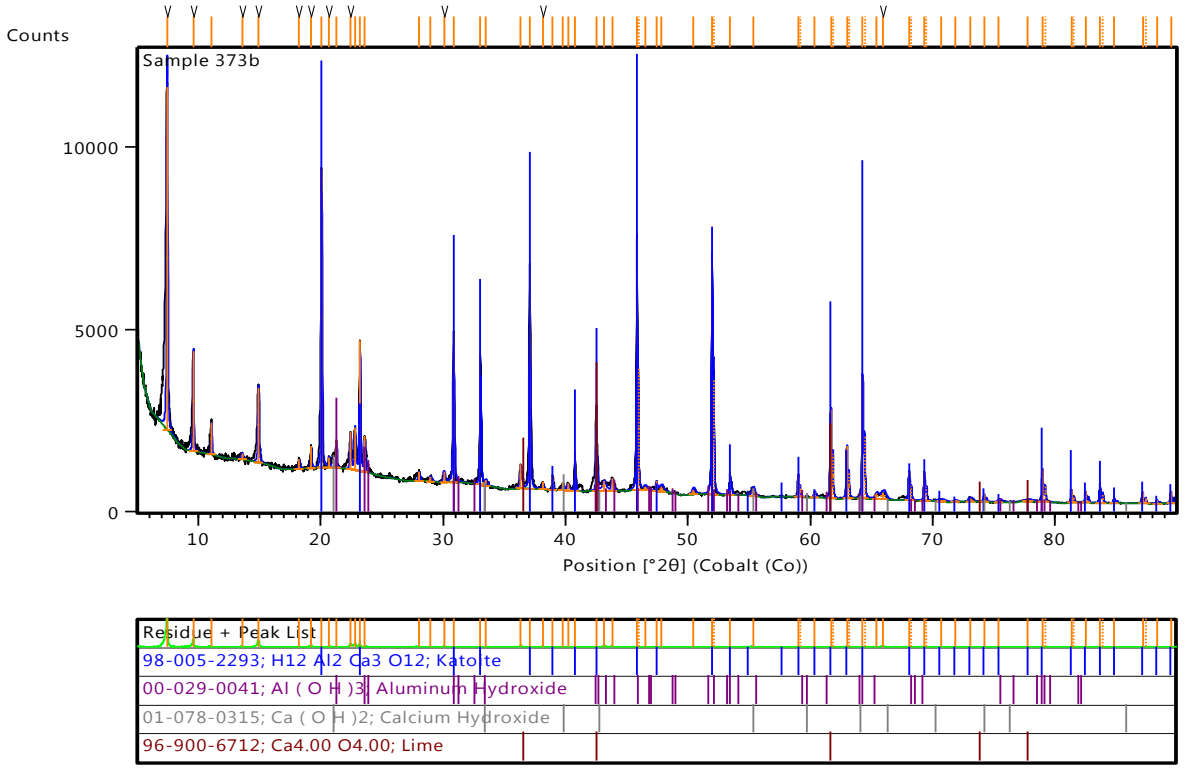

A-71: XRD graph for Ca/Al-chloride synthesis (pH = 13.00)

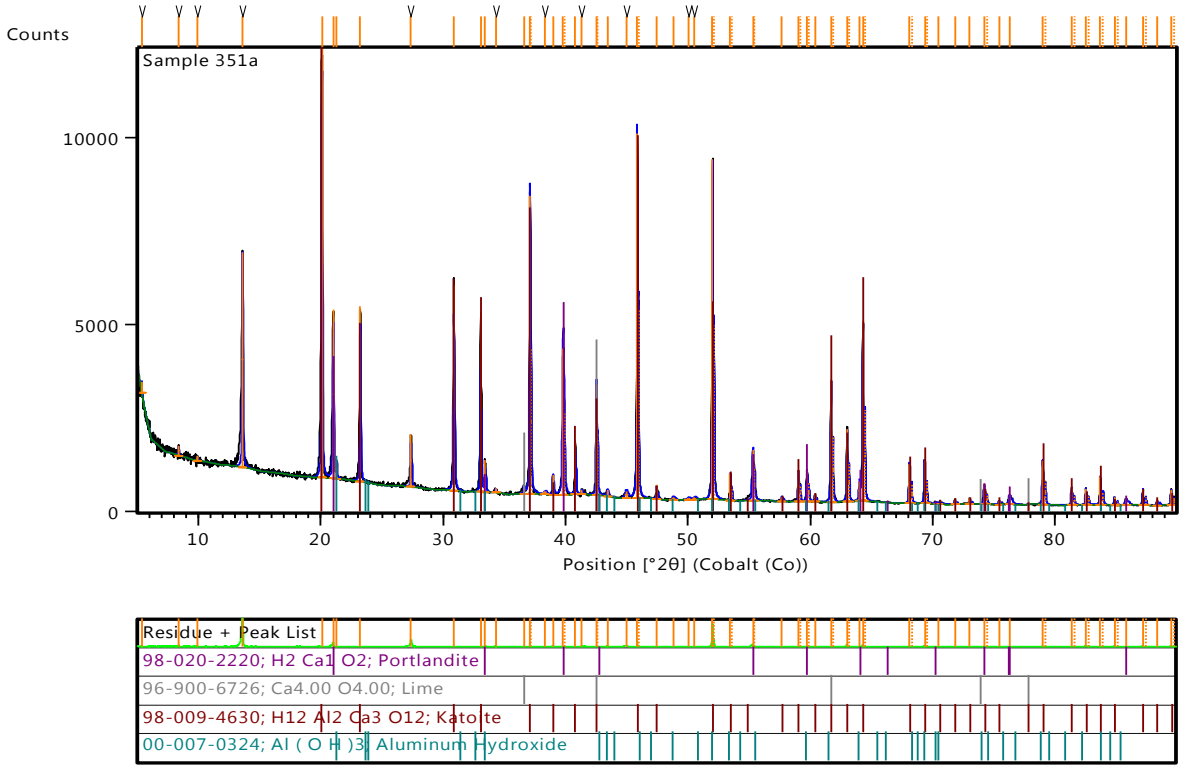

A-72: XRD graph for Ca/Al-chloride synthesis (pH = 11.11)

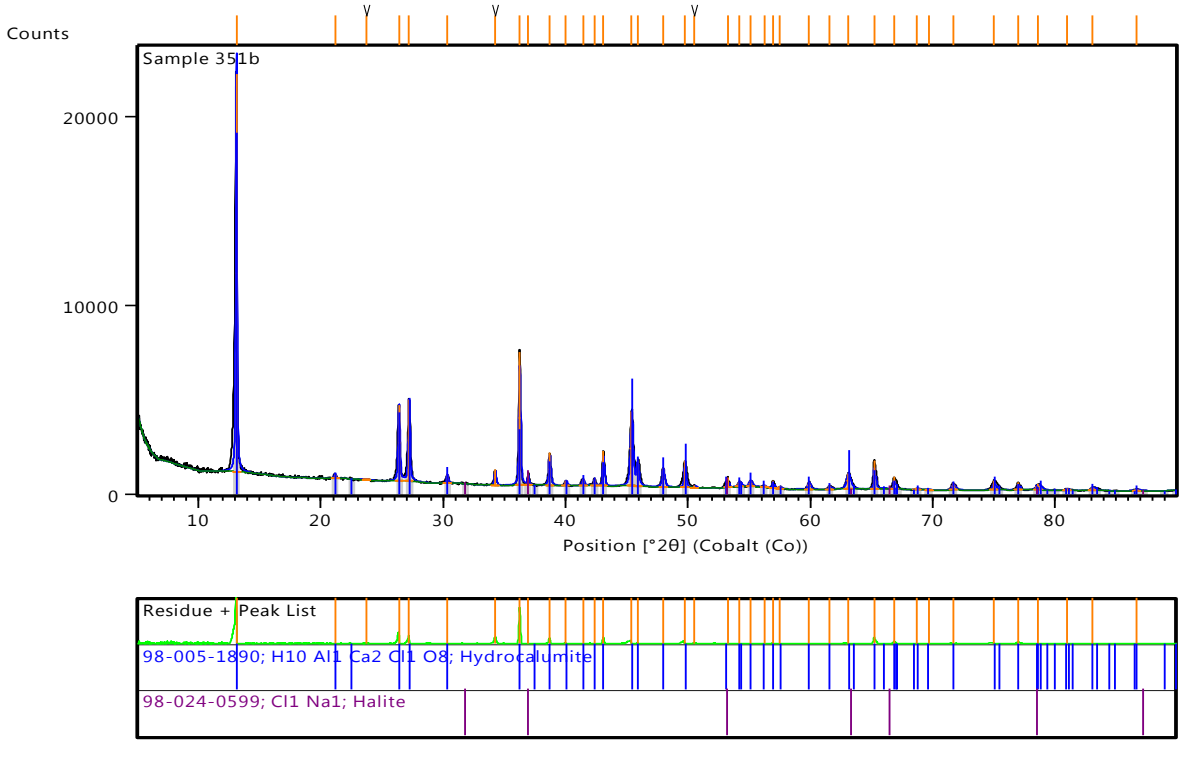

A-73: XRD graph for Ca/Al-chloride synthesis (pH = 4.68)

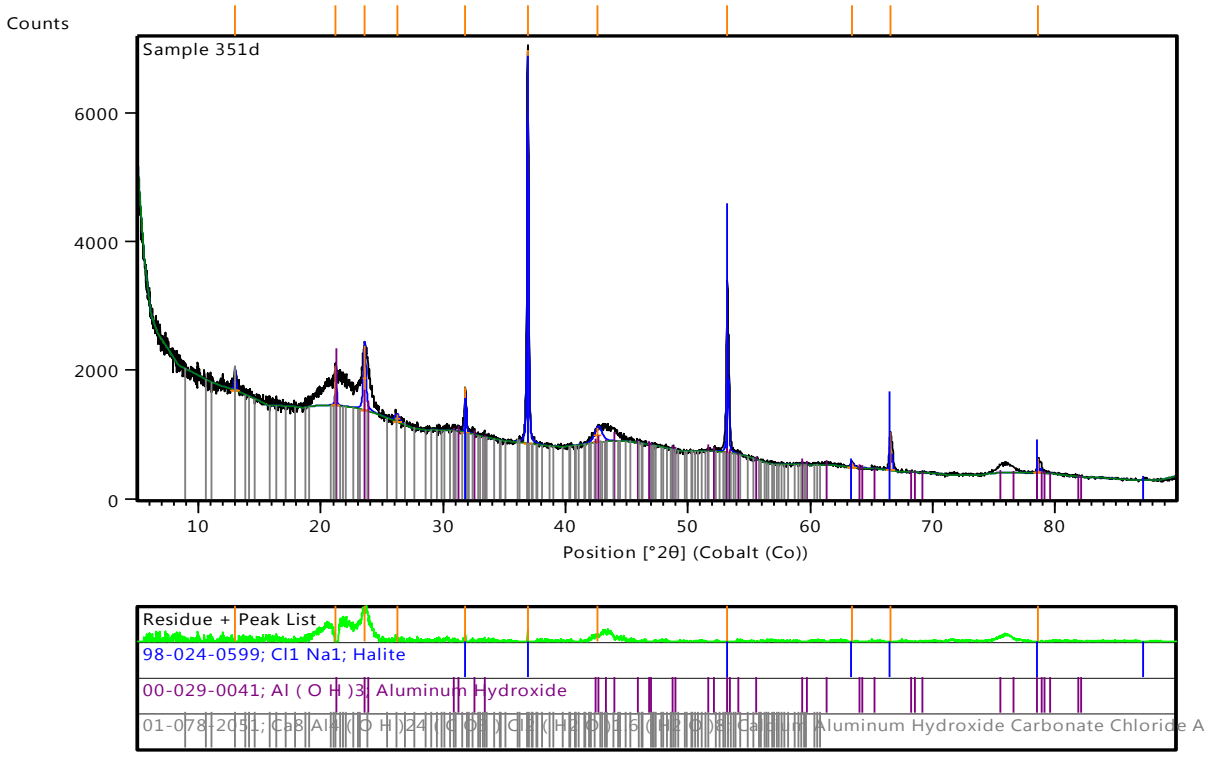

A-74: XRD graph for Ca/Al-chloride synthesis (pH = 3.23)

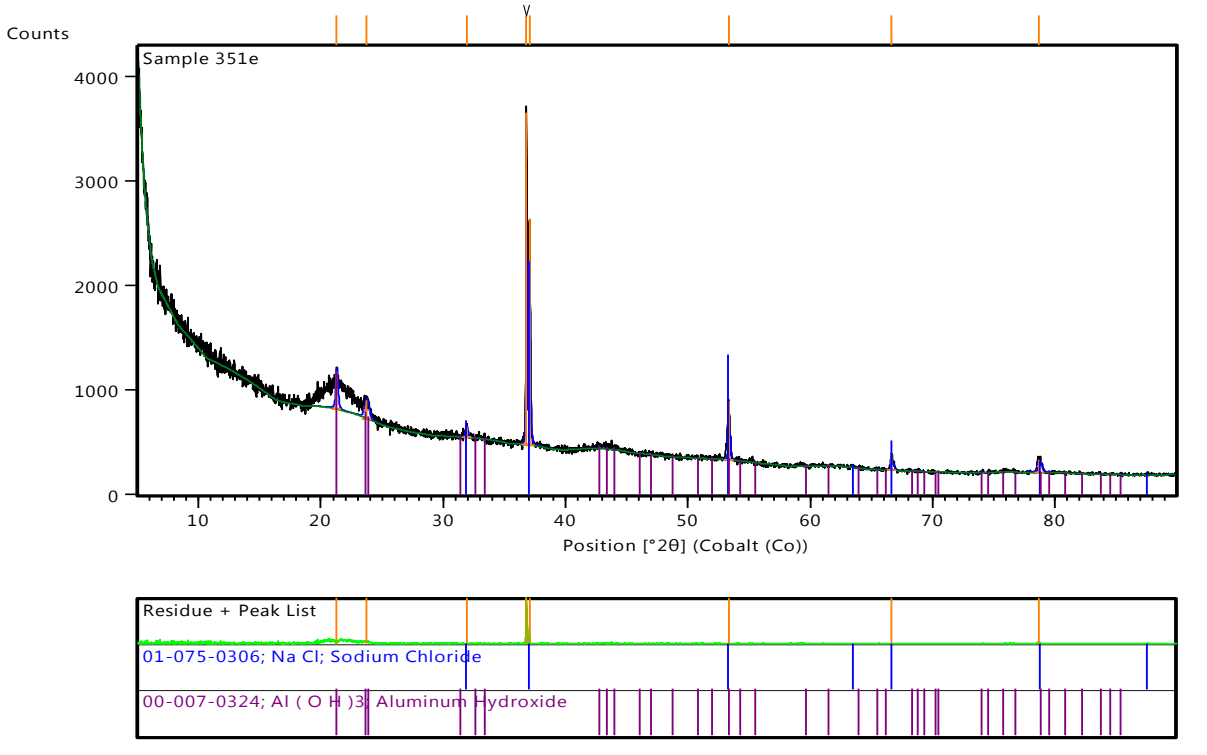

A-75: XRD graph for Ca/Al-nitrate synthesis (pH = 10.61)

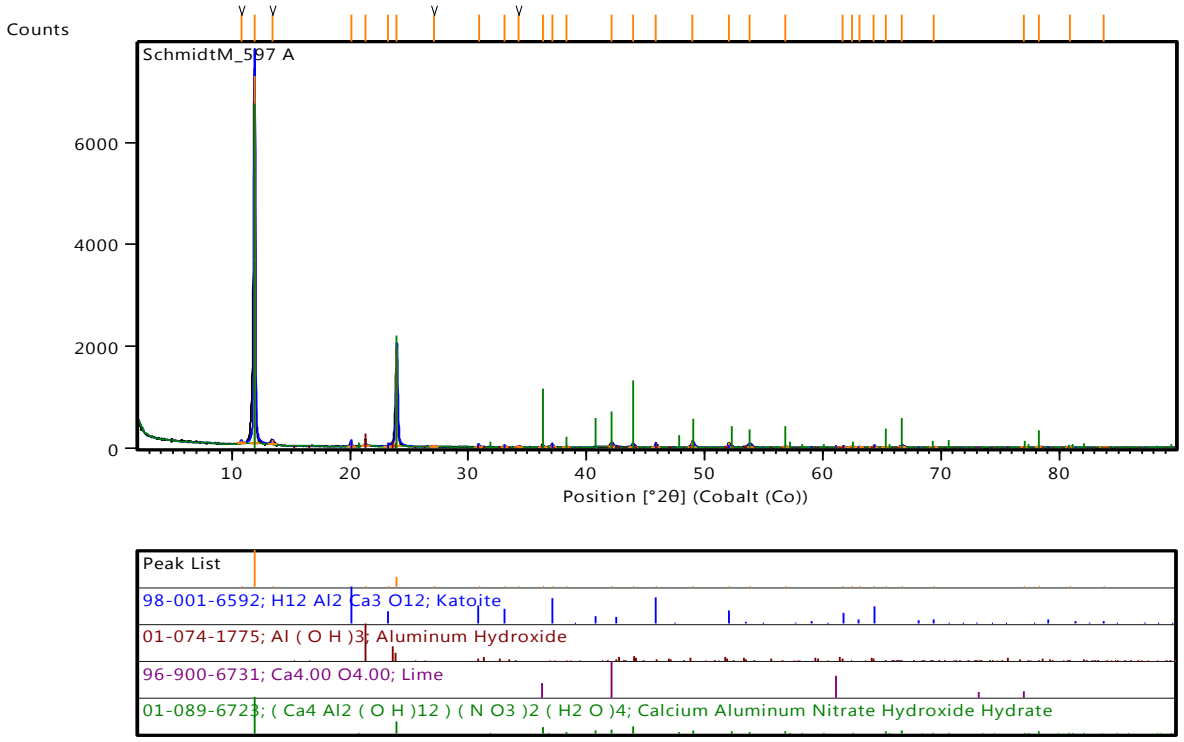

A-76: XRD graph for Ca/Al-nitrate synthesis (pH = 9.96)

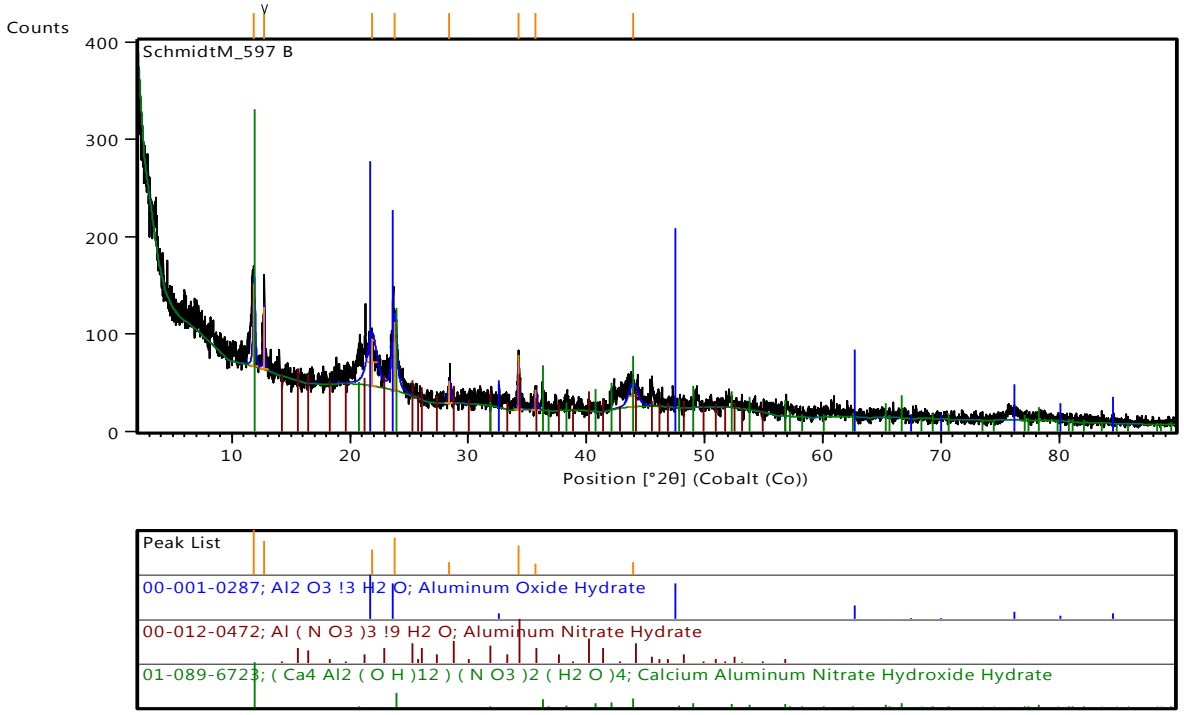

A-77: XRD graph for Ca/Al-sulphate synthesis (pH = 11.66)

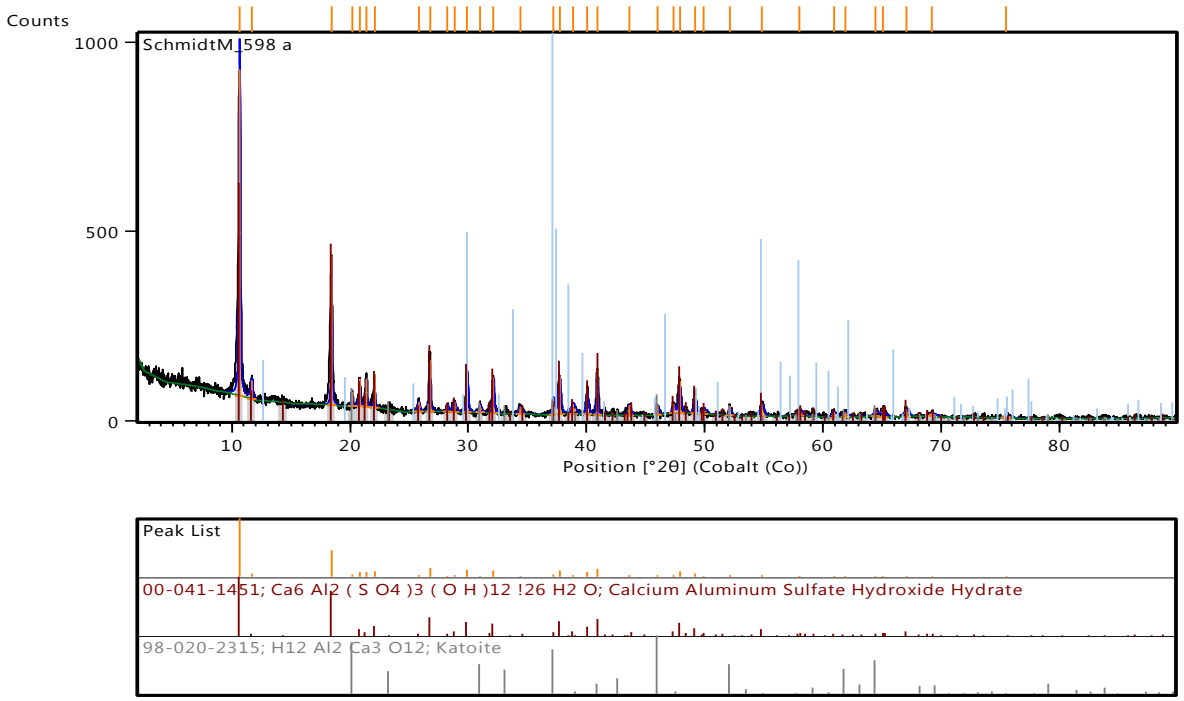

A-78: XRD graph for Ca/Al-sulphate synthesis (pH = 9.90)

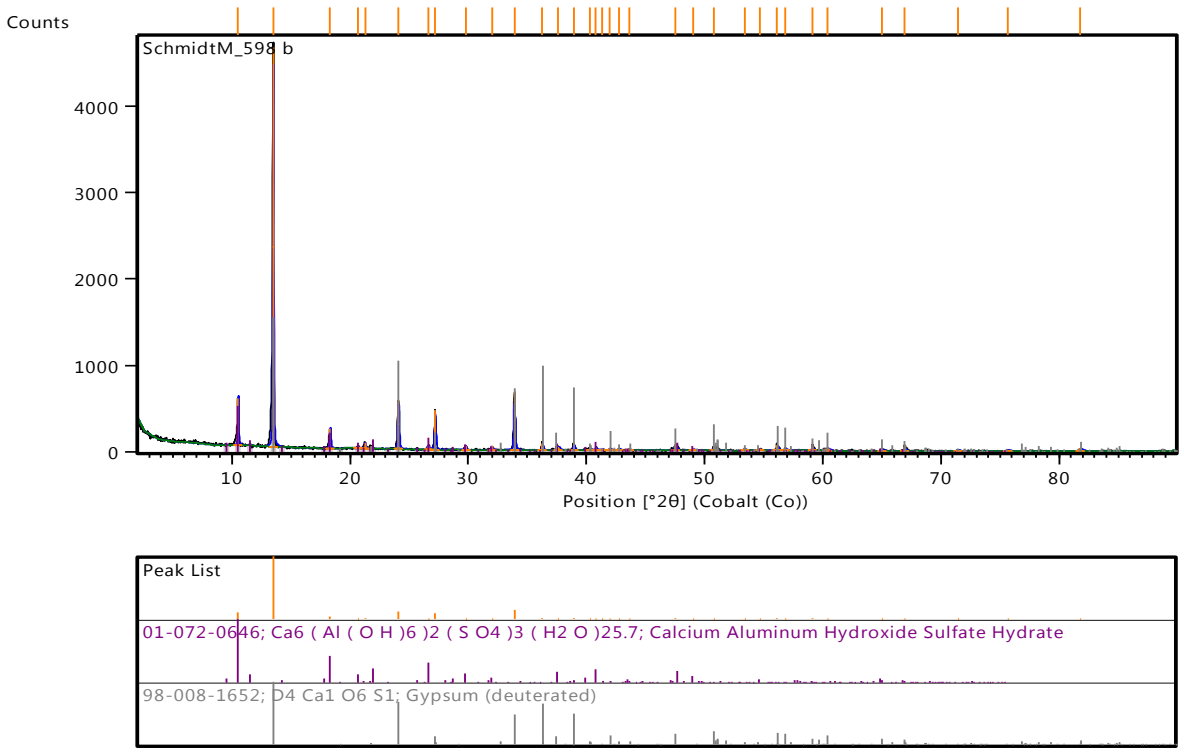

A-79: XRD graph for Ca/Al-sulphate synthesis (pH = 1.30)

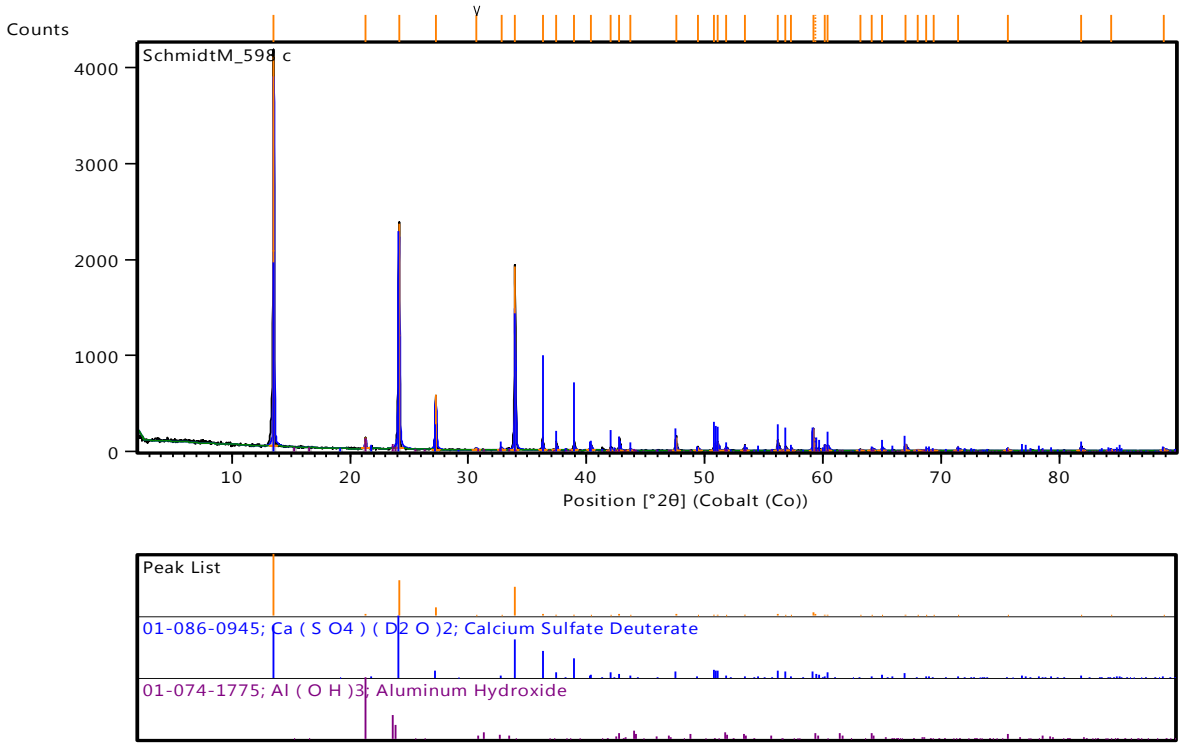

A-80: XRD graph for Ca/Al-citrate synthesis (pH = 10.59)

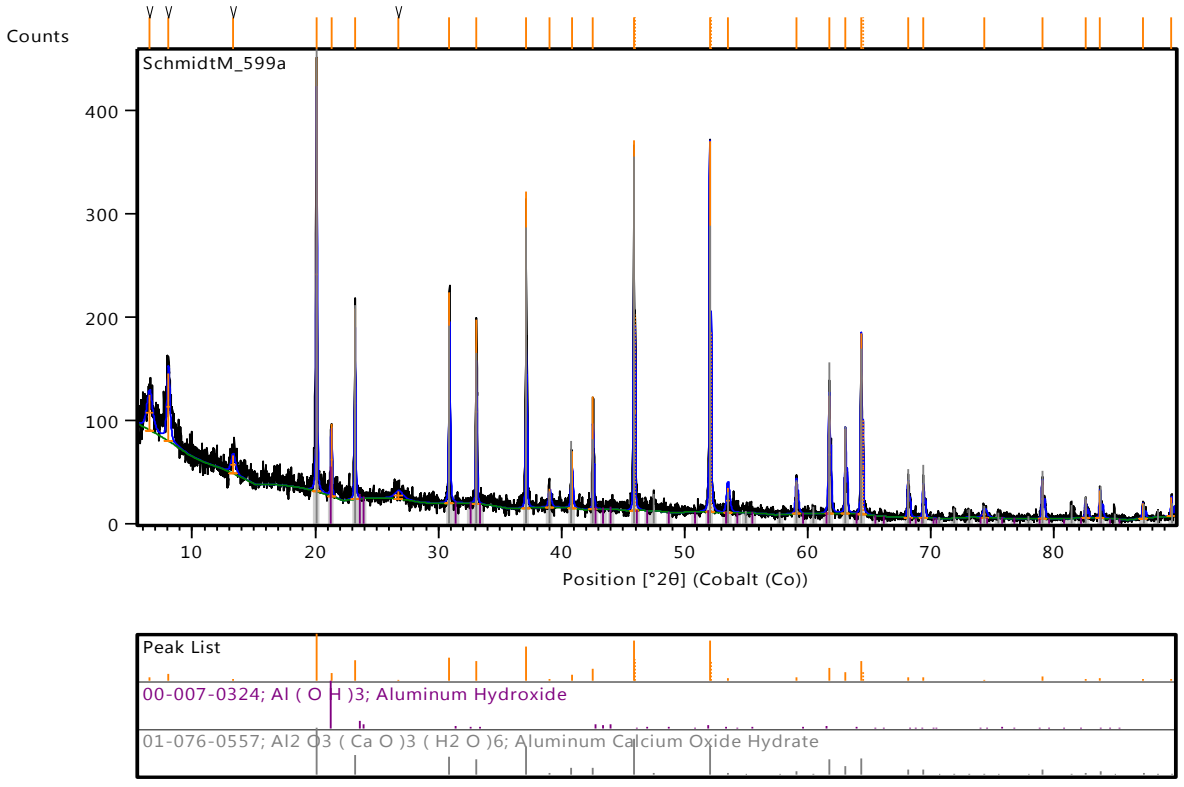

A-81: XRD graph for Ca/Al-citrate synthesis (pH = 9.70)

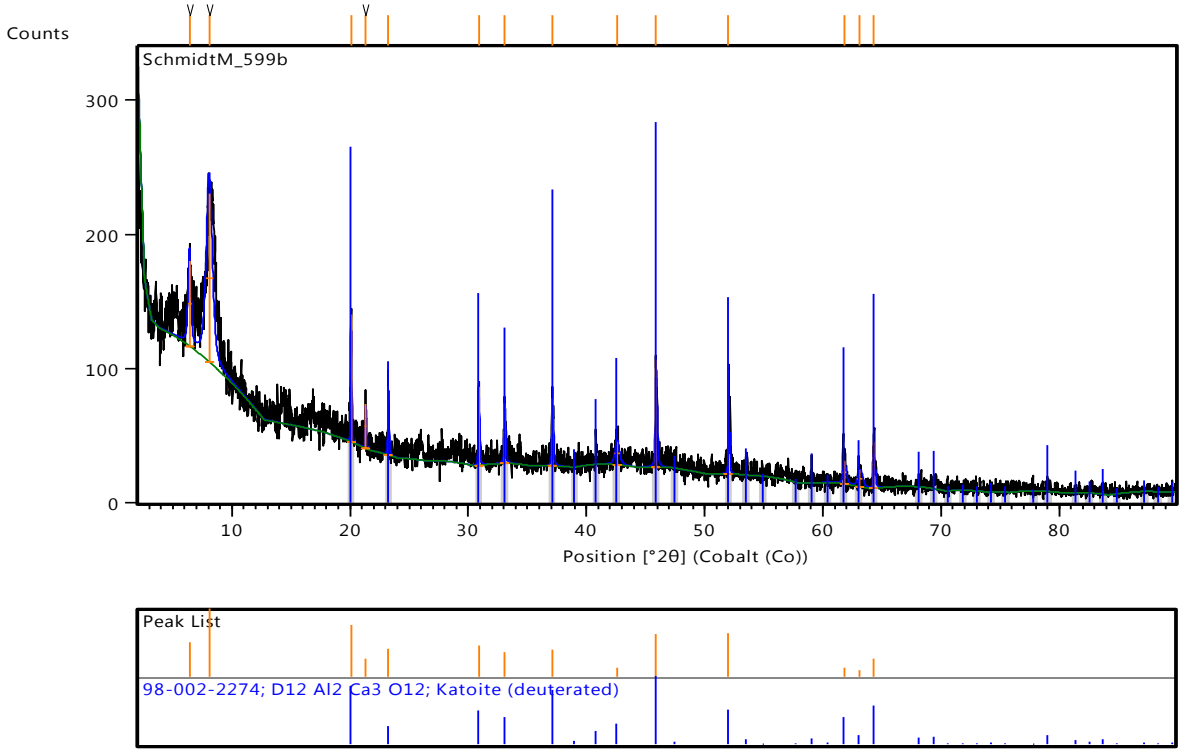

A-82: XRD graph for Ca/Al-citrate synthesis (pH = 2.86)

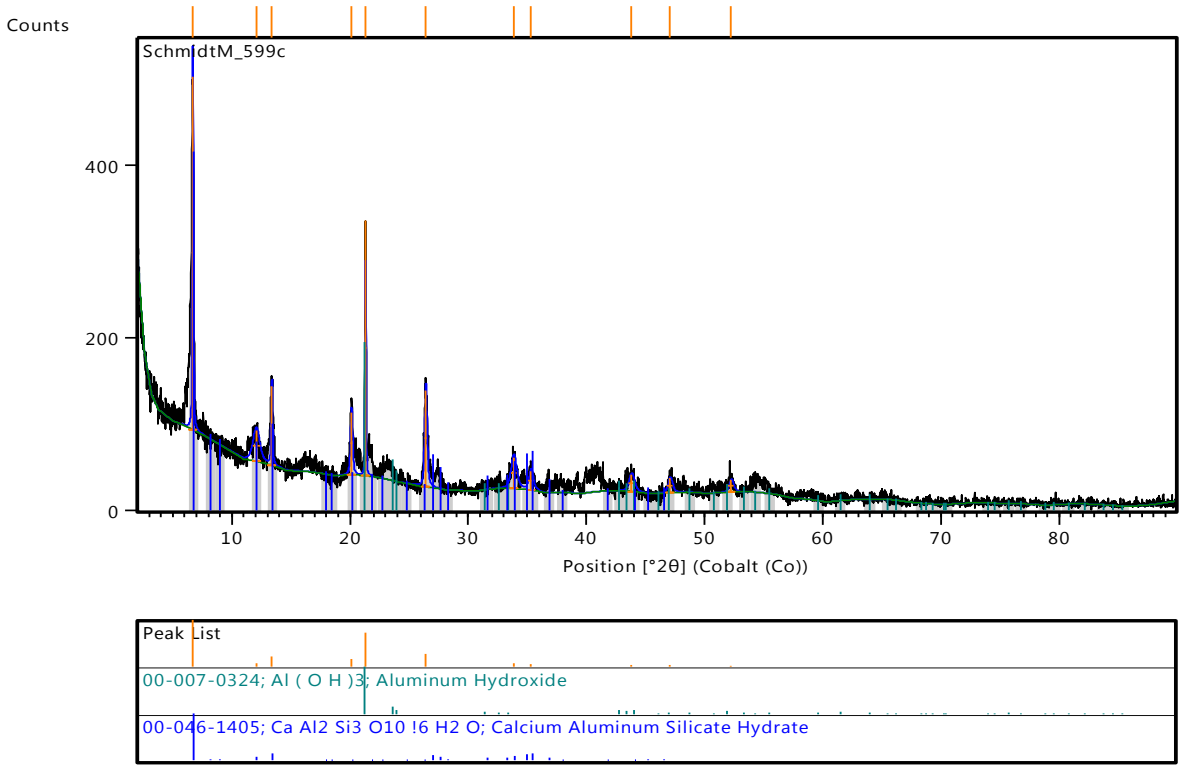

A-83: XRD graph for Ca/Al-acetate synthesis (pH = 12.61)

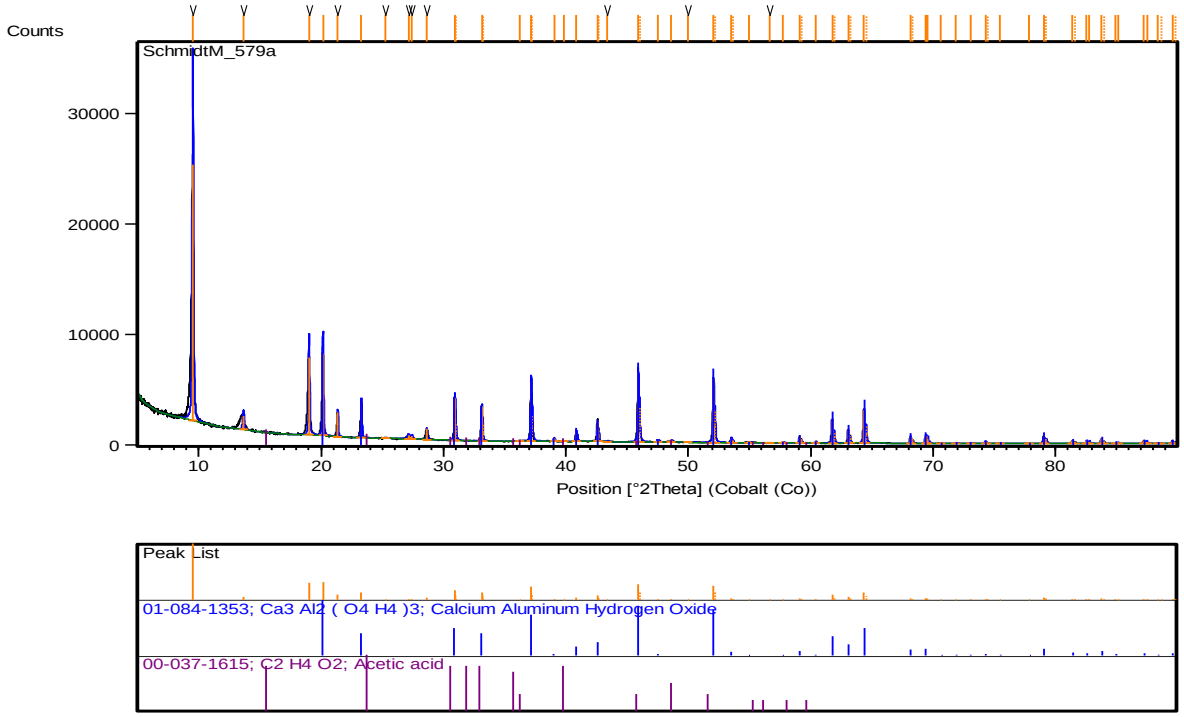

A-84: XRD graph for Ca/Al-acetate synthesis (pH = 11.50)

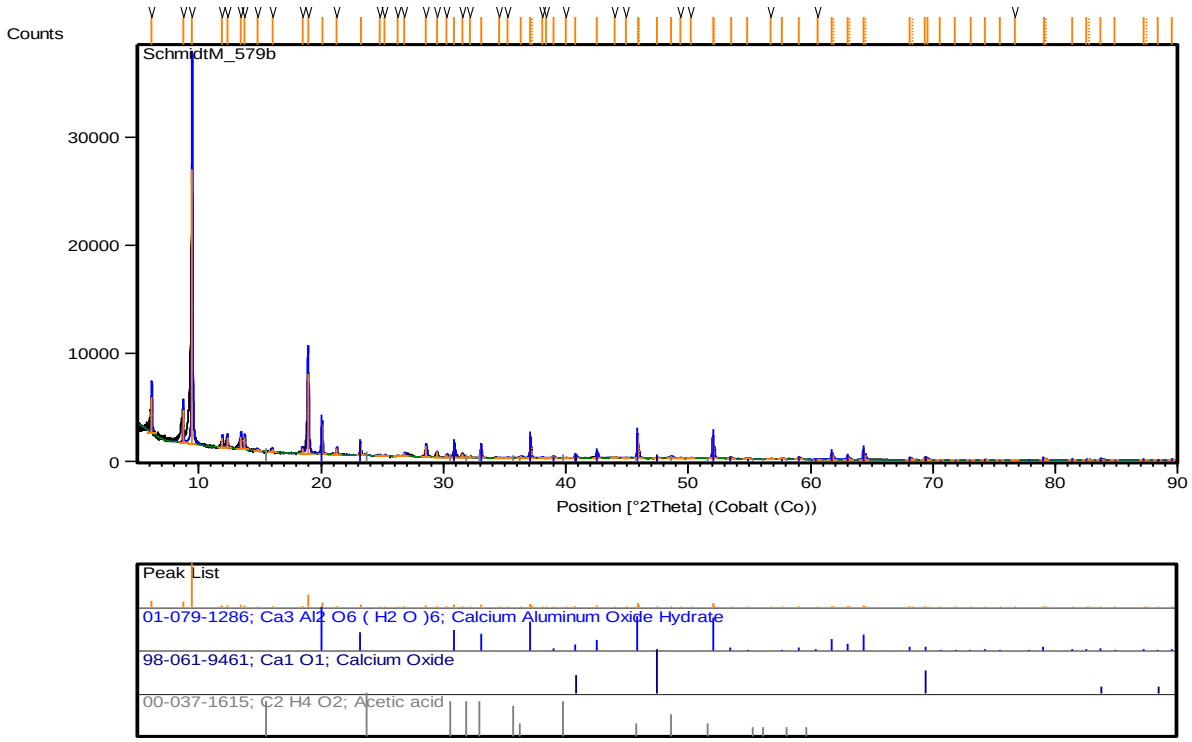

A-85: XRD graph for Ca/Al-acetate synthesis (pH = 5.43)

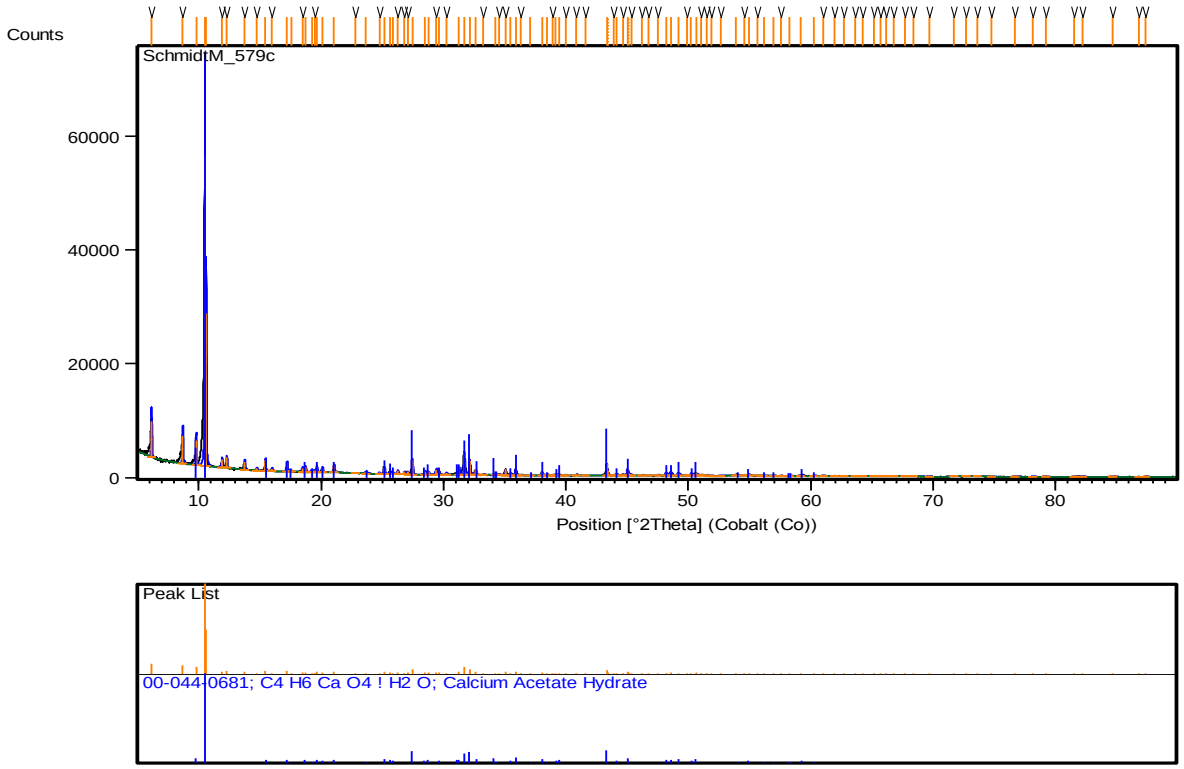

A-86: XRD graph for Ca/Al-thioglycolate synthesis (pH = 10.88)

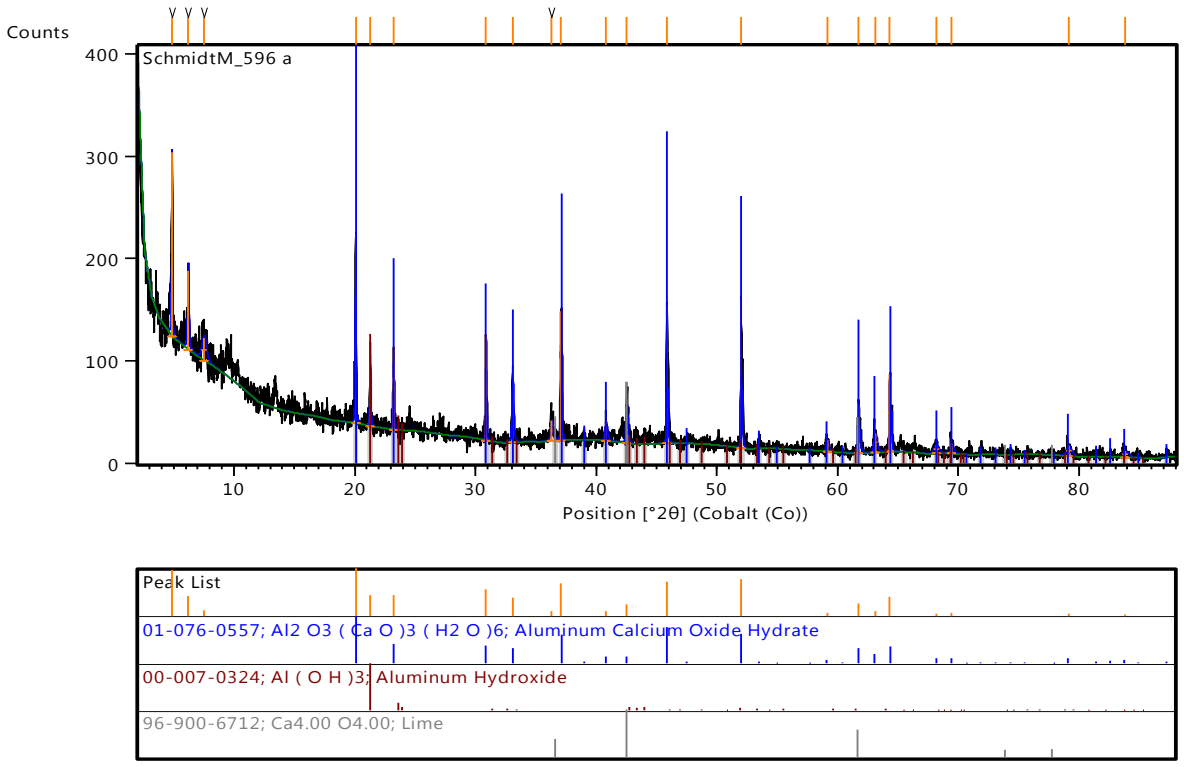

A-87: XRD graph for Ca/Al-thioglycolate synthesis (pH = 5.27)

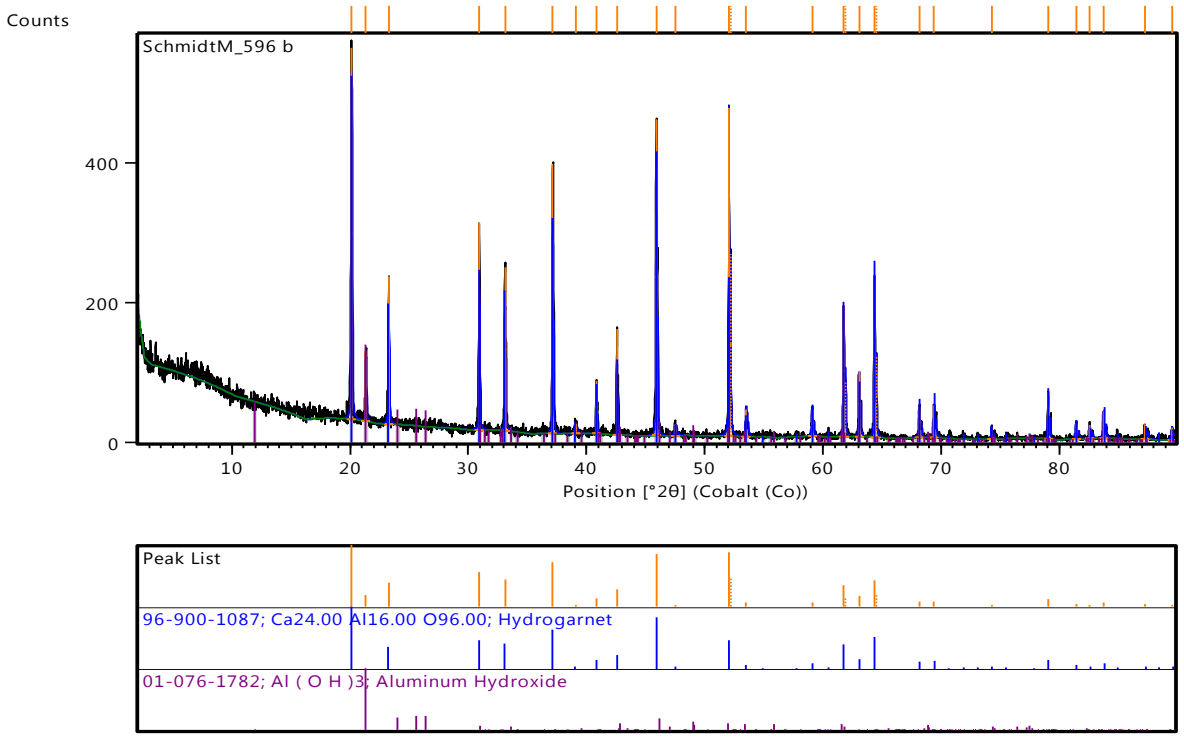

A-88: XRD graph for Ca/Al-thioglycolate synthesis (pH = 4.41)

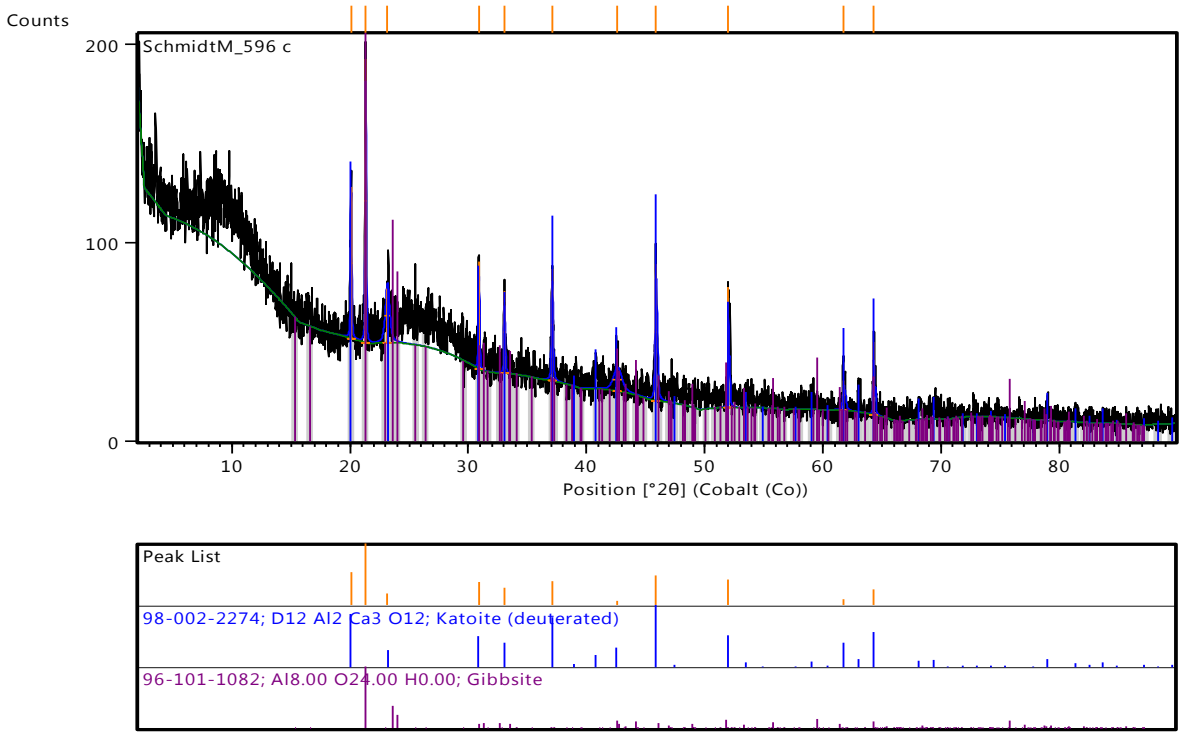

A-89: XRD graph for Ca/Al-carbonate synthesis (pH = 12.62)

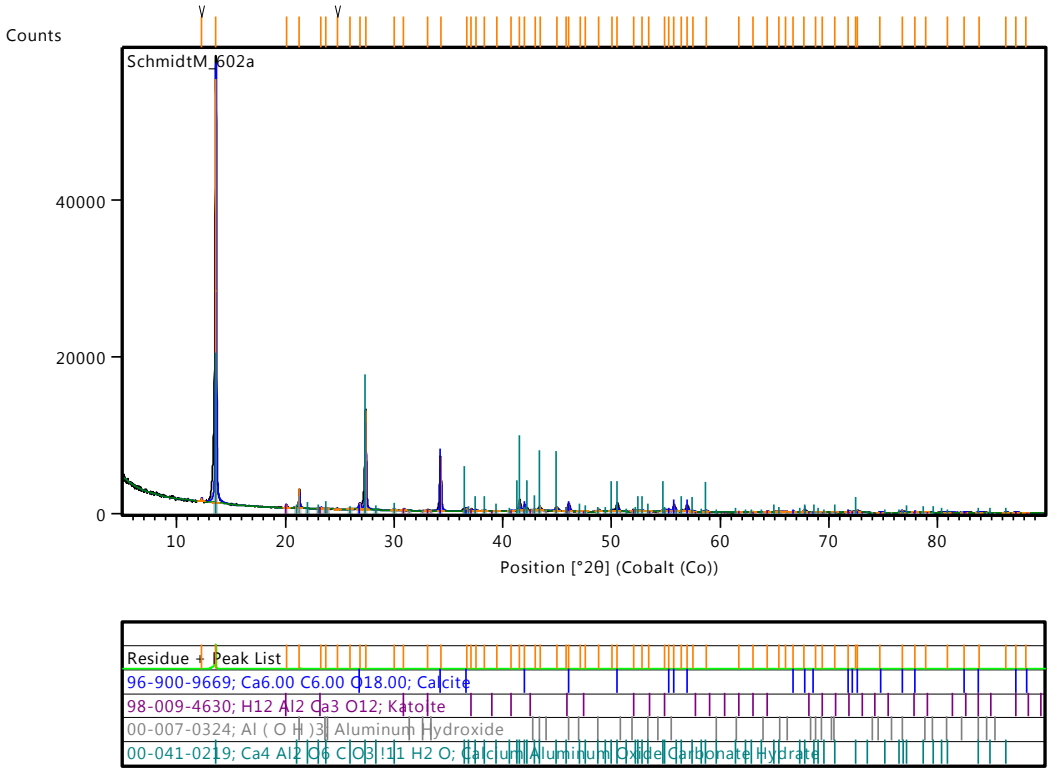

A-90: XRD graph for Ca/Al-carbonate synthesis (pH = 9.05)

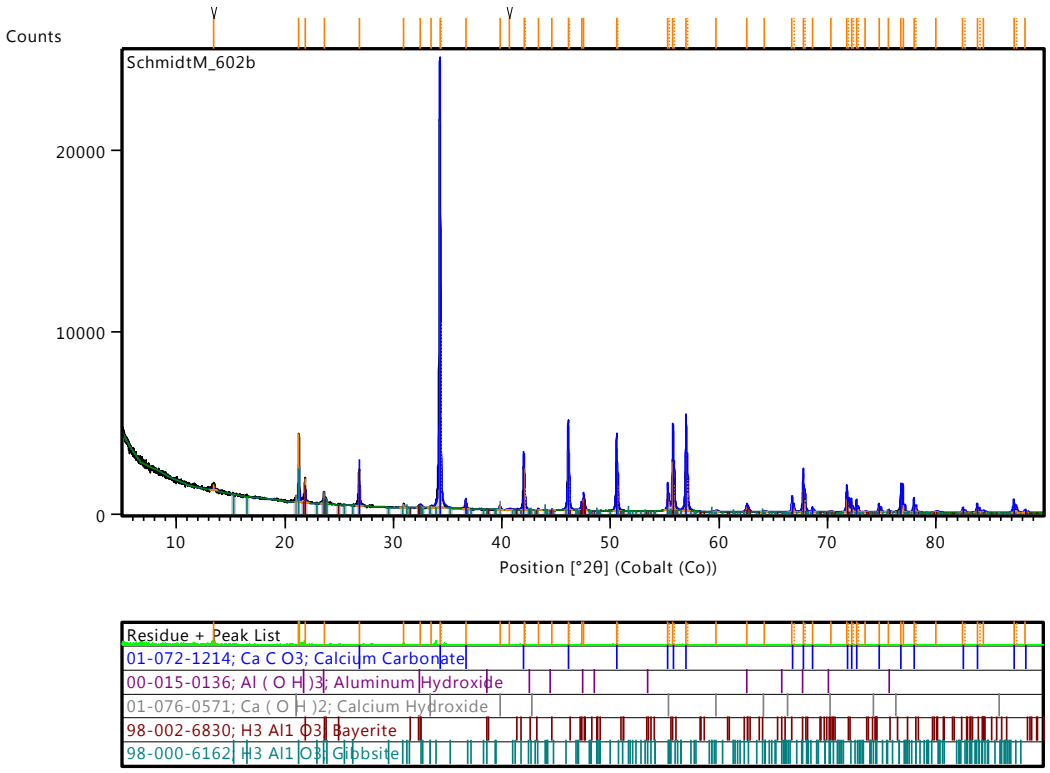

A-91: XRD graph for Ca/Al-carbonate synthesis (pH = 8.82)

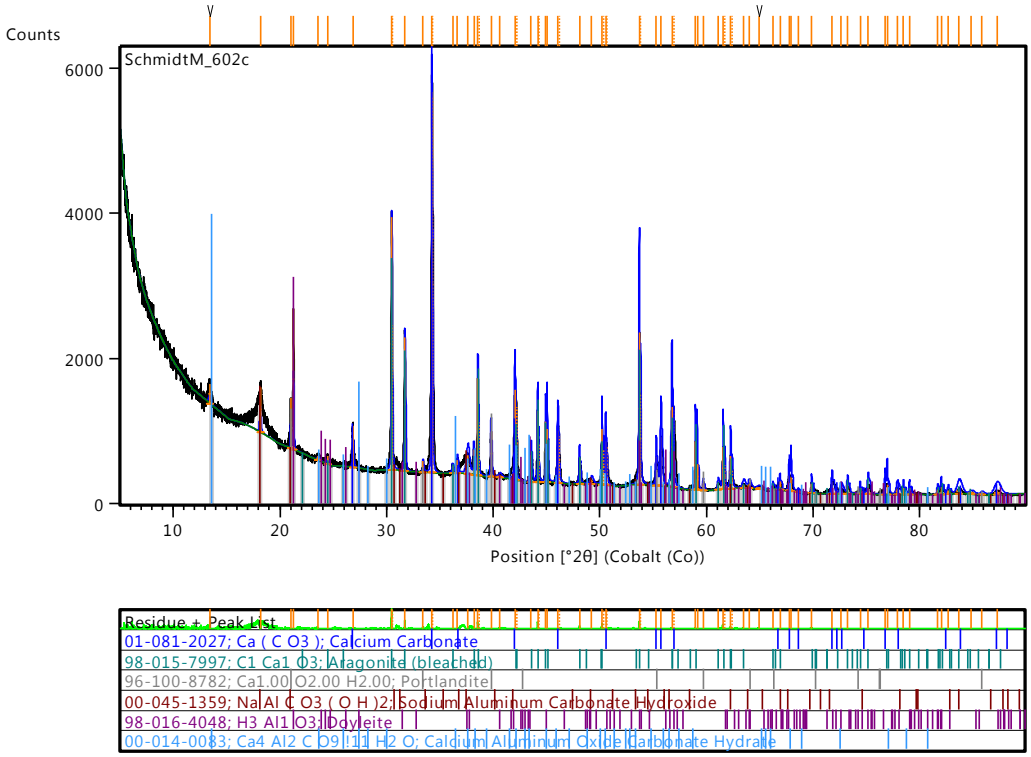

Appendix B: FTIR Results

B-1: FTIR graph for Ca/Al-benzoate synthesis (pH = 12.32)

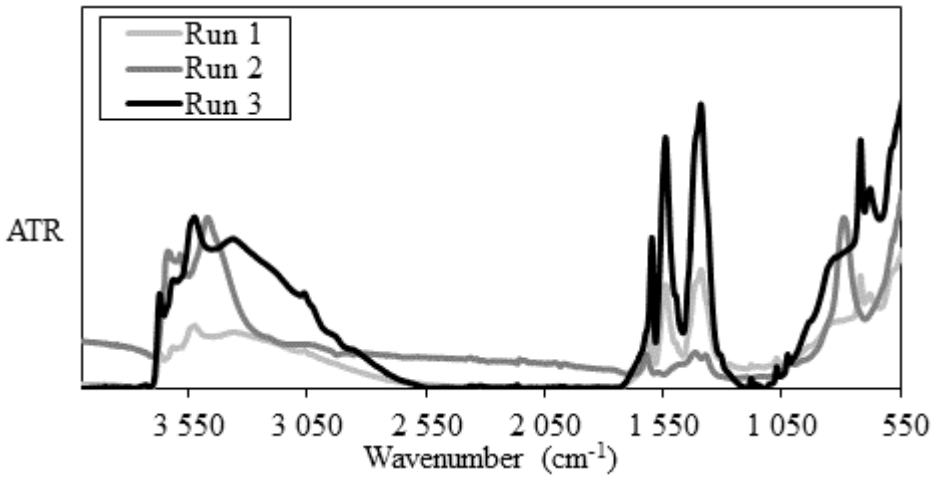

B-2: FTIR graph for Ca/Al-benzoate synthesis (pH = 11.24)

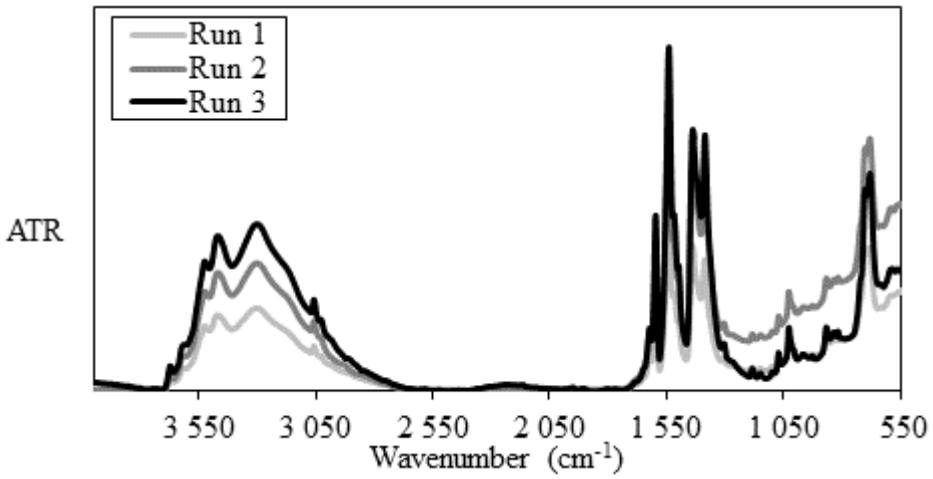

B-3: FTIR graph for Ca/Al-salicylate synthesis (pH = 11.69)

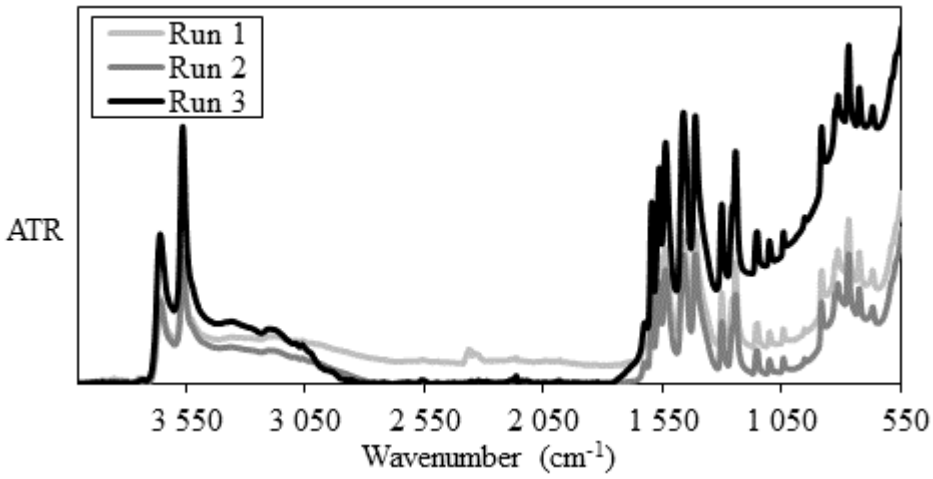

B-4: FTIR graph for Ca/Al-salicylate synthesis (pH = 11.11)

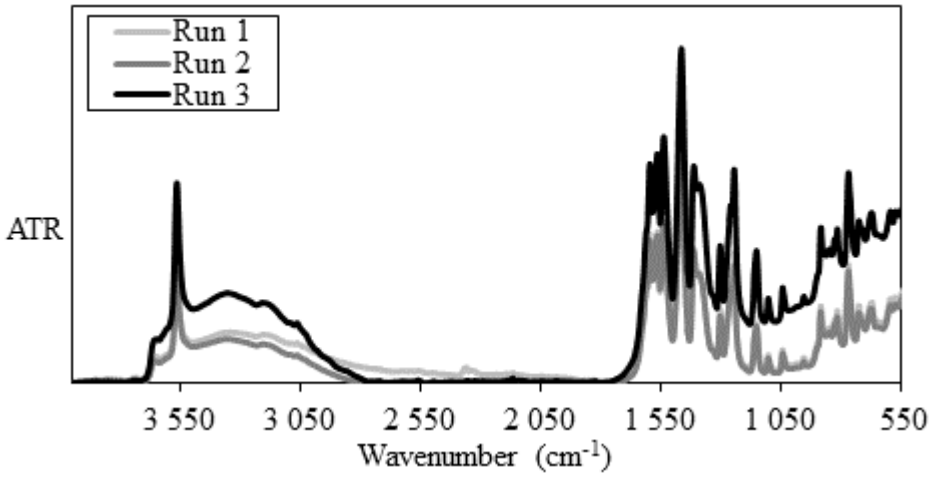

B-5: FTIR graph for Ca/Al-salicylate synthesis (pH = 3.69)

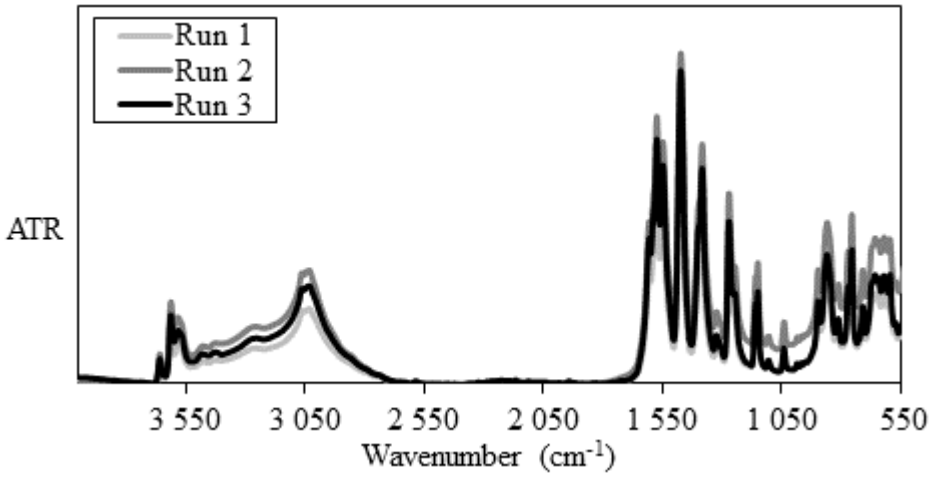

B-6: FTIR graph for Ca/Al-anthranilate synthesis (pH = 12.03)

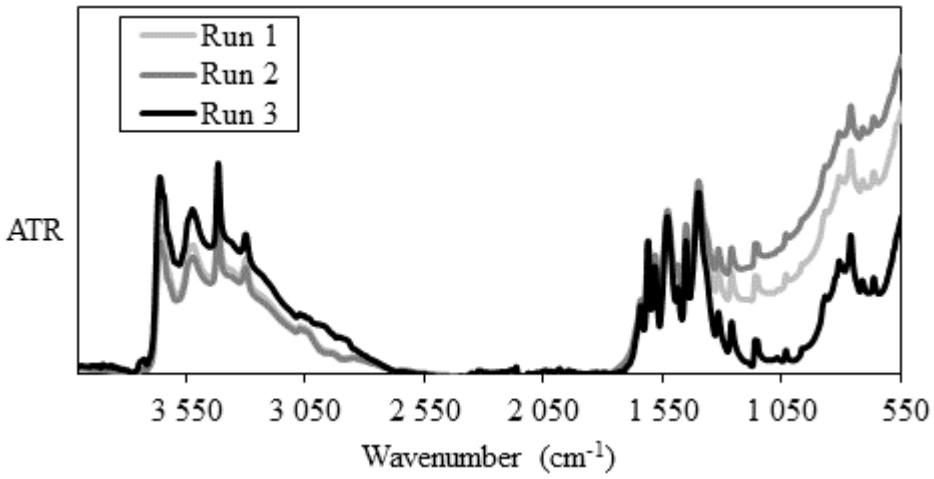

B-7: FTIR graph for Ca/Al-anthranilate synthesis (pH = 11.67)

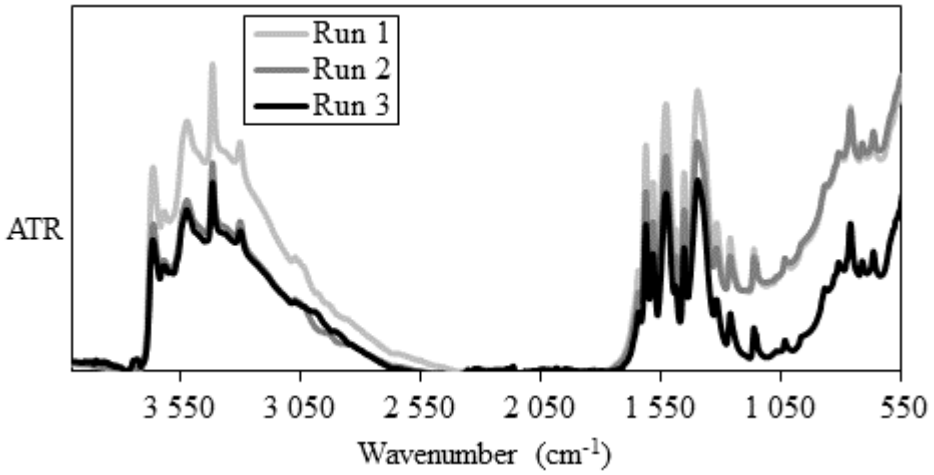

B-8: FTIR graph for Ca/Al-anthranilate synthesis (pH = 5.29)

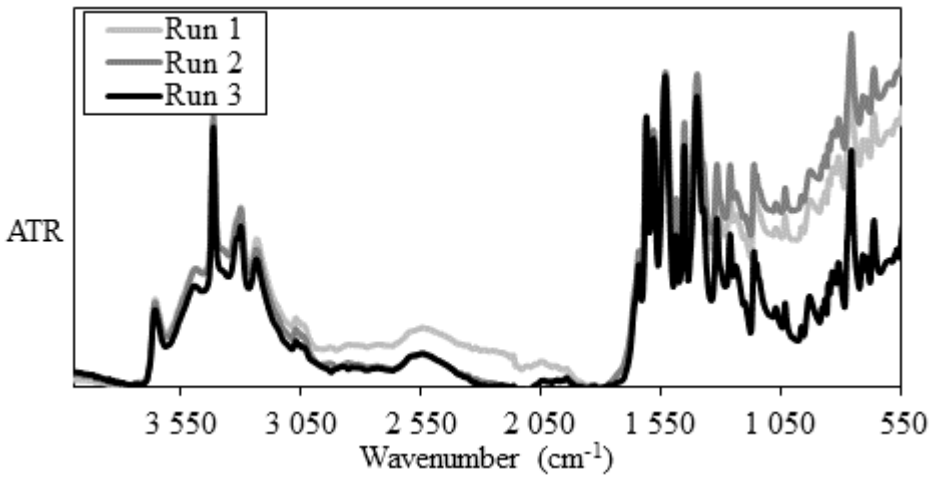

B-9: FTIR graph for Ca/Al-thiosalicylate synthesis (pH = 11.56)

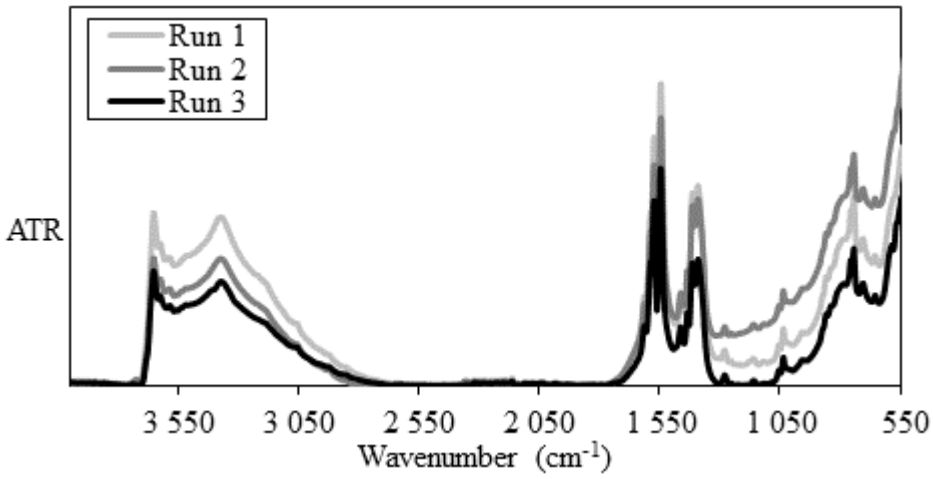

B-10: FTIR graph for Ca/Al-thiosalicylate synthesis (pH = 5.69)

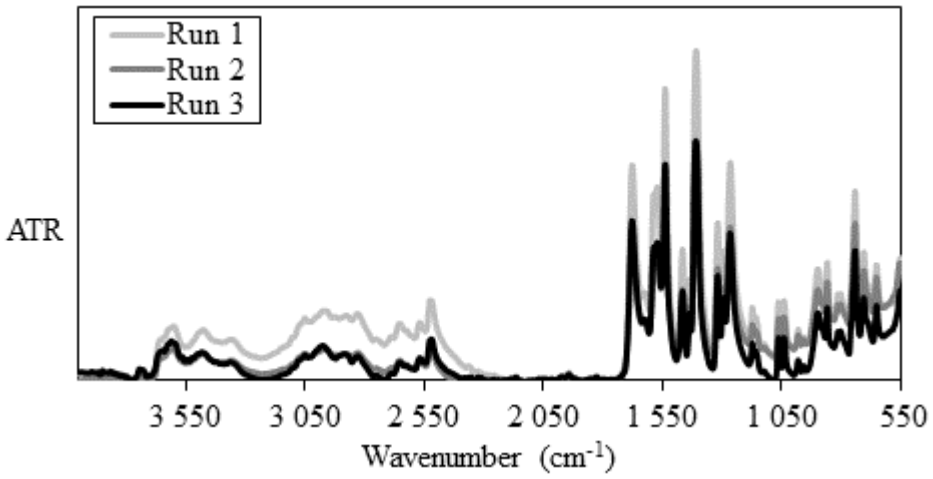

B-11: FTIR graph for Ca/Al-3-hydroxybenzoate synthesis (pH = 12.82)

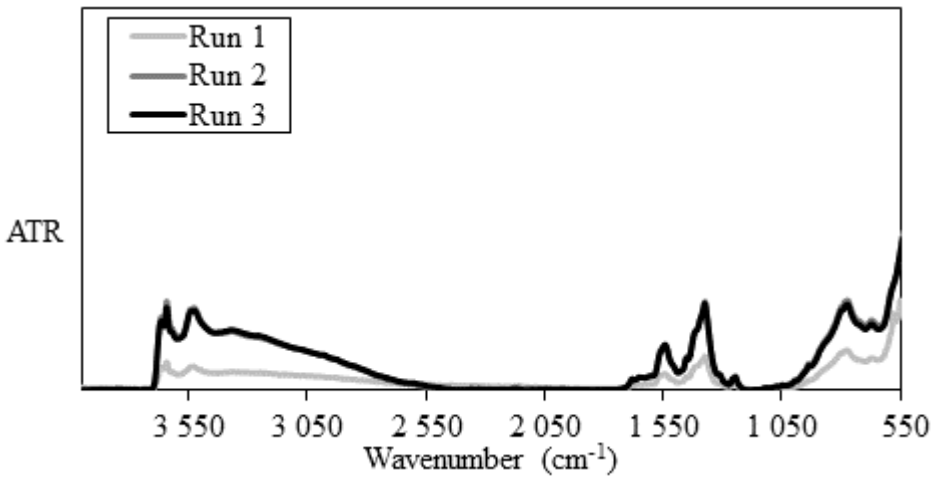

B-12: FTIR graph for Ca/Al-3-hydroxybenzoate synthesis (pH = 11.12)

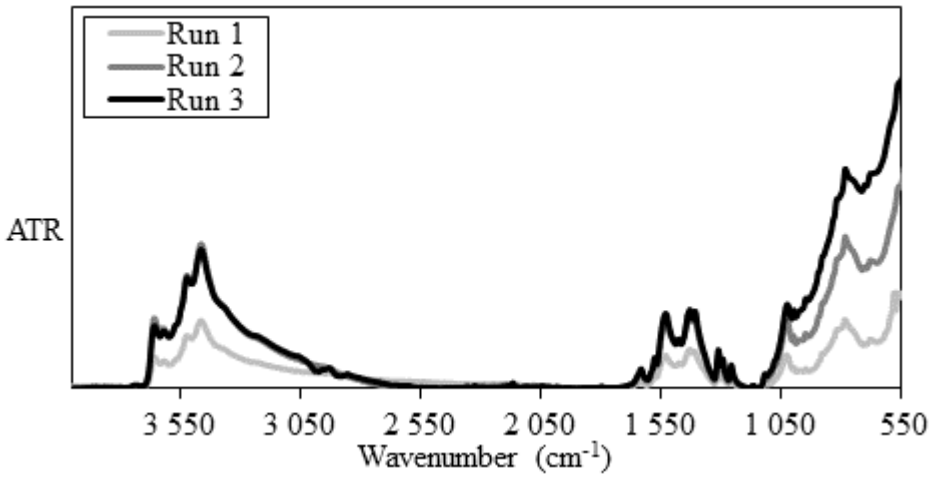

B-13: FTIR graph for Ca/Al-3-hydroxybenzoate synthesis (pH = 4.98)

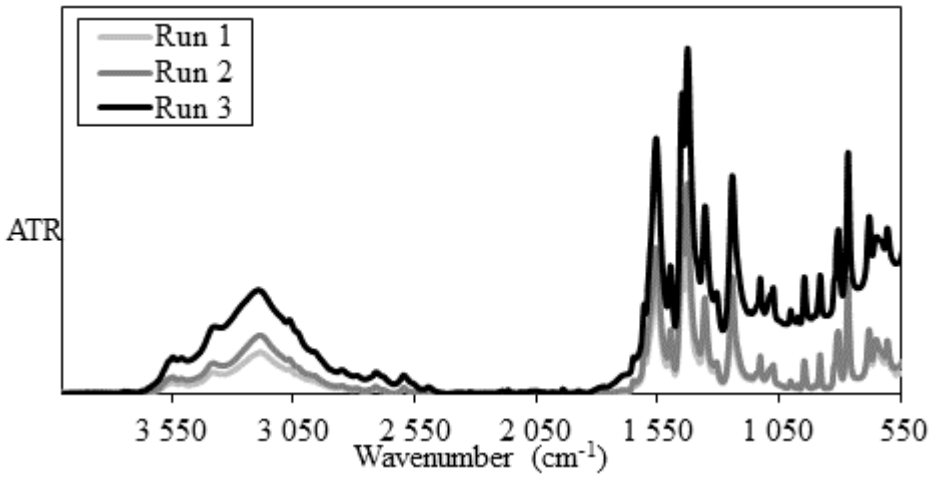

B-14: FTIR graph for Ca/Al-3-aminobenzoate synthesis (pH = 12.50)

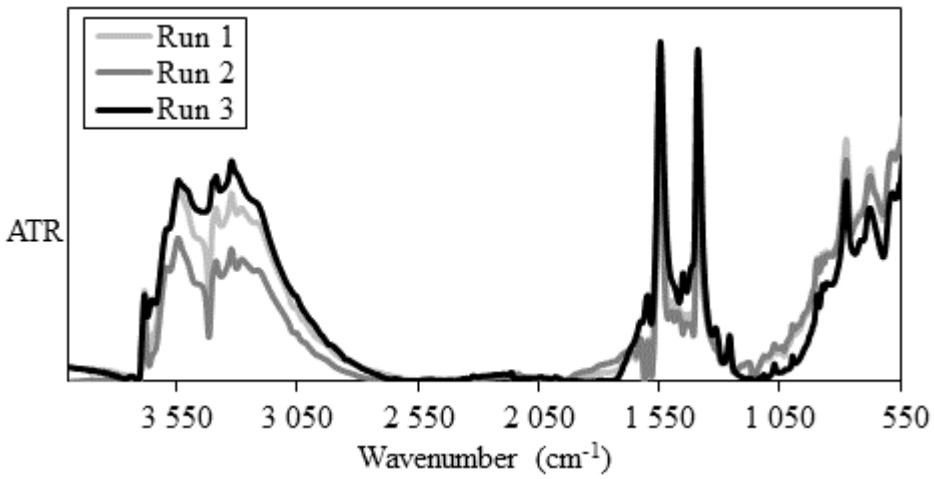

B-15: FTIR graph for Ca/Al-3-aminobenzoate synthesis (pH = 5.30)

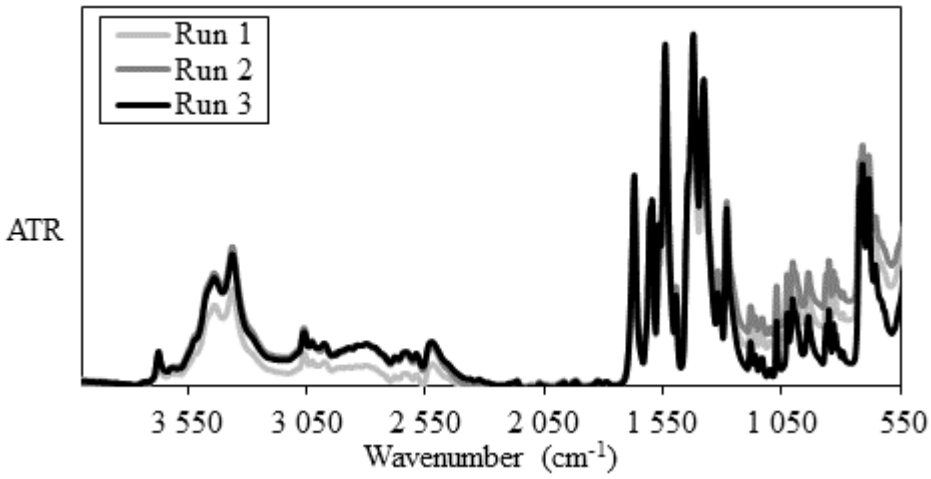

B-16: FTIR graph for Ca/Al-4-hydroxybenzoate synthesis (pH = 12.26)

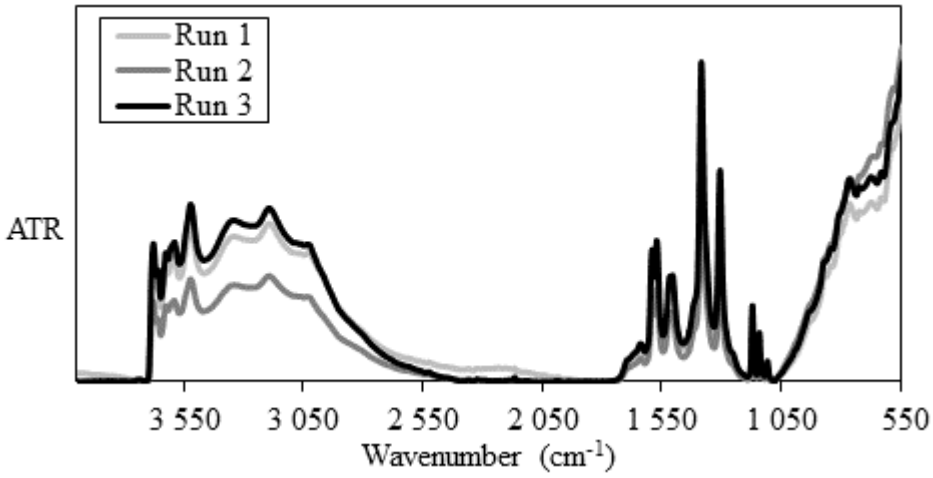

B-17: FTIR graph for Ca/Al-4-hydroxybenzoate synthesis (pH = 4.83)

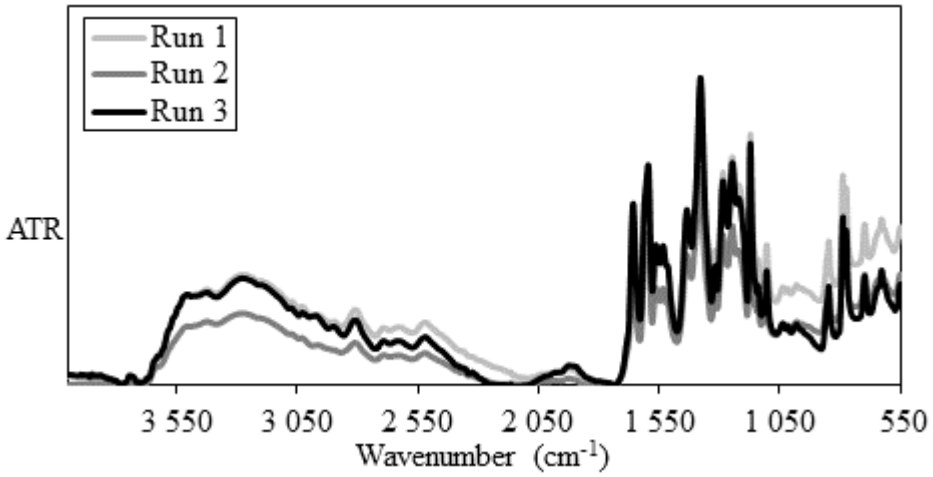

B-18: FTIR graph for Ca/Al-4-aminobenzoate synthesis (pH = 12.67)

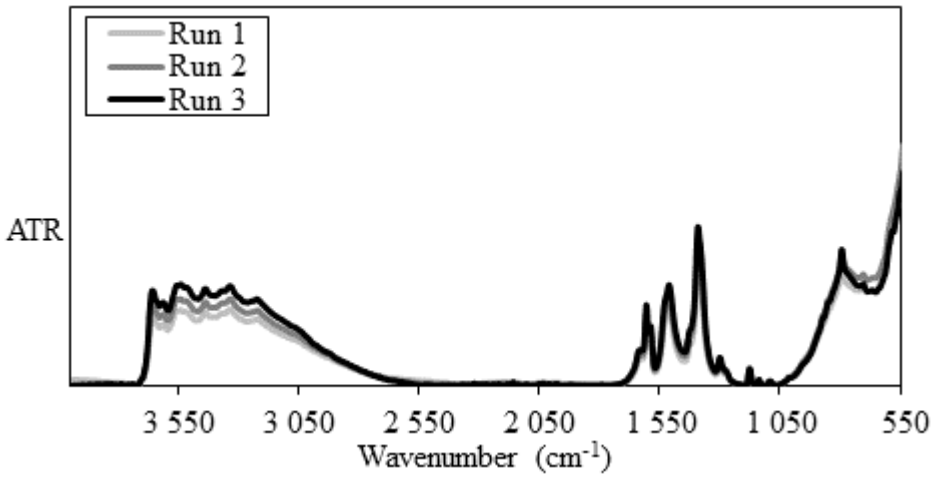

B-19: FTIR graph for Ca/Al-4-aminobenzoate synthesis (pH = 5.54)

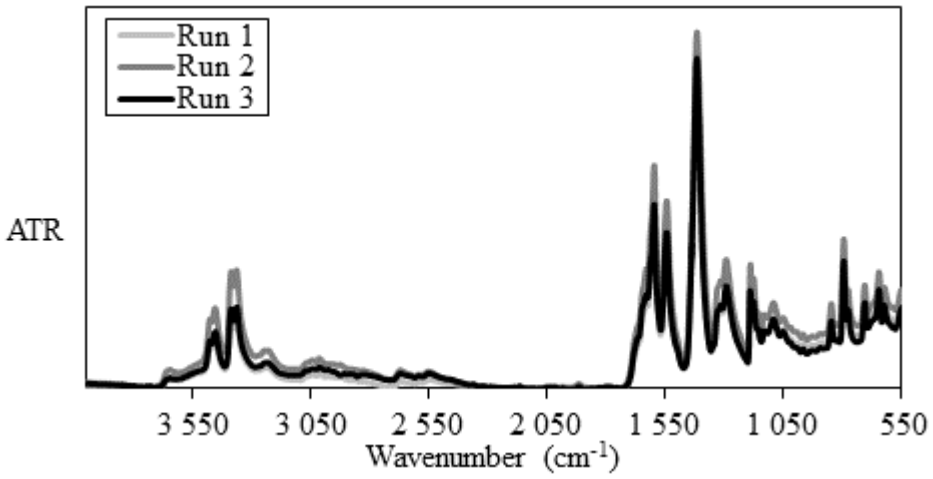

B-20: FTIR graph for Ca/Al-chloride synthesis (pH = 13.00)

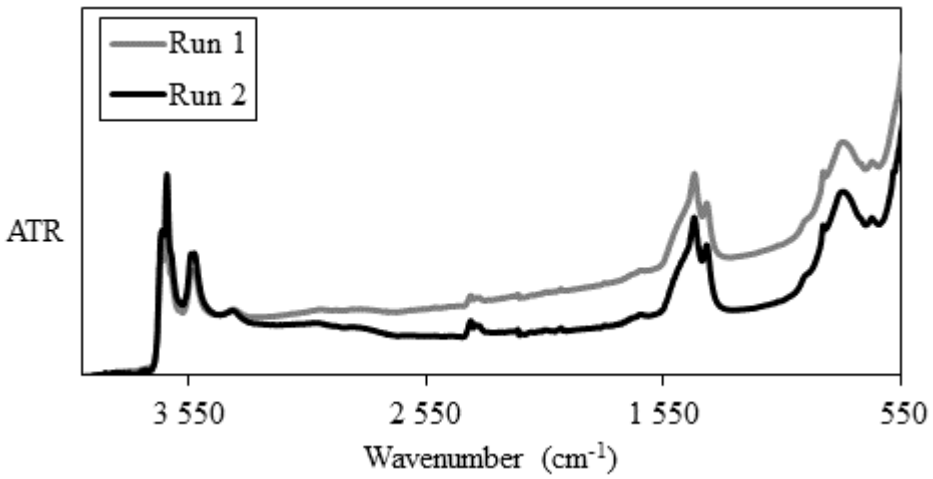

B-21: FTIR graph for Ca/Al-chloride synthesis (pH = 11.11)

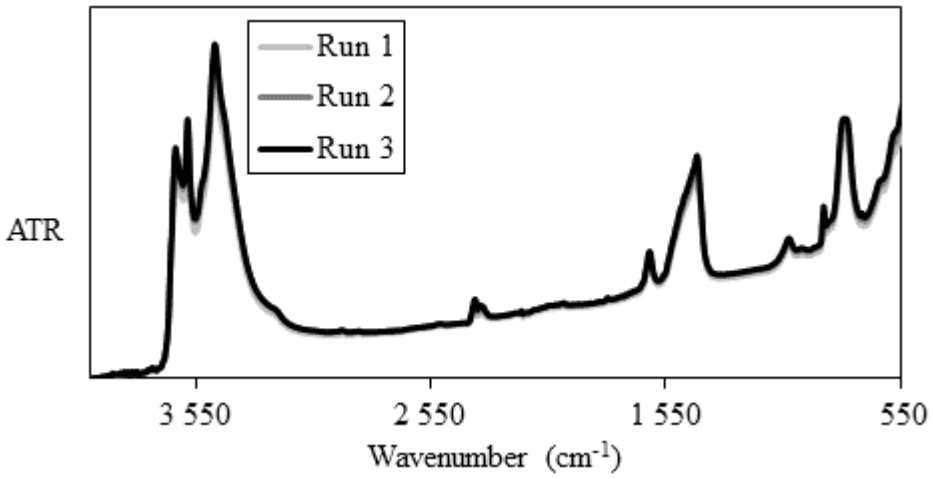

B-22: FTIR graph for Ca/Al-acetate synthesis (pH = 12.61)

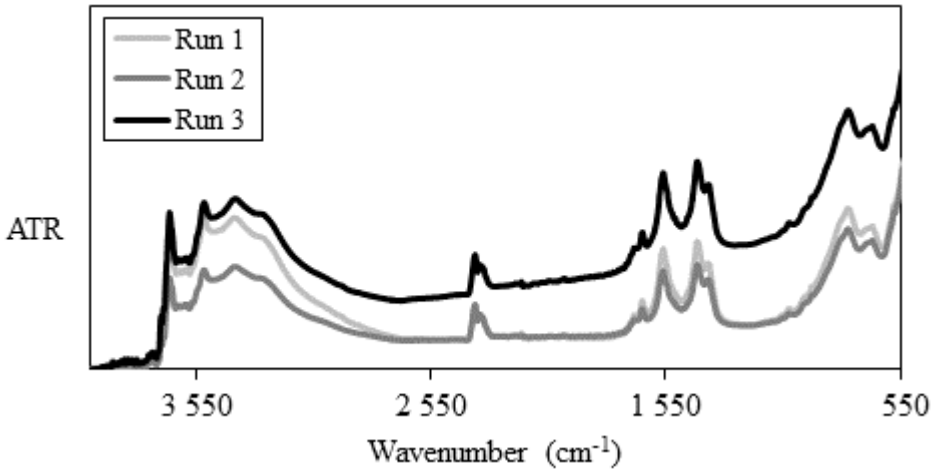

B-23: FTIR graph for Ca/Al-acetate synthesis (pH = 11.50)

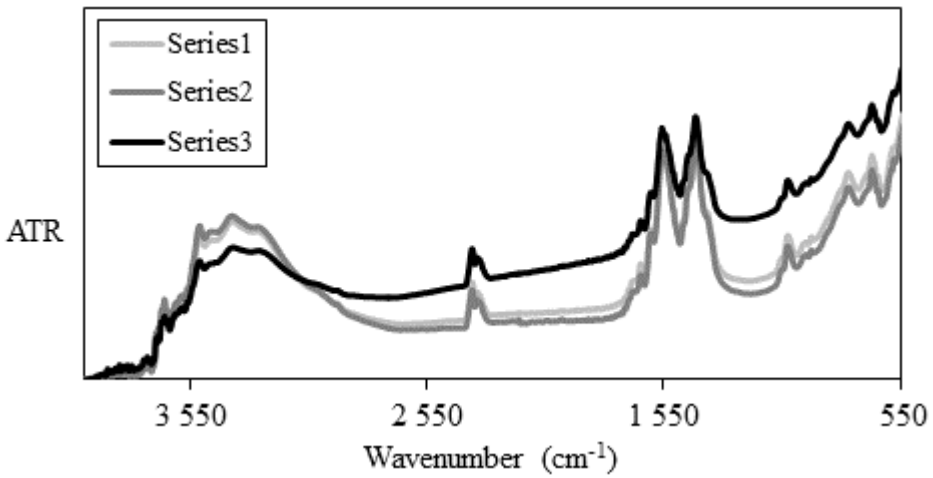

B-24: FTIR graph for Ca/Al-acetate synthesis (pH = 5.43)

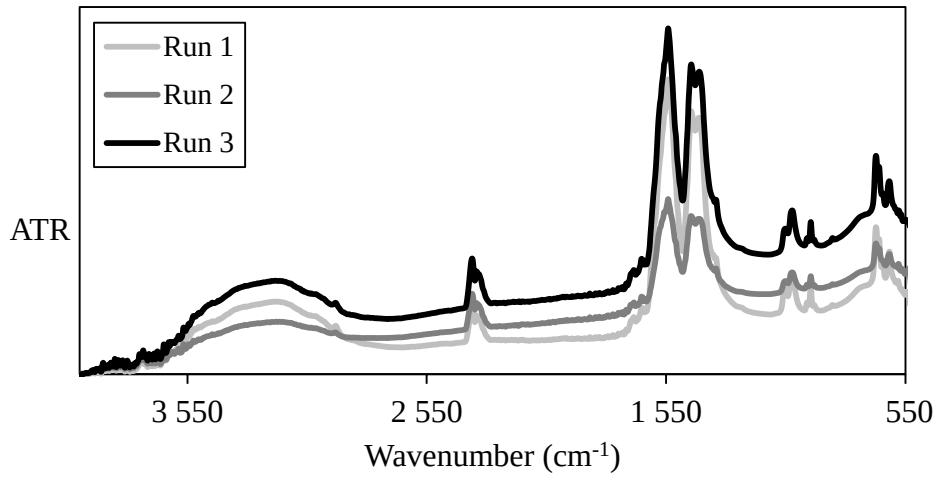

B-25: FTIR graph for Ca/Al-carbonate synthesis (pH = 12.62)

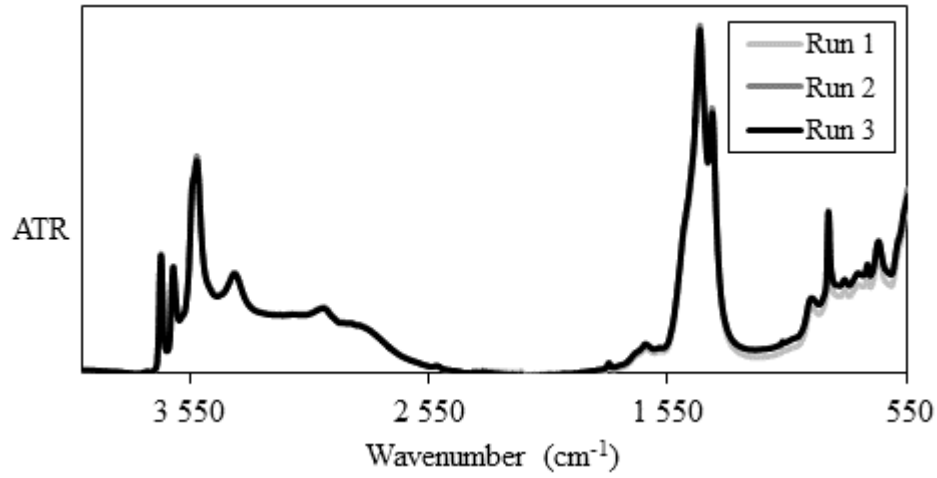

B-26: FTIR graph for Ca/Al-carbonate synthesis (pH =9.05)

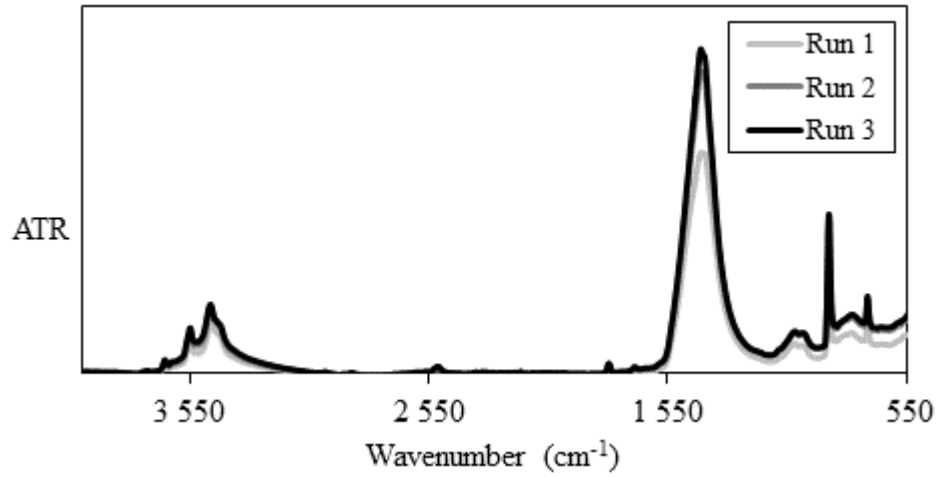

B-27: FTIR graph for Ca/Al-carbonate synthesis (pH = 8.82)

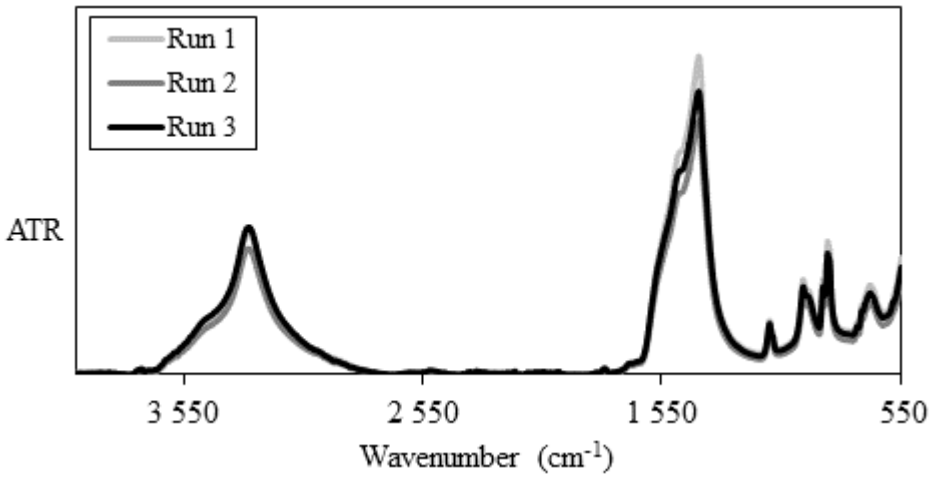

B-28: FTIR graph for Ca/Al-nitrate (pH = 10.61)

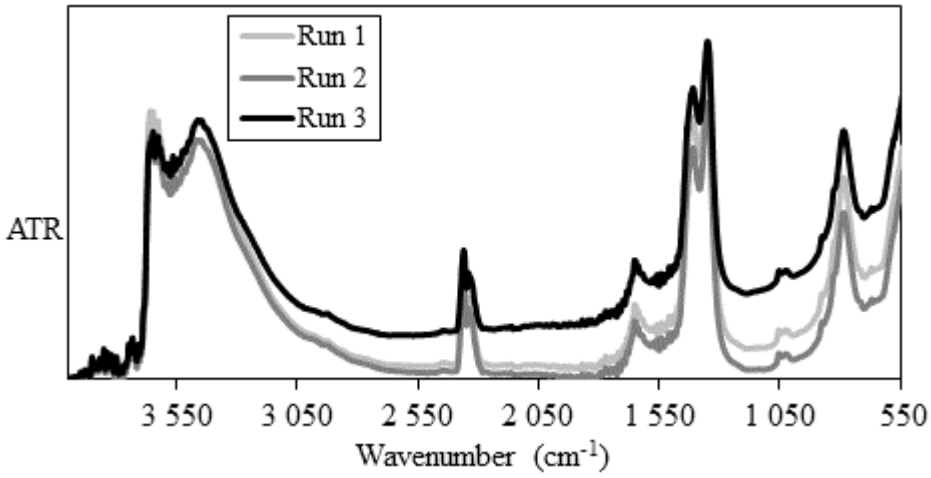

B-29: FTIR graph for Ca/Al-nitrate (pH = 9.96)

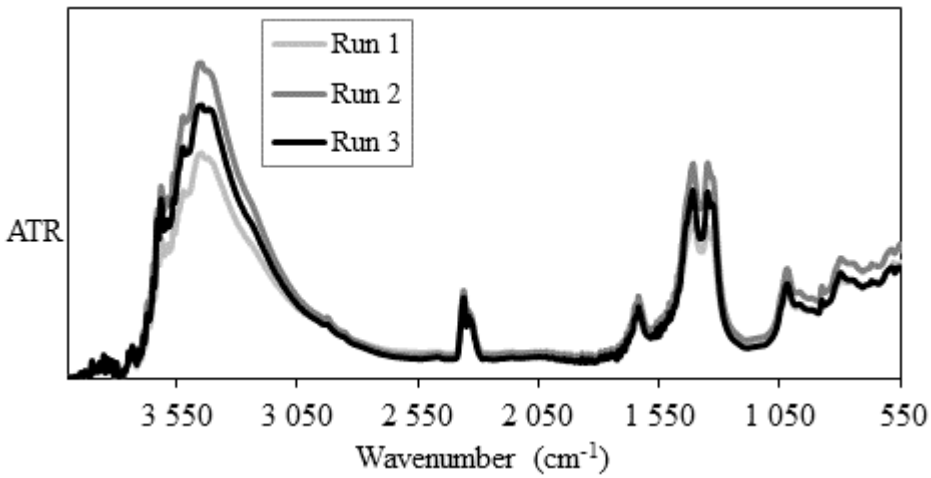

B-30: FTIR graph for Ca/Al-sulphate (pH = 11.66)

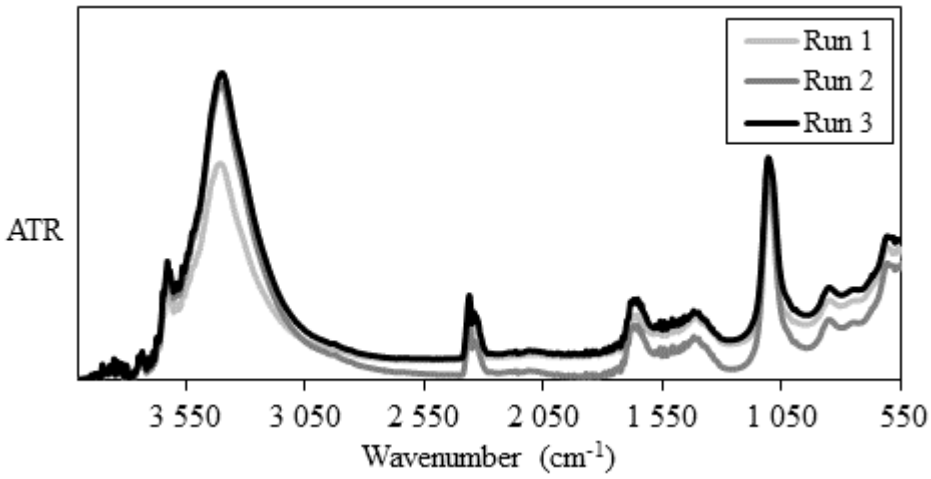

B-31: FTIR graph for Ca/Al-sulphate (pH = 9.90)

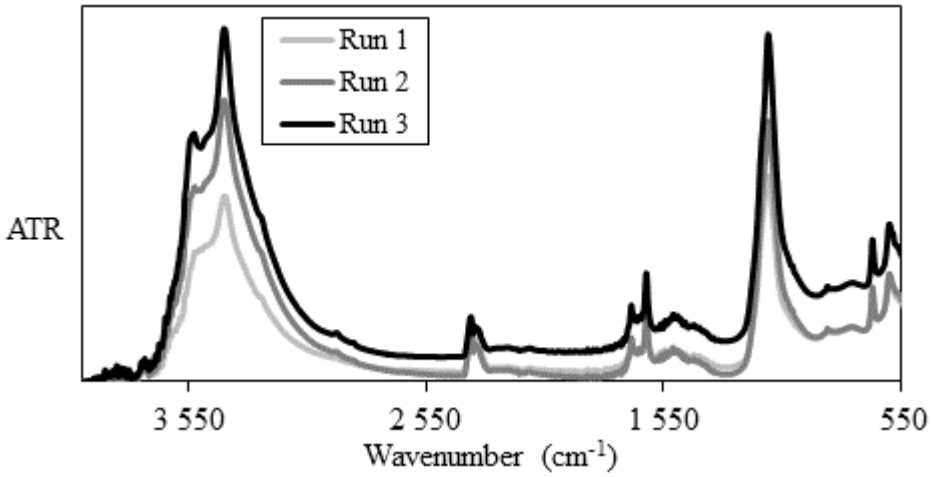

B-32: FTIR graph for Ca/Al-sulphate (pH = 1.30)

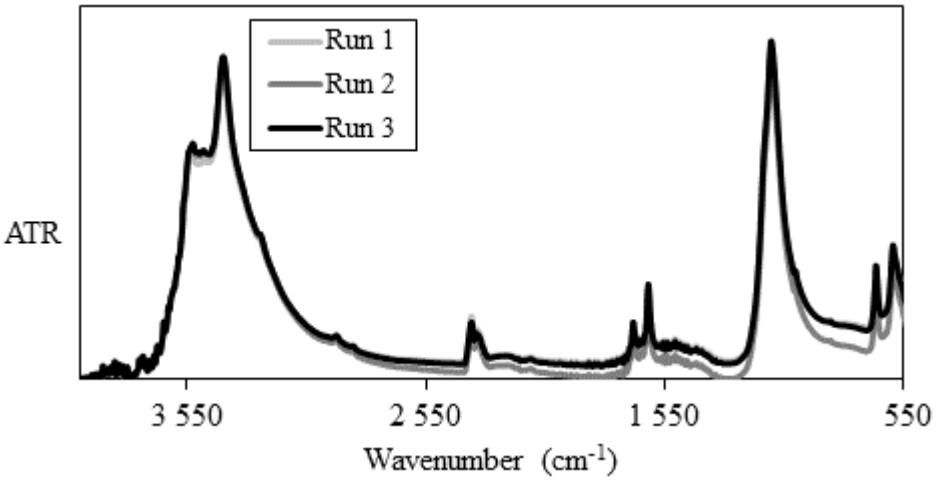

Appendix C: TGA Results

C-1: TGA curve for Ca/Al-sulphate

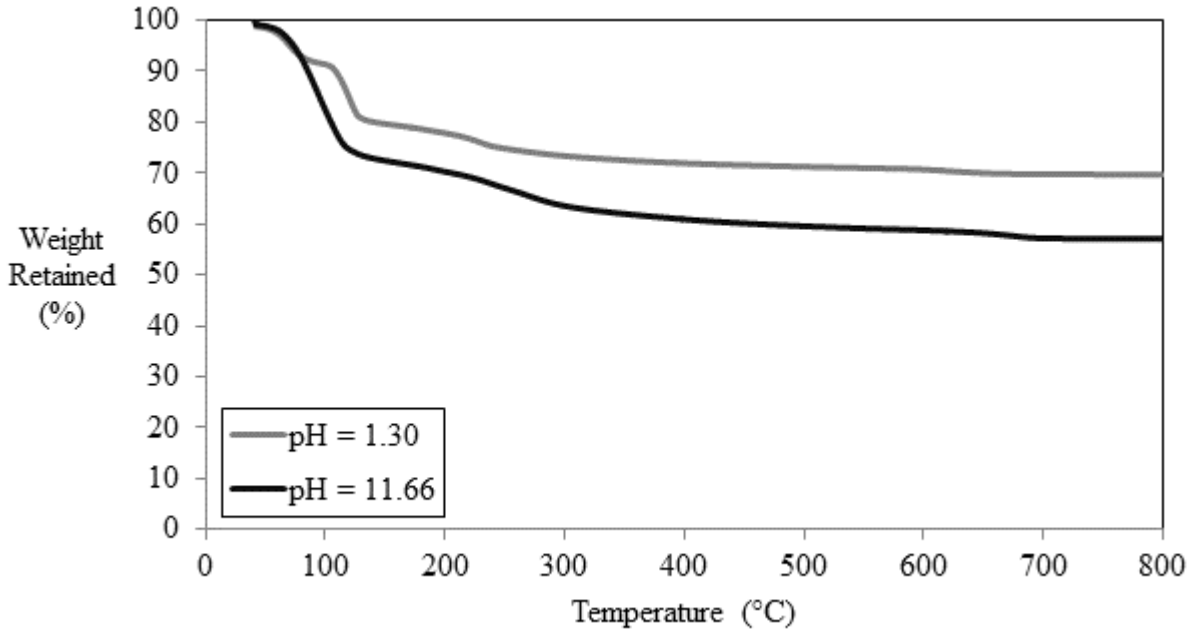

C-2: TGA curve for Ca/Al-thioglycolate